Third-order QCD corrections to heavy quark pair production near threshold

Von der Fakultät für Mathematik, Informatik und Naturwissenschaften der RWTH Aachen University zur Erlangung des akademischen Grades eines Doktors der Naturwissenschaften genehmigte Dissertation

vorgelegt von

Diplom-Physiker Kurt Schuller

aus

Mediasch (Rumänien)

Berichter: Universitätsprofessor Dr. Martin Beneke

Universitätsprofessor Dr. Werner Bernreuther

Tag der mündlichen Prüfung: 07. November 2008

Abstract

The measurement of the top quark mass is an important task at the future International Linear Collider. The most promising process is the top quark pair production in the threshold region. In this region the top quarks behave non-relativistically and a perturbative treatment using effective field theories is possible. Current second order theoretical predictions in a fixed order approach show an uncertainty which is bigger than the expected experimental errors. Therefore, an improvement of the cross section calculation is desirable. There are two ways to incorporate higher order effects, one is to calculate the full next order in the fixed order approach, another possibility is to resum large logarithms. In this work, the fixed order calculation has been extended to the third order in perturbation theory for the QCD corrections. The result is a strongly improved scale behavior and a better understanding of heavy quarkonium systems. The Green function result is given in a semi-analytic form. The energy levels and wave functions for heavy quarkonium states have been calculated from the poles of the Green function and are presented for arbitrary quantum number n. The results have been implemented in a Mathematica program which makes the data easily accessible. Once some missing matching coefficients are calculated, and a complete electroweak calculation is available, the results of this work can be used to improve the precision of the top quark mass measurement to an uncertainty of less than 50 MeV. An inclusion of initial state radiation and beam effects are essential for a realistic observable. In the future, the results obtained could be used for a third order resummation of large logarithms. Further applications are also the extraction of the bottom quark mass with sum rules.

Zusammenfassung

Die genaue Bestimmung der top-Quark Masse ist ein wichtiges Ziel des geplanten 'International Linear Collider'. Der Prozess, welcher die höchste Genauigkeit verspricht, ist die top-Quark Paarproduktion an der Erzeugungsschwelle. Bei diesen Energien haben die Quarks sehr kleine Geschwindigkeiten und können daher nicht-relativistisch beschrieben werden. Die aktuellen theoretischen Vorhersagen existieren bis zur zweiten Ordnung in der Störungstheorie und sind wesentlicher ungenauer als es die Messungen versprechen zu werden. Es ist daher wünschenswert diese Genauigkeit zu verbessern. Dies kann auf zwei Arten erreicht werden. Einerseits kann die Rechnung auf die nächst höhere Ordnung in der Störungstheorie ausgeweitet werden, und andererseits können die aktuellen Rechnungen mit Renormierungsgruppenmethoden resummiert werden. In dieser Arbeit wird der erste Weg eingeschlagen, das heißt die dritte Ordnung in der Störungstheorie wird berechnet. Das Ergebnis ist ein stark verbessertes Skalenverhalten des Wirkungsquerschnitts, sowie ein besseres Verständnis von schweren Quark-Anti-Quark-Systemen. Die Green Funktion, die eng mit dem Wirkungsquerschnitt verknüpft ist, wurde in semi-analytischer Form berechnet. Die Energieniveaus und Wellenfunktionen der Quark-Anti-Quark-Systeme wurden aus den Polen der Green Funktion für beliebige Hauptquantenzahl n bestimmt. Alle Ergebnisse wurden in ein Mathematica Paket implementiert, um die Weiterverwendung zu vereinfachen. Für eine vollständige QCD Rechnung fehlen noch einige Koeffizienten, welche recht einfach in das Programm eingefügt werden können. Zusammen mit den ebenfalls noch fehlenden elektroschwachen Korrekturen können die Ergebnisse dieser Arbeit zu der gewünschten Präzision der top-Quark Masse von weniger als 50 MeV führen. Das Ergebnis könnte außerdem mit Renormierungsgruppenmethoden weiter verbessert werden. Eine weitere Benutzung der Resultate zur Bestimmung der bottom-Quark Masse mit Summenregeln ist ebenfalls möglich.

Contents

Chapter 1

Introduction

In particle physics, since many years, the Standard Model (SM) has been very successful to explain almost every observed phenomenon. The mathematical concept of the SM is a quantum field theoretical description of three fundamental interactions (the electromagnetic, the weak and the strong force) and 37 elementary particles, described by the SM Lagrangian. One important failure of the SM is, that the gravitational interaction could not be included in this framework, without giving rise to infinities at high energies. This leads to the conclusion, that the SM might be only a low energy limit of a more fundamental 'Theory of Everything'. The concept of a limited theory, called effective theory, which is only valid up to a certain scale, is well known[1]. Such theories can be understood as an expansion in the small-scale limit. Field theoretically, this means that interactions in the Lagrangian are suppressed by the inverse of the limiting scale. So, at energies much lower than this scale, these terms become unimportant. This concept will return in the next chapter, when an effective non-relativistic theory will be introduced.

The particle content of the SM can be divided into half-integer-spin and integer-spin particles, called fermions and bosons, respectively. The fermions again will be classified into quarks, which feel the strong force, and leptons, which interact only by electromagnetic or weak forces. The bosons are the mediating particles of the three forces. A special role is assigned to the Higgs boson, which has been introduced to give masses to the particles via the so called Higgs mechanism. It is the only SM particle, which has not yet been observed experimentally.

Within the SM, the top quark is the heaviest elementary particle. Due to this high mass, the properties of the top quark are sensitive to high energy effects, beyond the reach of current accelerators. These effects might reveal some aspects of the more fundamental theory,

[1] Classical examples of low-energy effective theories are the Heisenberg-Euler effective theory in QED or Fermi's four-fermion theory of weak interactions.

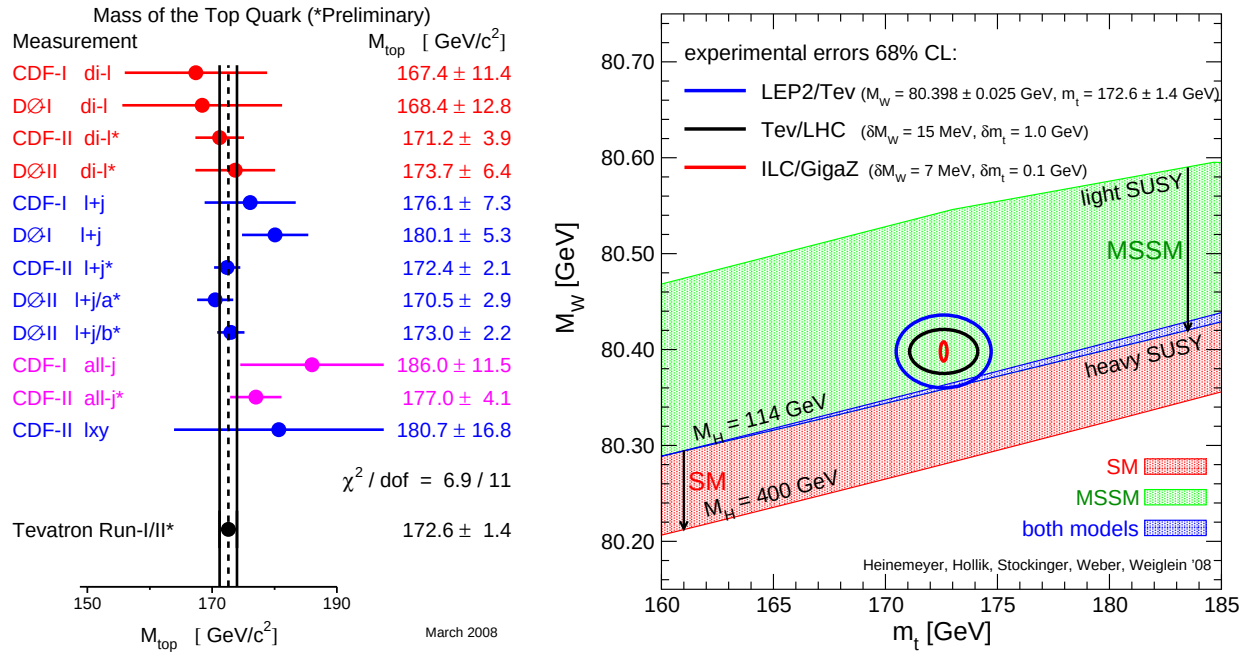

Figure 1.1: Left: Recent results for top quark mass measurements at the Tevatron (taken from [1]). Right: Effect of the top quark mass uncertainty on the exclusion limits for the Standard Model (taken/updated from [2,3], including two-loop corrections for the precision observables [4–7]).

described in the first paragraph, and therefore make the top quark a perfect playground for precision tests. An example of the importance of the top quark mass is shown in figure 1.1. The circle shows the 68 % confidence level interval of current and expected mass measurements. It reveals, that the precise measurement of the masses of the top quark, the W-boson and the Higgs in a combined fit can lead to an evidence for the model, which is favored by nature.

Therefore, it is not surprising, that strong efforts have been undertaken to measure the top quark mass since its discovery in 1995 at the Fermilab Tevatron collider by the CDF and D0 experiments [8,9]. The process that led to detection is the top quark pair production ($t\bar{t}$) in proton-antiproton ($p\bar{p}$) collisions. The protons are composed out of quarks (q) and gluons (g), so the production processes are $q\bar{q} \rightarrow t\bar{t}$ and $gg \rightarrow t\bar{t}$. The produced top quarks decay very rapidly ($\approx 0.5 \times 10^{-24}$s), mainly into a W-boson and a bottom quark ($t\bar{t} \rightarrow W^+bW^-\bar{b}$), which themselves decay into leptons (10%), leptons and quarks (44%) or only quarks (46%)[2]. Until today, the pair production is the only process where top quarks have been observed. The reason is, that other possible production channels, as for example the electroweak single-

[2]Due to confinement, quarks hadronize in the detector and show up in the form of jets. The three decay modes are therefore also called di-leptonic, semi-leptonic and hadronic (or all-jets) channels.

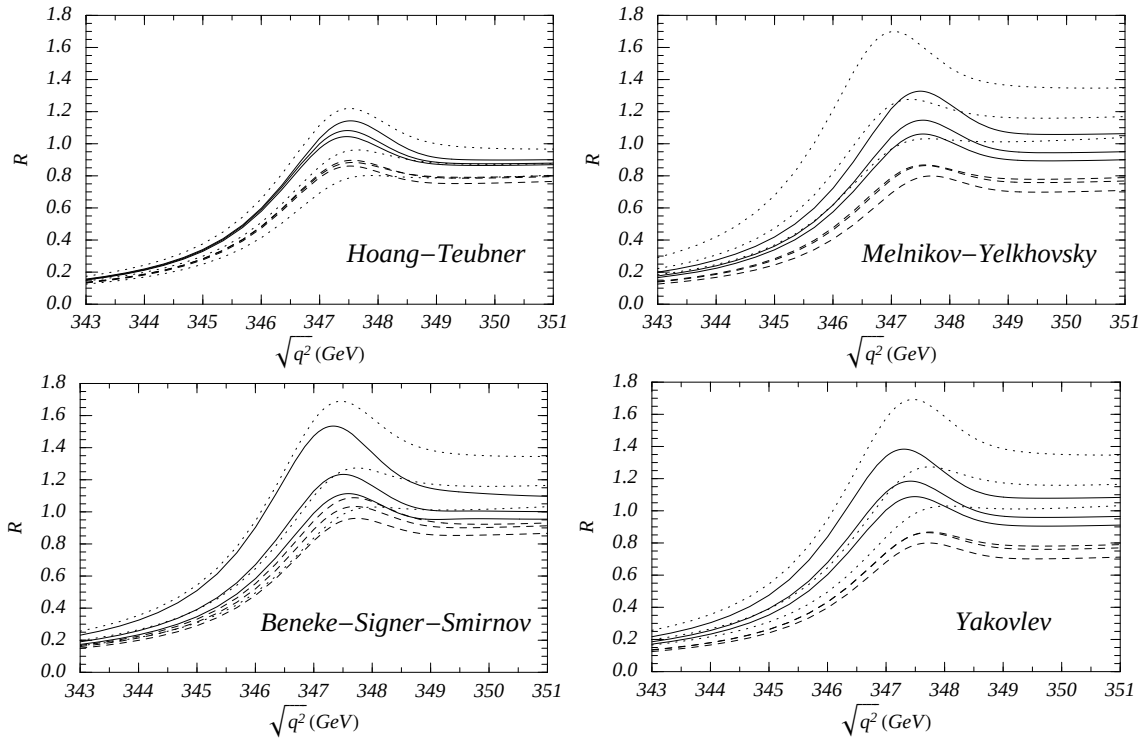

Figure 1.2: The total $e^+e^- \to \gamma \to t\bar{t}$ QCD cross section R at LO (dotted curves), NLO (dashed) and NNLO (solid) for three different scales by various groups (taken from [14]).

top production ($q\bar{q} \to t\bar{b}$ or $qb \to qt$ where b is the bottom quark), have a weaker signal and much higher backgrounds [10].

For the pair production of top quarks, the top quark mass has been measured at the Tevatron in all three decay channels (see figure 1.1). The current value is $m_t = 172.6 \pm 1.4$ GeV [1]. A more precise measurement will be done at the Large Hadron Collider (LHC), which will start operating soon. The expected accuracy is of the order of $\delta m_t = 1$ GeV [11,12]. The precision is limited at hadron colliders (with partonic initial states) due to large uncertainties in the parton density functions. This problem is avoided at linear colliders. The initial states consist of electrons, which form a much cleaner signal. Therefore, a high precision can be reached at the future International Linear Collider (ILC). At the ILC, the most sensitive process for mass measurements is the top quark pair production at threshold (energy of $E \sim 2m_t$). Assuming an uncertainty of 3% for the theoretical shape of the cross section, an accuracy of around 30 MeV can be reachable [13]. The aim of this work is to push the error of the theoretical calculation beyond this limit.

At the top quark pair production threshold, the shape of the cross section is strongly influenced by the position of the 1S peak of the top-antitop pair (toponium). The sharpness of the peak is affected mainly by the top quark width, and the peak position by the mass.

Due to the fast decay of the top quark, the 1S peak is very flat, and higher quantum state peaks are absent. The top quarks have small velocities, so the process can be described by a non-relativistic heavy quarkonium system, which has been examined since long ago [15–17]. A consistent field theoretical approach has been made possible by the invention of non-relativistic effective field theories [18]. Since that time, a lot of work has been done in the field, and several groups have calculated the next-to-next-to-leading order (NNLO) QCD corrections to the total pair production cross section [19–24]. Additional to the pure QCD corrections, electroweak (EW) and also the interference effects of EW and QCD corrections become important. Some work on the EW effects has been done in the past [25–27], but complete results still do not exist. Furthermore, a consistent treatment of finite width effects also becomes important at higher orders. In current calculations, only the leading order width effects are included.

The existing NNLO QCD calculations (see figure 1.2) show a good convergence for the peak position, but reveal a big uncertainty in the normalization. On the one hand, the successive addition of the higher orders does not converge rapidly, and on the other hand, the scale dependence of the second order is large. To cure this, there are essentially two possibilities, a renormalization group improvement by resummation of large logarithms or a full third-order calculation. The first approach, namely the resummation of logs up to next-to-next-to-leading-logarithmic (NNLL) order has been almost completed in two slightly different frameworks [28–30]. Also, first steps towards a full third-order calculation have been done in the past [31–42]. In this work, the full next-to-next-to-next-to-leading-order (NNNLO) QCD corrections to the cross section up to some yet unknown coefficients are presented. This includes not only the photon mediated contributions, but also those induced by a Z-boson exchange. These have been omitted in some earlier papers, because they are suppressed at threshold. They start contributing at NNLO, so only leading-order and first-order corrections are needed at third order. Some results at this order are available in a different regularization scheme [24, 43–45]. To combine the results, it is mandatory to use the same scheme, to ensure the correct cancelation of scheme dependent divergences. Therefore, these contributions were recalculated.

The thesis is structured as follows: In the next chapter, an introduction to effective field theories will be given, and the details of the non-relativistic expansion are provided. The relevant one-loop matching coefficients arising from the matching of QCD to the effective theories are calculated, and for higher loops the known results are provided. In the third part, the cross section in the effective theory will be calculated, and the results of the relevant Feynman diagrams are presented. The results have been implemented into a Mathematica package. The documentation of this program is the topic of chapter four. Finally, the results

for the energy levels, the wave function and the total cross section will be discussed. The effect of different contributions and parameters is analyzed and an overview of open issues is given.

Chapter 2

The $t\bar{t}$ cross section near threshold in the effective field theory

2.1 Heavy-quark correlation function

To study the QCD effects to the process $e^+e^- \to t\bar{t}$, the optical theorem is used to relate the total cross section $\sigma_{t\bar{t}}$ to the two point function $\Pi(q^2)$ of the electromagnetic heavy quark current. The current can come from the vector coupling (photon mediated, see first diagram in figure 2.1) and from the axial vector coupling to the Z boson coming from the second diagram in figure 2.1. The vector current is given by $j^v_\mu = \bar{t}\gamma_\mu t$ and the axial vector current by $j^a_\mu = \bar{t}\gamma_\mu\gamma_5 t$. The second effect is suppressed at threshold and contributes first at NNLO, as will be seen later.

In quarkonium physics it is common to use the R-ratio instead of the total cross section. In this work the term "cross section" will be used for the R-ratio:

$$R = \frac{\sigma(e^+e^- \to t\bar{t}+X)}{\sigma(e^+e^- \to \mu^+\mu^-)} = 12\pi \mathrm{Im}\Big[e_t^2\Pi^{(v)}(q^2) - \frac{2q^2}{q^2-M_Z^2}v_e v_t e_t \Pi^{(v)}(q^2) + \Big(\frac{q^2}{q^2-M_Z^2}\Big)^2 (v_e^2+a_e^2)(v_t^2\Pi^{(v)}(q^2) + a_t^2\Pi^{(a)}(q^2))\Big], \tag{2.1}$$

where $\sigma(e^+e^- \to \mu^+\mu^-) = 4\pi\alpha^2/(3s)$ is the high energy limit of $\mu^+\mu^-$ production, s the center-of-mass energy squared, e_t is the top quark electric charge and α is the fine-structure constant. "X" denotes an arbitrary final state of massless quarks and gluons. The vector and axial vector coupling of the fermion f to the Z-boson are given by

$$v_f = \frac{T_3^f - 2e_f \sin^2\theta_w}{2\sin\theta_w\cos\theta_w}, \tag{2.2}$$

$$a_f = \frac{T_3^f}{2\sin\theta_w\cos\theta_w}, \tag{2.3}$$

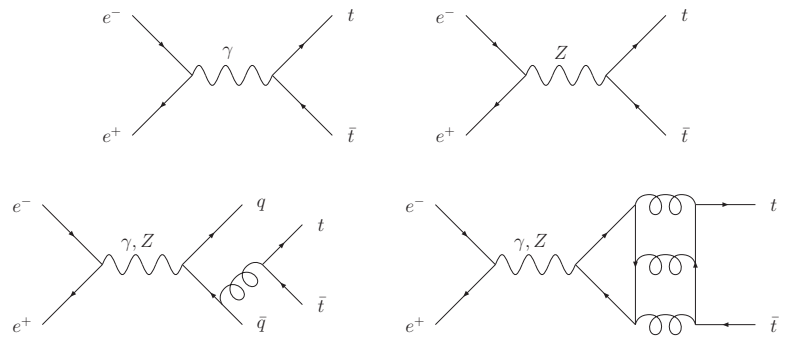

Figure 2.1: QCD diagrams for $t\bar{t}$ production.

where M_Z is the Z-boson mass, θ_w the weak mixing angle, e_f the charge of the fermion and T_3^f the third component of the weak isospin of the fermion. Relation (2.1) is not exactly true, because the radiation off light quarks and the annihilation contribution (shown in the third and forth diagram of figure 2.1) are not included in the correlation function, but also produce top quark pairs. As will be seen in section 2.2, the two effects are strongly suppressed near threshold, and don't contribute at third order. So, in this paper only on the first two diagrams and their QCD corrections will be studied. The corresponding current correlation function is given by:

$$\Pi^{(X)}(q^2) = (q_\mu q_\nu - q^2 g_{\mu\nu})\, i \int d^4x\, e^{iq\cdot x}\, \langle 0|T(j_\mu^{(X)}(x) j_\nu^{(X)}(0))|0\rangle, \tag{2.4}$$

where the X can stand for the vector or axial vector index. The two-point function at threshold can be expressed by the non-relativistic Green function G(E):

$$\Pi^{(v)} = \frac{N_c}{2m^2}\Big(c_v(c_v - \frac{E}{m}(1 + d_v/3))G^{(l=0)}(E)\Big), \tag{2.5}$$

$$\Pi^{(a)} = \frac{3N_c}{m^4} c_a^2 G^{(l=1)}(E), \tag{2.6}$$

where $N_c = 3$ denotes the number of colours. The coefficients c_v, d_v and c_a arise from short distance effects, which will not be cast into the Green function. They arise systematically in the effective theory approach, which will be shown later. The functions $G^{(l)}(E) = G^{(l)}(0, 0, E)$ come from the partial wave decomposition of the Green function:

$$G(\mathbf{r_1}, \mathbf{r_2}, E) = \sum_{l=0}^{\infty}(2l+1)(r_1 r_2)^l P_l(\mathbf{r_1}\cdot\mathbf{r_2}/r_1 r_2) G^{(l)}(r_1, r_2, E), \tag{2.7}$$

where $P_l(z)$ are the Legendre polynomials. The Green function describes the propagation of a $t\bar{t}$ pair, produced and annihilated at the origin. A more precise explanation of this quantity in the non-relativistic expansion and in the framework of an effective theory will be given in the sections 2.2 and 2.4.1.

The calculation is performed in the center of mass frame, so that the incoming momenta of the quark and antiquark are of opposite sign. The external heavy quark spinors in QCD are given by

$$u(p) = \frac{1}{(E_p + m)^{1/2}} \begin{pmatrix} (E_p + m)\,\xi \\ \boldsymbol{\sigma} \cdot \boldsymbol{p}\,\xi \end{pmatrix}, \qquad v(p) = \frac{1}{(E_p + m)^{1/2}} \begin{pmatrix} \boldsymbol{\sigma} \cdot \boldsymbol{p}\,\eta \\ (E_p + m)\,\eta \end{pmatrix}, \tag{2.8}$$

for external momentum $p = (E_p \equiv (m^2 + \boldsymbol{p}^2)^{1/2}, \boldsymbol{p})$. The variables ξ and η denote the quark and antiquark two-spinors, respectively. They are normalized according to $\xi^\dagger \xi = \eta^\dagger \eta = 1$.

2.2 Momentum regions and effective field theory

At the quark pair production threshold, one observes that the usual perturbation theory breaks down. This is due to the small quark velocity v. But, one can treat the system non-relativistically and make an expansion not only in the strong coupling constant α_s, as in the usual perturbation theory, but also in the velocity v, assuming that the velocity is of the same order as α_s. The power counting up to third order including the small velocity approximation is:

$$R = v \sum_k \left(\frac{\alpha_s}{v}\right)^k \{1(\mathrm{LO}); \alpha_s, v\,(\mathrm{NLO}); \alpha_s^2, \alpha_s v, v^2(\mathrm{NNLO}); \\ \alpha_s^3, \alpha_s^2 v, \alpha_s v^2, v^3(\mathrm{NNNLO})\}. \tag{2.9}$$

The expansion shows, that one has to take into account terms of the order $(\alpha_s/v)^k$ for all k. This means, the exchange of Coulomb gluons has to be summed up to all orders. At leading order, this is done by the use of the resummed Coulomb Green function, which includes all ladder diagrams from figure 2.2. At higher orders, the procedure is more complicated, because the quarkonium bound state system has different energy and three-momentum scales with respect to the given power counting. The relevant momentum scales are the top quark mass ($\sim$ 175 GeV), the non-relativistic top quark energy and the decay width (both $\sim$ 1.5 GeV), and the characteristic top quark momentum ($\sim$ 15 GeV). So, one can distinguish four regions:

$$\begin{aligned} \textbf{hard}: &\ \ l_0 \sim m, \ \ \mathbf{l} \sim m \\ \textbf{soft}: &\ \ l_0 \sim mv, \ \mathbf{l} \sim mv \\ \textbf{potential}: &\ l_0 \sim mv^2, \mathbf{l} \sim mv \\ \textbf{ultrasoft}: &\ l_0 \sim mv^2, \mathbf{l} \sim mv^2 \ , \end{aligned} \tag{2.10}$$

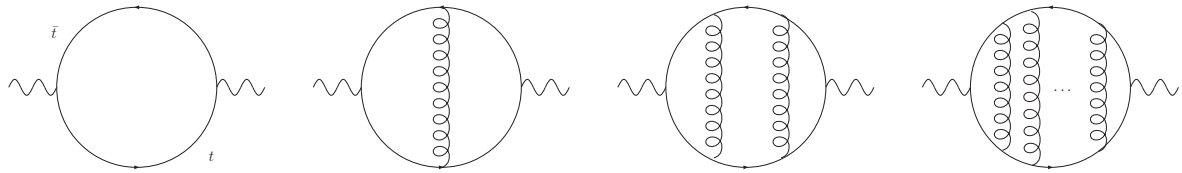

Figure 2.2: Ladder diagrams in the resummed Coulomb Green function.

where only massless particles (gluons, light quarks and ghosts) can be ultrasoft. The calculation of quantities describing such systems involve integrals with these scales. Therefore it is difficult to calculate these multiscale integrals in the non-relativistic expansion. With the use of the threshold expansion method [46], it is possible to separate the scales. This allows the correct expansion in α_s and v. To do so, the integrals are written as a sum over integrals coming from the different regions. Then, these integrals are expanded in the parameters which are small in the corresponding region. The integration is carried out over the complete phase space. Divergences coming from different regions cancel. In intermediate steps, these divergences have to be regularized consistently. In this work, dimensional regularization ($d = 4 - 2\epsilon$) will be used with $\overline{MS}$ subtraction in all parts of the calculation.

The threshold expansion allows to use separate field operators for the different regions, because every integral has to be evaluated only in one region, so that there is no overlap of loop momenta. The separation of fields makes it possible to use an effective theory framework. The idea behind this concept is to parameterize effects at small distances (or high energies) by local interactions of low-mass particles. The Lagrangian consists then of all possible local operators of the new fields. This procedure is called integrating out the short-distance (or high energy) modes. Here, the higher modes (hard, soft and potential) are integrated out step by step. In section 2.3, the hard modes are integrated out. Hard modes contribute on the one hand to an effective non-relativistic Lagrangian as well as to an external current, coming from the coupling to the photon. In the next step, the soft and potential modes are integrated out in section 2.4, and the result can be understood as an effective (instantaneous) heavy-quark potential.

To determine the scaling behavior of Feynman diagrams, the velocity scaling of loop integrations and propagators is examined. From equation (2.10) it follows, that the integration measure d^4k scales as v^0, v^4, v^5 and v^6, when k is hard, soft, potential and ultrasoft. The

denominator of a quark propagator with momentum $q/2 + l$ scales as:

$$\frac{1}{(q/2+l)^2 - m^2} = \begin{cases} \dfrac{1}{l^2 + q \cdot l} + \ldots & \text{hard } (v^0) \\ \dfrac{1}{2m}\dfrac{1}{l^0} + \ldots & \text{soft } (v^{-1}) \\ \dfrac{1}{2m}\dfrac{1}{E/2 + l^0 - \boldsymbol{l}^2/(2m)} + \ldots & \text{potential } (v^{-2}). \end{cases} \tag{2.11}$$

The velocity scaling is given in brackets. For the gluon propagator the scaling is:

$$\frac{1}{l^2} = \begin{cases} \dfrac{1}{l^2} & \text{hard } (v^0),\ \text{soft } (v^{-2}),\ \text{ultrasoft } (v^{-4}), \\ \dfrac{-1}{\boldsymbol{l}^2} + \ldots & \text{potential } (v^{-2}). \end{cases} \tag{2.12}$$

Using these scaling rules, it can now be shown why the radiation off light quarks is beyond NNNLO in the non-relativistic approximation. For the final states the kinetic energy available at threshold is limited to mv^2, since the final state consists of two top quarks. So, the two heavy quarks are potential and the light quarks must be ultrasoft. In the light quark correlation function this leads to a factor of v^{21} from the loop integration measure. Since there has to be a connected path of large momentum of order $2m$ from the production of the light quarks to the production of the top quark pair, one of the light quarks and the gluon are off-shell by an amount of order $4m^2$ and do not contribute powers of v. The two potential top quarks and the ultrasoft light quark propagator all scale as $1/v^2$ in the correlation function. So, the diagram scales as v^{13}, which corresponds to v^{12} relative to the leading-order cross section. Inspection of the analytic expression [47] confirms this result.

The dominant annihilation diagram in the colour singlet and spin triplet channel is the one shown in figure 2.1. This is of order α_s^3 from the vertices and v^2 from the potential quarks. So, it is also beyond NNNLO and can be neglected.

2.3 Non-relativistic QCD

The first step in the effective theory approach is to integrate out the hard modes. This corresponds to calculating (relativistic) effects of the order of the heavy quark mass, so that the remaining fields are non-relativistic and consist only of soft, potential and ultrasoft modes. This leads to the formulation of the non-relativistic QCD (NRQCD) [48–50] with the quark field ψ and the anti-quark field χ, the chromoelectric field E^i and the chromomagnetic interaction $\boldsymbol{\sigma} \cdot \mathbf{B}$. The Lagrangian can be divided into four parts:

$$\mathcal{L}_{NRQCD} = \mathcal{L}_{\psi\psi} + \mathcal{L}_{\chi\chi} + \mathcal{L}_{\psi\chi} + \mathcal{L}_g + \mathcal{L}_{light}, \tag{2.13}$$

where the antiquark part $\mathcal{L}_{\chi\chi}$ is the complex conjugated of the quark Lagrangian $\mathcal{L}_{\psi\psi}$, and $\mathcal{L}_{light}$ is the Lagrangian for light quarks and $\mathcal{L}_g$ for gluons. The light quark and gluon Lagrangian corresponds to the one in the full QCD without the heavy quark part. The heavy quark NRQCD Lagrangian is:

$$\begin{aligned}\mathcal{L}_{\psi\psi} &= \psi^\dagger\left(iD_0 + \frac{\mathbf{D}^2}{2m} + \frac{\mathbf{D}^4}{8m^3}\right)\psi \\ &+\psi^\dagger\Bigg(-\frac{d_1 g_s}{2m}\boldsymbol{\sigma}\cdot\mathbf{B} + \frac{d_2 g_s}{8m^2}[D^i, E^i] + i\,\frac{d_3 g_s}{8m^2}\sigma^{ij}[D^i, E^j] \\ &\quad +d_W g_s\frac{\{\mathbf{D}^2, \boldsymbol{\sigma}\cdot\mathbf{B}\}}{8m^3} + d_A g_s^2\frac{\mathbf{B}^2-\mathbf{E}^2}{8m^3} + d_B g_s^2\frac{\sigma^{ij}(B^iB^j - E^iE^j)}{8m^3}\Bigg)\psi + O\Big(\frac{1}{m^4}\Big),\end{aligned} \tag{2.14}$$

$$\begin{aligned}\mathcal{L}_{\psi\chi} &= \frac{d_{ss}}{m^2}\psi^\dagger\psi\,\chi^\dagger\chi + \frac{d_{sv}}{m^2}\psi^\dagger\boldsymbol{\sigma}\psi\,\chi^\dagger\boldsymbol{\sigma}\chi + \\ &\quad +\frac{d_{vs}}{m^2}\psi^\dagger\mathrm{T}^a\psi\,\chi^\dagger\mathrm{T}^a\chi + \frac{d_{vv}}{m^2}\psi^\dagger\mathrm{T}^a\boldsymbol{\sigma}\psi\,\chi^\dagger\mathrm{T}^a\boldsymbol{\sigma}\chi + O\Big(\frac{1}{m^3}\Big),\end{aligned} \tag{2.15}$$

$$\mathcal{L}_g = -\frac{d_4}{4}G^A_{\mu\nu}G^{A\mu\nu} + \frac{d_5}{m^2}G^A_{\mu\nu}D^2G^{A\mu\nu} + \frac{d_6}{m^2}gf^{ABC}G^A_{\mu\nu}G^B_{\mu\alpha}G^C_{\nu\alpha} + O\Big(\frac{1}{m^4}\Big), \tag{2.16}$$

where $A_\mu = A^A_\mu T^A$ is the gluon field, $G_{\mu\nu} = (i/g_s)\,[D_\mu, D_\nu]$ the corresponding field strength tensor and the chromoelectric and chromomagnetic fields are defined as:

$$\begin{aligned}E^i \equiv G^{i0} &= -\nabla^i A^0 - \frac{\partial}{\partial t}\,A^i - ig_s\left[A^i, A^0\right], \\ \boldsymbol{\sigma}\cdot\boldsymbol{B} &\equiv -\frac{1}{2}\,\sigma^{ij}G^{ij}.\end{aligned}$$

The Feynman rules for this Lagrangian are given in figure 2.3. The remnant of the hard modes is encoded in the Wilson coefficients d_i. They are normalized such that they are 1 at tree level (not for d_2, where the tree level contribution vanishes). Higher-loop orders have to be calculated by matching the QCD diagrams to the NRQCD diagrams order by order in the non-relativistic expansion. For reasons which will be explained later, the matching coefficients up to order ϵ are needed.

In the Lagrangian, all terms are kept that are relevant for the NNNLO calculation, so all terms that contribute to order v^3, $v^2\alpha_s$, $v\alpha_s^2$ and α_s^3 relative to the leading order. The scaling of the fields depends on the scaling region. Quarks fields can be potential and soft and from the scaling rules of the propagator (given in equation (2.11)) and the integration measure, one can see that in both cases the field scales as $v^{3/2}$. The same power counting can be done with the gluon field, which is either soft, potential or ultrasoft and the scalings of g_sA are $v^{3/2}$, v^2 and $v^{5/2}$ respectively, a factor of $v^{1/2}$ coming from the coupling constant g_s.

First, the two point interactions of the quark Lagrangian will be examined. For potential quarks, the kinetic term $\psi^\dagger(iD_0 + \mathbf{D}^2/(2m))\psi$, which is the leading-order Lagrangian, is of order v^5. The relativistic correction $\psi^\dagger(\mathbf{D}^4/(8m^3))\psi$ scales as v^7 and thus contributes to

NNLO. The next term in the expansion would be of order v^9 and is beyond NNNLO. For soft quarks, the quadratic kinetic energy term is an order v correction to the leading-order static Lagrangian $\psi^\dagger iD^0\psi$, which scales as v^4. In this case the quartic kinetic energy correction is a N^{3}LO effect.

Consider now interactions with the gauge field, i.e. terms of the form $g_s\psi^\dagger\psi A^n$, potentially with derivatives on the quark and gluon fields. The $g_s\psi^\dagger\psi A_0$ interaction that comes from $\psi^\dagger iD^0\psi$ scales as v^5 when all fields are potential. Therefore it is not suppressed relative to the terms that persist as $g_s \to 0$. In the potential region, this interaction has to be treated non-perturbatively; this is why the cross section near threshold requires a summation to all orders in α_s. When the gluon field is soft, the velocity scaling of the $g_s\psi^\dagger\psi A_0$ interaction is $v^{9/2}$, but since in this case the leading term $\psi^\dagger i\partial^0\psi$ scales as v^4, this interaction is a perturbation. It follows that all soft interactions can be treated in conventional perturbation theory. Further three-point interactions of the form above carry derivatives. Each derivative gives at least a suppression of v. So, the Lagrangian with up to three derivatives is needed at NNNLO. The requirement of gauge invariance restricts the possible interaction terms up to order v^6 to the so called chromomagnetic, Darwin and spin-orbit interactions, multiplied by the short-distance coefficients d_1, d_2 and d_3, respectively, and at order v^7 to the other terms given in (2.14). The Darwin and spin-orbit term contain two derivatives and start to contribute at NNLO. Hence, the one-loop short-distance coefficients are needed at NNNLO. For the particular case of the vector current correlation function, at least two vertices with a σ-matrix coupling to the heavy quarks are needed. Otherwise, one obtains a trace over three σ-matrices which vanishes. Consequently, one needs two chromomagnetic interactions at least, and since each is suppressed by v, the chromomagnetic interaction enters only at NNLO and d_1 is needed at one-loop order in this calculation. The contributions from the c_W and c_B terms don't contribute to third order by the same argument. The c_A part is suppressed by an additional coupling constants, and is therefore also of higher order.

The leading contribution of the four quark operator Lagrangian is suppressed by v^2 relative to leading order. So it appears first at NNLO. Terms of order v^3 relative to leading order would have again (similar to the two quark operators) an odd number of σ matrices and therefore vanish in the correlation function. Note that there is another possibility to write the Lagrangian using Fierz transformation. The representation given in (2.15) is useful when matching the Lagrangian to box diagrams rather than annihilation diagrams. Because at threshold the annihilation contribution is of higher order, the form given in (2.15) will be used throughout this work.

The pure gauge field Lagrangian is the same in QCD and NRQCD and thus it is fixed by the terms given in (2.16).

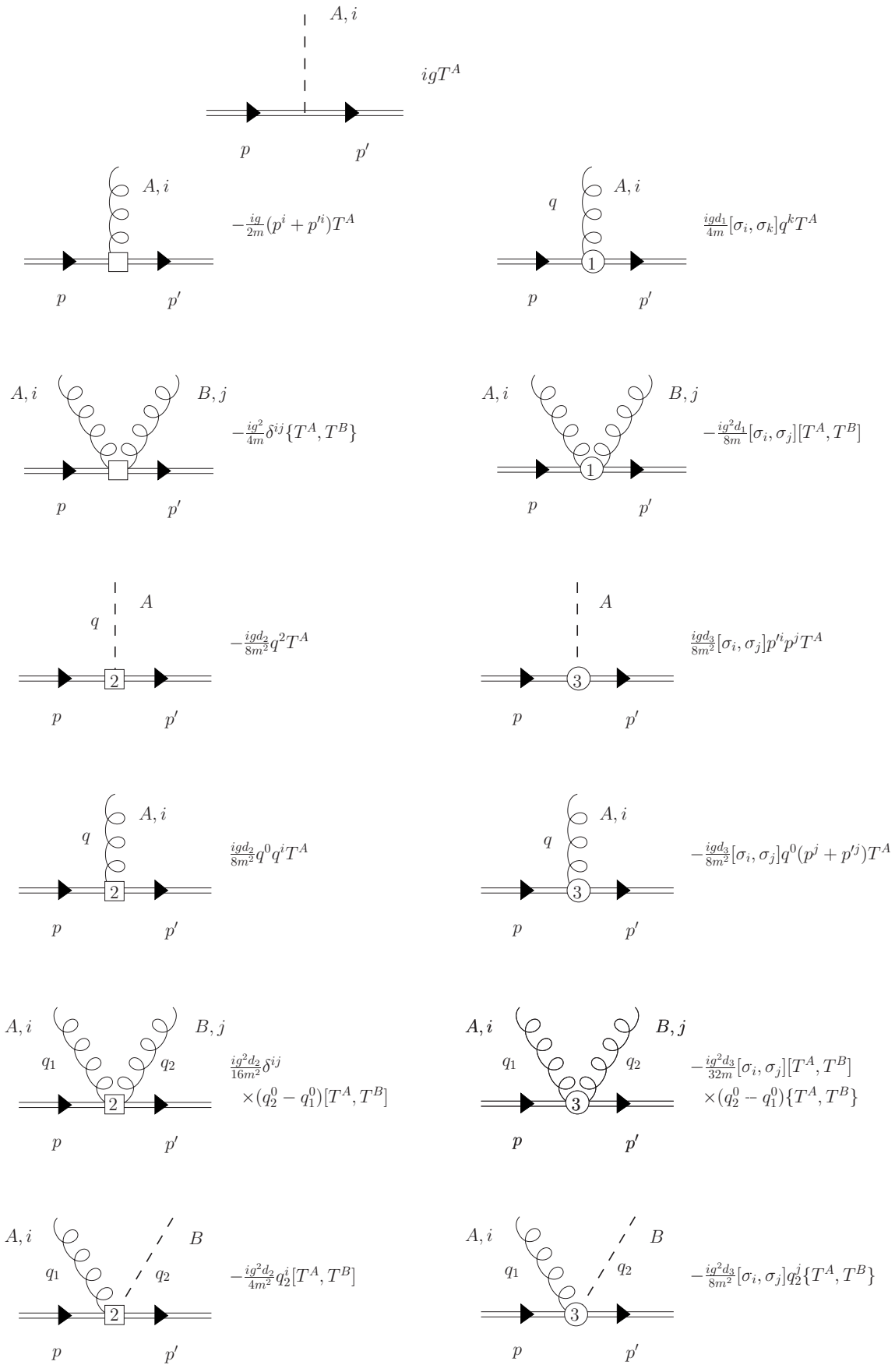

Figure 2.3: Feynman rules for NRQCD vertices up to order $1/m^2$.

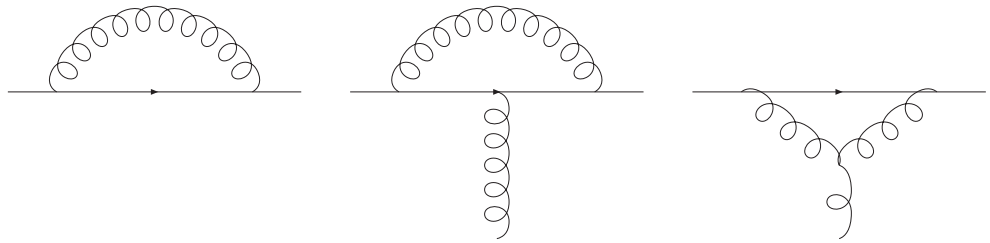

(a) (b) (c)

Figure 2.4: Formfactor contributions: wavefunction renormalization and vertex corrections.

Now, the matching at one-loop level will be performed and the results for higher loops are given, where available from the literature. The calculation is done in dimensional regularization. So, the d dimensional spin algebra must be used. This means the use of the ϵ tensor is avoided, since it is not defined in d dimensions. Note, that this convention has also been used in the definition of the Lagrangian. Instead, in the following calculations the expression:

$$\sigma^{ij} = \frac{1}{2i}\left[\sigma^i, \sigma^j\right], \tag{2.17}$$

will be used, and the products of σ matrices are evaluated with the identities:

$$\sigma^i\sigma^i = d - 1, \tag{2.18}$$

$$\sigma^i\sigma^j\sigma^i = (3-d)\,\sigma^j, \tag{2.19}$$

where $d = 4 - 2\epsilon$ and $tr(1) = 2$. As will be seen later, it is not sufficient to get the finite contributions of the matching coefficients. These coefficients multiply functions, which are divergent themselves. This means, the matching coefficients are also needed at higher orders in the ϵ expansion.

2.3.1 Two quark operators

This class of operators contains three fields, two quark fields and a gluon field (or its derivative). Therefore the matching will be done to the QCD three point function. Then, the result can be cast in the form written with the quark form factors, defined as:

$$-igT^a\bar{u}(p')\Big(F_1(q^2)\gamma^\mu + iF_2(q^2)\frac{\sigma^{\mu\nu}q_\nu}{2m}\Big)u(p). \tag{2.20}$$

The finite part of the one-loop quark form factors have been calculated some years ago [51]. However, the order ϵ coefficients are not given there. The form factors are calculated from the diagrams in figure 2.4 by calculating the on-shell wave function renormalization from figure

(a) and expressing the vertex corrections (b) and (c) in the form above. This expression is compared with the result for the three point function from NRQCD. The result for the wave function graph is:

$$-i\Sigma(p) = -iC_F\frac{\alpha_s}{4\pi}\Big(A(p^2)m + B(p^2)\Big), \tag{2.21}$$

with

$$A(p^2) = \int_0^1 dx \frac{\Gamma(\epsilon)(4-2\epsilon)}{(m^2x - p^2x(1-x))^\epsilon}, \tag{2.22}$$

$$B(p^2) = -\int_0^1 dx \frac{\Gamma(\epsilon)(2-2\epsilon)}{(m^2x - p^2x(1-x))^\epsilon}. \tag{2.23}$$

Then the correction to the wave function renormalization reads:

$$\delta Z = -C_F\frac{\alpha_s}{4\pi}\left[B(m^2) + 2m^2\Big(\frac{\partial A}{\partial p^2} + \frac{\partial B}{\partial p^2}\Big)_{p^2=m^2}\right] = -C_F\frac{\alpha_s}{4\pi}\Big(\frac{\mu}{m}\Big)^{2\epsilon}\frac{e^{\gamma_E}(3-2\epsilon)\Gamma(\epsilon)}{(-1+2\epsilon)}. \tag{2.24}$$

In the next step, the second diagram is considered, which is the abelian vertex corrections. The corresponding contributions are denoted with the superscript (V). The result for the form factors are:

$$F_1^{(V)} = \frac{\alpha_s}{4\pi}e^{\gamma_E\epsilon}\Gamma(\epsilon)\Big(C_F - \frac{C_A}{2}\Big)\Big(\frac{\mu}{m}\Big)^{2\epsilon}\Big(\frac{2\epsilon-3}{2\epsilon-1} + \frac{\mathbf{q}^2}{m^2}\frac{6\epsilon^2-5\epsilon+4}{12\epsilon-6}\Big), \tag{2.25}$$

$$F_2^{(V)} = \frac{\alpha_s}{4\pi}e^{\gamma_E\epsilon}\Gamma(\epsilon)\Big(C_F - \frac{C_A}{2}\Big)\Big(\frac{\mu}{m}\Big)^{2\epsilon}\Big(\frac{2\epsilon(2\epsilon+1)}{-2\epsilon+1} + \frac{\mathbf{q}^2}{m^2}\frac{\epsilon(\epsilon+1)(2\epsilon+1)}{-6\epsilon+3}\Big). \tag{2.26}$$

The last part is the non-abelian vertex corrections, which is the third relevant diagram. Background field Feynman gauge is used to assure gauge invariance. The contributions to the form factors are denoted with superscript (g) and read:

$$F_1^{(g)} = \frac{\alpha_s}{8\pi}e^{\gamma_E\epsilon}\Gamma(\epsilon)C_A\Big(\frac{\mu}{m}\Big)^{2\epsilon}\Big(\frac{2\epsilon-3}{2\epsilon-1} + \frac{\mathbf{q}^2}{m^2}\frac{2\epsilon+3}{8\epsilon^2-2}\Big), \tag{2.27}$$

$$F_2^{(g)} = \frac{\alpha_s}{8\pi}e^{\gamma_E\epsilon}\Gamma(\epsilon)C_A\Big(\frac{\mu}{m}\Big)^{2\epsilon}\Big(\frac{2\epsilon+2}{-2\epsilon+1} + \frac{\mathbf{q}^2}{m^2}\frac{\epsilon+2}{-4\epsilon^2+1}\Big). \tag{2.28}$$

Now, the complete on-shell form factors at one-loop can be computed by adding up the results obtained above. The form factors are given by:

$$F_1 = 1 - \delta Z + F_1^{(V)} + F_1^{(g)}, \tag{2.29}$$

$$F_2 = F_2^{(V)} + F_2^{(g)}. \tag{2.30}$$

So, the total result up to order α_s/m^2 is:

$$\begin{aligned} F_1 &= 1 + \frac{\alpha_s}{\pi}\Big(\frac{\mu}{m}\Big)^{2\epsilon}\frac{\Gamma(\epsilon)e^{\gamma_E\epsilon}}{48(4\epsilon^2-1)}\frac{\mathbf{q}^2}{m^2}\Big[C_A(-12\epsilon^3+4\epsilon^2+3\epsilon+5) + 2C_F(12\epsilon^3-4\epsilon^2+3\epsilon+4)\Big], \\ F_2 &= \frac{\alpha_s}{\pi}\Big(\frac{\mu}{m}\Big)^{2\epsilon}\frac{\Gamma(\epsilon)e^{\gamma_E\epsilon}}{24(4\epsilon^2-1)}\Big[C_A\Big(6(2\epsilon+1)(2\epsilon^2-1) + \frac{\mathbf{q}^2}{m^2}(4\epsilon^4+8\epsilon^3+5\epsilon^2-2\epsilon-6)\Big) \\ &\quad + C_F\Big(-12\epsilon(2\epsilon+1)^2 - \frac{\mathbf{q}^2}{m^2}2\epsilon(\epsilon+1)(2\epsilon+1)^2\Big)\Big]. \end{aligned} \tag{2.31}$$

By calculation of the corresponding diagrams in the effective theory the relations between the coefficients d_i and the form factors are obtained. First equation (2.20) can be expressed in the non-relativistic limit. In the non-relativistic case the zeroth component is separated. This reads:

$$igT^a\xi^\dagger\Big[F_1(q^2)\Big(1-\frac{\mathbf{q}^2}{8m^2}+\frac{p_i'p_j}{4m^2}[\sigma_i,\sigma_j]\Big)+F_2(q^2)\Big(-\frac{\mathbf{q}^2}{4m^2}+\frac{p_i'p_j}{4m^2}[\sigma_i,\sigma_j]\Big)\Big]\xi. \tag{2.32}$$

The space components of equation (2.20) are:

$$igT^a\xi^\dagger\Big[F_1(q^2)\Big(\frac{p_k+p_k'}{2m}+\frac{q_i}{4m}[\sigma_i,\sigma_k]\Big)+F_2(q^2)\frac{q_i}{4m}[\sigma_i,\sigma_j]\Big]\xi. \tag{2.33}$$

This is compared with the same quantity in NRQCD. The calculation is straightforward and the result for the time component is

$$igT^a\xi^\dagger\Big[1-\frac{d_2\mathbf{q}^2}{8m^2}+\frac{d_3p_i'p_j}{8m^2}[\sigma_i,\sigma_j]\Big]\xi\ , \tag{2.34}$$

and for space components

$$igT^a\xi^\dagger\Big[\frac{p_k+p_k'}{2m}-\frac{d_1q_i}{4m}[\sigma_i,\sigma_j]\Big]\xi\ . \tag{2.35}$$

Direct comparison of these results with the expanded form of the full theory yields:

$$d_1 = F_1(0)+F_2(0), \tag{2.36}$$

$$d_2 = F_1(0)+2F_2(0)+8F_1'(0), \tag{2.37}$$

$$d_3 = F_1(0)+2F_2(0), \tag{2.38}$$

where $F_i(0) = F_i|_{q^2=0}$ and $F_1'(0) = dF_1/d(q^2/m^2)|_{q^2=0}$. So, the coefficients of the bilinear parts in the NRQCD Lagrangian to full order in ϵ have been calculated. The result agrees with the expanded result presented in [51] up to the order given there.

2.3.2 Gauge field operators

For the gauge field matching the gluon self energy diagram (figure 2.5) has to matched to the two relevant NRQCD diagrams. Note that the diagram with a gluon loop is the same in QCD and NRQCD and therefore no matching is necessary. The result for the quark loop diagram is:

$$(q^2g_{\mu\nu}-q_\mu q_\nu)\delta_{ab}\Big(1-\frac{\alpha_s}{\pi}T_F\Gamma(\epsilon)e^{\gamma_E\epsilon}\Big(\frac{\mu}{m}\Big)^{2\epsilon}\Big(\frac{1}{3}+\frac{4q^2}{15m^2}\epsilon\Big)\Big). \tag{2.39}$$

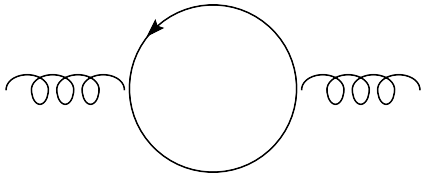

Figure 2.5: Gluon self energy diagram with one quark loop.

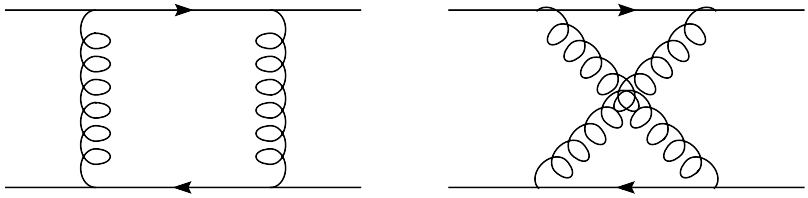

Figure 2.6: QCD diagrams for the 4 quark operators at one-loop.

The result in NRQCD is:

$$(q^2 g_{\mu\nu} - q_\mu q_\nu)\delta_{ab}\Big(f_1 + \frac{q^2}{m^2}16 f_2\Big). \tag{2.40}$$

This leads to corrections for the matching coefficients d_4 and d_5. They read:

$$d_4 = 1 + \frac{\alpha_s}{\pi}\Big(\frac{\mu}{m}\Big)^{2\epsilon}\frac{T_F\Gamma(\epsilon)e^{\gamma_E\epsilon}}{3}, \tag{2.41}$$

$$d_5 = \frac{\alpha_s}{\pi}\Big(\frac{\mu}{m}\Big)^{2\epsilon}\frac{T_F\epsilon\Gamma(\epsilon)e^{\gamma_E\epsilon}}{60}. \tag{2.42}$$

The results agree for $d = 4$ with the ones in [51]. The operator d_6 is not needed. The reason is, that in the final matching to the PNRQCD box diagram such a contribution is only possible at one-loop level. But since this correction is already of one-loop order, the additional loop would contribute only to higher orders.

2.3.3 Four quark operators

The last remaining part of the hard matching are the four quark operators. The four-dimensional results are given in [52]. Here the d-dimensional form of the matching coefficients is presented. Contributions from annihilation diagrams are not taken into account, because these are of higher orders for $t\bar{t}$ production in e^+e^- annihilation as described in section 2.1. For $t\bar{t}$ production in $\gamma\gamma$ collisions, these have to be considered. The only two relevant QCD diagrams for the process calculated in this work are shown in figure 2.6. These diagrams are of one-loop order (order α_s), so only the leading order in the v expansion is needed.

Therefore, all external momenta can be neglected and the quarks are put on-shell. After performing some algebra and using the master integrals from appendix B.1, the result for the two diagrams reads:

$$
\begin{aligned}
&(4\pi\alpha_s)\Big(C_F\Big(\frac{C_A}{2}-C_F\Big)+\Big(2C_F-\frac{C_A}{2}T^a\otimes T^a\Big)\Big) \\
&\times\int\frac{d^dk}{(2\pi)^d}\frac{2k^2-dk_0^2+4m^2-\frac{k_ik_j}{2}[\sigma_i,\sigma_k]\otimes[\sigma_j,\sigma_k]+\frac{k_0^2}{4}[\sigma_i,\sigma_j]\otimes[\sigma_i,\sigma_j]}{k^4(k^2+2mk_0)(k^2-2mk_0)} \\
&+(4\pi\alpha_s)\Big(C_F\Big(\frac{C_A}{2}-C_F\Big)+(2C_F-C_AT^a\otimes T^a)\Big) \\
&\times\int\frac{d^dk}{(2\pi)^d}\frac{-2k^2+dk_0^2-4k_0m+4m^2-\frac{k_ik_j}{2}[\sigma_i,\sigma_k]\otimes[\sigma_j,\sigma_k]+\frac{k_0^2}{4}[\sigma_i,\sigma_j]\otimes[\sigma_i,\sigma_j]}{k^4(k^2-2mk_0)^2} \\
=\;&\frac{\alpha_s^2}{m^2}\Big(\frac{m}{\mu}\Big)^{-2\epsilon}e^{\gamma_E\epsilon}\Big[C_F(C_A-2C_F)\frac{(2\epsilon-3)(2\epsilon^2+\epsilon+1)\Gamma(2+\epsilon)}{2\epsilon(8\epsilon^3+12\epsilon^2-2\epsilon-3)} \\
&+\frac{(-2\epsilon+3)(C_A(\epsilon(2\epsilon+1)(4\epsilon+3)+5)-8C_F(1+\epsilon)(2\epsilon^2+\epsilon+1))\Gamma(\epsilon)}{4(2\epsilon-1)(2\epsilon+1)(2\epsilon+3)}T^a\otimes T^a \\
&+\Big(C_F(C_A-2C_F)\frac{(1-\epsilon)\Gamma(1+\epsilon)}{2(2\epsilon+1)}+\frac{(\epsilon-1)(C_A+4C_A\epsilon-8C_F\epsilon)\Gamma(\epsilon)}{4(2\epsilon+1)}T^a\otimes T^a\Big)\sigma_i\otimes\sigma_i\Big],
\end{aligned}
\tag{2.43}
$$

where "$\otimes$" is the s-channel tensor product defined as $A\otimes B=A_{ij}B_{kl}$ and i, j are the indices of the quarks and k, j of the anti-quarks. In the effective theory the result is relatively simple and reads:

$$
\frac{1}{m^2}(d_{ss}+d_{vs}T^a\otimes T^a+(d_{sv}+d_{vv}T^a\otimes T^a)\sigma_i\otimes\sigma_i)\,. \tag{2.44}
$$

From the condition that the two results have to agree, the result for the effective four quark operators are obtained. The result is:

$$
d_{ss}=\alpha_s^2C_F(C_A-2C_F)\Big(\frac{\mu}{m}\Big)^{2\epsilon}\frac{e^{\gamma_E\epsilon}(2\epsilon-3)(2\epsilon^2+\epsilon+1)\Gamma(2+\epsilon)}{2\epsilon(8\epsilon^3+12\epsilon^2-2\epsilon-3)}, \tag{2.45}
$$

$$
d_{sv}=\alpha_s^2C_F(C_A-2C_F)\Big(\frac{\mu}{m}\Big)^{2\epsilon}\frac{e^{\gamma_E\epsilon}(-\epsilon+1)\Gamma(1+\epsilon)}{2(2\epsilon+1)}, \tag{2.46}
$$

$$
d_{vs}=\alpha_s^2\Big(\frac{\mu}{m}\Big)^{2\epsilon}\frac{e^{\gamma_E\epsilon}(-2\epsilon+3)(C_A(\epsilon(2\epsilon+1)(4\epsilon+3)+5)-8C_F(1+\epsilon)(2\epsilon^2+\epsilon+1))\Gamma(\epsilon)}{4(2\epsilon-1)(2\epsilon+1)(2\epsilon+3)}, \tag{2.47}
$$

$$
d_{vv}=\alpha_s^2\Big(\frac{\mu}{m}\Big)^{2\epsilon}\frac{e^{\gamma_E\epsilon}(\epsilon-1)(C_A+4C_A\epsilon-8C_F\epsilon)\Gamma(\epsilon)}{4(2\epsilon+1)}. \tag{2.48}
$$

The finite part of these coefficients agree with the result for the "unequal mass" case in [52].

2.3.4 Matching of currents

To get the two point function, the electromagnetic heavy quark currents $j_\mu^{(v)}$ and $j_\mu^{(a)}$ are needed in the effective theory. This contribution comes from the diagrams where the hard

loop connects to one of the external currents. For the vector current, the contribution comes from matching the $t\bar{t}\gamma$ vertex from NRQCD to QCD. For the axial vector current the matching to the $t\bar{t}Z$ vertex has to be calculated. The matching will be done by expansion of the current for small velocities v:

$$j_\mu^{(v)} = \bar{v}(-\mathbf{p})\gamma_\mu u(\mathbf{p}), \tag{2.49}$$

$$j_\mu^{(a)} = \bar{v}(-\mathbf{p})\gamma_\mu\gamma_5 u(\mathbf{p}). \tag{2.50}$$

First the vector current is considered. Using the definitions from equation (2.8), the time-like components of the vector current vanish and the spatial components contain the following operators [53]:

$$O_1 = \psi^\dagger\sigma^i\chi\,, \tag{2.51}$$

$$O_2 = \frac{1}{4m^2}\psi^\dagger\mathbf{D}\cdot\boldsymbol{\sigma}\,D^i\chi\,, \tag{2.52}$$

$$O_3 = \frac{1}{2m^2}\psi^\dagger\sigma^i\,\mathbf{D^2}\chi\,. \tag{2.53}$$

The operators O_2 and O_3 are already of order v^2, so only single insertions are needed. So, the spin projection to the triplet state, given as $A_{triplet} = \sigma^i_{\nu\xi}A_{\mu\nu,\xi\zeta}\sigma^i_{\mu\zeta}/(\sigma^i_{\nu\xi}\sigma^i_{\xi\nu})$ can be applied:

$$j_i^{(v)} = c_v\,\psi^\dagger\sigma^i\chi + \frac{d_v}{6m^2}\psi^\dagger\sigma_i\,\mathbf{D^2}\chi + O(1/m^4), \tag{2.54}$$

where the hard matching coefficients c_v and d_v have expansions $X_v = 1 + \sum_n X_v^{(n)}(\alpha_s/4\pi)^n$.

At NNNLO, the short-distance coefficient c_v is needed up to third order. Second-order corrections are given in [54, 55], the third-order corrections are not completed. Only the logarithmic part [33, 34] and the terms related to n_f are known [37]:

$$c_v^{(1)}(\mu) = -8C_F, \tag{2.55}$$

$$\begin{aligned} c_v^{(2)}(\mu) = {} & -2\pi^2 L_m\Big(4C_AC_F + \frac{8}{3}C_F^2 + \frac{\beta_0}{\pi^2}c_v^{(1)}\Big) + 16\bigg[\Big(\frac{23}{8} - \frac{79\pi^2}{36} + \pi^2\ln 2 - \frac{1}{2}\zeta(3)\Big)C_F^2 \\ & + \Big(-\frac{151}{72} + \frac{89\pi^2}{144} - \frac{5\pi^2}{6}\ln 2 - \frac{13}{4}\zeta(3)\Big)C_AC_F + \Big(\frac{22}{9} - \frac{2\pi^2}{9}\Big)C_FT_F + \frac{11}{18}C_FT_Fn_f\bigg], \end{aligned} \tag{2.56}$$

$$\begin{aligned} c_v^{(3)}(\mu) = {} & 4\pi^2L_m^2\bigg[-10C_F^3 - 15C_AC_F^2 - 4C_A^2C_F + \frac{8}{3}\beta_0C_F^2 + 4\beta_0C_AC_F - c_v^{(1)}\frac{\beta_0^2}{\pi^2}\bigg] \\ & + 32\pi^2L_m\bigg[C_F^3\Big(6\ln 2 - \frac{9}{4}\Big) - C_A^2C_F\Big(3\ln 2 + \frac{65}{36}\Big) - C_AC_F^2\Big(3\ln 2 + \frac{70}{27}\Big) \\ & - \frac{C_F^2T_F}{5} + \frac{49}{36}C_AC_Fn_fT_F + \frac{29}{27}C_F^2n_fT_F + \frac{C_AC_F\beta_0}{4} + \frac{C_F^2\beta_0}{9} + c_v^{(2)}\frac{\beta_0}{8\pi^2} + c_v^{(1)}\frac{\beta_1}{16\pi^2}\bigg] \\ & + 64n_fT_FC_F\bigg[46.7\,C_F + 39.6\,C_A + \Big(-\frac{557}{162} + \frac{26\pi^2}{81}\Big)T_F - \Big(\frac{163}{162} + \frac{4\pi^2}{27}\Big)n_fT_F\bigg] \\ & + c_{v,\not{n}_f}^{(3)}, \end{aligned} \tag{2.57}$$

where $L_m = \ln(\mu/m)$ and $c^{(3)}_{v,\not{n}_f}$ is the non-logarithmic part of $c^{(3)}_v$ not related to n_f.

For the derivative current d_v only the first-order corrections are relevant because these contribution is already of order v^2. They have been calculated in [53]. The result reads:

$$d^{(1)}_v(\mu) = -C_F \left[32 L_m + \frac{16}{3}\right]. \tag{2.58}$$

The scale dependence in the matching coefficients comes from the separation of the hard scale. It has to cancel against the hard scale dependence in the remaining parts. This has been checked explicitly. Note that the divergent part of $d^{(1)}_v$ has been dropped in (2.58) and will be added back to the ultrasoft part in equation (2.120).

Contributions from the axial vector current start at NNLO, so the matching at one-loop level is needed. Using equations (2.49) and (2.8) the time and space components of the axial vector current are:

$$j^{(a)}_0 = c_a \psi^\dagger \chi + O(1/m^2), \tag{2.59}$$

$$j^{(a)}_i = \frac{c_a}{2m} \psi^\dagger [\sigma_i, \mathbf{D}\cdot\boldsymbol{\sigma}] \chi + O(1/m^3). \tag{2.60}$$

Note, that in contrast to the vector current, here the time component does not vanish. The coefficient c_a is known up to two-loops [56]. However, here only the one-loop result is needed, because the axial vector contribution starts at second order. Using the same notation as for the vector current ($c_a = 1 + \sum_n c^{(n)}_a (\alpha_s/4\pi)^n$), the result reads:

$$c^{(1)}_a = -4 C_F \,. \tag{2.61}$$

Now, all relevant components for the hard matching are introduced, and the next step can be performed.

2.4 Potential NRQCD

In a second step the soft region and potential light fields (gluons and light quarks) are integrated out. This results in the potential NRQCD (PNRQCD) [57–60] with the Lagrangian

$$\begin{aligned}\mathcal{L}_{PNRQCD} = {} & \psi^\dagger \Big(i\partial_0 + \frac{\boldsymbol{\partial}^2}{2m} + \frac{\boldsymbol{\partial}^4}{8m^3} \Big) \psi + \chi^\dagger \Big(i\partial_0 - \frac{\boldsymbol{\partial}^2}{2m} - \frac{\boldsymbol{\partial}^4}{8m^3} \Big) \chi \\ & + \int d^{d-1}\mathbf{r} \left[\psi^\dagger_a \psi_b\right](x+\mathbf{r})\, V_{ab;cd}(r, \boldsymbol{\partial}) \left[\chi^\dagger_c \chi_d\right](x) \\ & - g_s \psi^\dagger(x) \boldsymbol{x}\boldsymbol{E}(t,\mathbf{0}) \psi(x) - g_s \chi^\dagger(x) \boldsymbol{x}\boldsymbol{E}(t,\mathbf{0}) \chi(x),\end{aligned} \tag{2.62}$$

where

$$V_{ab;cd}(r, \boldsymbol{\partial}) = T^A_{ab} T^A_{cd} V_0(r) + \delta V_{ab;cd}(r, \boldsymbol{\partial}).$$

The PNRQCD Lagrangian consists of a kinetic part (first line; including the relativistic corrections proportional to $\boldsymbol{\partial}^4/m^3$), a potential part (second line) and an ultrasoft part. The potentials are the Wilson coefficients from the matching to NRQCD, so from integrating out the soft modes. To separate the soft and ultrasoft gluon a multipole expansion [61] of the gluon interaction terms has been performed. This expansion about the center of mass coordinate $\mathbf{x}$ gives a contribution to the instantaneous potentials V (from soft gluons) and a higher-order term proportional to $\mathbf{x}$ which is the ultrasoft contribution and is given in the last line of equation (2.62).

For the potentials, the colour projection to the singlet state will be used in the following. This is the only relevant contribution for the top quark pair production, because the external current is a colour singlet. The singlet projection

$$\delta_{bc}\delta_{ad}V_{ab;cd}(r,\boldsymbol{\partial})$$

gives $\delta_{bc}\delta_{ad}1_{ab}1_{cd}=1$ and $\delta_{bc}\delta_{ad}T^A_{ab}T^A_{cd}=C_F$ for the different colour parts of the potential.

2.4.1 The S-wave Coulomb Green function

In this section, the relevant PNRQCD Feynman rules for the S-wave case will be explained. The P-wave contribution will be considered later.

In the center of mass system, the two particle propagator can be identified with the solution of the equation of motion, which is the non-relativistic Schrödinger equation:

$$\Big[-\frac{\boldsymbol{\partial}^2}{m}-\frac{\boldsymbol{\partial}^4}{4m^3}+V_{ab;cd}(r,\boldsymbol{\partial})\Big]G(\mathbf{x},\mathbf{x}+\mathbf{r},E)=\delta^{(3)}(\mathbf{r})\,, \tag{2.63}$$

where $G(\mathbf{x},\mathbf{x}+\mathbf{r},E)$ is the S-wave coordinate space Green function with its Fourier transform $G(\mathbf{p_1},\mathbf{p_2},E)$. The potential $V_{ab;cd}(r,\boldsymbol{\partial})$ can be interpreted as an instantaneous heavy quark potential.

At leading order, the Green function is given by the solution of the Schrödinger equation with a Coulomb potential. This will be called the Coulomb Green function $\tilde{G}_C(\mathbf{p}_3,\mathbf{p}_4;E)$. Diagrammatically, all Coulomb gluons are summed up in this Green function (since all exchanges are of leading order). Some useful representations are given in appendix A.

At higher order one can apply time independent perturbation theory to take into account the effect of higher-order potentials. This leads to integrals of the following form:

$$\int\prod_i\left(\frac{d^{d-1}\mathbf{p}_i}{(2\pi)^{d-1}}\right)\tilde{G}_C(\mathbf{p}_1,\mathbf{p}_2;E)\delta\widetilde{V}(\mathbf{p_2},\mathbf{p_3})\tilde{G}_C(\mathbf{p}_3,\mathbf{p}_4;E)\,, \tag{2.64}$$

where $\delta\widetilde{V}(\mathbf{p_2},\mathbf{p_3})$ is the Fourier transformed potential $\delta V(r,\boldsymbol{\partial})$. Here, the time integration has been done, so the remaining integral measure has is of order $d-1$. It is common to call

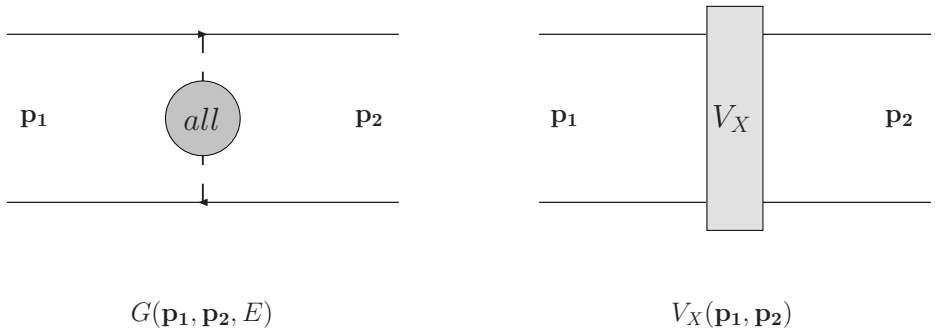

Figure 2.7: PNRQCD Feynman rules.

these corrections insertions of potentials and a diagrammatic form of Feynman diagrams is shown in figure 2.7.

The leading-order contribution comes from diagrams where no potentials are inserted. The result in the $\overline{MS}$-scheme is well known, and the details of the calculation are not given here. The result is:

$$G_C^{\overline{MS}}(0,0,E) = \frac{m^2\alpha_s C_F}{4\pi}\Big(-\frac{1}{2}\ln\frac{-4mE}{\mu^2} + \frac{1}{2} - \frac{\sqrt{-mE}}{mC_F\alpha_S} - \gamma_E - \Psi(1+\frac{mC_F\alpha_S}{2\sqrt{-mE}})\Big). \quad (2.65)$$

Note, that near the bound-state energy $E \to E_n$, the Green function has poles coming from the Ψ-function and is

$$G(E) \stackrel{E\to E_n}{=} \frac{|\Psi_n(0)|^2}{E_n - E - i\epsilon}. \quad (2.66)$$

So, in this region, the Green function is dominated by the energy levels (the pole position) and wave functions (the height of the pole). It is useful to introduce a variable λ, which is defined analogous to the quantum number n in the leading-order energy level:

$$E = -\frac{mC_F^2\alpha_s^2}{4\lambda^2}. \quad (2.67)$$

So, the Coulomb bound state poles are found at integer values of λ, and the absolute value of λ is of order 1 or larger in the threshold region.

2.4.2 Potentials

In this section, the corrections to the leading-order potential $\widetilde{V}(\mathbf{p},\mathbf{p}')$ are given, when available in the literature. For the one-loop coefficients the results for the order ϵ terms obtained in the previous sections are presented. The potential will be cast in the following general form:

$$\widetilde{V}(\mathbf{p},\mathbf{p}') = -\mathcal{V}_C(\alpha_s)\frac{4\pi C_F\alpha_s}{\mathbf{q}^2} + \mathcal{V}_{1/m}(\alpha_s)\frac{(4\pi)\pi^2 C_F\alpha_s}{m|\mathbf{q}|} + \mathcal{V}_\delta(\alpha_s)\frac{2\pi C_F\alpha_s}{m^2} \quad (2.68)$$

$$-\mathcal{V}_p(\alpha_s)\frac{2\pi C_F\alpha_s(\mathbf{p}^2+\mathbf{p}'^2)}{m^2\mathbf{q}^2}-\mathcal{V}_{so}(\alpha_s)\frac{3\pi C_F\alpha_s}{2m^2\mathbf{q}^2}\Big([\sigma_i,\sigma_j]q_ip_j\otimes 1-1\otimes[\sigma_i,\sigma_j]q_ip_j\Big)$$
$$+\mathcal{V}_{hf}(\alpha_s)\frac{\pi C_F\alpha_s}{4m^2\mathbf{q}^2}[\sigma_i,\sigma_j]q_j\otimes[\sigma_i,\sigma_k]q_k-\mathcal{V}_s(\alpha_s)\frac{\pi C_F\alpha_s}{4m^2}[\sigma_i,\sigma_j]\otimes[\sigma_i,\sigma_j].$$

The coefficients $\mathcal{V}_X$ of the potentials are α_s dependent:

$$\mathcal{V}_i(\alpha_s)=\mathcal{V}_i^{(0)}+\frac{\alpha_s}{4\pi}\mathcal{V}_i^{(1)}+\left(\frac{\alpha_s}{4\pi}\right)^2\mathcal{V}_i^{(2)}+\mathcal{O}(\alpha_s^3). \tag{2.69}$$

So, one can see that the corrections to leading order are an expansion in α_s and v (the momenta are of order mv). Here, a notation has been used which is valid in d dimensions and the use of vector products or the totally antisymmetric ϵ tensor has been avoided. The factors of the potentials are chosen in such a way that the leading-order coefficients are either one or zero. The calculation of the coefficients $\mathcal{V}_C^{(3)}$, $\mathcal{V}_{1/m}^{(2)}$, $\mathcal{V}_{1/m^2}^{(1)}$ and $\mathcal{V}_p^{(1)}$ results in infrared (IR) divergences [62, 63]. These divergences have been subtracted in the given results. They are added back to the ultrasoft calculation (see section 2.4.3). The subtracted potential is:

$$\delta\widetilde{V}_{c.t.}=-\frac{\alpha_sC_F}{6\epsilon}\Bigg[C_A^3\frac{\alpha_s^3}{\mathbf{q}^2}+4\left(C_A^2+2C_AC_F\right)\frac{\pi\alpha_s^2}{m|\mathbf{q}|}$$
$$+16\left(C_F-\frac{C_A}{2}\right)\frac{\alpha_s}{m^2}+16C_A\frac{\alpha_s}{m^2}\frac{(\mathbf{p^2}+\mathbf{p'^2})}{2\mathbf{q^2}}\Bigg]. \tag{2.70}$$

Now, the results for these coefficients will be presented, starting with the Coulomb potential which is needed up to three-loop order. The coefficients of the $1/m$ potential is then needed up to two-loop and the $1/m^2$ potential up to one-loop order.

Note, that not only higher order of the potential terms are needed for the calculation, but also relativistic corrections to the kinetic energy term ($\pm\boldsymbol{\partial}^4/(8m^3)$ in equation (2.62)), which are treated as an insertion to the Coulomb Green function, too. The corresponding potential from is given by

$$V_{kin}=-\frac{\mathbf{p^4}}{4m^3}(2\pi)^{d-1}\delta^{(d-1)}(\mathbf{p}-\mathbf{p}'). \tag{2.71}$$

The Coulomb potential The coefficients of order $O(1/m^0)$ are the Coulomb potential coefficients and known up to two-loop order. The one-loop coefficient will be given with the full ϵ dependence. The higher-order parts are presented in an expanded form omitting the non-finite orders. This can be done, because insertions of these potentials are always finite. So, the expansion of the potential can be done before the momentum integration. The result for the Coulomb part reads:

$$\mathcal{V}_C^{(0)}=1, \tag{2.72}$$
$$\mathcal{V}_C^{(1)}=\left[\left(\frac{\mu^2}{\mathbf{q^2}}\right)^\epsilon-1\right]\frac{\beta_0}{\epsilon}+\left(\frac{\mu^2}{\mathbf{q^2}}\right)^\epsilon a_1(\epsilon), \tag{2.73}$$

$$\mathcal{V}_C^{(2)} = a_2 + (2a_1\beta_0 + \beta_1)\ln\frac{\mu^2}{\mathbf{q^2}} + \beta_0^2\ln^2\frac{\mu^2}{\mathbf{q^2}}, \tag{2.74}$$

$$\begin{aligned}\mathcal{V}_C^{(3)} = {} & a_3 + \left(2a_1\beta_1 + \beta_2 + 3a_2\beta_0 + 8\pi^2 C_A^3\right)\ln\frac{\mu^2}{\mathbf{q^2}} \\ & + \left(\frac{5}{2}\beta_0\beta_1 + 3a_1\beta_0^2\right)\ln^2\frac{\mu^2}{\mathbf{q^2}} + \beta_0^3\ln^3\frac{\mu^2}{\mathbf{q^2}},\end{aligned} \tag{2.75}$$

with

$$a_1(\epsilon) = \left(C_A\left[11 - 8\epsilon\right] - 4\,T_F n_f\right)\frac{e^{\gamma_E\epsilon}\,\Gamma(1-\epsilon)\,\Gamma(2-\epsilon)\,\Gamma(\epsilon)}{(3-2\,\epsilon)\,\Gamma(2-2\,\epsilon)} - \frac{\beta_0}{\epsilon}, \tag{2.76}$$

$$a_2 = \left(\frac{4343}{162} + 4\pi - \frac{\pi^2}{4} + \frac{22}{3}\zeta_3\right)C_A^2 - \left(\frac{1798}{81} + \frac{56}{3}\zeta_3\right)C_A T_F n_l, \tag{2.77}$$

where $a_1 = a_1(\epsilon)$ is known since some time [64,65] and the d-dimensional expression for $a_1(\epsilon)$ is first shown in [66]. a_2 has been calculated in [67–69]. The three-loop coefficient a_3 is not known analytically, but a Padé estimate is available [70]:

$$\frac{a_3}{4^3} = \begin{cases} 142 \text{ for } n_l = 3 \\ 97.5 \text{ for } n_l = 4 \\ 60.1 \text{ for } n_l = 5 \end{cases}. \tag{2.78}$$

The β_i are the coefficients of the QCD β-function and are given in [71]:

$$\beta_0 = \frac{11}{3}C_A - \frac{4}{3}T_F n_l, \tag{2.79}$$

$$\beta_1 = \frac{34}{3}C_A^2 - \frac{20}{3}C_A T_F n_l - 4C_F T_F n_l, \tag{2.80}$$

$$\begin{aligned}\beta_2 = {} & \frac{2857}{54}C_A^3 - \frac{1415}{27}C_A^2 T_F n_l - \frac{205}{9}C_A C_F T_F n_l + 2C_F^2 T_F n_l \\ & + \frac{158}{27}C_A T_F^2 n_l^2 + \frac{44}{9}C_F T_F^2 n_l^2.\end{aligned} \tag{2.81}$$

Parts of the NNNNLO Coulomb potential are also known [72], but not needed for this calculation.

The insertions of Coulomb potentials are finite, so only the finite parts of the potential coefficients are needed, as long as only Coulomb insertions are taken into account. However, at third order also the double insertion of a Coulomb potential together with a (singular insertion of a) non-Coulomb potential has to be taken into account, so the order ϵ^1 parts of the Coulomb potential multiplies a divergent quantity and therefore contributes to the final result. The coefficient $\mathcal{V}_C^{(1)}$ is given with the full ϵ dependence.

As explained at the beginning of this section, the third-order Coulomb potential has an IR divergence [73], which has to cancel against a similar part from the ultrasoft calculation. The corresponding $1/\epsilon$ part is subtracted and does therefore not appear in 2.72, but the logarithmic part multiplied by C_A comes from this divergence.

The $1/m$ potential The coefficients of the order $O(1/m^1)$ potential are known up to two-loops and order ϵ^0. But since the insertion of these potential is divergent, the order ϵ^1 part of the coefficient contributes to the final part of the cross section. For the one-loop coefficient also the ϵ^2 is needed, since the corresponding divergence of the insertion has a higher power. The one-loop coefficient is known exactly, but the order ϵ^1 part of the two-loop coefficient is unknown and will be parameterized as $b_2^{(\epsilon)}$ in the following:

$$\mathcal{V}_{1/m}^{(0)} = 0, \tag{2.82}$$

$$\mathcal{V}_{1/m}^{(1)} = \left(\frac{\mu^2}{\mathbf{q^2}}\right)^{\epsilon} b_1(\epsilon), \tag{2.83}$$

$$\begin{aligned}\mathcal{V}_{1/m}^{(2)} = &\left[\left(\frac{\mu^2}{\mathbf{q^2}}\right)^{2\epsilon} - 1\right]\left(-\frac{8}{3\epsilon}\right)\left(2C_F C_A + C_A^2\right) \\ &+ \left[\left(\frac{\mu^2}{\mathbf{q^2}}\right)^{2\epsilon} - \left(\frac{\mu^2}{\mathbf{q^2}}\right)^{\epsilon}\right]\frac{2\beta_0}{\epsilon}\, b_1(\epsilon) + \left(\frac{\mu^2}{\mathbf{q^2}}\right)^{2\epsilon} 4b_2(\epsilon),\end{aligned} \tag{2.84}$$

with

$$b_1(\epsilon) = \left(\frac{C_F}{2}\left[1-2\epsilon\right] - C_A\left[1-\epsilon\right]\right)\frac{e^{\gamma_E \epsilon}\,\Gamma(\frac{1}{2}-\epsilon)^2\Gamma(\frac{1}{2}+\epsilon)}{\pi^{\frac{3}{2}}\,\Gamma(1-2\epsilon)}, \tag{2.85}$$

$$\begin{aligned}b_2(\epsilon) = &\left[\frac{65}{18} - \frac{8}{3}\ln 2\right] C_A C_F - \left[\frac{101}{36} + \frac{4}{3}\ln 2\right] C_A^2 \\ &+ \left[\frac{49}{36}\, C_A - \frac{2}{9} C_F\right] T_F n_f + \epsilon\, b_2^{(\epsilon)} + O(\epsilon^2),\end{aligned} \tag{2.86}$$

where $b_1(\epsilon)$ is taken from [21] and $b_2(\epsilon = 0)$ from [74]. Note that here the IR divergent part has again been subtracted, and will be added back to the ultrasoft result later.

The $1/m^2$ potential The coefficients of the order $O(1/m^2)$ potentials are known up to one-loop and order ϵ^0. The tree level result is known exactly:

$$\mathcal{V}_{\delta}^{(0)} = 1, \quad \mathcal{V}_{p}^{(0)} = 1, \quad \mathcal{V}_{so}^{(0)} = 1, \quad \mathcal{V}_{hf}^{(0)} = 1, \quad \mathcal{V}_{s}^{(0)} = 0. \tag{2.87}$$

At one-loop order, the result is needed again including the order ϵ^1 parts. In this section the exact form of the $O(1/m^2)$ potential in terms of ϵ is calculated (at one-loop). The relevant NRQCD diagrams for the matching calculation are given in figure 2.8 and 2.9. For the tree level parts the contribution at this order comes from higher-order matching coefficients and will be therefore called "hard". In the loop diagrams the soft and potential modes have to be integrated out. These contributions will be called "soft". The total contribution to the potentials is then $\mathcal{V}_X(\alpha_s) = \mathcal{V}_X^{(hard)}(\alpha_s) + \mathcal{V}_X^{(soft)}(\alpha_s)$. This potential is spin dependent. A projection to the triplet state will be done later. The IR divergence will be subtracted again, but after the spin projection. This is a useful convention here, because then after the spin

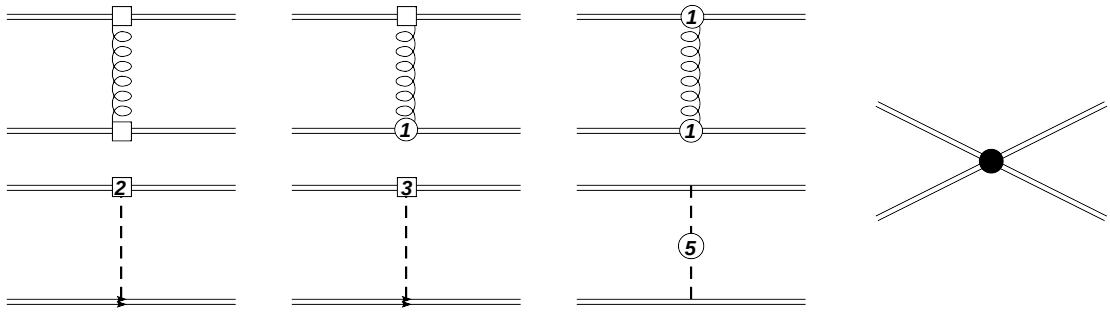

Figure 2.8: NRQCD tree level diagrams of order $1/m^2$.

projection, which is done in d dimensions, the counter term potential is purely divergent. If the IR divergence was subtracted from the beginning, the spin projection would introduce a finite contribution to the counter term.

The hard one-loop contributions can be easily calculated with the Feynman rules presented in figure 2.3, since all NRQCD matching coefficients are known exactly at one-loop order from the previous section. The result reads:

$$\mathcal{V}_\delta^{(hard)}(\alpha_s) = \frac{1}{2}(1+d_2-16d_5) + \frac{1}{2\pi C_F\alpha_s}(d_{ss}+C_F d_{vs}) + O(\alpha_s^2) \tag{2.88}$$

$$\begin{aligned} &= 1 + \frac{\alpha_s}{\pi}\left(\frac{\mu^2}{m^2}e^{\gamma_E}\right)^\epsilon \Gamma(\epsilon)\Big[C_A\frac{12\epsilon^3-44\epsilon^2+21\epsilon-13}{-96\epsilon^2+24} \\ &+ C_F\frac{12\epsilon^4-32\epsilon^3-63\epsilon^2-4\epsilon+3}{6(2\epsilon-1)(2\epsilon+1)(2\epsilon+3)} - \frac{2T_F}{15}\epsilon\Big] + O(\alpha_s^2), \end{aligned} \tag{2.89}$$

$$\mathcal{V}_p^{(hard)}(\alpha_s) = 1 + O(\alpha_s^2), \tag{2.90}$$

$$\mathcal{V}_{so}^{(hard)}(\alpha_s) = \frac{1}{3}(2d_1+d_3) + O(\alpha_s^2) \tag{2.91}$$

$$= 1 + \frac{\alpha_s}{\pi}\left(\frac{\mu^2}{m^2}e^{\gamma_E}\right)^\epsilon \Gamma(\epsilon)\Big[\frac{C_A(2\epsilon^2-1)-2C_F\epsilon(2\epsilon+1)}{6\epsilon-3}\Big] + O(\alpha_s^2),$$

$$\mathcal{V}_{hf}^{(hard)}(\alpha_s) = d_1^2 + O(\alpha_s^2) \tag{2.92}$$

$$= 1 + \frac{\alpha_s}{\pi}\left(\frac{\mu^2}{m^2}e^{\gamma_E}\right)^\epsilon \Gamma(\epsilon)\Big[\frac{C_A(2\epsilon^2-1)-2C_F\epsilon(2\epsilon+1)}{4\epsilon-2}\Big] + O(\alpha_s^2),$$

$$\mathcal{V}_s^{(hard)}(\alpha_s) = \frac{1}{(d-2)\pi C_F\alpha_s}(d_{sv}+C_F d_{vv}) + O(\alpha_s^2) \tag{2.93}$$

$$= \frac{\alpha_s}{\pi}\left(\frac{\mu^2}{m^2}e^{\gamma_E}\right)^\epsilon \Gamma(\epsilon)\Big[-C_A + \frac{4\epsilon}{2\epsilon+1}C_F\Big] + O(\alpha_s^2)\,.$$

In this notation the tree level parts are included and come only from hard diagrams. The soft contributions come from diagrams presented in figure 2.9, from diagrams of order $1/m^0$, where the denominator has been expanded to higher orders and from self energy diagrams

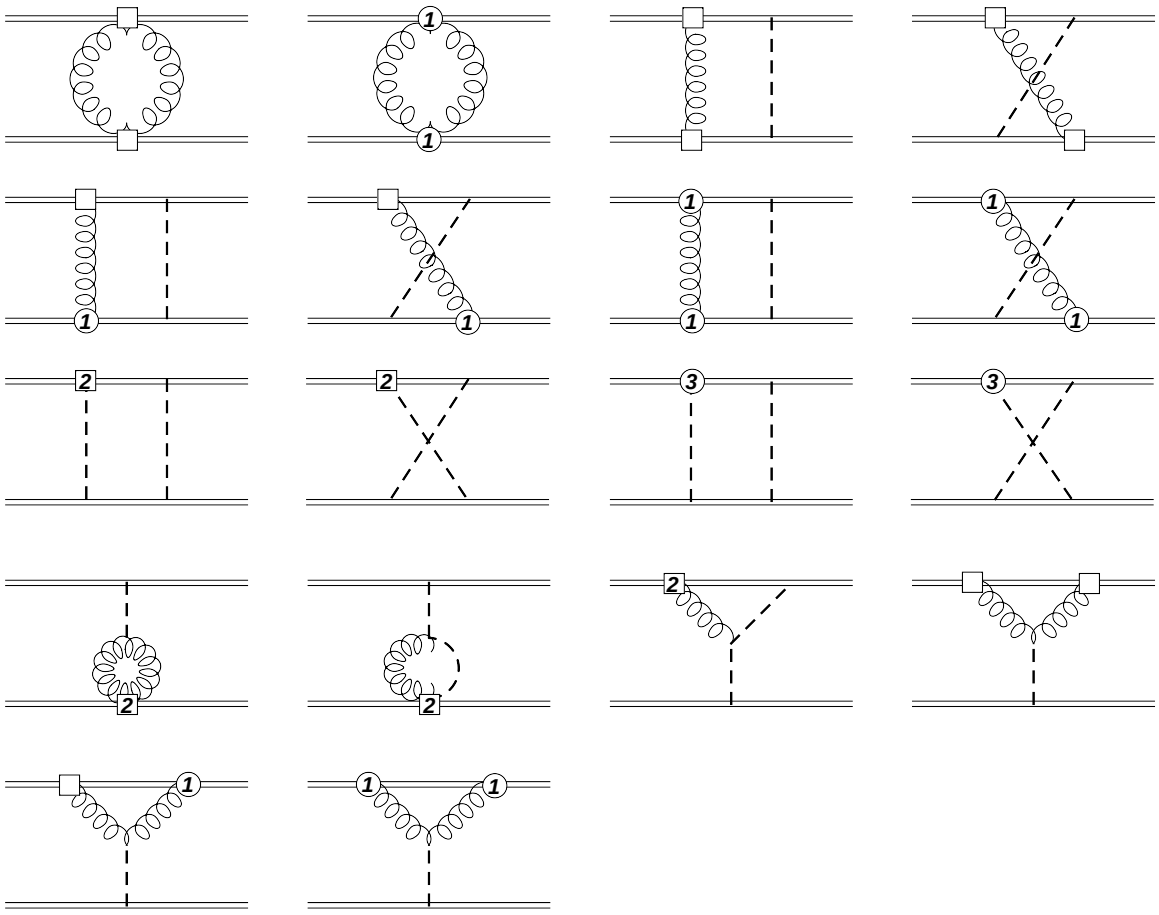

Figure 2.9: NRQCD one-loop diagrams of order $1/m^2$ (non-vanishing only, symmetric diagrams not included).

containing gluons and light quarks. The final result is:

$$\begin{aligned}\mathcal{V}_{\delta}^{(soft)}(\alpha_s) = \frac{\alpha_s}{4\pi}\Bigg[\left(\frac{\mu^2}{\mathbf{q}^2}\right)^{\epsilon}\frac{\epsilon\Gamma(-\epsilon)^2\Gamma(\epsilon)e^{\gamma_E\epsilon}}{12(4\epsilon^2-8\epsilon+3)\Gamma(-2\epsilon)}\Big(C_A(48\epsilon^3-230\epsilon^2+328\epsilon-138 \\ -3d_1^2(4\epsilon^2-9\epsilon+5))-4C_F(\epsilon-1)(16\epsilon^2-38\epsilon+21) \\ -12n_fT_F(\epsilon-1)(1+d_2)\Big)-\frac{d_2+1}{2}\frac{\beta_0}{\epsilon}\Bigg]+O(\alpha_s^2),\end{aligned} \tag{2.94}$$

$$\begin{aligned}\mathcal{V}_{p}^{(soft)}(\alpha_s) = \frac{\alpha_s}{4\pi}\Bigg[\left(\frac{\mu^2}{\mathbf{q}^2}\right)^{\epsilon}\frac{-\epsilon\Big(C_A(56\epsilon^2-121\epsilon+57)+12n_fT_F(\epsilon-1)\Big)\Gamma(-\epsilon)^2\Gamma(\epsilon)e^{\gamma_E\epsilon}}{6(4\epsilon^2-8\epsilon+3)\Gamma(-2\epsilon)} \\ -\frac{\beta_0}{\epsilon}\Bigg]+O(\alpha_s^2),\end{aligned} \tag{2.95}$$

$$\begin{aligned}\mathcal{V}_{so}^{(soft)}(\alpha_s) = \frac{\alpha_s}{4\pi}\Bigg[\left(\frac{\mu^2}{\mathbf{q}^2}\right)^{\epsilon}\frac{-\epsilon\Gamma(-\epsilon)^2\Gamma(\epsilon)e^{\gamma_E\epsilon}}{6(4\epsilon^2-8\epsilon+3)\Gamma(-2\epsilon)}\Big(C_A(d_3(8\epsilon^2-19\epsilon+11) \\ +2d_1(8\epsilon^2-15\epsilon+5))+4(2d_1+d_3)n_fT_F(\epsilon-1)\Big)-\frac{2d_1+d_3}{3}\frac{\beta_0}{\epsilon}\Bigg]\end{aligned}$$

$$+O(\alpha_s^2), \tag{2.96}$$

$$\mathcal{V}_{hf}^{(soft)}(\alpha_s) = \frac{\alpha_s}{4\pi}\left[\left(\frac{\mu^2}{\mathbf{q}^2}\right)^{\epsilon}\frac{-d_1^2\epsilon(\epsilon-1)\Big(C_A(4\epsilon-5)+4n_fT_F\Big)\Gamma(-\epsilon)^2\Gamma(\epsilon)e^{\gamma_E\epsilon}}{(8\epsilon^2-16\epsilon+6)\Gamma(-2\epsilon)} - d_1^2\frac{\beta_0}{\epsilon}\right]$$
$$+O(\alpha_s^2), \tag{2.97}$$

$$\mathcal{V}_{s}^{(soft)}(\alpha_s) = \frac{\alpha_s}{4\pi}\left(\frac{\mu^2}{\mathbf{q}^2}\right)^{\epsilon}\frac{d_1^2C_A\epsilon\Gamma(-\epsilon)^2\Gamma(\epsilon)e^{\gamma_E\epsilon}}{(8\epsilon-4)\Gamma(-2\epsilon)} + O(\alpha_s^2), \tag{2.98}$$

where the d_i can be put to one, since these parts are already of order α_s. An alternative way of calculating the soft corrections is by directly taking the soft limit to the QCD diagrams instead of the NRQCD diagrams. This calculation has also been performed and it has been checked that the results are exactly the same. Note that with the second method one cannot get the result in terms of the hard matching coefficients, but instead one gets the results given in (2.94) with $d_i = 1$.

Spin projection for S-waves The double insertion of the spin dependent potential is of higher order, so at NNNLO only single insertions of spin dependent potentials and double insertions of a Coulomb potential with spin dependent potentials have to be considered, but never the double insertion of two spin dependent potentials (this would be of forth order). Therefore, it is possible to take the spin projection to the singlet or triplet state directly in the potentials. For the process considered in this work, only the triplet contribution is relevant. The results for the spin projection to the spin triplet state are:

$$[\sigma_i,\sigma_j]q_ip_j\otimes 1 - 1\otimes[\sigma_i,\sigma_j]q_ip_j \to 0, \tag{2.99}$$

$$[\sigma_i,\sigma_j]q_j\otimes[\sigma_i,\sigma_k]q_k \to \frac{10-7d+d^2}{1-d}4\mathbf{q}^2, \tag{2.100}$$

$$[\sigma_i,\sigma_j]\otimes[\sigma_i,\sigma_j] \to -4(10-7d+d^2). \tag{2.101}$$

Now, these relations are applied to the potentials from equation (2.68). Then, the counter term for the $1/m^2$ potential is subtracted from equation (2.70) and one arrives at the result presented in [38]:

$$\widetilde{V}(\mathbf{p},\mathbf{p}') = -\frac{4\pi\alpha_sC_F}{\mathbf{q^2}}\Big[\,\mathcal{V}_C - \mathcal{V}_{1/m}\,\frac{\pi^2\,|\mathbf{q}|}{m} + \mathcal{V}_{1/m^2}\,\frac{\mathbf{q^2}}{m^2} + \mathcal{V}_p\,\frac{\mathbf{p^2}+\mathbf{p'^2}}{2m^2}\,\Big]. \tag{2.102}$$

with

$$\mathcal{V}_p^{(0)} = 1, \tag{2.103}$$

$$\mathcal{V}_{1/m^2}^{(0)} = v_0(\epsilon) = -\frac{4-\epsilon-2\,\epsilon^2}{6-4\epsilon}, \tag{2.104}$$

$$\mathcal{V}_p^{(1)} = \left[\left(\frac{\mu^2}{\mathbf{q^2}}\right)^{\epsilon}-1\right]\frac{1}{\epsilon}\left(\frac{8}{3}C_A+\beta_0\right) + \left(\frac{\mu^2}{\mathbf{q^2}}\right)^{\epsilon}v_p^{(1)}(\epsilon). \tag{2.105}$$

$$\mathcal{V}^{(1)}_{1/m^2} = \left[\left(\frac{\mu^2}{\mathbf{q^2}}\right)^{\epsilon} - 1\right]\frac{1}{\epsilon}\left(\frac{7}{3}C_F - \frac{11}{6}C_A + \beta_0\, v_0(\epsilon)\right) + \left[\left(\frac{\mu^2}{m^2}\right)^{\epsilon} - 1\right]\frac{1}{\epsilon}\left(\frac{C_F}{3} + \frac{C_A}{2}\right) + \left(\frac{\mu^2}{\mathbf{q^2}}\right)^{\epsilon} v_q^{(1)}(\epsilon) + \left(\frac{\mu^2}{m^2}\right)^{\epsilon} v_m^{(1)}(\epsilon). \quad (2.106)$$

The relevant coefficients (up to order ϵ) are:

$$v_q^{(1)}(\epsilon) = \left\{-\frac{C_F}{3} - \frac{11}{27}C_A + \frac{40}{27}T_F n_f\right\} + \epsilon\left\{\left(-\frac{419}{81} + \frac{77\pi^2}{216}\right)C_A + \left(2 - \frac{7\pi^2}{36}\right)C_F + \left(\frac{274}{81} - \frac{2\pi^2}{27}\right)T_F n_f\right\} + O(\epsilon^2), \quad (2.107)$$

$$v_m^{(1)}(\epsilon) = -\frac{C_F}{3} - \frac{29}{9}C_A + \frac{4}{15}T_F + \epsilon\left\{\left(\frac{379}{54} + \frac{\pi^2}{24}\right)C_A + \left(-10 + \frac{\pi^2}{36}\right)C_F\right\} + O(\epsilon^2), \quad (2.108)$$

$$v_p^{(1)}(\epsilon) = \frac{31}{9}C_A - \frac{20}{9}T_F n_f + \epsilon\left\{\left(\frac{188}{27} - \frac{19\pi^2}{36}\right)C_A + \left(-\frac{112}{27} + \frac{\pi^2}{9}\right)T_F n_f\right\} + O(\epsilon^2), \quad (2.109)$$

where $v_i^{(1)}(\epsilon = 0)$ for $i = \{q, m, p\}$ agree with those obtained from [62, 75], and the order ϵ agrees with [75].

Equation of motion After applying the spin projection, only six different types of insertions are left:

$$\frac{1}{\mathbf{q}^2}\left(\frac{\mu^2}{\mathbf{q}^2}\right)^{a\epsilon},\ \frac{1}{|\mathbf{q}|}\left(\frac{\mu^2}{\mathbf{q}^2}\right)^{a\epsilon},\ \left(\frac{\mu^2}{\mathbf{q}^2}\right)^{a\epsilon},\ \frac{\mathbf{p^2} + \mathbf{p'^2}}{2\mathbf{q}^2}\left(\frac{\mu^2}{\mathbf{q}^2}\right)^{a\epsilon},\ \mathbf{p^4}\delta^{(\mathbf{3})}(\mathbf{q}),\ \mathbf{p^2}\delta^{(\mathbf{3})}(\mathbf{q}), \quad (2.110)$$

where the first four come from the potentials in equation (2.102), the fifth is the kinetic correction and the last one might be used for the threshold mass implementation (not used in the calculation here, see section 3.6 for more details), and is given here for completeness. The last three can be reduced by using the equation of motion to the first three and an additional delta potential. At third order, both, single and double insertions with Coulomb potentials have to be considered. The equation of motion

$$\frac{\mathbf{p}_2^2}{m^2}G_C(\mathbf{p}_1, \mathbf{p_2}) = \frac{E}{m}G_C(\mathbf{p}_1, \mathbf{p}_2) + \frac{(2\pi)^{d-1}}{m}\delta^{(d-1)}(\mathbf{p}_1 - \mathbf{p}_2) + \frac{4\pi C_F \alpha_s}{m}\int \frac{d^{d-1}\mathbf{k}}{(2\pi)^{d-1}}\frac{G_C(\mathbf{p}_1, \mathbf{k})}{(\mathbf{k} - \mathbf{p}_2)^2}, \quad (2.111)$$

is then applied, and the result for the single insertions (with $\mathbf{q} = \mathbf{p}_3 - \mathbf{p}_2$) is:

$$\delta^{d-1}(\mathbf{q})\frac{\mathbf{p}_2^2}{m}: \quad \int \prod_{i=1}^{4}\frac{d^{d-1}\mathbf{p}_i}{(2\pi)^{d-1}}G_C(\mathbf{p}_1, \mathbf{p}_2)(2\pi)^{d-1}\delta^{d-1}(\mathbf{q})\frac{\mathbf{p}_2^2}{m}G_C(\mathbf{p}_3, \mathbf{p}_4)$$
$$= E\int \prod_{i=1}^{3}\frac{d^{d-1}\mathbf{p}_i}{(2\pi)^{d-1}}G_C(\mathbf{p}_1, \mathbf{p}_2)G_C(\mathbf{p}_2, \mathbf{p}_3) + \int \prod_{i=1}^{2}\frac{d^{d-1}\mathbf{p}_i}{(2\pi)^{d-1}}G_C(\mathbf{p}_1, \mathbf{p}_2)$$

$$+ 4\pi C_F\alpha_s \int \prod_{i=1}^{4} \frac{d^{d-1}\mathbf{p}_i}{(2\pi)^{d-1}} G_C(\mathbf{p}_1,\mathbf{p}_2)\frac{1}{\mathbf{q}^2}G_C(\mathbf{p}_3,\mathbf{p}_4), \tag{2.112}$$

$$\begin{aligned}
\delta^{d-1}(\mathbf{q})\frac{\mathbf{p}_2^4}{m^3}: \quad & \int \prod_{i=1}^{4} \frac{d^{d-1}\mathbf{p}_i}{(2\pi)^{d-1}} G_C(\mathbf{p}_1,\mathbf{p}_2)(2\pi)^{d-1}\delta^{d-1}(\mathbf{q})\frac{\mathbf{p}_2^4}{m^3}G_C(\mathbf{p}_3,\mathbf{p}_4) \\
&= \frac{E^2}{m}\int \prod_{i=1}^{3} \frac{d^{d-1}\mathbf{p}_i}{(2\pi)^{d-1}} G_C(\mathbf{p}_1,\mathbf{p}_2)G_C(\mathbf{p}_2,\mathbf{p}_3) + \frac{2E}{m}\int \prod_{i=1}^{2} \frac{d^{d-1}\mathbf{p}_i}{(2\pi)^{d-1}} G_C(\mathbf{p}_1,\mathbf{p}_2) \\
&+ \frac{8\pi C_F\alpha_s E}{m}\int \prod_{i=1}^{4} \frac{d^{d-1}\mathbf{p}_i}{(2\pi)^{d-1}} G_C(\mathbf{p}_1,\mathbf{p}_2)\frac{1}{\mathbf{q}^2}G_C(\mathbf{p}_3,\mathbf{p}_4) \\
&+ \frac{(4\pi C_F\alpha_s)^2}{m}\int \prod_{i=1}^{4} \frac{d^{d-1}\mathbf{p}_i}{(2\pi)^{d-1}} G_C(\mathbf{p}_1,\mathbf{p}_2)\frac{1}{[\mathbf{q}^2]^{\frac{1}{2}+\epsilon}}\frac{k(0)}{8}G_C(\mathbf{p}_3,\mathbf{p}_4),
\end{aligned} \tag{2.113}$$

$$\begin{aligned}
\frac{\mathbf{p}_2^2+\mathbf{p}_3^2}{2m^2\mathbf{q}^2}: \quad & \int \prod_{i=1}^{4} \frac{d^{d-1}\mathbf{p}_i}{(2\pi)^{d-1}} G_C(\mathbf{p}_1,\mathbf{p}_2)\frac{\mathbf{p}_2^2+\mathbf{p}_3^2}{2m^2\mathbf{q}^2}G_C(\mathbf{p}_3,\mathbf{p}_4) \\
&= \int \prod_{i=1}^{4} \frac{d^{d-1}\mathbf{p}_i}{(2\pi)^{d-1}} G_C(\mathbf{p}_1,\mathbf{p}_2)\left[\frac{E}{m}\frac{1}{\mathbf{q}^2} + \frac{4\pi C_F\alpha_s}{m}\frac{1}{[\mathbf{q}^2]^{\frac{1}{2}+\epsilon}}\frac{k(0)}{8}\right]G_C(\mathbf{p}_3,\mathbf{p}_4).
\end{aligned} \tag{2.114}$$

The result for the double insertions with a Coulomb potential (with $\mathbf{q_1} = \mathbf{p}_3 - \mathbf{p}_2$ and $\mathbf{q_2} = \mathbf{p}_5 - \mathbf{p}_4$) reads:

$$\begin{aligned}
\delta^{d-1}(\mathbf{q_1})\frac{\mathbf{p}_2^2}{m}: \quad & \int \prod_{i=1}^{6} \frac{d^{d-1}\mathbf{p}_i}{(2\pi)^{d-1}} G_C(\mathbf{p}_1,\mathbf{p}_2)(2\pi)^{d-1}\delta^{d-1}(\mathbf{q_1})\frac{\mathbf{p}_2^2}{m}\frac{G_C(\mathbf{p}_3,\mathbf{p}_4)G_C(\mathbf{p}_5,\mathbf{p}_6)}{[\mathbf{q_2}^2]^{u+1}} \\
&= E\int \prod_{i=1}^{5} \frac{d^{d-1}\mathbf{p}_i}{(2\pi)^{d-1}} \frac{G_C(\mathbf{p}_1,\mathbf{p}_2)G_C(\mathbf{p}_2,\mathbf{p}_3)G_C(\mathbf{p}_4,\mathbf{p}_5)}{[(\mathbf{p}_4-\mathbf{p}_3)^2]^{u+1}} \\
&+ \int \prod_{i=1}^{4} \frac{d^{d-1}\mathbf{p}_i}{(2\pi)^{d-1}} \frac{G_C(\mathbf{p}_1,\mathbf{p}_2)G_C(\mathbf{p}_3,\mathbf{p}_4)}{[\mathbf{q_1}^2]^{u+1}} \\
&+ 4\pi C_F\alpha_s \int \prod_{i=1}^{6} \frac{d^{d-1}\mathbf{p}_i}{(2\pi)^{d-1}} \frac{G_C(\mathbf{p}_1,\mathbf{p}_2)G_C(\mathbf{p}_3,\mathbf{p}_4)G_C(\mathbf{p}_5,\mathbf{p}_6)}{\mathbf{q_1}^2[\mathbf{q_2}^2]^{u+1}},
\end{aligned} \tag{2.115}$$

$$\begin{aligned}
\delta^{d-1}(\mathbf{q_1})\frac{\mathbf{p}_2^4}{m^3}: \quad & \int \prod_{i=1}^{6} \frac{d^{d-1}\mathbf{p}_i}{(2\pi)^{d-1}} G_C(\mathbf{p}_1,\mathbf{p}_2)(2\pi)^{d-1}\delta^{d-1}(\mathbf{q_1})\frac{\mathbf{p}_2^4}{m^3}\frac{G_C(\mathbf{p}_3,\mathbf{p}_4)G_C(\mathbf{p}_5,\mathbf{p}_6)}{[\mathbf{q_2}^2]^{u+1}} \\
&= \frac{E^2}{m}\int \prod_{i=1}^{5} \frac{d^{d-1}\mathbf{p}_i}{(2\pi)^{d-1}} G_C(\mathbf{p}_1,\mathbf{p}_2)\frac{1}{[\mathbf{q_1}^2]^{u+1}}G_C(\mathbf{p}_3,\mathbf{p}_4)G_C(\mathbf{p}_4,\mathbf{p}_5) \\
&+ \frac{1}{m}\int \prod_{i=1}^{4} \frac{d^{d-1}\mathbf{p}_i}{(2\pi)^{d-1}} G_C(\mathbf{p}_1,\mathbf{p}_2)\left[\frac{2E}{[\mathbf{q_1}^2]^{u+1}} + \frac{k(u)}{8}\frac{4\pi C_F\alpha_s}{[\mathbf{q_1}^2]^{u+\epsilon+\frac{1}{2}}}\right]G_C(\mathbf{p}_3,\mathbf{p}_4) \\
&+ \frac{4\pi C_F\alpha_s}{m}\int \prod_{i=1}^{6} \frac{d^{d-1}\mathbf{p}_i}{(2\pi)^{d-1}} G_C(\mathbf{p}_1,\mathbf{p}_2)\left[\frac{2E}{\mathbf{q_1}^2} + \frac{k(0)}{8}\frac{4\pi C_F\alpha_s}{[\mathbf{q_1}^2]^{\frac{1}{2}+\epsilon}}\right] \\
&\times \frac{G_C(\mathbf{p}_3,\mathbf{p}_4)G_C(\mathbf{p}_5,\mathbf{p}_6)}{[\mathbf{q_2}^2]^{u+1}},
\end{aligned} \tag{2.116}$$

$$\frac{\mathbf{p}_2^2+\mathbf{p}_3^2}{2m^2\mathbf{q_1}^2}: \quad \int \prod_{i=1}^{6} \frac{d^{d-1}\mathbf{p}_i}{(2\pi)^{d-1}} G_C(\mathbf{p}_1,\mathbf{p}_2)\frac{\mathbf{p}_2^2+\mathbf{p}_3^2}{2m^2\mathbf{q_1}^2}\frac{G_C(\mathbf{p}_3,\mathbf{p}_4)G_C(\mathbf{p}_5,\mathbf{p}_6)}{[\mathbf{q_2}^2]^{u+1}}$$

$$= \int \prod_{i=1}^{6} \frac{d^{d-1}\mathbf{p}_i}{(2\pi)^{d-1}} G_C(\mathbf{p}_1,\mathbf{p}_2) \left[\frac{E}{m}\frac{1}{{\mathbf{q_1}}^2} + \frac{4\pi C_F \alpha_s}{m}\frac{k(0)}{8}\frac{1}{[{\mathbf{q_1}}^2]^{\frac{1}{2}+\epsilon}} \right] G_C(\mathbf{p}_3,\mathbf{p}_4)$$
$$\times \frac{1}{[{\mathbf{q_2}}^2]^{u+1}} G_C(\mathbf{p}_5,\mathbf{p}_6) + \frac{k(u)}{16m} \int \prod_{i=1}^{4} \frac{d^{d-1}\mathbf{p}}{(2\pi)^{d-1}} \frac{G_C(\mathbf{p}_1,\mathbf{p}_2) G_C(\mathbf{p}_3,\mathbf{p}_4)}{[{\mathbf{q_1}}^2]^{u+\epsilon+\frac{1}{2}}}, \quad (2.117)$$

where

$$k(u) = \frac{8\Gamma(u-\frac{d-5}{2})\Gamma(\frac{d-3}{2}-u)\Gamma(\frac{d-3}{2})}{(4\pi)^{\frac{d-1}{2}}\Gamma(1+u)\Gamma(d-3-u)} \frac{e^{\gamma_E \epsilon}}{(4\pi)^{\epsilon}}. \quad (2.118)$$

So, finally only Coulomb, delta and $1/r^2$ potentials are left, and a new potential type, $\delta(\mathbf{q})$, which will be called contact potential in the following.

2.4.3 Ultrasoft interaction

The calculation of the ultrasoft part has not been done in this work. Instead the results from [42] were used for the calculation. For completeness a short overview of the ultrasoft calculation is presented here and some issues of the factorization which are important to understand the splitting of various divergent parts are briefly discussed.

The ultrasoft calculation first appears at third order. So, this is a new effect which has not yet been considered in lower-order calculations. The ultrasoft term in the Lagrangian (see equation (2.62)) is:

$$-g_s \psi^\dagger(x) \boldsymbol{x} \boldsymbol{E}(t,\mathbf{0}) \psi(x) - g_s \chi^\dagger(x) \boldsymbol{x} \boldsymbol{E}(t,\mathbf{0}) \chi(x).$$

The corresponding corrections can be expressed in the form

$$\delta^{us} G(E) = i g_s^2 C_F \int d^3\mathbf{r} d^3\mathbf{r}' \int \frac{d^4k}{(2\pi)^4} \left[\frac{k_0^2\, \mathbf{r}\mathbf{r}' - (\mathbf{r}\mathbf{k})(\mathbf{r}'\mathbf{k})}{k^2 + i\varepsilon} \right.$$
$$\left. \times G_C^{(s)}(0,\mathbf{r};E) G_C^{(o)}(\mathbf{r},\mathbf{r}';E-k_0) G_C^{(s)}(\mathbf{r}',0;E) \right], \quad (2.119)$$

where $G_C^{(s)}$ is the colour singlet and $G_C^{(s)}$ the colour octet Green function. This expression is ultraviolet (UV) divergent. To get a finite contribution it has to be combined with the IR poles of the potential calculation. This is done in practice by adding a counter term to the potentials and subtracting this counterterm from the ultrasoft calculation. Then, the ultrasoft corrections read:

$$\delta^{us} G(E) = \left[\tilde{\mu}^{2\epsilon}\right]^2 \int \frac{d^{d-1}\mathbf{l}}{(2\pi)^{d-1}} \frac{d^{d-1}\mathbf{l}'}{(2\pi)^{d-1}} \left\{ (-\delta d_v^{\mathrm{div}}) \frac{\ell^{\mathbf{2}} + \ell'^{\mathbf{2}}}{6m^2} \tilde{G}_C^{(s)}(\ell,\ell';E) \right.$$
$$\left. + \left[\tilde{\mu}^{2\epsilon}\right]^2 \int \frac{d^{d-1}\mathbf{p}}{(2\pi)^{d-1}} \frac{d^{d-1}\mathbf{p}'}{(2\pi)^{d-1}} \tilde{G}_C^{(s)}(\ell,\mathbf{p};E) \left[\delta U - \delta \tilde{V}_{c.t.}\right] \tilde{G}_C^{(s)}(\mathbf{p}',\ell';E) \right\}, \quad (2.120)$$

where d_v^{div} is the divergent part of the short distance coefficient d_v (see explanation below equation (2.58)) and δU is the ultrasoft insertion (containing the octet Green function). This result is then finite and can be calculated with the same methods as the potential insertions. The numerical evaluation will be done by a numerical integration. The routine is taken from [42] for the calculations in this work and is implemented in the Mathematica package.

2.5 Top quark width effects

The application of the calculations presented in the previous sections to the top quark pair production is not possible by treating the top quark as a stable particle, due to the large top quark width. The Standard Model prediction at NLO is [76] (NNLO also available but small [77, 78]):

$$\Gamma_t = \frac{G_F m_t^3}{8\pi\sqrt{2}}\left(1-\frac{M_W^2}{m_t^2}\right)^2\left(1+2\frac{M_W^2}{m_t^2}\right)\left[1-\frac{2\alpha_s}{3\pi}\left(\frac{2\pi^2}{3}-\frac{5}{2}\right)\right], \tag{2.121}$$

where terms of the order m_b^2/m_t^2 have been neglected. For a top quark mass of $m_t = 175$ GeV the width is about $\Gamma_t = 1.5$ GeV. So, the top quark is decaying very rapidly ($\approx 0.5\times 10^{-24}$s), even faster than the typical hadronisation time, which makes it behave like a free particle [79, 80]. The main decay channel in the Standard Model is to a b-quark and a W-boson $t \to Wb$. The other channels are suppressed by at least one order of magnitude [10]. Measurements of the total width are very difficult and the experiment gives currently a limit of $\Gamma_t < 12.7$ GeV at 95% confidence level [81].

To take into account the width effect properly, one has to apply the power counting $\Gamma_t/m \sim \alpha_s^2 \sim v^2$ for the width. This leads to additional terms in the Lagrangian [45, 82]:

$$\mathcal{L}_\Gamma = \psi^\dagger\left(i\frac{\Gamma_t}{2}+i\frac{\Gamma_t\mathbf{D}^2}{4m^2}-\frac{\Gamma_t^2}{8m}\right)\psi - \chi^\dagger\left(i\frac{\Gamma_t}{2}+i\frac{\Gamma_t\mathbf{D}^2}{4m^2}-\frac{\Gamma_t^2}{8m}\right)\chi\,. \tag{2.122}$$

The first term in both brackets is a leading-order effect, the second and third term contribute to the second order. The implementation of the leading order is particularly simple. It can be achieved by adding an additional width dependent term into the denominator of the propagator:

$$\frac{i\delta^{ij}}{E-\frac{\mathbf{p}^2}{2m}+i\frac{\Gamma_t}{2}}. \tag{2.123}$$

This is equivalent to shifting the center of mass energy into the complex plane $E \to E + i\Gamma_t$, which results in a broadening of the toponium 1S resonance in the cross section. In the following, the leading-order effects will be implemented in this way. At third order, the LO

implementation of the width effect is not sufficient. This shows up in the fact that there are uncanceled divergences of the form Γ/ϵ left in the QCD result obtained here. They are given in equation (3.172). When adding electroweak effects, these divergencies should cancel in the final result. First steps towards this have been done, but a full result is not yet available [25–27]. Also recently a new framework has been developed to include finite width effects and first phenomenological calculations are available within this approach [82–84].

Chapter 3

Calculation of the potential insertions

As seen in section 2.4.1, the calculation of Feynman diagrams in PNRQCD leads to insertions of potentials. In higher orders one needs to take into account multiple insertions, too. In this section the master integrals for all relevant insertions at NNNLO are calculated. The effect from higher-order potentials can be calculated in a quantum mechanical way. The leading-order Green function is:

$$G_C(E) \equiv \langle 0|\hat{G}_0|0\rangle = \langle 0|\frac{1}{H_0 - E - i\epsilon}|0\rangle. \tag{3.1}$$

Now, one can apply perturbation theory and take into account higher iterations of the potentials up to the appropriate order. The insertions of the potentials in perturbation theory at third order read:

$$\delta_3 G = -\langle 0|\hat{G}_0\delta V_1\hat{G}_0\delta V_1\hat{G}_0\delta V_1\hat{G}_0|0\rangle + 2\,\langle 0|\hat{G}_0\delta V_1\hat{G}_0\delta V_2\hat{G}_0|0\rangle - \langle 0|\hat{G}_0\delta V_3\hat{G}_0|0\rangle. \tag{3.2}$$

For a single insertion $\langle 0|\hat{G}_0\delta V\hat{G}_0|0\rangle$ of the potential of the form $\delta V = \frac{1}{(\mathbf{q}^2)^x}\left(\frac{\mu^2}{\mathbf{q}^2}\right)^{a\epsilon}$ the notation, which will be used in this work is:

$$I[x + a\epsilon] = \int \prod_i \left(\frac{d^{d-1}\mathbf{p}_i}{(2\pi)^{d-1}}\right)\tilde{G}_C(\mathbf{p}_1, \mathbf{p}_2; E)\frac{1}{(\mathbf{q}_{23}^2)^x}\left(\frac{\mu^2}{\mathbf{q}_{23}^2}\right)^{a\epsilon}\tilde{G}_C(\mathbf{p}_3, \mathbf{p}_4; E), \tag{3.3}$$

where $\mathbf{q_{ij}} = \mathbf{p}_i - \mathbf{p}_j$. Correspondingly for higher iterations $\langle 0|\hat{G}_0\delta V_x\hat{G}_0\delta V_y\hat{G}_0...|0\rangle$:

$$\begin{aligned} I[x + a\epsilon, y + b\epsilon \cdots] = \int \prod_i \left(\frac{d^{d-1}\mathbf{p}_i}{(2\pi)^{d-1}}\right)\tilde{G}_C(\mathbf{p}_1, \mathbf{p}_2; E)\frac{1}{(\mathbf{q}_{23}^2)^x}\left(\frac{\mu^2}{\mathbf{q}_{23}^2}\right)^{a\epsilon}\tilde{G}_C(\mathbf{p}_3, \mathbf{p}_4; E) \\ \times\frac{1}{(\mathbf{q}_{45}^2)^y}\left(\frac{\mu^2}{\mathbf{q}_{45}^2}\right)^{b\epsilon}\tilde{G}_C(\mathbf{p}_5, \mathbf{p}_6; E)\cdots . \end{aligned} \tag{3.4}$$

Using this notation and the results from section 2.4.2 four types of single insertions are needed:

$$I[1 + a_{c1}\epsilon], I[1/2 + a_{nc}\epsilon], I[a_{nc}\epsilon], I[\delta],$$

four types of double insertions:

$$I[1+a_{c2}\epsilon, 1+\epsilon], I[1/2+\epsilon, 1+\epsilon], I[0, 1+\epsilon], I[\delta, 1+\epsilon],$$

and one type of triple insertion:

$$I[1+\epsilon, 1+\epsilon, 1+\epsilon],$$

where $a_{c1} = 1, 2, 3$ and $a_{c2}, a_{nc} = 1, 2$. The δ in the argument of I stands for the insertion of $\delta^{(d-1)}(\mathbf{q})$. Some of the potential insertions are multiplied by a divergent coefficient function. This means, one has to calculate $I[x+a\epsilon, \cdots]$ to order ϵ. However, these divergent coefficient functions always come with a counter term, so that the expanded potential is finite. The form of the coefficient functions with divergent part can be written as:

$$\left(\frac{\mu^2}{\mathbf{q^2}}\right)^{a\epsilon} w(\epsilon) - \frac{w^{(1/\epsilon)}}{\epsilon},$$

where $w(\epsilon) = \frac{w^{(1/\epsilon)}}{\epsilon} + w + w^{(\epsilon)}\epsilon + O(\epsilon^2)$. The most elegant way to deal with these parts is to define a counter term subtracted insertion consisting of the complete coefficient function. The reason is that in the subtracted form, terms of order ϵ in $I[x+a\epsilon]$, which are independent of a, do not contribute to the complete result. This is because they appear in both, the insertion of $\left(\frac{\mu^2}{\mathbf{q^2}}\right)^{a\epsilon} \frac{w^{(1/\epsilon)}}{\epsilon}$ and of $\frac{w^{(1/\epsilon)}}{\epsilon}$. This simplifies the calculation and makes the presentation of the results more compact. In this work, the following notation for the counter term subtracted single insertion will be used:

$$J[x+a\epsilon; w(\epsilon)] = \frac{1}{\epsilon} w^{(1/\epsilon)} \Big(I[x+a\epsilon] - I[x] \Big) + \Big(w + w^{(\epsilon)}\epsilon \Big) I[x+a\epsilon]. \tag{3.5}$$

In the case of the double insertion the subtraction is in general more complicated. But at third order, one can make use of the fact that the double insertion always comes with at least one Coulomb potential. The case of two Coulomb potentials will be discussed later. Then the other potential is a second-order non-Coulomb potential and has therefore a finite (tree level) coefficient function. So, the only counter term comes with the β function of the Coulomb potential:

$$J[x+a\epsilon, 1+\epsilon; w(\epsilon)] = w(\epsilon) \Big(\frac{\beta_0}{\epsilon} + a_1(\epsilon) \Big) I[x+a\epsilon, 1+\epsilon] - \frac{w(\epsilon)\beta_0}{\epsilon} I[x+a\epsilon, 1], \tag{3.6}$$

where a can be either 0 or 1 at third order. In the case of only Coulomb insertions, the calculation can be simplified, because the imaginary part of these insertions is always finite. So, one does not need the $O(\epsilon)$ dependence of the potential, and can use instead the finite part of the ϵ expanded coefficient function. However, when dealing with the double insertion of Coulomb and non-Coulomb potentials, some parts will be encountered, where the imaginary

part of the (NLO-)Coulomb insertion is also needed. In that case the same definition as above will be used. For all other cases the superscript "(C)" will be added to denote that the expanded potentials ($w(\epsilon) = w^{(c)} + w^{(L)} L_q + \cdots$ with $L_q = \ln \frac{\mu^2}{\mathbf{q}^2}$) is used:

$$J^{(C)}[1; w^{(c)} + w^{(L)} L_q + w^{(L^2)} L_q^2 + w^{(L^3)} L_q^3] = \int \prod_i \left(\frac{d^{d-1}\mathbf{p}_i}{(2\pi)^{d-1}} \right) \tilde{G}_C(\mathbf{p}_1, \mathbf{p}_2; E)$$
$$\times \frac{1}{\mathbf{q}_{23}^2} \left(w^{(c)} + w^{(L)} \ln \frac{\mu^2}{\mathbf{q}_{23}^2} + w^{(L^2)} \ln^2 \frac{\mu^2}{\mathbf{q}_{23}^2} + w^{(L^3)} \ln^3 \frac{\mu^2}{\mathbf{q}_{23}^2} \right) \tilde{G}_C(\mathbf{p}_3, \mathbf{p}_4; E), \tag{3.7}$$

$$J^{(C)}[1, 1; w^{(c)} + w^{(L)} L_q + w^{(L^2)} L_q^2] = \int \prod_i \left(\frac{d^{d-1}\mathbf{p}_i}{(2\pi)^{d-1}} \right) \tilde{G}_C(\mathbf{p}_1, \mathbf{p}_2; E) \frac{1}{\mathbf{q}_{23}^2} \left(a_1 + \beta_0 \ln \frac{\mu^2}{\mathbf{q}_{23}^2} \right)$$
$$\times \tilde{G}_C(\mathbf{p}_3, \mathbf{p}_4; E) \frac{1}{\mathbf{q}_{45}^2} \left(w^{(c)} + w^{(L)} \ln \frac{\mu^2}{\mathbf{q}_{45}^2} + w^{(L^2)} \ln^2 \frac{\mu^2}{\mathbf{q}_{45}^2} \right) \tilde{G}_C(\mathbf{p}_5, \mathbf{p}_6; E), \tag{3.8}$$

$$J^{(C)}[1, 1, 1; w^{(c)} + w^{(L)} L_q] = \int \prod_i \left(\frac{d^{d-1}\mathbf{p}_i}{(2\pi)^{d-1}} \right) \tilde{G}_C(\mathbf{p}_1, \mathbf{p}_2; E) \frac{1}{\mathbf{q}_{23}^2} \left(a_1 + \beta_0 \ln \frac{\mu^2}{\mathbf{q}_{23}^2} \right) \tilde{G}_C(\mathbf{p}_3, \mathbf{p}_4; E)$$
$$\times \frac{1}{\mathbf{q}_{45}^2} \left(a_1 + \beta_0 \ln \frac{\mu^2}{\mathbf{q}_{45}^2} \right) \tilde{G}_C(\mathbf{p}_5, \mathbf{p}_6; E) \frac{1}{\mathbf{q}_{67}^2} \left(w^{(c)} + w^{(L)} \ln \frac{\mu^2}{\mathbf{q}_{67}^2} \right) \tilde{G}_C(\mathbf{p}_7, \mathbf{p}_8; E), \tag{3.9}$$

again with $\mathbf{q}_{ij} = \mathbf{p}_i - \mathbf{p}_j$.

Since the remaining $1/\epsilon$-poles must cancel against the same poles from the hard matching coefficient part, one must factorize the divergent part in the form that a divergent coefficient multiplies the LO and NLO Green function. For simplicity, if not stated otherwise, the J-functions will be given in such a way, that all parts which don't contribute to the imaginary part are left away. With this definition of the J-functions it is possible to express the final result only in terms of J-functions, even if the coefficient of the potential is not divergent (by setting the corresponding coefficient to zero in the argument of the J-function), so the I-functions are only needed in intermediate steps. For the final functions, also the poles in the limit $\lambda \to n$ are needed to extract the energy levels and wave function corrections. The notation for the pole parts will be $\hat{J}[x + a\epsilon, \cdots; w(\epsilon)]$ or $\hat{J}^{(C)}[1, \cdots; w^{(c)} + w^{(L)} L_q + \cdots]$ for the insertions of only Coulomb potentials.

In the results several short notations are used. The logarithms of λ are written as $L_\lambda = \ln(\lambda\mu/(C_F m \alpha_s))$, in the limit $\lambda \to n$ the corresponding logs are written as $L_n = \ln(n\mu/(C_F m \alpha_s))$. Ψ_i are Euler's Psi-functions and $\gamma_E = 0.577216...$ is Euler's constant. Euler's constant always appears together with the zeroth Psi-function and is therefore combined in the following way: $\hat{\Psi}(x) = \Psi_0(x) + \gamma_E$.

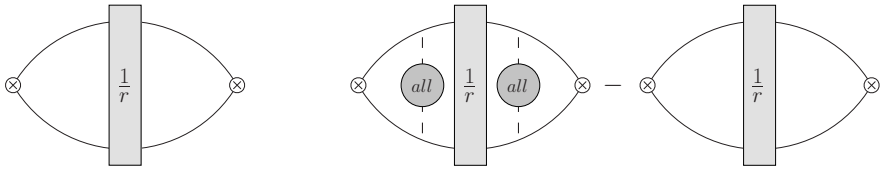

(a) (b)

Figure 3.1: The 2 parts of the Coulomb potential insertion which have to be separated.

3.1 Single insertions

3.1.1 Coulomb potential

The imaginary part of the Coulomb single insertion is finite. But the diagram from figure 3.1(a) without gluon exchange (denoted in the following with subscript a) has a pole in the real part. This will not appear in the result for $J^{(C)}$, because in this notation the real parts are omitted. However, it is included in equation (3.24), where the full real part is given. Due to the divergence, this diagram has to be calculated in d dimensions and the finite diagram (b) can be done in $d = 4$ dimensions:

$$I[1+a\epsilon] = \int \prod_i \left(\frac{d^{d-1}\mathbf{p}_i}{(2\pi)^{d-1}}\right) \frac{\tilde{G}_C^{(0ex)}(\mathbf{p}_1,\mathbf{p}_2;E)\tilde{G}_C^{(0ex)}(\mathbf{p}_3,\mathbf{p}_4;E)}{(\mathbf{q}_{23}^2)^x} \left(\frac{\mu^2}{\mathbf{q}_{23}^2}\right)^{a\epsilon} \tag{3.10}$$
$$+ \int \prod_i \left(\frac{d^3\mathbf{p}_i}{(2\pi)^3}\right) \frac{\tilde{G}_C(\mathbf{p}_1,\mathbf{p}_2;E)\tilde{G}_C(\mathbf{p}_3,\mathbf{p}_4;E) - \tilde{G}_C^{(0ex)}(\mathbf{p}_1,\mathbf{p}_2;E)\tilde{G}_C^{(0ex)}(\mathbf{p}_3,\mathbf{p}_4;E)}{(\mathbf{q}_{23}^2)^x} \left(\frac{\mu^2}{\mathbf{q}_{23}^2}\right)^{a\epsilon}.$$

The two parts will be discussed separately. The calculation has already been performed in [85]. But there, the part b of the insertion of the triple logarithm was only done by a numerical integration. This is not safe for all parameters of the calculation. Especially for small scales and small width the numerical integration can produce large errors, which are beyond the desired accuracy. Another additional point here is, that the pole parts could be written completely with harmonic sums and Zeta functions, while in [85], there were still some parts non-analytic.

Part a

The Green function without gluon exchange is given by

$$\tilde{G}_C^{(0ex)}(\mathbf{p}_1,\mathbf{p}_2;E) = \frac{m\delta^{(d-1)}(\mathbf{p}_1-\mathbf{p}_2)}{\mathbf{p}_1^2 - mE}. \tag{3.11}$$

So, the first integral reduces to:

$$\int \frac{d^{d-1}\mathbf{p}_2}{(2\pi)^{d-1}} \frac{d^{d-1}\mathbf{p}_3}{(2\pi)^{d-1}} \frac{m^2}{(\mathbf{p}_2^2 - mE)(\mathbf{q}_{23}^2)^x(\mathbf{p}_3^2 - mE)} \left(\frac{\mu^2}{\mathbf{q}_{23}^2}\right)^{a\epsilon}. \tag{3.12}$$

Similar diagrams with a finite number of gluon exchanges will appear in the following sections. The calculation of this type of diagrams in d dimensions is straightforward with standard methods (Feynman parameters, integration by parts and Mellin Barnes integrals). However, technically the more gluon exchanges one has to take into account, the more complicated the calculation becomes. This case has no gluon exchanges, so the integral is simple and the relevant master formula is the first one from appendix B.2. The result relevant for NNNLO is:

$$J_a^{(C)}[1; w^{(c)} + w^{(L)} L_q + w^{(L^2)} L_q^2 + w^{(L^3)} L_q^3] = \frac{m^2}{16\pi^2}\Bigg[w^{(c)} L_\lambda + w^{(L)} L_\lambda^2 + w^{(L^2)}\left(\pi^2 L_\lambda + \frac{4}{3} L_\lambda^3\right) + w^{(L^3)}\left(3\pi^2 L_\lambda^2 + 2L_\lambda^4\right)\Bigg]. \tag{3.13}$$

So this result has up to L_λ^4, which is plausible, because the leading-order Green function (which corresponds the insertion of $1/q^2$) has already one logarithms, and at each order an additional logarithm is added.

Part b

The second integral is finite, and can be calculated in coordinate space. A specific representation of the Green function will be used, here the integral representation given in appendix A. To use this form, the integral is transformed from momentum space into coordinate space. The zero exchange Green function in coordinate space can be derived by suppressing α_s, which corresponds to taking the limit $\lambda \to 0$ in the integral representation of the Green function defined in appendix A. So, one can write:

$$G_C(0,x;E)G_C(x,0;E) - G_C^{(0ex)}(0,x;E)G_C^{(0ex)}(x,0;E) = \frac{-m^3 E}{4\pi^2}\int_0^\infty dt_1 \int_0^\infty dt_2 e^{-2\sqrt{-mE}x(1+t_1+t_2)}\left[\left(\frac{t_1+1}{t_1}\right)^\lambda \left(\frac{t_2+1}{t_2}\right)^\lambda - 1\right]. \tag{3.14}$$

To generate the logs in the potential the function

$$W(\boldsymbol{r}) = \frac{1}{4\pi\Gamma(1+2u)\cos(\pi u)}\left(\boldsymbol{r}^2\right)^{u-\frac{1}{2}} \tag{3.15}$$

is introduced. Then by taking the nth derivative in u at the point $u = 0$ the logs to power n can be generated. The result up to the third derivative is needed for the single insertion of the third-order potential, because this potential contains up to $\ln^3(\mu^2/\boldsymbol{q}^2)$.

$$J_b^{(C)}[1, L_q^n] = \frac{\partial^n}{\partial u^n}\Bigg\{\frac{m^4 C_F^2 \alpha_s^2}{16\pi^2\lambda^2}\frac{1}{4\pi\Gamma(1+2u)\cos\pi u}\int d^3\mathbf{r}\int_0^\infty dt_1 \times \int_0^\infty dt_2 e^{-2\sqrt{-mE}r(1+t_1+t_2)}\left(\mathbf{r}^2\right)^{u-\frac{1}{2}}\left[\left(\frac{t_1+1}{t_1}\right)^\lambda\left(\frac{t_2+1}{t_2}\right)^\lambda - 1\right]\Bigg\}_{u=0}. \tag{3.16}$$

The r integrals can be done with Mathematica and one remains with a double integral over the parameters from the Green function representation. This integral is not trivial. After the substitution $z = \frac{1+t_1+t_2}{t_1 t_2}$ and $y = \frac{t_1}{1+t_1+t_2}$ the result is:

$$J_b^{(C)}[1, L_q^n] = \frac{\partial^n}{\partial u^n}\Bigg\{ \frac{m^2}{(4\pi)^2}\frac{1+2u}{\cos \pi u}(-4mE)^{-u}\int_0^\infty dz \left[(1+z)^\lambda - 1\right] z^{-1+2u} \\ \times \int_0^1 dy y^{2u}(1-y)^{2u}(1+yz)^{-2u-1}\Bigg\}_{u=0}. \tag{3.17}$$

At this point the derivative can be taken. Then the integral over y can be done. For some parts of the third derivative the function HypExpInt from the HypExp program package [86, 87] is used here. For the case of the zeroth and first derivative, the remaining integral has been done analytically. But already for the second derivative an analytic formula could not be derived. Instead, the following relation has been used:

$$(1+z)^\lambda - 1 = \sum_{k=1}^{\infty} \frac{\Gamma(k-\lambda)(-z)^k}{\Gamma(-\lambda)\Gamma(k+1)}. \tag{3.18}$$

Then, the z-integral can be performed. The result is a single sum. This sum can be partially done. The result up to the third derivative is:

$$J_b^{(C)}[1; w^{(c)} + w^{(L)}L_q + w^{(L^2)}L_q^2 + w^{(L^3)}L_q^3] = \frac{m^2}{16\pi^2}\Bigg[w^{(c)}j_0 + w^{(L)}\Big(j_1 + 2j_0 L_\lambda\Big) \\ + w^{(L^2)}\Big(4j_0 L_\lambda^2 + 4j_1 L_\lambda + j_2\Big) + w^{(L^3)}\Big(8j_0 L_\lambda^3 + 12 j_1 L_\lambda^2 + 6 j_2 L_\lambda + j_3\Big)\Bigg], \tag{3.19}$$

with

$$j_0 = -\hat{\Psi}(1-\lambda) + \lambda\Psi_1(1-\lambda), \tag{3.20}$$

$$j_1 = 4{}_4F_3(1,1,1,1;2,2,1-\lambda;1) - \frac{\pi^2}{6} + \hat{\Psi}(1-\lambda)^2 - 2\lambda\hat{\Psi}(1-\lambda)\Psi_1(1-\lambda) - 3\Psi_1(1-\lambda) \\ + \lambda\Psi_2(1-\lambda), \tag{3.21}$$

$$j_2 = 48 + \frac{88}{3}\zeta_3 - 8\Big[2 + \hat{\Psi}(1-\lambda)\Big]\,{}_4F_3(1,1,1,1;2,2,1-\lambda;1) \\ -32\,{}_5F_4(1,1,1,1,1;2,2,2,1-\lambda;1) + \hat{\Psi}(1-\lambda)\Big[16(\lambda\zeta_3 - 1) - 3\pi^2 \\ -4(1+2\lambda)\Psi_1(1-\lambda) + 4\lambda\Psi_2(1-\lambda) + 4\lambda\Psi_1(1-\lambda)\hat{\Psi}(1-\lambda) - \frac{4}{3}\hat{\Psi}(1-\lambda)^2\Big] \\ +\Psi_1(1-\lambda)\Big[3\pi^2\lambda + 32\lambda - 8 + 4\lambda\Psi_1(1-\lambda)\Big] + \frac{32}{3}\Psi_2(1-\lambda) - \frac{8}{3}\lambda\Psi_3(1-\lambda) \\ +16\sum_{k=1}^{\infty}\frac{(k-\lambda)\hat{\Psi}(k-\lambda)}{k^3} + 8\sum_{k=1}^{\infty}\frac{\Gamma(k)\Gamma(1-\lambda)\left[\hat{\Psi}(k-\lambda+1) - 2\hat{\Psi}(k)\right]}{(k+1)^2\Gamma(k-\lambda+1)}. \tag{3.22}$$

The coefficient j_3 would cover several pages and is therefore not given here in analytic form. Instead, in table 3.1 several values for the imaginary part of j_3 as a function of λ are given.

$Im(j_3)$	0.0	0.1	0.2	0.3	0.4	0.5	0.6	0.7	0.8
0.05 i	-12.10	-12.07	-11.61	-10.25	-6.77	2.01	25.90	102.73	438.69
0.15 i	-36.48	-36.59	-35.67	-32.59	-24.76	-5.99	39.81	157.27	457.34
0.25 i	-61.30	-62.04	-61.69	-59.16	-52.32	-37.09	-6.55	45.18	85.50
0.35 i	-86.60	-88.49	-89.72	-89.72	-87.72	-83.10	-77.42	-81.46	-131.85
0.45 i	-112.19	-115.57	-118.93	-122.29	-125.99	-131.41	-142.67	-169.69	-229.76
0.55 i	-137.72	-142.67	-148.20	-154.68	-162.95	-174.81	-193.71	-225.15	-274.84
0.65 i	-162.86	-169.23	-176.58	-185.41	-196.60	-211.56	-232.40	-261.42	-299.52
0.75 i	-187.31	-194.83	-203.54	-213.90	-226.58	-242.52	-262.73	-287.87	-317.31
0.85 i	-210.90	-219.28	-228.89	-240.09	-253.34	-269.15	-287.91	-309.61	-333.34

Table 3.1: $Im(j_3)$ for several values of the imaginary and real part of λ.

The imaginary part is varied vertically and the real part horizontally. Intermediate values can be obtained by interpolation.

To examine the size of this part, the ratio R_{j3} is defined as:

$$R_{j3} = \frac{C_F \alpha_s^4}{(4\pi)^2} \beta_0^3 \frac{m^2}{16\pi^2} j_3 / G(E). \tag{3.23}$$

This is the relative contribution of j_3 to the total cross section. The results for R_{j3} are given in table 3.2 for some specific values of the energy, the width and the scale. The size of j_3 is of the order of some percent in the relevant region.

The sums which appear in the formula above as well as the sums in j_3 are evaluated numerically. At this point some issues which are relevant for all sums which appear in the Green function (also in the other parts of the calculation) will be discussed. Single sums which contain only Ψ-functions are done numerically without a cutoff in Mathematica. Double sums and sums with Γ functions are calculated with a cutoff. This cutoff is chosen such, that the error of each individual sum is negligible in the threshold region. Sums with a bad convergence are also evaluated up to a cutoff, and then an approximation in the limit of high summation parameter is used to get an exact value for the approximate sum up to infinity. The results have been checked with a numerical integration in the regions where this integration (see equation (3.17)) is well convergent. The integration is not converging near zero energy or near zero width. Everywhere else, both methods agree with an error of below 0.1%.

μ=20	-8	-6	-4	-2	0	2
1.4	0.010	0.020	0.032	0.092	0.087	0.040
1.6	0.011	0.022	0.034	0.091	0.085	0.041
μ=30	-8	-6	-4	-2	0	2
1.4	0.019	0.059	0.041	0.050	0.059	0.025
1.6	0.021	0.054	0.042	0.053	0.058	0.026
μ=60	-8	-6	-4	-2	0	2
1.4	0.067	0.045	0.018	0.023	0.032	0.010
1.6	0.050	0.044	0.019	0.025	0.031	0.011

Table 3.2: Values for R_{j3} for energies in the range $E = (-8; 2)$, for width $\Gamma = (1.4; 1.6)$ and scales $\mu = (20; 60)$.

Full real part

For some parts of the double insertion of singular potentials with a Coulomb potential the real part is also needed. But since the singular potentials are already of NNLO, only up to the first-order correction to the Coulomb potential are needed in this form. The result is:

$$\begin{aligned} J_a[1+a\epsilon; w(\epsilon)] = &-\frac{am^2 w^{(1/\epsilon)}}{64(2+a)\pi^2\epsilon^2} + \frac{m^2(w - aw^{(1/\epsilon)})}{32(2+a)\pi^2\epsilon} \\ &+\frac{m^2}{16(2+a)\pi^2}\left[\frac{w^{(\epsilon)}}{2} + w\Big(1 + (2+a)L_\lambda\Big)\right. \\ &\left.+aw^{(1/\epsilon)}\Big(\frac{\pi^2}{24}(11+6a) - 1 + (2+a)L_\lambda^2\Big)\right], \end{aligned} \tag{3.24}$$

$$J_b[1+\epsilon; w(\epsilon)] = J_b^{(C)}[1; w + w^{(1/\epsilon)}L_q]. \tag{3.25}$$

Note, that here the convention for $J^{(C)}$ is not used, to indicate that the difference between the two results. Here the finite part remains unchanged. This is because the real parts in $J_b^{(C)}$ have not been dropped and the expanded potential with the logarithm L_q corresponds exactly to the form used in the convention for J.

Poles

The calculation of the poles for this part turns out to be quite complicated. The other single insertions are much easier (although for the other parts the calculation of the full Green function is more complicated). This is, because the the insertions of high powers of

logarithms leads to high orders of harmonic sums. A general discussion of the calculation of the poles is given in appendix C. The result is written in terms of harmonic sums and Zeta functions and reduced to a simpler structure where possible. Useful formulas for this reduction are given in appendix C.1. Here, only the second part of this insertion has poles in the $\lambda \to n$ limit. This is a general observation. Only parts which include the full Green function have these poles. Diagrams with a finite number of gluon exchanges will never contribute in this limit, and therefore play no role for the calculation of the energy levels and wave functions. The correction for the Coulomb single insertion reads:

$$\begin{aligned}
\hat{J}^{(C)}[1; w^{(c)} + w^{(L)} L_q + w^{(L^2)} L_q^2 + w^{(L^3)} L_q^3] = \frac{m^2}{16\pi^2} \Bigg\{ & \frac{n}{(n-\lambda)^2} \Bigg\{ w^{(c)} + 2w^{(L)}[L_n + S_1] \\
& + w^{(L^2)} \Big[\pi^2 + 4L_n^2 - \frac{8}{n} S_1 + 8 L_n S_1 + 4 S_1^2 + 4 S_2 \Big] + 24 w^{(L^3)} \Big[-2 S_{2,1} + 2 S_{1,1,1} \\
& + \frac{\pi^2 L_n}{4} + \frac{{L_n}^3}{3} + {S_1}^2 L_n + S_2 L_n + S_1 \Big(\frac{\pi^2}{4} - \frac{2 L_n}{n} + {L_n}^2 \Big) \Big] \Bigg\} \\
& - \frac{2}{(n-\lambda)} \Bigg\{ w^{(L)} \Big[1 + \frac{n\pi^2}{3} + 2 S_1 - 2 n S_2 \Big] + 8 w^{(L^2)} \Big[-n S_3 + n S_{2,1} - n \zeta_3 + \frac{L_n}{2} + \frac{n \pi^2 L_n}{6} \\
& + S_1 \Big(\frac{1}{2} + \frac{n\pi^2}{6} - n S_2 + L_n \Big) + S_2 \Big(1 - n L_n \Big) \Big] + 24 w^{(L^3)} \Big[\frac{\pi^2}{8} + \frac{23 n \pi^4}{360} - \frac{{S_1}^3}{6} + n {S_2}^2 \\
& + {S_1}^2 \Big(\frac{1}{2} + \frac{n\pi^2}{6} - n S_2 \Big) + 4 n S_{3,1} + 3 S_{1,1,1} - 4 n S_{2,1,1} - 2 n \zeta_3 L_n + \frac{{L_n}^2}{2} + \frac{n \pi^2 {L_n}^2}{6} \\
& + S_3 \Big(-\frac{1}{3} - 2 n L_n \Big) + S_{2,1} \Big(-2 + 2 n L_n \Big) + S_2 \Big(\frac{1}{2} - \frac{n\pi^2}{12} + 2 L_n - n {L_n}^2 \Big) \\
& + S_1 \Big(-\frac{1}{n} - \frac{\pi^2}{12} - 2 n S_3 + 2 n S_{2,1} - 2 n \zeta_3 + L_n + \frac{n \pi^2 L_n}{3} + {L_n}^2 - S_2 \Big(\frac{1}{2} + 2 n L_n \Big) \Big) \Big] \Bigg\} \Bigg\},
\end{aligned} \tag{3.26}$$

where the harmonic sums are defined as follows:

$$S_a(n) = \sum_{k=1}^{n} 1/k^a, \qquad S_{a,b}(n) \equiv \sum_{k=1}^{n} \frac{1}{k^a} S_b(k), \qquad S_{a,b,c}(n) \equiv \sum_{k=1}^{n} \frac{1}{k^a} S_{b,c}(k). \tag{3.27}$$

The argument n (principal quantum number) of the harmonic sums has been omitted to make the expressions more compact.

3.1.2 $1/r^2$ potential

This potential starts contributing at NNLO and is the first insertion with a non-finite imaginary part. While for the Coulomb potentials, the divergence appeares only in the real part, the $1/r^2$ potential single insertion will generate $1/\epsilon$-poles also in the imaginary part. Of course, all physical observables must be finite. The point here is, that the divergence from this part will cancel against a divergence which appears in the NNLO short distance coefficient. Another contribution from this coefficient multiplying the leading-order Green

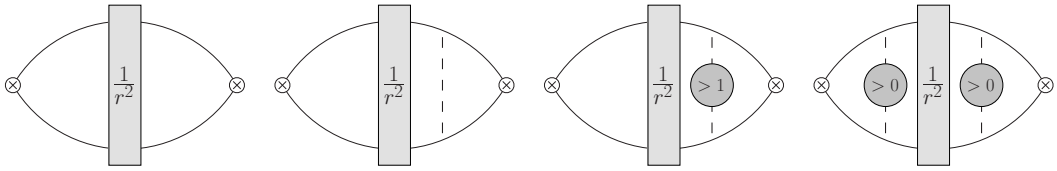

(a) (b) (c) (d)

Figure 3.2: The 4 parts of the $\frac{1}{r^2}$ potential insertion which have to be separated.

function is of the same order as the $1/r^2$ potential (and also the delta potential from the next section). To assure the correct cancelation of the divergences, one has to factorize the singular part in such a way, that it multiplies the imaginary part of the leading-order Green function at NNLO and correspondingly for the third order. This will be done by dividing the integral into different parts, each with another divergent structure. Power counting shows, that the integral for this insertion has an overall divergence coming from diagrams with less then two gluon exchanges, and a subdivergence, when there is no gluon exchange near the potential. The imaginary part of the overall divergence is vanishing, as it was the case for the Coulomb potential where only the overall divergence occurred. The relevant factorization has to be made for the diagram with the divergence in the subgraph. To treat the factorization correctly, four different parts are identified, as far as the divergent structure is concerned:

$$I[\frac{1}{2}+a\epsilon] = I_a[\frac{1}{2}+a\epsilon] + 2I_b[\frac{1}{2}+a\epsilon] + 2I_c[\frac{1}{2}+a\epsilon] + I_d[\frac{1}{2}+a\epsilon], \tag{3.28}$$

and the similar notation for J. The subdiagrams $I_x[\frac{1}{2}+a\epsilon]$ are shown in figure 3.2, and a subscript is used to denote the type of diagram. The first two diagrams have the overall divergence and additionally a divergence in the subgraph without gluon exchanges, the third one has only a divergence in the left subgraph and the last one is finite. Now, the calculation of the diagrams will be presented and the results will be briefly discussed.

Part a

The calculation of the first diagram is straightforward and similar to the Coulomb insertion part a. In fact, one can get the result directly by using $u = -1/2 + a\epsilon$ in the Coulomb result. The result is:

$$\begin{aligned} I_a[\frac{1}{2}+a\epsilon] &= \int \frac{d^{d-1}\mathbf{p}}{(2\pi)^{d-1}} \frac{d^{d-1}\mathbf{p'}}{(2\pi)^{d-1}} \frac{m^2}{(\mathbf{p}^2 - mE)\left[(\mathbf{p}-\mathbf{p'})^2\right]^{\frac{1}{2}+a\epsilon}(\mathbf{p'}^2 - mE)} \\ &= \frac{m^2\Gamma((2+a)\epsilon - \frac{1}{2})}{(4\pi)^{3-2\epsilon}(-mE)^{(2+a)\epsilon-\frac{1}{2}}} \frac{\Gamma\left((1+a)\epsilon\right)^2\Gamma\left(1-(1+a)\epsilon\right)}{\Gamma(2(1+a)\epsilon)\Gamma\left(\frac{3}{2}-\epsilon\right)}. \end{aligned} \tag{3.29}$$

The result for the corresponding J-function is:

$$J_a[\frac{1}{2}+a\epsilon;w(\epsilon)] = -\frac{amw^{(1/\epsilon)}}{2\pi^2(a+1)\epsilon^2}G_C^{(0ex)}(E) + \frac{m\Big(2a(\ln 2-1)w^{(1/\epsilon)}+w\Big)}{2\pi^2(a+1)\epsilon}G_C^{(0ex)}(E) \quad (3.30)$$
$$+\frac{m^3C_F\alpha_s}{8\pi^3(a+1)\lambda}\Bigg[aw^{(1/\epsilon)}\Big(\ln^2 2-2\ln 2-\frac{\pi^2}{24}(2a+5)-2a-2(a+1)L_\lambda-(a+1)L_\lambda^2\Big)$$
$$+w\Big(\ln 2-(a+1)L_\lambda-2-a\Big)-\frac{1}{2}w^{(\epsilon)}\Bigg].$$

The divergent part has been written here in the form of a coefficient times the Green function without gluon exchange. In the end, the sum of all parts must add up to the complete Green function, so that the divergence can cancel when combined with the short distance coefficient.

Part b

The second part has no gluon exchange on the left hand side of the potential and one exchange on the right. So, it has a subdivergence on the left side and on top of that an overall divergence. Like for part a, it will be done in momentum space. One can use integration by parts (IBP) relations to reduce the integral to more simpler ones. The idea behind this method is to use the fact that an integral of a total derivative vanishes. By performing this total derivative one gets to relations among Feynman integrals with different exponents. These relations can be used to write the integrals in terms of simpler ones, called master integrals, which can be done by other methods, for example with Feynman parameters. For a more detailed explanation of this method see [88]. The integration that has to be done for this part is:

$$I_b[\frac{1}{2}+a\epsilon] = \int \frac{d^{d-1}\mathbf{p}}{(2\pi)^{d-1}}\frac{d^{d-1}\mathbf{k}}{(2\pi)^{d-1}}\frac{d^{d-1}\mathbf{l}}{(2\pi)^{d-1}}\frac{C_F g_s^2 m^3}{(\mathbf{p}^2-mE)(\mathbf{k}^2-mE)(\mathbf{l}^2-mE)(\mathbf{p}-\mathbf{k})^2[(\mathbf{l}-\mathbf{k})^2]^{\frac{1}{2}+a\epsilon}}. \quad (3.31)$$

Now, using IBP with $\partial/\partial\mathbf{p}(\mathbf{p}-\mathbf{k})$ one finds:

$$\frac{\partial}{\partial\mathbf{p}}\ \frac{(\mathbf{p}-\mathbf{k})}{(\mathbf{p}^2-mE)^{a_1}(\mathbf{k}^2-mE)^{a_2}(\mathbf{l}^2-mE)^{a_3}[(\mathbf{p}-\mathbf{k})^2]^{a_4}[(\mathbf{l}-\mathbf{k})^2]^{a_5}} \quad (3.32)$$
$$= \frac{d-1-a_1\frac{2\mathbf{p}(\mathbf{p}-\mathbf{k})}{(\mathbf{p}^2-mE)}-2a_4\frac{(\mathbf{p}-\mathbf{k})^2}{(\mathbf{p}-\mathbf{k})^2}}{(\mathbf{p}^2-mE)^{a_1}(\mathbf{k}^2-mE)^{a_2}(\mathbf{l}^2-mE)^{a_3}[(\mathbf{p}-\mathbf{k})^2]^{a_4}[(\mathbf{l}-\mathbf{k})^2]^{a_5}} \quad (3.33)$$
$$= \frac{d-1-a_1-2a_4+a_1\frac{(\mathbf{k}^2-mE)-(\mathbf{p}-\mathbf{k})^2}{(\mathbf{p}^2-mE)}}{(\mathbf{p}^2-mE)^{a_1}(\mathbf{k}^2-mE)^{a_2}(\mathbf{l}^2-mE)^{a_3}[(\mathbf{p}-\mathbf{k})^2]^{a_4}[(\mathbf{l}-\mathbf{k})^2]^{a_5}}. \quad (3.34)$$

To write this expression in a more compact form an increasing and a lowering operator is introduced, x^+ and x^- respectively, which raises or lowers the power of a_x in the denominator. Then the integration by parts relation takes the form:

$$d-1-a_1-2a_4+a_1 1^+(2^- - 4^-) = 0\,, \quad (3.35)$$

where the integration is implicit and left away in this short notation, as well as the integrand to which the operators are applied. The equation equals zero, because the integration of a total derivative vanishes. Using this equation, the original integral reads:

$$
\begin{aligned}
I_b[\frac{1}{2}+a\epsilon] &= \frac{1^+(4^- - 2^-)}{d-4} I_b[\frac{1}{2}+a\epsilon] = \frac{C_F g_s^2 m^3}{d-4} \\
&\times \left[\int \frac{d^{d-1}\mathbf{p}}{(2\pi)^{d-1}} \frac{1}{(\mathbf{p}^2 - mE)^2} \int \frac{d^{d-1}\mathbf{k}}{(2\pi)^{d-1}} \frac{d^{d-1}\mathbf{l}}{(2\pi)^{d-1}} \frac{1}{(\mathbf{k}^2 - mE)(\mathbf{l}^2 - mE)[(\mathbf{l}-\mathbf{k})^2]^{\frac{1}{2}+a\epsilon}} \right. \\
&\left. - \int \frac{d^{d-1}\mathbf{p}}{(2\pi)^{d-1}} \frac{d^{d-1}\mathbf{k}}{(2\pi)^{d-1}} \frac{d^{d-1}\mathbf{l}}{(2\pi)^{d-1}} \frac{1}{(\mathbf{p}^2 - mE)^2 (\mathbf{l}^2 - mE)(\mathbf{p}-\mathbf{k})^2 [(\mathbf{l}-\mathbf{k})^2]^{\frac{1}{2}+a\epsilon}} \right] \\
&= \frac{C_F g_s^2 m^3 \Gamma(\frac{7}{2}+a\epsilon-d)\Gamma(\frac{d-1}{2}-\frac{1}{2}-a\epsilon)}{(d-4)(4\pi)^{\frac{3}{2}(d-1)}(-mE)^{6-\frac{3d}{2}+a\epsilon}\Gamma(\frac{d-1}{2})} \left[\frac{\Gamma(2-\frac{d-1}{2})\Gamma(\frac{3}{2}+a\epsilon-\frac{d-1}{2})^2}{\Gamma(4+2a\epsilon-d)} \right. \\
&\left. - \frac{\Gamma(\frac{9}{2}+a\epsilon-3\frac{d-1}{2})\Gamma(\frac{9}{2}-d+a\epsilon)\Gamma(d-a\epsilon-\frac{5}{2})}{\Gamma(8+2a\epsilon-2d)} \frac{\Gamma(\frac{3}{2}+a\epsilon-\frac{d-1}{2})}{\Gamma(a\epsilon+\frac{1}{2})} \frac{\Gamma(\frac{d-1}{2}-1)}{\Gamma(d-\frac{5}{2}-a\epsilon)} \right].
\end{aligned}
\tag{3.36}
$$

In the second step the master integrals from appendix B.2 have been used again. From this result one can easily get the expression for the J function:

$$
\begin{aligned}
2J_b[\frac{1}{2}+a\epsilon; w(\epsilon)] &= -\frac{amw^{(1/\epsilon)}}{2\pi^2(a+1)\epsilon^2} G_C^{(1ex)}(E) + \frac{m\Big(2a(\ln 2 - 1)w^{(1/\epsilon)} + w\Big)}{2\pi^2(a+1)\epsilon} G_C^{(1ex)}(E) \\
&+ \frac{m^3 C_F \alpha_s}{8\pi^3(a+1)} \Bigg\{ aw^{(1/\epsilon)} \Bigg[\Big(2(2a + 2\ln 2 - \ln^2 2) - \frac{2a+1}{4}\pi^2 \Big) L_\lambda + 2(a+1)L_\lambda^2 \\
&+ \frac{2}{3}(a+1)L_\lambda^3 \Bigg] + w\Big[2(2 + a - \ln 2)L_\lambda + (a+1)L_\lambda^2 \Big] + w^{(\epsilon)} L_\lambda \Bigg\}.
\end{aligned}
\tag{3.37}
$$

The divergent part is again written as a coefficient times a part of the Green function. Since the divergence in this part comes from the left subgraph, and in the right subgraph there is one gluon exchange, the remaining Green function is also that with one exchange. Note, that the result for $2J_B$ is written here, because in the final result there is not only this diagram, but also the symmetric part with one gluon exchange on the left hand side. Then the coefficient of the divergent part times the Green function is the same as for part a. This is necessary, so that the complete result adds up to the full Green function in the end.

Part c

The third part of the $1/r^2$-potential is the most complicated one. This part has a subdivergence in the left subgraph, but no overall divergence. So, this subgraph will be treated in d dimensions. Then, one can expand in ϵ, because the remaining part is finite. With this treatment one gets automatically the correct factorization of the divergent part. The starting

integral is:

$$I_c[\frac{1}{2}+a\epsilon] = \int \prod_{i=1}^{4} \left(\frac{d^{d-1}\mathbf{p}_i}{(2\pi)^{d-1}}\right) \frac{(2\pi)^{d-1}\delta^{(d-1)}(\mathbf{p}_1-\mathbf{p}_2)}{\mathbf{p}_1^2 - mE} \frac{m\tilde{G}_C^{(>1ex)}(\mathbf{p}_3,\mathbf{p}_4;E)}{[(\mathbf{p}_2-\mathbf{p}_3)^2]^{\frac{1}{2}+a\epsilon}}. \tag{3.38}$$

The divergence comes from the integral over $\mathbf{p}_1$ and $\mathbf{p}_2$. So, these integrals are done by first using results from appendix B.2. Then, the Fourier transformation is taken and the integration over $\mathbf{p}_4$ performed, so that one can use the coordinate space representation of the Green function. The result is:

$$\begin{aligned} I_c[\frac{1}{2}+a\epsilon] = \int_0^1 dx \frac{m\Gamma(a\epsilon+\frac{3}{2}-\frac{d-1}{2})x^{a\epsilon-\frac{1}{2}}\bar{x}^{\frac{d-1}{2}-a\epsilon-\frac{3}{2}}}{(4\pi)^{\frac{d-1}{2}}\Gamma(\frac{1}{2}+a\epsilon)} \int d^{d-1}\mathbf{r} G_C^{(>1ex)}(r,0;E) \\ \times \int \frac{d^{d-1}\mathbf{p}_3}{(2\pi)^{d-1}} \frac{e^{i\mathbf{p}_3\mathbf{r}}}{[x\mathbf{p}_3^2 - mE]^{a\epsilon+\frac{3}{2}-\frac{d-1}{2}}}. \end{aligned} \tag{3.39}$$

Now, the singularity comes only from the first x-integral. So, one can expand in ϵ and perform the other integrals in $d=4$ dimensions. This factors out a part which is a coefficient times the full Green function with more than one exchanges, because there are more than one exchanges on the right hand side of the original integral. This Green function multiplies a divergent coefficient, and it is important to keep in mind, that this is indeed the full Green function including also the parts of order ϵ. The result reads:

$$\begin{aligned} I_c[\frac{1}{2}+a\epsilon] &= \frac{m}{8(1+a)\pi^2}\int_0^1 \frac{dx}{\sqrt{x}} \int d^{d-1}\mathbf{r} G_C^{(>1ex)}(r,0;E) \int \frac{d^{d-1}\mathbf{p}_3}{(2\pi)^{d-1}} e^{i\mathbf{p}_3\mathbf{r}} \Big\{ \frac{1}{\epsilon} + \\ &+\Big(a\ln 4x - (1+a)\ln(1-x) - (1+a)\ln(x\mathbf{p}^2 - mE)\Big) + \Big(\frac{\pi^2}{6}(1+2a-2a^2) + \\ &+((1+a)\ln(1-x) - a\ln 4x + (1+a)\ln(x\mathbf{p}^2-mE))^2\Big)\frac{\epsilon}{2} + O(\epsilon^2)\Big\} \end{aligned} \tag{3.40}$$

$$\begin{aligned} &= \frac{m}{4(1+a)\pi^2}\Big\{ G_C^{(>1ex)}(0,0;E)\Big[\frac{1}{\epsilon} + 2(1-\ln 2) + \epsilon\Big(4 + (a^2+2a-\frac{1}{2})\frac{\pi^2}{6} - 4\ln 2 + \\ &+2\ln^2 2\Big)\Big] - \frac{(1+a)}{2}\int d^3\mathbf{r} G_C^{(>1ex)}(r,0;E)\int_0^1 \frac{dx}{\sqrt{x}}\int \frac{d^3\mathbf{p}_3}{(2\pi)^3} e^{i\mathbf{p}_3\mathbf{r}} \ln(x\mathbf{p}_3^2 - mE) + \\ &+\epsilon\frac{(1+a)}{2}\int d^3\mathbf{r} G_C^{(>1ex)}(r,0;E)\int_0^1 \frac{dx}{\sqrt{x}}\int \frac{d^3\mathbf{p}_3}{(2\pi)^3} e^{i\mathbf{p}_3\mathbf{r}}((1+a)\ln(1-x) - \\ &-a\ln 4x)\ln(x\mathbf{p}_3^2 - mE) + \epsilon\frac{(1+a)^2}{4}\int d^3\mathbf{r} G_C^{(>1ex)}(r,0;E)\int_0^1 \frac{dx}{\sqrt{x}} \\ &\times \int \frac{d^3\mathbf{p}_3}{(2\pi)^3} e^{i\mathbf{p}_3\mathbf{r}} \ln^2(x\mathbf{p}_3^2 - mE)\Big\} \end{aligned} \tag{3.41}$$

$$\begin{aligned} &= \frac{m}{8\pi^2}\Big\{ 2\frac{G_C^{(>1ex)}(E)}{a+1}\Big[\frac{1}{\epsilon} + 2(1-\ln 2) + \epsilon\Big(4 + (a^2+2a-\frac{1}{2})\frac{\pi^2}{6} \\ &-4\ln 2 + 2\ln^2 2\Big)\Big] + \int d^3\mathbf{r} G_C^{(>1ex)}(r,0;E)\int_0^1 \frac{dx}{\sqrt{x}}\Big[L^{(1)}(\mathbf{r}) \end{aligned}$$

$$+\epsilon\Big(a\ln 4x-(1+a)\ln(1-x)\Big)L^{(1)}(\mathbf{r})+\epsilon\frac{1+a}{2}L^{(2)}(\mathbf{r})+O(\epsilon^2)\Big]\Big\}. \tag{3.42}$$

In the second step the energy dependent logarithm is replaced by

$$L^{(i)}(\mathbf{r}):=(-1)^i\int\frac{d^{d-1}\mathbf{p}}{(2\pi)^{d-1}}e^{i\mathbf{pr}}[\ln(x\mathbf{p}^2-mE)]^i=\frac{\partial^i}{\partial u^i}\int\frac{d^{d-1}\mathbf{p}}{(2\pi)^{d-1}}\frac{e^{i\mathbf{pr}}}{(x\mathbf{p}^2-mE)^u}\bigg|_{u=0}. \tag{3.43}$$

This replacement is useful, because the u parameter regulates the integral and the integral becomes easier and can be done analytically. The integral depends only on the absolute value p of $\mathbf{p}$, so one can use spherical coordinates and do the integral in two steps:

$$L^{(i)}(\mathbf{r})=\frac{\partial^i}{\partial u^i}\left(\frac{1}{2\pi^2 r}\int_0^\infty dp\frac{p\sin(pr)}{(xp^2-mE)^u}\right)_{u=0} \tag{3.44}$$

$$=\frac{\partial^i}{\partial u^i}\left(\frac{1}{2^{u+\frac{1}{2}}}\frac{(-\frac{r^2mE}{x})^{\frac{3+2u}{4}}}{\pi^{\frac{3}{2}}(-mE)^u r^3\Gamma(u)}K_{\frac{3}{2}-u}\Big(r\sqrt{-mE/x}\Big)\right)_{u=0}, \tag{3.45}$$

where $K_n(x)$ is the modified Bessel function of the second kind. Now, the integral representation of the Green function is used and the remaining integrals are done:

$$\int_0^1 dx\int d^3\mathbf{r}G_C^{(>1ex)}(r,0;E)\frac{1}{\sqrt{x}}L^{(1)}=\frac{m\sqrt{-mE}}{2\pi}\Big[4(1-\lambda)\hat\Psi(1-\lambda)+2\lambda\hat\Psi(1-\lambda)^2$$
$$+2\lambda\Big(\frac{\pi^2}{2}-\Psi_1(1-\lambda)\Big)\Big]-2\ln(-4mE)G_C^{(>1ex)}(E)\,. \tag{3.46}$$

These integrals can be done with Mathematica. But if one goes to the the order ϵ terms, this is not possible in this way. Instead, one can write the exponential as a Taylor expansion, then do the integral first and after this the sum from the expansion. This procedure is mathematically not safe, because formally the sum from the Taylor expansion can be divergent. However, if this sum can be done analytically with Mathematica, and the final result after performing the sum is always finite. So, the analytical continuation gives the correct result in the end. The procedure has been checked numerically in the relevant parameter regions. For technical reasons it is useful to combine the parts with $L^{(1)}$ and $L^{(2)}$, because there are some cancelations among the two. The result is:

$$\int_0^1 dx\int d^3\mathbf{r}G_C^{(>1ex)}(r,0;E)\frac{1}{\sqrt{x}}\Big([a\ln 4x-(1+a)\ln(1-x)]L^{(1)}+\frac{1+a}{2}L^{(2)}\Big) \tag{3.47}$$

$$=\frac{4am\sqrt{-mE}}{2\pi}\Big\{\frac{\pi^2}{6}(3\lambda-1)+(\lambda-1)\hat\Psi(1-\lambda)^2-\frac{\lambda}{3}\hat\Psi(1-\lambda)^3 \tag{3.48}$$

$$-(\lambda-1)\Psi_1(1-\lambda)+\hat\Psi(1-\lambda)\Big(2-2\lambda-\frac{\pi^2\lambda}{6}+\lambda\Psi_1(1-\lambda)\Big)-\frac{1}{3}\lambda\Psi_2(1-\lambda)-\frac{8}{3}\lambda\zeta_3$$

$$+\ln(-4mE)\Big[(\lambda-1)\hat\Psi(1-\lambda)-\frac{\lambda}{2}\hat\Psi(1-\lambda)^2-\frac{\lambda}{2}\Big(\frac{\pi^2}{2}-\Psi_1(1-\lambda)\Big)\Big]\Big\}+\delta_{\not a}\,,$$

where the $\Psi_i(x)$ are the Polygamma functions (including Euler's constant if denoted with a hat) and $\delta_{\not a}$ is an a-independent term, which drops out in the counter term subtracted result. For the total cross section only this form is needed, so the calculation of $\delta_{\not a}$ is not necessary. The final result for the J-function is:

$$\begin{aligned}
2J_c[\frac{1}{2}+a\epsilon;w(\epsilon)] = &-\frac{amw^{(1/\epsilon)}}{2\pi^2(a+1)\epsilon^2}G_C^{(>1ex)}(E)+\frac{m\Big(2a(\ln 2-1)w^{(1/\epsilon)}+w\Big)}{2\pi^2(a+1)\epsilon}G_C^{(>1ex)}(E)\\
&+\frac{m^3C_F\alpha_s}{4\pi^3}\Bigg\{aw^{(1/\epsilon)}\Bigg[\hat\Psi(1-\lambda)\Big(\Psi_1(1-\lambda)-2L_\lambda+\frac{2}{\lambda}L_\lambda-L_\lambda^2+\frac{2}{\lambda}\\
&+\frac{1}{8(1+a)}(-16a-(3+2a)\pi^2-16\ln 2+8\ln^2 2)\Big)-\frac{1}{3}\hat\Psi(1-\lambda)^3-\frac{1}{3}\Psi_2(1-\lambda)\\
&+\Big(\hat\Psi(1-\lambda)^2-\Psi_1(1-\lambda)\Big)\Big(1-\frac{1}{\lambda}+L_\lambda\Big)-\frac{\pi^2}{6\lambda}+\frac{\pi^2}{2}L_\lambda\Bigg]\\
&+w\Bigg[\hat\Psi(1-\lambda)\Big(\frac{1}{\lambda}-\frac{2+a-\ln 2}{(1+a)}-L_\lambda\Big)+\frac{1}{2}\Big(\hat\Psi(1-\lambda)^2-\Psi_1(1-\lambda)\Big)\Bigg]\\
&-\frac{w^{(\epsilon)}}{2(1+a)}\hat\Psi(1-\lambda)\Bigg\}. \qquad (3.49)
\end{aligned}$$

Now, all divergent parts of this insertion have been calculated and one can see that the divergent part indeed adds up to a coefficient times the full Green function ($G_C(E) = G_C(E)^{(0ex)} + G_C(E)^{(1ex)} + G_C(E)^{(>1ex)}$). In this case the divergent part of the sum is:

$$J[\frac{1}{2}+a\epsilon;w(\epsilon)] = -\frac{amw^{(1/\epsilon)}}{2\pi^2(a+1)\epsilon^2}G_C(E)+\frac{m\Big(2a(\ln 2-1)w^{(1/\epsilon)}+w\Big)}{2\pi^2(a+1)\epsilon}G_C(E)+O(\epsilon^0)\,. \qquad (3.50)$$

As mentioned above, this Green function contains all orders in ϵ and not only the finite parts. But since one gets exactly the same type of contribution from the short distance coefficient these parts are never needed for the final result.

Part d

The last part is finite, so it can be done directly in coordinate space. On both sides, the integral representation of the Green function is used and procedure is analogous to the Coulomb part. One remains with the integrals over the t-variables from the Green function representation:

$$I_d[\frac{1}{2}+a\epsilon] = \frac{m^2}{8\pi^2}\frac{a\epsilon(-4mE)^{\frac{1}{2}-a\epsilon}}{\cos[\pi(a\epsilon-\frac{1}{2})]}\int_0^\infty dt_1dt_2\frac{\Big[\Big(\frac{1+t_1}{t_1}\Big)^\lambda-1\Big]\Big[\Big(\frac{1+t_2}{t_2}\Big)^\lambda-1\Big]}{(1+t_1+t_2)^{2a\epsilon+1}} \qquad (3.51)$$

$$= \frac{m^2}{16\pi^2}\frac{(-4mE)^{\frac{1}{2}-a\epsilon}\Gamma(2a\epsilon)}{\cos[\pi(a\epsilon-\frac{1}{2})]}\sum_{k=1}^\infty\frac{[\Gamma(k+2a\epsilon)\Gamma(k-\lambda)-\Gamma(k)\Gamma(k+2a\epsilon-\lambda)]^2}{\Gamma(k)\Gamma(k+2a\epsilon)\Gamma(k+2a\epsilon-\lambda)^2} \qquad (3.52)$$

$$= \frac{m^2}{8\pi^2}\frac{a\epsilon(-4mE)^{\frac{1}{2}-a\epsilon}}{\cos[\pi(a\epsilon-\frac{1}{2})]}\int_0^1 dxdy[(1-x)(1-y)]^{2a\epsilon-1}(1-xy)^{-1-2a\epsilon}\left[\left(x^{-\lambda}-1\right)\left(y^{-\lambda}-1\right)\right]. \tag{3.53}$$

In the second step, the substitutions $t_1 = x/(1-x)$ and $t_1 = y/(1-y)$ are made. Then x is small and one can use the expansion:

$$x^{-\lambda} - 1 = \sum_{k=1}^{\infty}\frac{\Gamma(k+\lambda)(1-x)^k}{\Gamma(\lambda)\Gamma(k+1)}. \tag{3.54}$$

This introduces an additional sum, but then the integrals can be done with Mathematica. The result of the first integration is a Hypergeometric function. This function will be written in the standard sum representation form and the result is:

$$I_d[\frac{1}{2}+a\epsilon] = \frac{m^2}{8\pi^2}\frac{a\epsilon(-4mE)^{\frac{1}{2}-a\epsilon}}{\cos[\pi(a\epsilon-\frac{1}{2})]}\sum_{k=1}^{\infty}\frac{\Gamma(k+\lambda)}{(k+2a\epsilon)\Gamma(1+k)\Gamma(\lambda)} \tag{3.55}$$
$$\times\int_0^1 dy(1-y)^{2a\epsilon-1}(y^{-\lambda}-1){}_2F_1(1,1+2a\epsilon;1+k+2a\epsilon;y)$$
$$= \frac{m^2}{8\pi^2}\frac{a\epsilon(-4mE)^{\frac{1}{2}-a\epsilon}}{\cos[\pi(a\epsilon-\frac{1}{2})]}\sum_{k=1}^{\infty}\frac{\Gamma(k+\lambda)\Gamma(1+k+2a\epsilon)}{(k+2a\epsilon)\Gamma(1+k)\Gamma(\lambda)\Gamma(1+2a\epsilon)} \tag{3.56}$$
$$\times\sum_{n=0}^{\infty}\frac{\Gamma(1+2a\epsilon+n)}{\Gamma(1+k+2a\epsilon+n)}\int_0^1 dy(1-y)^{2a\epsilon-1}(y^{-\lambda}-1)y^n$$
$$= \frac{m^2}{8\pi^2}\frac{a\epsilon(-4mE)^{\frac{1}{2}-a\epsilon}}{\cos[\pi(a\epsilon-\frac{1}{2})]}\sum_{k=1}^{\infty}\frac{\Gamma(k\lambda)\Gamma(1+k+2a\epsilon)}{(k+2a\epsilon)\Gamma(1+k)\Gamma(\lambda)\Gamma(1+2a\epsilon)} \tag{3.57}$$
$$\times\sum_{n=0}^{\infty}\frac{\Gamma(1+2a\epsilon+n)}{\Gamma(1+k+2a\epsilon+n)}\Gamma(2a\epsilon)\left(\frac{\Gamma(1+n-\lambda)}{\Gamma(1+n+2a\epsilon-\lambda)}-\frac{\Gamma(1+n)}{\Gamma(1+n+2a\epsilon)}\right)$$
$$= \frac{m^2}{16\pi^2}\frac{(-4mE)^{\frac{1}{2}-a\epsilon}\Gamma(2a\epsilon)}{\cos[\pi(a\epsilon-\frac{1}{2})]}\sum_{k=1}^{\infty}\frac{(\Gamma(k+2a\epsilon)\Gamma(k-\lambda)-\Gamma(k)\Gamma(k+2a\epsilon-\lambda))^2}{\Gamma(k)\Gamma(k+2a\epsilon)\Gamma(k+2a\epsilon-\lambda)^2}. \tag{3.58}$$

Then, the result can be expanded in ϵ. In the expanded form, some parts of the last sum can be done. The finite part can be given in a completely analytic form, for the order ϵ part a single sum is left:

$$I_d[\frac{1}{2}+a\epsilon] = \frac{m^2\sqrt{-mE}}{4\pi^3}\Big(-\lambda\frac{\pi^2}{3}-\hat{\Psi}(1-\lambda)+\lambda\Psi_1(1-\lambda)\Big) \tag{3.59}$$
$$-a\epsilon\frac{m^2\sqrt{-mE}}{4\pi^3}\Bigg[\Big(-\lambda\frac{\pi^2}{3}-\hat{\Psi}(1-\lambda)+\lambda\Psi_1(1-\lambda)\Big)\ln(-4mE)$$
$$+2\sum_{k=1}^{\infty}(\hat{\Psi}(k)-\hat{\Psi}(k-\lambda))\Big(\hat{\Psi}(k)\hat{\Psi}(k-\lambda)-\hat{\Psi}(k-\lambda)^2-\Psi_1(k)+\Psi_1(k-\lambda)\Big)\Bigg].$$

The corresponding result for the J function is:

$$J_d[\frac{1}{2}+a\epsilon;w(\epsilon)] = \frac{m^3C_F\alpha_s}{8\pi^3\lambda}\Bigg\{-2aw^{(1/\epsilon)}\Bigg[\Big(\lambda\frac{\pi^2}{3}+\hat{\Psi}(1-\lambda)-\lambda\Psi_1(1-\lambda)\Big)L_\lambda \tag{3.60}$$

$$+\sum_{n=0}^{\infty}(\hat{\Psi}(1+n)-\hat{\Psi}(1+n-\lambda))\Big(\hat{\Psi}(1+n)\hat{\Psi}(1+n-\lambda)-\hat{\Psi}(1+n-\lambda)^2$$
$$-\Psi_1(1+n)+\Psi_1(1+n-\lambda)\Big)\Big]+w\Big[-\lambda\frac{\pi^2}{3}-\hat{\Psi}(1-\lambda)+\lambda\Psi_1(1-\lambda)\Big]\Big\}.$$

Poles

Finally, the result for the poles in the limit $\lambda \to n$ are given. Only the last two parts have such poles. They were calculated with the methods described in appendix C and read:

$$2\hat{J}_c[\frac{1}{2}+a\epsilon;w(\epsilon)] = -\frac{amw^{(1/\epsilon)}}{2\pi^2(a+1)\epsilon^2}G_C^{\lambda\to n}(E)+\frac{m\Big(2a(\ln 2-1)w^{(1/\epsilon)}+w\Big)}{2\pi^2(a+1)\epsilon}G_C^{\lambda\to n}(E) \quad (3.61)$$
$$+\frac{m^3C_F\alpha_s}{4\pi^3(n-\lambda)}\Big\{aw^{(1/\epsilon)}\Big[\frac{1}{(1+a)}\Big(2a+\frac{5\pi^2}{24}+\frac{\pi^2}{12}a+2\ln 2-\ln^2 2\Big)-2S_1+S_1^2-S_2$$
$$+2L_n(1-S_1)+L_n^2\Big]+w\Big[L_n+\frac{(2+a-\ln 2)}{(1+a)}-S_1\Big]+w^{(\epsilon)}\frac{1}{2(1+a)}\Big\}$$
$$\hat{J}_d[\frac{1}{2}+a\epsilon;w(\epsilon)] = \frac{m^3C_F\alpha_s}{4\pi^3(n-\lambda)^2}\Big\{aw^{(1/\epsilon)}\Big[1+L_n-S_1\Big]+\frac{w}{2}\Big\} \quad (3.62)$$
$$+\frac{m^3C_F\alpha_s}{4\pi^3(\lambda-n)}\Big\{aw^{(1/\epsilon)}\Big[\frac{\pi^2}{3}+\frac{1}{n}(S_1-L_n)\Big]-\frac{w}{2n}\Big\}.$$

Note, that although the calculation of the full Green function was more complicated than for the Coulomb part, due to the higher order of divergence, the result for the pole structure is much simpler. This is, because the power of the logarithms which correspond to the needed order in the ϵ expansion is two orders less than for the Coulomb potential. So, one can expect harmonic sums up to second order, which is here indeed the case in the final result.

3.1.3 Delta potential

The single insertion of the delta potential is the most complicated part of the calculation. Naively, one might think that a delta potential is easy to calculate, because the left and right side of the potential factorize. This is indeed the case at second order, where there is only the pure delta potential insertion. Then:

$$\int\prod_i\left(\frac{d^{d-1}\mathbf{p}_i}{(2\pi)^{d-1}}\right)\tilde{G}_C(\mathbf{p}_1,\mathbf{p}_2;E)\tilde{G}_C(\mathbf{p}_3,\mathbf{p}_4;E)=G_C(E)^2\,, \quad (3.63)$$

where the d-dimensional expression for $G_C(E)$ should be used:

$$G_C(0,0,E)=\frac{m^2\,C_F\alpha_s}{4\pi}\Big[\frac{1}{4\epsilon}+L_\lambda+\frac{1}{2}-\frac{1}{2\lambda}-\hat{\Psi}(1-\lambda)\Big]+O(\epsilon). \quad (3.64)$$

After adding the appropriate counter term to this insertion, the order ϵ term of $G_C(E)$ does not contribute to the imaginary part of the insertion.

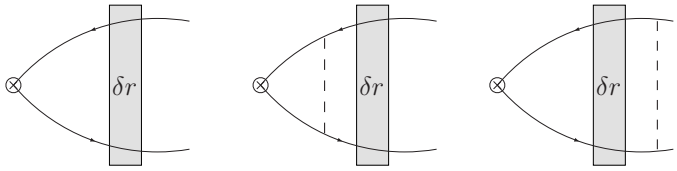

(1) (2) (3)

Figure 3.3: The three types of (naively) divergent subdiagrams for the single insertion of a delta potential.

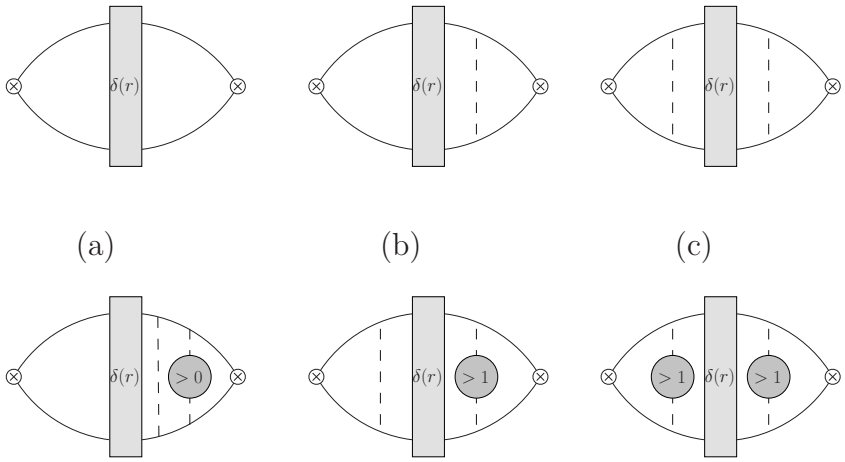

(a) (b) (c)

(d) (e) (f)

Figure 3.4: The delta potential single insertion is divided into six different parts.

But at third order, one has to take into account corrections to the tree level delta potential. These corrections have an extra $(\mu^2/q^2)^\epsilon$ factor, which leads to logarithms in the expanded form. Therefore, the result does not simplify as at second order, instead one has to perform the calculation in the same way as for the $1/r^2$ potential.

Power counting shows, that there are several divergent subdiagrams, shown in figure 3.3. On the one hand there is the diagram without and with one gluon exchange on the left side, but also the one which has no exchange on the left side but one exchange on the right hand side. The overall divergence is present only for the first diagram without gluon exchange. So, the insertion is divided into six different parts, shown in figure 3.4:

$$I[a\epsilon] = I_a[a\epsilon] + 2I_b[a\epsilon] + I_c[a\epsilon] + 2I_d[a\epsilon] + 2I_e[a\epsilon] + I_f[a\epsilon]. \tag{3.65}$$

Some diagrams have to be counted twice in the formula above, due to the left-right symmetry of the corresponding diagrams.

Part a

This part is similar to the first part of the Coulomb and the $1/r^2$ calculation. The integral can be easily done with Feynman parameters. The result reads:

$$\begin{aligned} I_a[a\epsilon] &= \int \frac{d^{d-1}\mathbf{p}}{(2\pi)^{d-1}} \frac{d^{d-1}\mathbf{p\prime}}{(2\pi)^{d-1}} \frac{m^2}{(\mathbf{p}^2 - mE)\left[(\mathbf{p}-\mathbf{p\prime})^2\right]^{a\epsilon}(\mathbf{p\prime}^2 - mE)} \\ &= \frac{m^2\Gamma((a+2)\epsilon - 1)}{(4\pi)^{3-2\epsilon}(-mE)^{(a+2)\epsilon-1}} \frac{\Gamma\left(-\frac{1}{2} + (a+1)\epsilon\right)^2 \Gamma\left(\frac{3}{2} - (a+1)\epsilon\right)}{\Gamma(2(a+1)\epsilon - 1)\Gamma\left(\frac{3}{2} - \epsilon\right)} . \end{aligned} \tag{3.66}$$

The result for the J-function of this part is:

$$J_a[\epsilon; w(\epsilon)] = -\frac{i\Gamma m^3 w^{(1/\epsilon)}}{48\pi^2\epsilon} + \frac{m^4 C_F^2 \alpha_s^2}{48\pi^2\lambda^2}(w^{(1/\epsilon)}(2 + 3L_\lambda) + w) . \tag{3.67}$$

Note that $J_a[\epsilon; w(\epsilon)]$ has a divergent part proportional to the width Γ. This part will remain uncanceled in the QCD calculation. Additional parts of these sort will arise from the insertion of the p^2/q^2 potential and the kinetic insertion and some issues concerning these parts were discussed in section 2.5. Interestingly, this part does only arise at third order. At second order, one needs instead of $J_a[\epsilon]$ the expression for $J_a[0]$, which has no such Γ/ϵ term. This coincides with the observation that there is no such term in the result for the squared Green function in equation (3.63), which is actually used in the second-order calculation as described above.

Part b

This part is similar to the second part of the $1/r^2$ insertion. One can use the result obtained in section 3.1.2 with $a\epsilon = a\epsilon - 1/2$ to get the result for this part. The result is:

$$\begin{aligned} I_b[a\epsilon] = \frac{C_F g_s^2 m^3 \Gamma(3 + a\epsilon - d)\Gamma(\frac{d-1}{2} - a\epsilon)}{(d-4)(4\pi)^{\frac{3}{2}(d-1)}(-mE)^{\frac{11}{2} - \frac{3d}{2} + a\epsilon}\Gamma(\frac{d-1}{2})} \Bigg[& \frac{\Gamma(2 - \frac{d-1}{2})\Gamma(1 + a\epsilon - \frac{d-1}{2})^2}{\Gamma(3 + 2a\epsilon - d)} \\ & - \frac{\Gamma(4 + a\epsilon - 3\frac{d-1}{2})\Gamma(4 - d + a\epsilon)}{\Gamma(7 + 2a\epsilon - 2d)} \frac{\Gamma(1 + a\epsilon - \frac{d-1}{2})\Gamma(\frac{d-1}{2} - 1)}{\Gamma(a\epsilon)} \Bigg] . \end{aligned} \tag{3.68}$$

The expression for the J-function is:

$$\begin{aligned} 2J_b[\epsilon; w(\epsilon)] = & -\frac{m^2 C_F \alpha_s w^{(1/\epsilon)}}{24\pi\epsilon^2} G_C^{(0ex)}(E) - \frac{m^2 C_F \alpha_s (2w^{(1/\epsilon)} - w)}{12\pi\epsilon} G_C^{(0ex)}(E) \\ & + \frac{m^4 C_F^2 \alpha_s^2}{96\pi^2\lambda} \left\{ w^{(1/\epsilon)} \left[19 + \frac{7\pi^2}{12} + 6L_\lambda - 6L_\lambda^2 \right] - w[1 + 6L_\lambda] - w^{(\epsilon)} \right\} . \end{aligned} \tag{3.69}$$

The divergent part has been cast again in the form of a coefficient times the relevant part of the Green function.

Part c

The third part has on both sides one gluon exchange. So, this is a three-loop integral. To calculate this, one can use again IBP relations and relate it to an integral of the same kind as in part b, but with slightly different exponents:

$$I_c[a\epsilon] = \int \prod_{i=1}^{4} \frac{d^{d-1}\mathbf{p}_i}{(2\pi)^{d-1}} \times \frac{C_F^2 g_s^4 m^4}{(\mathbf{p}_1^2 - mE)(\mathbf{p}_2^2 - mE)(\mathbf{p}_3^2 - mE)(\mathbf{p}_4^2 - mE)(\mathbf{p}_1 - \mathbf{p}_2)^2[(\mathbf{p}_2 - \mathbf{p}_3)^2]^{a\epsilon}(\mathbf{p}_3 - \mathbf{p}_4)^2} \,. \tag{3.70}$$

One can use the same IBP relation as in part b, but due to a different numbering this acts now on different parts of the denominator. The relation coming from $\partial/\partial\mathbf{p}_1(\mathbf{p}_1 - \mathbf{p}_2)$ is:

$$d - 1 - a_1 - 2a_5 + a_1 1^+(2^- - 5^-) = 0 \,. \tag{3.71}$$

This is the same notation used in section 3.1.2. Using this relation, the original integral can be written as two easier integrals:

$$I_c[a\epsilon] = \frac{C_F^2 g_s^4 m^4}{d-4}(1^+5^- - 1^+2^-) I_c[a\epsilon] \,. \tag{3.72}$$

One can now treat both integrals separately. The first one is relatively easy, because it factorizes into an easy one-loop integral and a second integral which is exactly the same as the integral calculated in the previous part:

$$\begin{aligned} 1^+5^- &= \int \prod_{i=1}^{4} \frac{d^{d-1}\mathbf{p}_i}{(2\pi)^{d-1}} \frac{1}{(\mathbf{p}_1^2 - mE)^2(\mathbf{p}_2^2 - mE)(\mathbf{p}_3^2 - mE)(\mathbf{p}_4^2 - mE)[(\mathbf{p}_2 - \mathbf{p}_3)^2]^{a\epsilon}(\mathbf{p}_3 - \mathbf{p}_4)^2} \\ &= \frac{\Gamma(2 - \frac{d-1}{2})}{(4\pi)^{\frac{d-1}{2}}(-mE)^{2-\frac{d-1}{2}}} \frac{\Gamma(3 + a\epsilon - d)\Gamma(\frac{d-1}{2} - a\epsilon)\Gamma(1 + a\epsilon - \frac{d-1}{2})}{(4-d)(4\pi)^{\frac{3}{2}(d-1)}(-mE)^{\frac{11}{2} - \frac{3d}{2} + a\epsilon}\Gamma(\frac{d-1}{2})} \\ &\quad \times \left[\frac{\Gamma(2 - \frac{d-1}{2})\Gamma(1 + a\epsilon - \frac{d-1}{2})}{\Gamma(3 + 2a\epsilon - d)} - \frac{\Gamma(4 + a\epsilon - 3\frac{d-1}{2})\Gamma(4 - d + a\epsilon)}{\Gamma(7 + 2a\epsilon - 2d)} \frac{\Gamma(\frac{d-1}{2} - 1)}{\Gamma(a\epsilon)} \right] . \end{aligned} \tag{3.73}$$

The second part is more complicated. First, the $\mathbf{p}_3$ integral will be done. This leads again to an integral similar to the one in part b, with the difference that the exponent of the first part of the denominator is two instead of one. This is still useful, because now one can apply the same IBP relation again. This reduces the result to simpler integrals, which can be done with the master formulas from appendix B.2:

$$\begin{aligned} 1^+2^- &= \int \prod_{i=1}^{4} \frac{d^{d-1}\mathbf{p}_i}{(2\pi)^{d-1}} \frac{1}{(\mathbf{p}_1^2 - mE)^2(\mathbf{p}_3^2 - mE)(\mathbf{p}_4^2 - mE)(\mathbf{p}_1 - \mathbf{p}_2)^2[(\mathbf{p}_2 - \mathbf{p}_3)^2]^{a\epsilon}(\mathbf{p}_3 - \mathbf{p}_4)^2} \\ &= \frac{1}{(4\pi)^{\frac{d-1}{2}}} \frac{\Gamma(a\epsilon + 1 - \frac{d-1}{2})}{\Gamma(a\epsilon)} \frac{\Gamma(\frac{d-1}{2} - a\epsilon)\Gamma(\frac{d-1}{2} - 1)}{\Gamma(d - 2 - a\epsilon)} \int \prod_{i=1}^{3} \frac{d^{d-1}\mathbf{p}_i}{(2\pi)^{d-1}} \end{aligned} \tag{3.74}$$

$$
\begin{aligned}
&\times \frac{1}{(\mathbf{p}_1^2 - mE)^2(\mathbf{p}_2^2 - mE)(\mathbf{p}_3^2 - mE)[(\mathbf{p}_1 - \mathbf{p}_2)^2]^{a\epsilon+1-\frac{d-1}{2}}(\mathbf{p}_2 - \mathbf{p}_3)^2} \\
&= \frac{1}{(d-4)(4\pi)^{\frac{d-1}{2}}} \frac{\Gamma(a\epsilon + 1 - \frac{d-1}{2})}{\Gamma(a\epsilon)} \frac{\Gamma(\frac{d-1}{2} - a\epsilon)\Gamma(\frac{d-1}{2} - 1)}{\Gamma(d - 2 - a\epsilon)} \int \prod_{i=1}^{3} \frac{d^{d-1}\mathbf{p}_i}{(2\pi)^{d-1}} \qquad (3.75) \\
&\times \Bigg[\frac{1}{(\mathbf{p}_1^2 - mE)^2(\mathbf{p}_2^2 - mE)(\mathbf{p}_3^2 - mE)^2[(\mathbf{p}_1 - \mathbf{p}_2)^2]^{a\epsilon+1-\frac{d-1}{2}}} \\
&- \frac{1}{(\mathbf{p}_1^2 - mE)^2(\mathbf{p}_3^3 - mE)^2[(\mathbf{p}_1 - \mathbf{p}_2)^2]^{a\epsilon+1-\frac{d-1}{2}}(\mathbf{p}_2 - \mathbf{p}_3)^2} \Bigg] \\
&= \frac{1}{(d-4)(4\pi)^{\frac{d-1}{2}}} \frac{\Gamma(a\epsilon + 1 - \frac{d-1}{2})}{\Gamma(a\epsilon)} \frac{\Gamma(\frac{d-1}{2} - a\epsilon)\Gamma(\frac{d-1}{2} - 1)}{\Gamma(d - 2 - a\epsilon)} \int \prod_{i=1}^{2} \frac{d^{d-1}\mathbf{p}_i}{(2\pi)^{d-1}} \qquad (3.76) \\
&\times \Bigg[\frac{\Gamma(2 - \frac{d-1}{2})}{(4\pi)^{\frac{d-1}{2}}(-mE)^{2-\frac{d-1}{2}}} \frac{1}{(\mathbf{p}_1^2 - mE)^2(\mathbf{p}_2^2 - mE)[(\mathbf{p}_1 - \mathbf{p}_2)^2]^{a\epsilon+1-\frac{d-1}{2}}} \\
&- \frac{1}{(4\pi)^{\frac{d-1}{2}}} \frac{\Gamma(3 + a\epsilon - d)}{\Gamma(a\epsilon + 1 - \frac{d-1}{2})} \frac{\Gamma(d - a\epsilon - 2)\Gamma(\frac{d-1}{2} - 1)}{\Gamma(d - 3 - a\epsilon + \frac{d-1}{2})} \\
&\times \frac{1}{(\mathbf{p}_1^2 - mE)^2(\mathbf{p}_2^3 - mE)^2[(\mathbf{p}_1 - \mathbf{p}_2)^2]^{3+a\epsilon-d}} \Bigg] \\
&= \frac{\Gamma(a\epsilon + 1 - \frac{d-1}{2})\Gamma(\frac{d-1}{2} - a\epsilon)\Gamma(\frac{d-1}{2} - 1)}{(d-4)(4\pi)^{2d-2}(-mE)^{8-2d+a\epsilon}\Gamma(a\epsilon)\Gamma(\frac{d-1}{2})} \qquad (3.77) \\
&\times \Bigg[\frac{\Gamma(2 - \frac{d-1}{2})\Gamma(5 - d + a\epsilon - \frac{d-1}{2})\Gamma(a\epsilon + 4 - d)\Gamma(a\epsilon + 3 - d)}{\Gamma(7 + 2a\epsilon - 2d)} \\
&- \frac{\Gamma(3 + a\epsilon - d)\Gamma(\frac{d-1}{2} - 1)\Gamma(8 - 2d + a\epsilon)\Gamma(5 + a\epsilon - d - \frac{d-1}{2})^2}{\Gamma(11 - 3d + 2a\epsilon)\Gamma(a\epsilon + 1 - \frac{d-1}{2})} \Bigg].
\end{aligned}
$$

Now, the two parts can be put together and the result for the J function can be derived. The results reads:

$$
\begin{aligned}
J_c[\epsilon; w(\epsilon)] = &-\frac{m^2 C_F \alpha_s w^{(1/\epsilon)}}{24\pi\epsilon^2} G_C^{(1ex)}(E) - \frac{m^2 C_F \alpha_s (w^{(1/\epsilon)} - w)}{12\pi\epsilon} G_C^{(1ex)}(E) \qquad (3.78) \\
&+ \frac{m^4 C_F^2 \alpha_s^2}{48\pi^2} \Bigg\{ w^{(1/\epsilon)} \Big[\Big(\frac{5\pi^2}{12} - 8 \Big) L_\lambda + 2L_\lambda^3 \Big] + w \Big[2L_\lambda + 3L_\lambda^2 \Big] + w^{(\epsilon)} L_\lambda \Bigg\}.
\end{aligned}
$$

Note, that the divergent part multiplies the Green function with one gluon exchange $G_C^{(1ex)}(E)$ and the coefficient is the same as for part b.

Part d

The part d has a divergence in the left subgraph. Basically, one can proceed first in the same way as for part c of the $1/r^2$ potential and calculate the divergent subdiagram in d dimensions, then expand in ϵ and calculate the remaining part in $d = 4$ dimensions. However, it turns out that this integral is more complicated. The reason is that this strategy leads to Hypergeometric function, which cannot be expanded easily for small ϵ. In principle one can

use the summation representation for Hypergeometric functions and proceed as before. But this gives an additional sum in the end. Unfortunately, this sum shows a slow convergence, so that the actual numerical evaluation is also very slow. A faster way is to do the integration numerically. This is possible, when using a momentum space representation of the Green function. Such a numerical integration has also been performed in [42].

The result for the J-function is:

$$\begin{aligned}
2J_d[\epsilon; w(\epsilon)] = &-\frac{m^2 C_F \alpha_s w^{(1/\epsilon)}}{12\pi\epsilon} G_C^{(>0ex)}(E) \\
&+\frac{m^4 C_F^2 \alpha_s^2}{8\pi^2}\Bigg\{ w^{(1/\epsilon)}\Big[C_{NInt}^{Log}[-C_F^2/(2\lambda)^2]\ln(m^2\alpha_s^2/\mu^2) - C_{NInt}^{const}[-C_F^2/(2\lambda)^2] \\
&-\frac{1}{2}\Big(\frac{11}{6}+3L_\lambda-\ln 2\Big)(1+2L_\lambda-2\hat{\Psi}(1-\lambda))\Big] \\
&+\frac{w}{6}\Big[\frac{\pi^2}{2}+\hat{\Psi}(1-\lambda)\Big(\frac{3}{\lambda}+1\Big)-L_\lambda\Big]\Bigg\},
\end{aligned} \tag{3.79}$$

where C_{NInt} comes from the numerical integration and is given by:

$$\begin{aligned}
C_{NInt}^{Log}(\tilde{E}) = &\frac{3}{4}\ln(-\tilde{E}) + 2\ln 2 - \frac{11}{12} + i\int_0^\infty Im\Bigg\{ \frac{-\sqrt{-\tilde{E}}(2\ln(1/p_t)-1)}{\pi(p_t^2-\tilde{E})} \\
&+\frac{9}{4}\Bigg[\frac{\sqrt{-\tilde{E}}}{9\pi(\tilde{E}-p_t^2)}\Big(8-3ip_t\ln\frac{\sqrt{-\tilde{E}}}{\sqrt{-\tilde{E}}-ip_t}+3ip_t\ln\frac{\sqrt{-\tilde{E}}}{\sqrt{-\tilde{E}}+ip_t}+8\ln\frac{p_t}{2\sqrt{-\tilde{E}}} \\
&-8\hat{\Psi}(1-2/(3\sqrt{-\tilde{E}}))\Big) - \frac{i\tilde{E}p_t}{\pi(\tilde{E}-p_t^2)^2(2\sqrt{-\tilde{E}}+3\tilde{E})} \\
&\times\Big((\tilde{E}(\sqrt{-\tilde{E}}-2ip_t)+\sqrt{-\tilde{E}}p_t^2)\,{}_2F_1(1,1-\frac{2}{3\sqrt{-\tilde{E}}},2-\frac{2}{3\sqrt{-\tilde{E}}};\frac{ip_t-\sqrt{-\tilde{E}}}{ip_t+\sqrt{-\tilde{E}}}) \\
&-(\tilde{E}(\sqrt{-\tilde{E}}+2ip_t)+\sqrt{-\tilde{E}}p_t^2)\,{}_2F_1(1,1-\frac{2}{3\sqrt{-\tilde{E}}},2-\frac{2}{3\sqrt{-\tilde{E}}};\frac{ip_t+\sqrt{-\tilde{E}}}{ip_t-\sqrt{-\tilde{E}}})\Big)\Bigg]\Bigg\}dp_t\,,
\end{aligned} \tag{3.80}$$

$$\begin{aligned}
C_{NInt}^{const}(\tilde{E}) = &\frac{9i}{32\pi}\int_0^\infty Im\Bigg\{\Big(-i(p_t^2+\tilde{E})\ln\frac{\sqrt{-\tilde{E}}+ip_t}{\sqrt{-\tilde{E}}-ip_t}+2p_t\sqrt{-\tilde{E}}+2p_t\sqrt{-\tilde{E}}\ln\frac{1}{p_t^2-\tilde{E}}\Big) \\
&\times\Bigg[\frac{16(1-2\ln(1/p_t))}{9p_t(p_t^2-\tilde{E})}+\frac{-32}{9p_t(p_t^2-\tilde{E})}\Big(1+\ln\frac{p_t}{2\sqrt{-\tilde{E}}}-\hat{\Psi}(1-2/(3\sqrt{-\tilde{E}}))\Big) \\
&+\frac{4i}{3(p_t^2-\tilde{E})}\Big(\ln\frac{\sqrt{-\tilde{E}}}{\sqrt{-\tilde{E}}-ip_t}-\ln\frac{\sqrt{-\tilde{E}}}{\sqrt{-\tilde{E}}+ip_t}\Big)+\frac{4\tilde{E}}{(\tilde{E}-p_t^2)^2(2\sqrt{-\tilde{E}}+3\tilde{E})} \\
&\times\Big((-i\tilde{E}+p_t(2\sqrt{-\tilde{E}}-ip_t))\,{}_2F_1(1,1-\frac{2}{3\sqrt{-\tilde{E}}},2-\frac{2}{3\sqrt{-\tilde{E}}};\frac{ip_t-\sqrt{-\tilde{E}}}{ip_t+\sqrt{-\tilde{E}}}) \\
&+(i\tilde{E}+p_t(2\sqrt{-\tilde{E}}+ip_t))\,{}_2F_1(1,1-\frac{2}{3\sqrt{-\tilde{E}}},2-\frac{2}{3\sqrt{-\tilde{E}}};\frac{ip_t+\sqrt{-\tilde{E}}}{ip_t-\sqrt{-\tilde{E}}})\Big)\Bigg]\Bigg\}dp_t\,.
\end{aligned} \tag{3.81}$$

In this numerical integration the imaginary part has been taken before the integration, so that divergencies in the real part do not appear. To compensate for this, the result is multiplied with i.

Part e

The part e has also a divergence in the left subgraph. In contrast to the previous part, the strategy from the $1/r^2$ single insertion can be used here and leads to a useful result. First the left part is calculated in d dimensions. This is done by using integration by parts relations and Feynman parameters. The starting point is:

$$I_e[a\epsilon] = \int \prod_{i=1}^{4} \frac{d^{d-1}\mathbf{p}_i}{(2\pi)^{d-1}} \frac{C_F g^2 m^2}{(\mathbf{p}_1^2 - mE)(\mathbf{p}_1 - \mathbf{p}_2)^2(\mathbf{p}_2^2 - mE)} \frac{1}{[(\mathbf{p}_2 - \mathbf{p}_3)^2]^{a\epsilon}} \tilde{\tilde{G}}_C^{(1)}(\mathbf{p}_3, \mathbf{p}_4)\,. \tag{3.82}$$

Then, using the IBP relation $d - 1 - 2a_2 - a_1 + a_1 1^+(3^- - 2^-) = 0$, one gets to two easier integrals:

$$I_e[a\epsilon] = \frac{C_F g_s^2 m^2 (1^+2^- - 1^+3^-)}{d-4}\,. \tag{3.83}$$

The remaining integrals can be done separately by using the master integrals from B.2. The result is:

$$\begin{aligned}
1^+3^- &= \int \prod_{i=1}^{4} \frac{d^{d-1}\mathbf{p}_i}{(2\pi)^{d-1}} \frac{1}{(\mathbf{p}_1^2 - mE)^2(\mathbf{p}_1 - \mathbf{p}_2)^2} \frac{1}{[(\mathbf{p}_2 - \mathbf{p}_3)^2]^{a\epsilon}} \tilde{\tilde{G}}_C^{(1)}(\mathbf{p}_3, \mathbf{p}_4) && (3.84)\\
&= \frac{1}{(4\pi)^{\frac{d-1}{2}}} \frac{\Gamma(1 + a\epsilon - \frac{d-1}{2})\Gamma(\frac{d-1}{2} - 1)\Gamma(\frac{d-1}{2} - a\epsilon)}{\Gamma(a\epsilon)\Gamma(d - 2 - a\epsilon)} \\
&\quad \times \int \prod_{i=1}^{3} \frac{d^{d-1}\mathbf{p}_i}{(2\pi)^{d-1}} \frac{1}{(\mathbf{p}_1^2 - mE)^2[(\mathbf{p}_1 - \mathbf{p}_2)^2]^{1+a\epsilon-\frac{d-1}{2}}} \tilde{\tilde{G}}_C^{(1)}(\mathbf{p}_2, \mathbf{p}_3) && (3.85)\\
&= \frac{1}{(4\pi)^{d-1}} \frac{\Gamma(\frac{d-1}{2} - 1)\Gamma(\frac{d-1}{2} - a\epsilon)\Gamma(4 - d + a\epsilon)}{\Gamma(a\epsilon)\Gamma(d - 2 - a\epsilon)} \int_0^1 dx x^{a\epsilon - \frac{d-1}{2}} \bar{x}^{d-3-a\epsilon} && (3.86)\\
&\quad \times \int \prod_{i=1}^{2} \frac{d^{d-1}\mathbf{p}_i}{(2\pi)^{d-1}} \frac{1}{(x\mathbf{p}_1^2 - mE)^{4-d+a\epsilon}} \tilde{\tilde{G}}_C^{(1)}(\mathbf{p}_1, \mathbf{p}_2)\,, \\
1^+2^- &= \int \prod_{i=1}^{4} \frac{d^{d-1}\mathbf{p}_i}{(2\pi)^{d-1}} \frac{1}{(\mathbf{p}_1^2 - mE)^2(\mathbf{p}_2^2 - mE)} \frac{1}{[(\mathbf{p}_2 - \mathbf{p}_3)^2]^{a\epsilon}} \tilde{\tilde{G}}_C^{(1)}(\mathbf{p}_3, \mathbf{p}_4) && (3.87)\\
&= \frac{\Gamma(2 - \frac{d-1}{2})}{(4\pi)^{\frac{d-1}{2}}(-mE)^{2-\frac{d-1}{2}}} \int \prod_{i=2}^{4} \frac{d^{d-1}\mathbf{p}_i}{(2\pi)^{d-1}} \frac{C_F g^2 m^2}{(\mathbf{p}_2^2 - mE)[(\mathbf{p}_2 - \mathbf{p}_3)^2]^{a\epsilon}} \tilde{\tilde{G}}_C^{(1)}(\mathbf{p}_3, \mathbf{p}_4) && (3.88)\\
&= \frac{\Gamma(2 - \frac{d-1}{2})\Gamma(1 + a\epsilon - \frac{d-1}{2})}{(4\pi)^{d-1}(-mE)^{2-\frac{d-1}{2}}\Gamma(a\epsilon)} \int_0^1 dx x^{a\epsilon-1} \bar{x}^{\frac{d-1}{2} - a\epsilon - 1} \int \prod_{i=1}^{2} \frac{d^{d-1}\mathbf{p}_i}{(2\pi)^{d-1}} \frac{C_F g^2 m^2 \tilde{\tilde{G}}_C^{(1)}(\mathbf{p}_1, \mathbf{p}_2)}{(x\mathbf{p}_1^2 - mE)^{1+a\epsilon-\frac{d-1}{2}}}\,. && (3.89)
\end{aligned}$$

At this point, one can combine both integrals:

$$I_e[a\epsilon] = \frac{C_F \alpha_s m^2}{(4\pi)^{d-2}(d-4)} \int \prod_{i=1}^{2} \frac{d^{d-1}\mathbf{p}_i}{(2\pi)^{d-1}} \frac{\tilde{G}_C^{(>1ex)}(\mathbf{p}_1, \mathbf{p}_2)}{\Gamma(a\epsilon)} \int_0^1 dx \left[\frac{\Gamma(2 - \frac{d-1}{2})\Gamma(1 + a\epsilon - \frac{d-1}{2})}{(-mE)^{2-\frac{d-1}{2}}} \right.$$

$$\times\frac{x^{a\epsilon-1}\bar{x}^{\frac{d-1}{2}-a\epsilon-1}}{(x\mathbf{p}_1^2-mE)^{1+a\epsilon-\frac{d-1}{2}}}-\frac{\Gamma(\frac{d-1}{2}-1)\Gamma(\frac{d-1}{2}-a\epsilon)\Gamma(4-d+a\epsilon)}{\Gamma(d-2-a\epsilon)}\frac{x^{a\epsilon-\frac{d-1}{2}}\bar{x}^{d-3-a\epsilon}}{(x\mathbf{p}_1^2-mE)^{4-d+a\epsilon}}\Big]. \tag{3.90}$$

Now, the x integral is done, the resulting Hypergeometric function is written as a sum and the remaining integrals are performed using the Laguerre representation of the Green function. This representation gives an additional sum. Some parts of this double sum can be done analytically, but the sums of the form:

$$\sum_{n=1}^{\infty}\sum_{k=1}^{n-1}\frac{(-1)^k(1+k)\Gamma(k)^2\Gamma(n-k)}{(1+2k)(n-\lambda)\Gamma(1+k+n)}\,, \tag{3.91}$$

and

$$\sum_{k=1}^{\infty}\sum_{n=1}^{k}\frac{(-1)^n(1+k)\Gamma(k)^2}{(1+2k)(n-\lambda)\Gamma(1+k-n)\Gamma(1+k+n)}\Big[\hat{\Psi}(1+k-n)+\hat{\Psi}(1+k+n)$$
$$-2\hat{\Psi}(k)-\frac{4k}{1+2k}\Big]\,, \tag{3.92}$$

are not further simplified. The numerical evaluation of these sums is stable and the convergence is good. The complete result for J_e is:

$$\begin{aligned}2J_e[\epsilon;w(\epsilon)] &= -\frac{m^2C_F\alpha_s w^{(1/\epsilon)}}{24\pi\epsilon^2}G_C^{(>1ex)}(E)-\frac{m^2C_F\alpha_s(w^{(1/\epsilon)}-w)}{12\pi\epsilon}G_C^{(>1ex)}(E) \\ &+\frac{m^4C_F^2\alpha_s^2}{8\pi^2}\Big\{\frac{w^{(1/\epsilon)}}{2\lambda}\Big[\frac{\pi^2}{3}-\frac{\pi^2\lambda}{4}+3\lambda\zeta_3+\hat{\Psi}(1-\lambda)\Big(\frac{1}{\lambda}-2+\frac{14}{3}\lambda-\frac{5\pi^2}{36}\lambda\Big)+\hat{\Psi}(1-\lambda)^2 \\ &-\Psi_1(1-\lambda)+\hat{\Psi}(1-\frac{\lambda}{2})-2\lambda L_\lambda^2\hat{\Psi}(1-\lambda)-\lambda^2\sum_{n=1}^{\infty}\sum_{k=1}^{n-1}\frac{(-1)^k(1+k)\Gamma(k)^2\Gamma(n-k)}{(1+2k)(n-\lambda)\Gamma(1+k+n)} \\ &-\lambda^2\sum_{k=1}^{\infty}\sum_{n=1}^{k}\frac{(-1)^n(1+k)\Gamma(k)^2}{(1+2k)(n-\lambda)\Gamma(1+k-n)\Gamma(1+k+n)}\Big(\hat{\Psi}(1+k-n)+\hat{\Psi}(1+k+n) \\ &-2\hat{\Psi}(k)-\frac{4k}{1+2k}\Big)-2\lambda^2\sum_{n=1}^{\infty}\frac{\hat{\Psi}(n)^2}{n(n-\lambda)}\Big]-\frac{1}{3}\Big[w(1+3L_\lambda)+\frac{w^{(\epsilon)}}{2}\Big]\hat{\Psi}(1-\lambda)\Big\}.\end{aligned} \tag{3.93}$$

Again, the divergent parts of this insertion add to the full Green function, similar to the case of the $1/r^2$ single insertion.

Part f

This last part is finite, so it can be done completely in coordinate space. The integral representation of the Green function is used on both sides of the potential. This gives two integrals over t_1 and t_2. Then, the same substitution as for the finite part of the $1/r^2$ potential is made ($t_1 = x/(1-x)$ and $t_1 = y/(1-y)$):

$$I_f[a\epsilon]=\frac{m^2}{8\pi^2}\frac{(a\epsilon-\frac{1}{2})(-4mE)^{1-a\epsilon}}{\cos[\pi(a\epsilon-1)]}\int_0^\infty dt_1\int_0^\infty dt_2(1+t_1+t_2)^{-2a\epsilon} \tag{3.94}$$

$$\begin{aligned}
&\left\{\left[\left(\frac{1+t_1}{t_1}\right)^{-\lambda}-1+\lambda\ln\left(\frac{1+t_1}{t_1}\right)\right]\left[\left(\frac{1+t_2}{t_2}\right)^{-\lambda}-1+\lambda\ln\left(\frac{1+t_2}{t_2}\right)\right]\right\}\\
&=\frac{m^2}{8\pi^2}\frac{(a\epsilon+\frac{1}{2})(-4mE)^{1-a\epsilon}}{\cos[\pi(a\epsilon-1)]}\int_0^1 dxdy((1-x)(1-y))^{2a\epsilon-2}(1-xy)^{-2a\epsilon} \qquad (3.95)\\
&\quad\left[\left(x^{-\lambda}-1+\lambda\ln x\right)\left(y^{-\lambda}-1+\lambda\ln y\right)\right].
\end{aligned}$$

Now, one can perform the x-integral with Mathematica. The resulting Hypergeometric function is expressed as a sum, and the remaining y-integral can be done:

$$\begin{aligned}
I_f[a\epsilon] = -\frac{m^3E}{4\pi^2}\Bigg\{&\left(1-\lambda\hat{\Psi}(-\lambda)\right)^2+a\epsilon\Bigg[2\lambda\left(1-\lambda\hat{\Psi}(-\lambda)\right)\left(\hat{\Psi}(-\lambda)^2-\Psi_1(-\lambda)+\frac{\pi^2}{2}\right)\\
&+\left(2-\ln(-4mE)\right)\left(1-\lambda\hat{\Psi}(-\lambda)\right)^2+\sum_{k=1}^{\infty}\frac{2}{k}\left((\lambda-k)\left(\hat{\Psi}(k)-\hat{\Psi}(k-\lambda)\right)+k\lambda\Psi_1(k)\right)^2\Bigg]\Bigg\}. \qquad (3.96)
\end{aligned}$$

The result partly contains the sum from the Hypergeometric function, which has to be evaluated numerically. Expressed with the notation of the J function the result reads:

$$\begin{aligned}
J_f[\epsilon;w(\epsilon)] = \frac{m^4C_F^2\alpha_s^2}{16\pi^2}\Bigg[&w\hat{\Psi}(1-\lambda)^2+2w^{(1/\epsilon)}\Bigg(\hat{\Psi}(1-\lambda)\left(\Psi_1(1-\lambda)-\hat{\Psi}(1-\lambda)^2-\frac{\pi^2}{2}\right)\\
&+\left(1-\frac{2}{\lambda}+L_\lambda\right)\hat{\Psi}(1-\lambda)^2+\frac{1}{\lambda^2}\sum_{k=1}^{\infty}\frac{1}{k}\left((\lambda-k)\left(\hat{\Psi}(k)-\hat{\Psi}(k-\lambda)\right)+k\lambda\Psi_1(k)\right)^2\Bigg)\Bigg] \qquad (3.97)
\end{aligned}$$

Poles

The last three parts have poles for $\lambda \to n$. The calculation of the poles for the parts d and e are more complicated than for other parts. Obtaining the results for specific n is straightforward. But the expression for arbitrary n can not be derived directly. Instead a kind of smart guessing is used to get this result. Details of the procedure are explained in the appendix C. The results are:

$$\begin{aligned}
2\hat{J}_d[\epsilon;w(\epsilon)] &= -\frac{m^2C_F\alpha_s w^{(1/\epsilon)}}{12\pi\epsilon}G_C^{\lambda\to n}(E) \qquad (3.98)\\
&-\frac{m^4C_F^2\alpha_s^2}{8\pi^2(n-\lambda)}\left\{w^{(1/\epsilon)}\left[\frac{11}{6}+\frac{1}{2n}-S_1-\frac{S_1}{n}+\left(1+\frac{1}{n}\right)L_n\right]+w\frac{3+n}{6n}\right\},\\
2\hat{J}_e[\epsilon;w(\epsilon)] &= -\frac{m^2C_F\alpha_s w^{(1/\epsilon)}}{24\pi\epsilon^2}G_C^{\lambda\to n}(E)-\frac{m^2C_F\alpha_s(w^{(1/\epsilon)}-w)}{12\pi\epsilon}G_C^{\lambda\to n}(E) \qquad (3.99)\\
&-\frac{m^4C_F^2\alpha_s^2}{8\pi^2(n-\lambda)}\left\{w^{(1/\epsilon)}\left[\frac{4}{3}-\frac{5\pi^2}{72}+\frac{n\pi^2}{6}-\frac{S_1}{n}+S_1^2-nS_2-L_n^2\right]\right.\\
&\left.-\frac{1}{3}w(1+3L_n)-\frac{1}{6}w^{(\epsilon)}\right\},\\
\hat{J}_f[\epsilon;w(\epsilon)] &= \frac{m^4C_F^2\alpha_s^2}{8\pi^2}\left\{w\left[\frac{1}{2(n-\lambda)^2}+\frac{\frac{1}{n}-S_1}{n-\lambda}\right]+w^{(1/\epsilon)}\left[\frac{\frac{1}{n}-1+2L_n-2S_1}{2(n-\lambda)^2}\right.\right. \qquad (3.100)
\end{aligned}$$

$$+\frac{1}{n-\lambda}\Big(\frac{1}{n^2}-\frac{1}{n}+\frac{2}{n}L_n-\frac{\pi^2}{6}+\frac{n\pi^2}{6}-2L_nS_1-\frac{3}{n}S_1+2S_1^2-(1+n)S_2\Big)\Big]\Big\}\,.$$

One can see here again that in the complete result the divergent part always adds up to the full Green function. Note also, that the divergent term coming from part a of the form Γ/ϵ does not appear here, because this part has no poles in the limit $\lambda \to n$.

3.1.4 Contact potential

This insertion does not appear in the original Lagrangian. But it arises when applying the equation of motion to reduce the kinetic correction and the $\mathbf{p}^2/\mathbf{q}^2$ to other known insertions. It is finite for single insertion as well as for the double insertion with a Coulomb potential. The single insertion can be done straightforwardly by using the results from the Coulomb single insertion for $u = 1/2$ and taking into account that the subtraction of the diagram without gluon exchange is not necessary here. The insertion is:

$$I[\delta] = \int \prod_{i=1}^{3} \frac{d^{d-1}\mathbf{p}_i}{(2\pi)^{d-1}} G_C(\mathbf{p}_1,\mathbf{p}_2)G_C(\mathbf{p}_2,\mathbf{p}_3) = \frac{m\lambda}{2\pi C_F\alpha_s}\int_0^\infty dz(1+z)^\lambda \frac{(2+z)\ln(1+z)-2z}{z^3} \tag{3.101}$$

$$= \frac{m\lambda}{2\pi C_F\alpha_s}\left(\frac{1}{2}+\lambda+\lambda^2\Psi_1(1-\lambda)\right). \tag{3.102}$$

Considering that this potential always comes with a finite coefficient, the counter term subtracted result and the pole part are:

$$J[\delta;w(\epsilon)] = \frac{mw\lambda}{2\pi C_F\alpha_s}\left[\frac{1}{2}+\lambda+\lambda^2\Psi_1(1-\lambda)\right], \tag{3.103}$$

$$\hat{J}[\delta;w(\epsilon)] = \frac{mw}{2\pi C_F\alpha_s}\left[\frac{n^3}{(n-\lambda)^2}-\frac{3n^2}{(n-\lambda)}\right]. \tag{3.104}$$

This finishes the single insertion at third order, and in the next section the results for the double insertion are presented.

3.2 Double insertions

3.2.1 Coulomb potential

The double insertion of the Coulomb potential is finite and can be done completely in coordinate space. The logs in the potential are once more generated by

$$W_i(\boldsymbol{r}_i) = \frac{1}{4\pi\Gamma(1+2u_i)\cos(\pi u_i)}\left(\boldsymbol{r}_i^2\right)^{u_i-\frac{1}{2}}. \tag{3.105}$$

So, the calculation reduces to the calculation of $I[1+u_1, 1+u_2]$ and taking the zeroth, the first and the second derivative with respect to u. The sum representation for the Green function is used in the middle and the integral representation for the left and right one. Then, the two integrals factorize and can be written in the following form:

$$\Big(\frac{\partial}{\partial u_1}\Big)^{x_1}\Big(\frac{\partial}{\partial u_2}\Big)^{x_2} I[1+u_1, 1+u_2] = \tag{3.106}$$

$$\Big(\frac{\partial}{\partial u_1}\Big)^{x_1}\Big(\frac{\partial}{\partial u_2}\Big)^{x_2} \int \prod_{i=1}^{2} d^3\boldsymbol{r}_i\, G_C(0,\boldsymbol{r}_1;E) W_1(\boldsymbol{r}_1) G_C(\boldsymbol{r}_1,\boldsymbol{r}_2;E) W_2(\boldsymbol{r}_2) G_C(\boldsymbol{r}_2,0;E)$$

$$= \Big(\frac{m}{4\pi}\Big)^3 \frac{\lambda}{mC_F\alpha_s} \sum_{j=1}^{\infty} \frac{H^{(x_1)}(j) H^{(x_2)}(j)}{j(j-\lambda)}\,, \tag{3.107}$$

with

$$H(u,j) = \frac{1}{\Gamma(1+2u)\cos\pi u}\left(\frac{e^{i\pi}}{4m^2v^2}\right)^u \int_0^\infty dt \left(\frac{1+t}{t}\right)^\lambda \int_0^\infty ds\, e^{-(1+t)s} s^{2u+1} L_{j-1}^{(1)}(s) \tag{3.108}$$

$$= \frac{j\Gamma(1-\lambda)}{\cos(\pi u)(-4mE)^u} \sum_{k=0}^{j-1} \frac{(-1)^k (j-1)!}{k!(j-1-k)!} \frac{\Gamma(2+k+2u)\Gamma(1+k+2u)}{\Gamma(1+2u)\Gamma(k+2)\Gamma(2+k+2u-\lambda)}\,, \tag{3.109}$$

and

$$H^{(x)}(j) = \Big(\frac{\partial}{\partial u}\Big)^x H(u,j)\,. \tag{3.110}$$

In the last step the remaining integral is performed. The results for H after taking the derivatives are:

$$H^{(0)}(k) = \frac{k}{k-\lambda}\,, \tag{3.111}$$

$$H^{(1)}(k) = \frac{2}{k-\lambda}\bigg[kL_\lambda - k\hat\Psi(k-\lambda) + \lambda\Big(\hat\Psi(1-\lambda) - \hat\Psi(k+1-\lambda)\Big)\bigg]\,, \tag{3.112}$$

$$\begin{aligned} H^{(2)}(k) = \frac{4}{k-\lambda}\bigg[&kL_\lambda^2 - \frac{2\lambda L_\lambda}{k-\lambda} + \frac{5k\pi^2}{12} + \frac{2\lambda}{(k-\lambda)^2} + \frac{2k(k-1)\,{}_4F_3(1,1,1,2-k;2,2,2-\lambda;1)}{\lambda-1} \\ &+\hat\Psi(1-\lambda)\Big(-\frac{2\lambda}{k-\lambda} + 2\lambda L_\lambda + k\hat\Psi(1-\lambda) - 2(k+\lambda)\hat\Psi(k-\lambda)\Big) \\ &+\hat\Psi(k-\lambda)\Big(\frac{4\lambda}{k-\lambda} - 2(k+\lambda)L_\lambda + 2(k+\lambda)\hat\Psi(k-\lambda)\Big) - k\Psi_1(1-\lambda)\bigg]\,. \end{aligned} \tag{3.113}$$

For the J functions, the special notation for insertion with only Coulomb potentials, defined in the beginning of this chapter, is used. The result in terms of the H functions reads:

$$J^{(C)}[1,1;w^{(c)} + w^{(L)}L_q + w^{(L^2)}L_q^2] = \frac{m^2\lambda}{64\pi^3 C_F\alpha_s}\bigg\{a_1 w^{(c)}\Big[\Psi_1(1-\lambda) - \frac{\lambda}{2}\Psi_2(1-\lambda)\Big]$$

$$+(a_1 w^{(L)} + w^{(c)}\beta_0)\Big[- \lambda\hat{\Psi}(1-\lambda)\Psi_2(1-\lambda) - \frac{\lambda}{3}\Psi_3(1-\lambda) - 2\sum_{k=1}^{\infty}\frac{(k+\lambda)\hat{\Psi}(k-\lambda)}{(k-\lambda)^3}$$
$$+L_\lambda(2\Psi_1(1-\lambda) - \lambda\Psi_2(1-\lambda))\Big] + a_1 w^{(L^2)}\sum_{k=1}^{\infty}\frac{H^{(0)}(k)H^{(2)}(k)}{k(k-\lambda)}$$
$$+w^{(L)}\beta_0\sum_{k=1}^{\infty}\frac{H^{(1)}(k)H^{(1)}(k)}{k(k-\lambda)} + w^{(L^2)}\beta_0\sum_{k=1}^{\infty}\frac{H^{(1)}(k)H^{(2)}(k)}{k(k-\lambda)}\Bigg\}. \tag{3.114}$$

Parts of the sums in the last line of equation (3.114) are known analytically but the result is too lengthy and not given here.

Poles

The poles in the limit $\lambda \to n$ of this part are not so easy to calculate for arbitrary quantum number n. There are several complicated sums and double sums. Nevertheless, after a tedious reduction of harmonic-like sums, the result can be written completely with the usual harmonic sums and nested harmonic sums:

$$\hat{J}^{(C)}[1,1;w^{(c)} + w^{(L)}L_q + w^{(L^2)}L_q^2] = \frac{m^2}{(4\pi)^3 C_F\alpha_s}\Bigg\{\frac{n^2}{(n-\lambda)^3}\Big[a_1 w^{(c)} \tag{3.115}$$
$$+2(a_1 w^{(L)} + w^{(c)}\beta_0)(L_n + S_1) + 4a_1 w^{(L^2)}\Big(\frac{\pi^2}{4} + {S_1}^2 + S_2 + {L_n}^2 + 2S_1\Big(-\frac{1}{n} + L_n\Big)\Big)$$
$$+4w^{(L)}\beta_0({S_1}^2 + 2S_1L_n + {L_n}^2) + 8w^{(L^2)}\beta_0\Big({S_1}^3 + \frac{\pi^2 L_n}{4} + S_2L_n + {L_n}^3 + {S_1}^2\Big(\frac{-2}{n} + 3L_n\Big)$$
$$+S_1\Big(\frac{\pi^2}{4} + S_2 - \frac{2L_n}{n} + 3{L_n}^2\Big)\Big)\Big]$$
$$-\frac{n}{(n-\lambda)^2}\Big[a_1 w^{(c)} + 2(a_1 w^{(L)} + w^{(c)}\beta_0)(1 + L_n + \frac{n\pi^2}{6} + 2S_1 - nS_2)$$
$$+4a_1 w^{(L^2)}\Big(\frac{\pi^2}{4} + {S_1}^2 + 2nS_{2,1} - 2nS_3 - 2n\zeta_3 + 2L_n + \frac{n\pi^2}{3}L_n + {L_n}^2 + S_1\Big(2 - \frac{2}{n} + \frac{n\pi^2}{3}$$
$$-2nS_2 + 4L_n\Big) + S_2\Big(3 - 2nL_n\Big)\Big) + 4w^{(L)}\beta_0\Big(\frac{\pi^2}{6} + 3{S_1}^2 + nS_3 - n\zeta_3 + 2L_n$$
$$+\frac{n\pi^2 L_n}{3} + {L_n}^2 + S_1\Big(2 - \frac{1}{n} + \frac{n\pi^2}{3} - 2nS_2 + 4L_n\Big) + S_2\Big(-1 - 2nL_n\Big)\Big)$$
$$+4w^{(L^2)}\beta_0\Big(\frac{\pi^2}{2} + \frac{17n\pi^4}{180} + 4{S_1}^3 - 2n{S_2}^2 - 4S_3 + 4nS_4 - 12nS_{3,1} + \frac{7\pi^2 L_n}{6} + 6{L_n}^2$$
$$+n\pi^2{L_n}^2 + 2{L_n}^3 + {S_1}^2\Big(6 - \frac{6}{n} + n\pi^2 - 6nS_2 + 14L_n\Big) + \zeta_3\Big(-4 - 8nL_n\Big)$$
$$+S_{2,1}\Big(4 + 4nL_n\Big) + S_2\Big(2 + \frac{2}{n} + \frac{n\pi^2}{2} + 2L_n - 6n{L_n}^2\Big) + S_1\Big(\frac{-4}{n} + \frac{\pi^2}{3} + 4nS_{2,1}$$
$$-8n\zeta_3 + 12L_n - \frac{8L_n}{n} + 2n\pi^2 L_n + 12{L_n}^2 + S_2\Big(12 - 12nL_n\Big)\Big)\Big)\Big]$$
$$+\frac{1}{(n-\lambda)}\Big[(a_1 w^{(L)} + w^{(c)}\beta_0)\Big(1 + \frac{\pi^2 n}{3} + 2S_1 - 2nS_2\Big) + 4a_1 w^{(L^2)}\Big(1 + \frac{n\pi^2}{3}$$

$$
\begin{aligned}
&-2nS_3 + 2nS_{2,1} - 2n\zeta_3 + L_n + \frac{n\pi^2}{3}L_n \\
&+S_1\Big(3 + \frac{n\pi^2}{3} - 2nS_2 + 2L_n\Big) + S_2\Big(2 - 2n - 2nL_n\Big)\Big) \\
&+4w^{(L)}\beta_0\Big(1 + \frac{n\pi^2}{3} + \frac{n^2\pi^4}{36} + 2{S_1}^2 + n^2{S_2}^2 + 6nS_3 - 5n^2S_4 - 2nS_{2,1} + 4n^2S_{3,1} \\
&-2n\zeta_3 + L_n + \frac{n\pi^2 L_n}{3} + S_1\Big(3 + n\pi^2 - 6nS_2 + 2L_n\Big) + S_2\Big(-2n - \frac{n^2\pi^2}{3} - 2nL_n\Big)\Big) \\
&+8w^{(L^2)}\beta_0\Big(\frac{11\pi^2}{24} + \frac{73n\pi^4}{360} + {S_1}^3 - 12n^2S_5 + \frac{20S_{1,1}}{n} + 20n^2S_{3,2} + 28n^2S_{4,1} \\
&+4nS_{2,1,1} + 4n^2S_{2,2,1} - 24n^2S_{3,1,1} - 2n^2\zeta_5 + 3L_n + n\pi^2L_n + \frac{n^2\pi^4L_n}{18} + \frac{3{L_n}^2}{2} \\
&+\frac{n\pi^2{L_n}^2}{2} + {S_1}^2\Big(\frac{11}{2} - \frac{10}{n} + \frac{7n\pi^2}{6} - 7nS_2 + 4L_n\Big) + \zeta_3\Big(-4n - \frac{2n^2\pi^2}{3} - 6nL_n\Big) \\
&+S_{2,1}\Big(2n + \frac{2n^2\pi^2}{3} - 2nL_n\Big) + S_3\Big(-4 - \frac{2n^2\pi^2}{3} + 10nL_n\Big) + S_4\Big(11n - 10n^2L_n\Big) \\
&+{S_2}^2\Big(-6n + 2n^2L_n\Big) + S_{3,1}\Big(-24n + 8n^2L_n\Big) + S_2\Big(\frac{1}{2} - \frac{10}{n} + \frac{n\pi^2}{4} - 4n^2S_{2,1} \\
&+2L_n - 6nL_n - \frac{2n^2\pi^2L_n}{3} - 3n{L_n}^2\Big) + S_1\Big(3 - \frac{3}{n} - \frac{3\pi^2}{4} + n\pi^2 + \frac{n^2\pi^4}{18} + 2n^2{S_2}^2 \\
&-2nS_3 - 10n^2S_4 + 6nS_{2,1} + 8n^2S_{3,1} - 10n\zeta_3 + 9L_n + \frac{7n\pi^2L_n}{3} + 3{L_n}^2 \\
&+S_2\Big(9 - 6n - \frac{2n^2\pi^2}{3} - 14nL_n\Big)\Big)\Big)\Big]\Big\}.
\end{aligned}
$$

The result contains up to fifth-order harmonic sums. This can be understood again by counting the highest order of logarithms in the relevant potentials.

3.2.2 Coulomb and $1/r^2$ potential

The double insertion calculation of the Coulomb and the $1/r^2$ potential is similar to the single insertion of the $1/r^2$ potential. The insertion has an overall divergence coming from the diagram with no gluon exchange and a logarithmic divergence coming from the diagram with no gluon exchange on the left side of the $1/r^2$ potential insertion. Therefore, the diagram is divided into three parts (as shown in figure 3.5):

$$
I[\frac{1}{2} + \epsilon, 1 + \epsilon] = I_a[\frac{1}{2} + a\epsilon, 1 + \epsilon] + I_b[\frac{1}{2} + a\epsilon, 1 + \epsilon] + I_c[\frac{1}{2} + a\epsilon, 1 + \epsilon]. \tag{3.116}
$$

Each part appears only ones. Nevertheless, there is a symmetric diagram, which has the order of the two potentials interchanged. This will be considered in the final result, not at this stage.

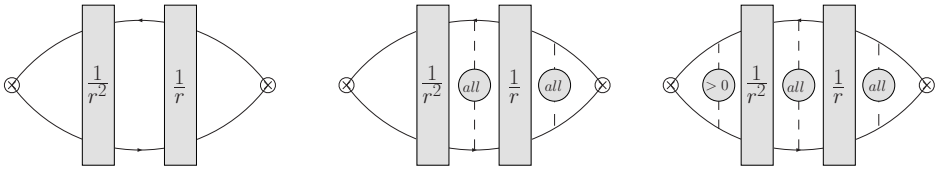

(a) (a+b) (c)

Figure 3.5: The 3 parts of the $\frac{1}{r^2}$ and Coulomb potential double insertion which have to be separated.

Part a

The first diagram without gluon exchange has an overall divergence and a divergence in the left subgraph. It can be done with Feynman parameters and the Mellin Barnes representation:

$$I_a[1+\epsilon,\frac{1}{2}+\epsilon] = \int \prod_{i=1}^{3} \frac{d^{d-1}\mathbf{p}_i}{(2\pi)^{d-1}} \frac{m}{\mathbf{p}_1^2 - mE} \frac{1}{[(\mathbf{p}_1-\mathbf{p}_2)^2]^{a_1}} \frac{m}{\mathbf{p}_2^2 - mE} \frac{1}{[(\mathbf{p}_2-\mathbf{p}_3)^2]^{a_2}} \frac{m}{\mathbf{p}_3^2 - mE} \tag{3.117}$$

$$= \int \frac{d^{d-1}\mathbf{p}}{(2\pi)^{d-1}} \int_0^1 dx \int_0^1 dy \frac{m^3}{(4\pi)^{d-1}} \frac{\Gamma(1+a_1-\frac{d-1}{2})\Gamma(1+a_2-\frac{d-1}{2})}{\Gamma(a_1)\Gamma(a_2)} \tag{3.118}$$
$$\frac{x^{a_1-1}(1-x)^{\frac{d-1}{2}-a_1-1} y^{a_2-1}(1-y)^{\frac{d-1}{2}-a_2-1}}{(x\mathbf{p}^2-mE)^{a_1+1-\frac{d-1}{2}}(y\mathbf{p}^2-mE)^{a_2+1-\frac{d-1}{2}}(\mathbf{p}^2-mE)}$$

$$= \left(\frac{1}{2\pi i}\right)^2 \int_{-i\infty}^{i\infty} dz_1 \int_{-i\infty}^{i\infty} dz_2 \Gamma(a_1+1-\frac{d-1}{2}+z_1)\Gamma(a_2+1-\frac{d-1}{2}+z_2)$$
$$\Gamma(-z_1)\Gamma(-z_2) \int \frac{d^{d-1}\mathbf{p}}{(2\pi)^{d-1}} \int_0^1 dx \int_0^1 dy \frac{m^3}{(4\pi)^{d-1}} \frac{1}{\Gamma(a_1)\Gamma(a_2)} \tag{3.119}$$
$$\frac{x^{\frac{d-1}{2}-z_1-2}(1-x)^{\frac{d-1}{2}-a_1-1} y^{\frac{d-1}{2}-z_2-2}(1-y)^{\frac{d-1}{2}-a_2-1}(-mE)^{z_1+z_2}}{(\mathbf{p}^2)^{a_1+a_2+z_1+z_2-d+3}(\mathbf{p}^2-mE)}$$

$$= \left(\frac{1}{2\pi i}\right)^2 \int_{-i\infty}^{i\infty} dz_1 \int_{-i\infty}^{i\infty} dz_2 \Gamma(a_1+1-\frac{d-1}{2}+z_1)\Gamma(a_2+1-\frac{d-1}{2}+z_2)\Gamma(-z_1)\Gamma(-z_2)$$
$$\frac{m^3}{(4\pi)^{d-1}} \frac{1}{\Gamma(a_1)\Gamma(a_2)} \frac{\Gamma(\frac{d-1}{2}-z_1-1)\Gamma(\frac{d-1}{2}-a_1)\Gamma(\frac{d-1}{2}-z_2-1)\Gamma(\frac{d-1}{2}-a_2)(-mE)^{z_1+z_2}}{\Gamma(d-2-a_1-z_1)\Gamma(d-2-a_2-z_2)}$$
$$\int_0^1 dx x^{\xi-1} \frac{\Gamma(\xi+1)}{\Gamma(\xi)} \int \frac{d^{d-1}\mathbf{p}}{(2\pi)^{d-1}} \frac{1}{(\mathbf{p}^2-mE(1-x))^{\xi+1}} \tag{3.120}$$

$$= \left(\frac{1}{2\pi i}\right)^2 \int_{-i\infty}^{i\infty} dz_1 \int_{-i\infty}^{i\infty} dz_2 \Gamma(a_1+1-\frac{d-1}{2}+z_1)\Gamma(a_2+1-\frac{d-1}{2}+z_2)\Gamma(-z_1)\Gamma(-z_2)$$
$$\frac{m^3}{(4\pi)^{d-1}} \frac{1}{\Gamma(a_1)\Gamma(a_2)} \frac{\Gamma(\frac{d-1}{2}-z_1-1)\Gamma(\frac{d-1}{2}-a_1)\Gamma(\frac{d-1}{2}-z_2-1)\Gamma(\frac{d-1}{2}-a_2)(-mE)^{z_1+z_2}}{\Gamma(d-2-a_1-z_1)\Gamma(d-2-a_2-z_2)}$$
$$\int_0^1 dx x^{\xi-1} \frac{\Gamma(\xi+1)}{\Gamma(\xi)} \frac{\Gamma(\xi+1-\frac{d-1}{2})(1-x)^{\frac{d-1}{2}-\xi-1}}{(4\pi)^{\frac{d-1}{2}}(-mE)^{\xi+1-\frac{d-1}{2}}\Gamma(\xi+1)} \tag{3.121}$$

$$= \left(\frac{1}{2\pi i}\right)^2 \int_{-i\infty}^{i\infty} dz_1 \int_{-i\infty}^{i\infty} dz_2 \Gamma(a_1+1-\frac{d-1}{2}+z_1)\Gamma(a_2+1-\frac{d-1}{2}+z_2)\Gamma(-z_1)\Gamma(-z_2)$$
$$\frac{m^3}{(4\pi)^{d-1}} \frac{1}{\Gamma(a_1)\Gamma(a_2)} \frac{\Gamma(\frac{d-1}{2}-z_1-1)\Gamma(\frac{d-1}{2}-a_1)\Gamma(\frac{d-1}{2}-z_2-1)\Gamma(\frac{d-1}{2}-a_2)(-mE)^{z_1+z_2}}{\Gamma(d-2-a_1-z_1)\Gamma(d-2-a_2-z_2)}$$
$$\frac{\Gamma(\xi+1-\frac{d-1}{2})\Gamma(\frac{d-1}{2}-\xi)}{(4\pi)^{\frac{d-1}{2}}(-mE)^{\xi+1-\frac{d-1}{2}}\Gamma(\frac{d-1}{2})}\,, \tag{3.122}$$

with $a_1 = \frac{1}{2}+\epsilon$, $a_2 = 1+\epsilon$ and $\xi = a_1+a_2+z_1+z_2-d+3$. Again, the integrals from the appendix have been used. Now, the values for $a_{1,2}$ and $d = 4-2\epsilon$ can be inserted and the result is:

$$I_a[1+\epsilon, \frac{1}{2}+\epsilon] = -\frac{4m^3\Gamma(\frac{1}{2}-2\epsilon)\Gamma(1-2\epsilon)}{(4\pi)^{13/2-3\epsilon}(-mE)^{5\epsilon}\Gamma(\frac{3}{2}-\epsilon)\Gamma(\frac{1}{2}+\epsilon)\Gamma(1+\epsilon)} \tag{3.123}$$
$$\int_{-i\infty}^{i\infty} dz_1 \int_{-i\infty}^{i\infty} dz_2 \frac{\Gamma(-z_1)\Gamma(-z_2)\Gamma(1-z_1-z_2-5\epsilon)\Gamma(z_1+2\epsilon)\Gamma(z_1+z_2+5\epsilon)}{\Gamma(\frac{3}{2}-z_1-3\epsilon)\Gamma(1-z_2-3\epsilon)}$$
$$\Gamma(\frac{1}{2}-z_1-\epsilon)\Gamma(\frac{1}{2}-z_2-\epsilon)\Gamma(\frac{1}{2}+z_2+2\epsilon)\,.$$

The λ dependence comes only in the $(-mE)$ part, so the Mellin Barnes integral is independent of λ. Therefore this integral can be easily done. The divergent part has been computed analytically, the remaining part numerically. This is because one needs for the imaginary part only the divergent contribution, which leads to logarithms of the energy if expanded. The complete result for the I-function, including the not needed real part, is given here for completeness:

$$I_a[1+\epsilon, \frac{1}{2}+\epsilon] = \frac{m^3}{1280\pi^4\epsilon^2} + \frac{m^3}{1280\pi^4\epsilon}\left(8-2\ln 2-5\ln(-4mE)\right) \tag{3.124}$$
$$+\frac{m^3}{128\pi^4}\left(\frac{5}{4}\ln^2(-4mE)+(\ln 2-4)\ln(-4mE)-\frac{\pi^2}{24}+\frac{26}{5}-\frac{8}{5}\ln 2+\frac{1}{5}\ln^2 2\right)$$
$$+\frac{m^3\epsilon}{256\pi^4}\Bigg(-\frac{25}{6}\ln^3(-4mE)-5(\ln 2-4)\ln^2(-4mE)$$
$$\ln(-4mE)\left(\frac{5\pi^2}{12}-52+16\ln 2-2\ln^2 2\right)+55.9293\Bigg)+O(\epsilon^2)\,.$$

This leads to the following J-function:

$$J_a[\frac{1}{2}+\epsilon, 1+\epsilon; w(\epsilon)] = \frac{mw}{8\pi^2\epsilon}\left[\frac{\delta^{(1)}G_C^{(0ex)}(E)}{4\pi C_F\alpha_s}\right] + \frac{m^3}{64\pi^4}\Bigg\{w\beta_0\left[(3-\ln 2)L_\lambda^2+\frac{4}{3}L_\lambda^3\right]$$
$$+wa_1\left[(3-\ln 2)L_\lambda+L_\lambda^2\right]+\frac{1}{2}w^{(\epsilon)}\beta_0 L_\lambda^2+\frac{1}{2}w^{(\epsilon)}a_1L_\lambda\Bigg\}\,, \tag{3.125}$$

where $\left[\frac{\delta^{(1)}G_C^{(0ex)}(E)}{4\pi C_F\alpha_s}\right] =< G_C^{(0ex)}[\frac{1}{q^2}\frac{\mu^{2\epsilon}}{q^{2\epsilon}}(\beta_0/\epsilon+a_1(\epsilon))]G_C^{(0ex)} >$ is the first-order correction to the Green function without gluon exchanges on both sides of the Coulomb potential. This

quantity has to be considered to all order in ϵ, because it multiplies a divergent part. It will add up to a full Green function in the final result for this part, and in the end it will cancel with other divergent parts.

Part b

This part is more complicated, because it has a divergence in the left subgraph. This is extracted in the same way as for the $1/r^2$-potential single insertion part c. First, the left subgraph is calculated in d dimensions. Then, the result is expanded in ϵ and the remaining (finite) part can be done in $d = 4$ dimensions. Again this automatically factorizes the divergences in the required form. For the finite part, the integral is Fourier transformed into coordinate space. For a shorter notation, the expressions for $I_{a+b}[\frac{1}{2}+\epsilon, 1+a\epsilon]$ is shown instead of $I_b[\frac{1}{2}+\epsilon, 1+a\epsilon]$, and $I_a[\frac{1}{2}+\epsilon, 1+a\epsilon]$ is subtracted in the end to get the correct result.

$$I_{a+b}[\frac{1}{2}+\epsilon, 1+a\epsilon] = \frac{m}{8\pi^2}\Bigg\{\left[\frac{1}{\epsilon}+2(1-\ln 2)\right]I[1+a\epsilon] - \int d^3\mathbf{r}\int_0^1 \frac{dx}{\sqrt{x}} \tag{3.126}$$
$$\int \frac{d^3\mathbf{p}}{(2\pi)^3} e^{i\mathbf{pr}} \ln(xp^2 - mE) \int d^3\mathbf{r}' G_C(r, r'; E) W(r') G_C(r', 0; E)\Bigg\}$$
$$= \frac{m}{8\pi^2}\left[\frac{1}{\epsilon}+2(1-\ln 2)\right]I[1+a\epsilon] + \frac{m^3}{128\pi^4}\int_0^\infty dr e^{-r\sqrt{-mE}}\int_0^1 \frac{dx}{\sqrt{x}} \tag{3.127}$$
$$\frac{\partial}{\partial u}\int_0^\infty dp \frac{2pr\sin(pr)}{\pi}\frac{1}{(xp^2-mE)^u}\sum_{j=1}^\infty \frac{L_{j-1}^{(1)}(2r\sqrt{-mE})H(a\epsilon, j)}{j(j-\lambda)},$$

with $W(r) = \frac{1}{4\pi\Gamma(1+2a\epsilon)\cos(\pi a\epsilon)}(r^2)^{a\epsilon-\frac{1}{2}}$. In the second step the derivative representation of the logarithm is used again. Then the first Green function is written using the Laguerre representation and for the second one the integral representation is used. The right subpart is the same as for the Coulomb double insertion, so the results from section 3.2.1 can be used and the p-integral performed, which already appeared in calculation the single insertion of the $1/r^2$-potential:

$$I_{a+b}[\frac{1}{2}+\epsilon, 1+a\epsilon] = \frac{m}{8\pi^2}\left[\frac{1}{\epsilon}+2(1-\ln 2)\right]I[1+a\epsilon] + \frac{m^3}{16\pi^2}\sum_{j=1}^\infty \frac{N(j)H(a\epsilon, j)}{j(j-\lambda)}, \tag{3.128}$$

where

$$N(j) := \frac{\partial}{\partial u}\left(\int_0^\infty dr e^{imvr}\frac{2^{\frac{5}{2}-u}r^{-\frac{1}{2}+u}(-mE)^{\frac{1}{4}-\frac{u}{2}}}{8\pi^2\sqrt{\pi}\Gamma(u)}K_{\frac{1}{2}-u}(r\sqrt{-mE})L_{j-1}^{(1)}(2r\sqrt{-mE})\right)_{u=0}. \tag{3.129}$$

This can be solved analytically:

$$N(j) = \frac{j}{2\pi^2}\left(1 - \hat{\Psi}(j+1) - \frac{1}{2}\ln(-4mE)\right). \tag{3.130}$$

The remaining sum with $N(j)$ and $H(a\epsilon, j)$ has still a divergence, because the first part of this insertion is included, so one has to subtract

$$I_a[\frac{1}{2}+\epsilon, 1+a\epsilon] = \lim_{\lambda\to 0} I_{(a+b)}[\frac{1}{2}+\epsilon, 1+a\epsilon]. \tag{3.131}$$

Then the imaginary part is finite:

$$\begin{aligned} I_b[\frac{1}{2}+\epsilon, 1+a\epsilon] = {} & \frac{m}{8\pi^2}\left[\frac{1}{\epsilon} + 2(1-\ln 2)\right] I_b[1+a\epsilon] \\ & + \frac{m^3}{64\pi^4}\sum_{j=1}^{\infty}\left[\frac{2-2\hat{\Psi}(1+j)-\ln(-4mE)}{j-\lambda} H(a\epsilon, j)\right. \\ & \left. - \lim_{\lambda\to 0}\frac{2-2\hat{\Psi}(1+j)-\ln(-4mE)}{j-\lambda} H(a\epsilon, j)\right]. \end{aligned} \tag{3.132}$$

Inserting the formulas for $H^{(i)}(j)$ (the expanded form of $H(a\epsilon, j)$) most parts of the sum can be done analytically. The results are

$$I_b[\frac{1}{2}+\epsilon, 1+a\epsilon] = \frac{m}{8\pi^2}\left\{\frac{1}{\epsilon} + 2(1-\ln 2)\right\} I_b[1] \tag{3.133}$$

$$\begin{aligned} & + \frac{m^3}{64\pi^4}\left\{\left[\ln(-4mE) - 2 + \hat{\Psi}(1-\lambda) - 2\lambda\Psi_1(1-\lambda)\right]\hat{\Psi}(1-\lambda)\right. \\ & \left. + \left[2\lambda - 3 - \lambda\ln(-4mE)\right]\Psi_1(1-\lambda) + \lambda\Psi_2(1-\lambda) + \frac{\pi^2}{2}\right\} \end{aligned} \tag{3.134}$$

$$\begin{aligned} & + a\epsilon\frac{m}{8\pi^2}\left\{\frac{1}{\epsilon} + 2(1-\ln 2)\right\} I_b[1+\epsilon] \\ & + a\epsilon\frac{m^3}{64\pi^4}\left\{\ln^2(-4mE)\Big(\lambda\Psi_1(1-\lambda) - \hat{\Psi}(1-\lambda)\Big) + 2\ln(-4mE)\Big(-\frac{\pi^2}{6} + \hat{\Psi}(1-\lambda)\right. \\ & - \hat{\Psi}(1-\lambda)^2 + (1-\lambda)\Psi_1(1-\lambda) - \lambda\Psi_2(1-\lambda) + 2\lambda\sum_{k=1}^{\infty}\frac{\hat{\Psi}(k-\lambda)}{(k-\lambda)^2}\Big) \\ & + 2\Big[-\frac{4}{3}\zeta_3 - \frac{\pi^2}{6} - \Big(\frac{\pi^2}{3} + \frac{2}{\lambda^2}\Big)\hat{\Psi}(1-\lambda) + \Big(1-\frac{2}{\lambda}\Big)\Big(\hat{\Psi}(1-\lambda)^2 + \Psi_1(1-\lambda)\Big) \\ & + \lambda\Psi_2(1-\lambda) - \lambda\Psi_1^2(1-\lambda) - \frac{2}{3}\Big(\hat{\Psi}(1-\lambda)^3 + \Psi_2(1-\lambda)\Big) + \frac{\lambda}{2}\Psi_3(1-\lambda) \\ & - 2\Big(1 + \lambda(-1+\hat{\Psi}(1-\lambda))\Big)\hat{\Psi}(1-\lambda)\Psi_1(1-\lambda) + 4\lambda\sum_{k=1}^{\infty}\frac{\hat{\Psi}(k)\hat{\Psi}(k-\lambda)}{(k-\lambda)^2} \\ & \left. + 2\sum_{k=1}^{\infty}\frac{(k+\lambda-2k\lambda)\hat{\Psi}(k-\lambda)}{k(k-\lambda)^2}\Big]\right\}. \end{aligned}$$

The remaining sums have to be calculated numerically. This can be done with high accuracy. The final result for the J function reads:

$$
\begin{aligned}
J_b[\frac{1}{2}+\epsilon,1+\epsilon;w(\epsilon)] &= \frac{mw}{8\pi^2\epsilon}\Big[\frac{\delta^{(1)}G_C^{(>0ex)}(E)}{4\pi C_F\alpha_s}\Big]+\frac{m}{8\pi^2}\Big(w^{(\epsilon)}+2(1-\ln 2)w\Big)J_b[1+\epsilon;\beta_0/\epsilon+a_1]\\
&+\frac{m^3w}{64\pi^4}\Big\{\beta_0\Big[4L_\lambda^2\Big(\lambda\Psi_1(1-\lambda)-\hat\Psi(1-\lambda)\Big)-4L_\lambda\Big(-\frac{\pi^2}{6}+\hat\Psi(1-\lambda)-\hat\Psi(1-\lambda)^2\\
&+(1-\lambda)\Psi_1(1-\lambda)-\lambda\Psi_2(1-\lambda)+2\lambda\sum_{k=1}^{\infty}\frac{\hat\Psi(k-\lambda)}{(k-\lambda)^2}\Big)\\
&+2\Big[-\frac{4}{3}\zeta_3-\frac{\pi^2}{6}-\Big(\frac{\pi^2}{3}+\frac{2}{\lambda^2}\Big)\hat\Psi(1-\lambda)+\Big(1-\frac{2}{\lambda}\Big)\Big(\hat\Psi(1-\lambda)^2+\Psi_1(1-\lambda)\Big)\\
&+\lambda\Psi_2(1-\lambda)-\lambda\Psi_1^2(1-\lambda)-\frac{2}{3}\Big(\hat\Psi(1-\lambda)^3+\Psi_2(1-\lambda)\Big)+\frac{\lambda}{2}\Psi_3(1-\lambda)\\
&-2\Big(1+\lambda(-1+\hat\Psi(1-\lambda))\Big)\hat\Psi(1-\lambda)\Psi_1(1-\lambda)+4\lambda\sum_{k=1}^{\infty}\frac{\hat\Psi(k)\hat\Psi(k-\lambda)}{(k-\lambda)^2}\\
&+2\sum_{k=1}^{\infty}\frac{(k+\lambda-2k\lambda)\hat\Psi(k-\lambda)}{k(k-\lambda)^2}\Big]\Big]\\
&+a_1\Big[\Big(-2L_\lambda-2+\hat\Psi(1-\lambda)-2\lambda\Psi_1(1-\lambda)\Big)\hat\Psi(1-\lambda)\\
&+\Big(2\lambda-3+2\lambda L_\lambda\Big)\Psi_1(1-\lambda)+\lambda\Psi_2(1-\lambda)+\frac{\pi^2}{2}\Big]\Big\},
\end{aligned}
\tag{3.135}
$$

where $\Big[\frac{\delta^{(1)}G_C^{(>0ex)}(E)}{4\pi C_F\alpha_s}\Big] =< G_C[\frac{1}{q^2}\frac{\mu^{2\epsilon}}{q^{2\epsilon}}(\beta_0/\epsilon+a_1(\epsilon))]G_C > -\Big[\frac{\delta^{(1)}G_C^{(0ex)}(E)}{4\pi C_F\alpha_s}\Big]$ is the first-order correction to the Green function with more than one gluon exchange.

Part c

This part is finite and can be calculated in $d=4$ dimensions. The procedure is the same as for the Coulomb double insertion, with the difference, that one has to subtract the Green functions without gluon exchange on the left side, and the exponent of the potential is $1/2+a\epsilon$ instead of $1+a\epsilon$. The result using the same functions from section 3.2.1 is:

$$
I_c[\frac{1}{2}+\epsilon,1+a\epsilon]=\Big(\frac{m}{4\pi}\Big)^3\frac{\lambda}{mC_F\alpha_s}\sum_{j=1}^{\infty}\frac{\bar H(-\frac{1}{2},j)H(a\epsilon,j)}{j(j-\lambda)}\,. \tag{3.136}
$$

$\bar H$ is a modified version of H and given by $\bar H = H-(H)_{\lambda\to 0}$. Then, $\bar H(-\frac{1}{2},j)$ can be calculated analytically:

$$
\bar H(-\frac{1}{2},j)=\frac{2mC_F\alpha_s}{\pi\lambda}\Big(j\hat\Psi(1+j)-(j-\lambda)\hat\Psi(j-\lambda)-\lambda\hat\Psi(-\lambda)\Big)\,. \tag{3.137}
$$

Inserting this result and the result from 3.2.1 into equation (3.136), most parts of the last summation could be done and the result is:

$$I_c[\frac{1}{2}+\epsilon,1+\epsilon] = \frac{m^3}{32\pi^4}\Big(-\frac{\pi^2}{6}+\Psi_1(1-\lambda)-\frac{\lambda}{2}\Psi_2(1-\lambda)\Big) \tag{3.138}$$
$$+a\epsilon\frac{m^3}{32\pi^4}\Big[\ln(-4mE)\Big(\frac{\pi^2}{6}-\Psi_1(1-\lambda)+\frac{\lambda}{2}\Psi_2(1-\lambda)\Big)-\frac{2}{\lambda}\hat{\Psi}(1-\lambda)^2$$
$$-\hat{\Psi}(1-\lambda)\Big(2\Psi_1(1-\lambda)+\lambda\Psi_2(1-\lambda)\Big)+\lambda\hat{\Psi}(1-\lambda)^2-2\hat{\Psi}(1-\lambda)^3-\frac{\lambda}{2}\Psi_3(1-\lambda)$$
$$+2\lambda\Big(1+2\lambda\hat{\Psi}(1-\lambda)\Big)\sum_{k=1}^{\infty}\frac{\hat{\Psi}(k-\lambda)}{k(k-\lambda)^2}+2\sum_{k=1}^{\infty}\frac{(k+\lambda)\hat{\Psi}(k-\lambda)}{k-\lambda}\Big(\frac{\hat{\Psi}(k-\lambda)}{k}-\frac{\hat{\Psi}(k)}{k-\lambda}\Big)\Big].$$

The final result for the J function reads:

$$J_c[\frac{1}{2}+\epsilon,1+\epsilon;w(\epsilon)] = \frac{m^3\beta_0 w}{32\pi^4}\Big[-2L_\lambda\Big(\frac{\pi^2}{6}-\Psi_1(1-\lambda)+\frac{\lambda}{2}\Psi_2(1-\lambda)\Big)-\frac{2}{\lambda}\hat{\Psi}(1-\lambda)^2$$
$$-\hat{\Psi}(1-\lambda)\Big(2\Psi_1(1-\lambda)+\lambda\Psi_2(1-\lambda)\Big)-2\hat{\Psi}(1-\lambda)^3+\lambda\Psi_1(1-\lambda)^2-\frac{\lambda}{2}\Psi_3(1-\lambda)$$
$$+2\lambda\Big(1+2\lambda\hat{\Psi}(1-\lambda)\Big)\sum_{k=1}^{\infty}\frac{\hat{\Psi}(k-\lambda)}{k(k-\lambda)^2}+2\sum_{k=1}^{\infty}\frac{(k+\lambda)\hat{\Psi}(k-\lambda)}{k-\lambda}\Big(\frac{\hat{\Psi}(k-\lambda)}{k}-\frac{\hat{\Psi}(k)}{k-\lambda}\Big)\Big]$$
$$+\frac{m^3 a_1 w}{32\pi^4}\Big[-\frac{\pi^2}{6}+\Psi_1(1-\lambda)-\frac{\lambda}{2}\Psi_2(1-\lambda)\Big]. \tag{3.139}$$

Poles

The last two parts have poles in the limit $\lambda \to n$. The calculation is straightforward and the result reads::

$$\hat{J}_b[\frac{1}{2}+\epsilon,1+\epsilon;w(\epsilon)] = \frac{mw}{8\pi^2\epsilon}\Big[\frac{\delta^{(1)}G_C(E)}{4\pi C_F\alpha_s}\Big]^{\lambda\to n}+\frac{m^3}{32\pi^4}\Big\{\frac{n}{(n-\lambda)^2}\Big[wa_1\Big(\frac{3}{2}+L_n-\frac{1}{2}\ln 2-S_1\Big)$$
$$+w\beta_0(3+2L_n-\ln 2-2S_1)(L_n+S_1)+\frac{\beta_0 w^{(\epsilon)}}{2}(L_n+S_1)+\frac{a_1 w^{(\epsilon)}}{4}\Big]$$
$$+\frac{1}{n-\lambda}\Big[-wa_1-w\beta_0\Big(3+n\pi^2-\ln 2-\frac{n\pi^2}{3}\ln 2+L_n\Big(4+\frac{2n\pi^2}{3}\Big)$$
$$+S_1\Big(6-\frac{2n\pi^2}{3}+4L_n-2\ln 2-4S_1+4nS_2\Big)+(2-6n-4nL_n+2n\ln 2)S_2$$
$$-4nS_3+4nS_{2,1}-4n\zeta_3\Big)-\beta_0 w^{(\epsilon)}\Big(\frac{1}{2}+n\frac{\pi^2}{6}+S_1-nS_2\Big)\Big]\Big\}, \tag{3.140}$$

$$\hat{J}_c[\frac{1}{2}+\epsilon,1+\epsilon;w(\epsilon)] = \frac{m^3}{32\pi^4}\Big\{\frac{a_1 wn+2\beta_0 wn(L_n+S_1)}{(n-\lambda)^3} \tag{3.141}$$
$$-\beta_0 w\Big(\frac{1}{(n-\lambda)^2}\Big(2+\frac{2n\pi^2}{3}+2S_1-4nS_2\Big)+\frac{\frac{1}{n}+4n\zeta_3+2S_2-4nS_3}{n-\lambda}\Big)\Big\}.$$

The first term in the expression for $\hat{J}_b$ is a divergent part, which is proportional to the single Coulomb insertion. This is expected, because such a divergence comes also from

the second-order correction to the short distance coefficient (which multiplies the first-order Green function). It is important to keep in mind that again the multiplicative part of the divergence, in this case the function $\hat{J}[1+\epsilon, \frac{\beta_0}{\epsilon} + a_1(\epsilon)]$ is kept to all orders in ϵ.

3.2.3 Coulomb and delta potential

The double insertion of the Coulomb potential and delta potential is easy to calculate, because the integral factorizes into two parts, which have already been calculated in the single insertion of the Coulomb potentials. This factorization can be done, because this is a double insertion of a tree level delta potential and a Coulomb potential and so, no factors of $(\mu^2/\mathbf{q}^2)$ appear in the delta potential (contrary to the single insertion at this order). The result for the insertion is then:

$$I[0, 1+a\epsilon] = G_C(E) I[1+a\epsilon]. \tag{3.142}$$

The divergences in the imaginary part of $I[0, 1+a\epsilon]$ come from divergences in the real parts of $I[0, 1+a\epsilon]$ and $G_C(E)$. In the J-function they are factorized in such a way, that they cancel the divergences from the hard Wilson coefficient:

$$\begin{aligned}
J[0, 1+\epsilon; w(\epsilon)] = {} & \frac{C_F \alpha_s m^2 w}{16\pi\epsilon}\Big[\frac{\delta^{(1)} G_C(E)}{4\pi C_F \alpha_s}\Big] - \frac{m^2 w \beta_0}{192\pi^2\epsilon^2} G_C(E) \\
& + \frac{m^2}{192\pi^2\epsilon} G_C(E)(2a_1 w - 2\beta_0 w - \beta_0 w^{(\epsilon)}) + \frac{C_F \alpha_s m^2 w^{(\epsilon)}}{16\pi} J[1+\epsilon, \beta_0/\epsilon + a_1(\epsilon)] \\
& + \frac{m^2}{192\pi^2} G_C(E)(2a_1 w^{(\epsilon)} - 2\beta_0 w^{(\epsilon)} - \beta_0 w^{(\epsilon^2)} + 2a_1^{(\epsilon)} w) \\
& + \frac{m^4 C_F \alpha_s w}{64\pi^3}\Bigg\{\beta_0\Bigg[L_\lambda^3 + L_\lambda^2\Big(\frac{1}{2} - \frac{1}{2\lambda} - 3\hat{\Psi}(1-\lambda) + 2\lambda\Psi_1(1-\lambda)\Big) \\
& + L_\lambda\Big(\frac{5\pi^2}{72} - \frac{1}{3} + (\lambda-4)\Psi_1(1-\lambda) + \lambda\Psi_2(1-\lambda) \\
& + \hat{\Psi}(1-\lambda)\Big(\frac{1}{\lambda} - 1 + 3\hat{\Psi}(1-\lambda) - 4\lambda\Psi_1(1-\lambda)\Big) + {}_4F_3(1,1,1,1;2,2,1-\lambda;1)\Big) \\
& + \Big(1 - \frac{1}{\lambda}\Big)\Big(\frac{5\pi^2}{144} - \frac{1}{6}\Big) + \hat{\Psi}(1-\lambda)\Big(\frac{1}{3} - \frac{5\pi^2}{72} + (4-\lambda)\Psi_1(1-\lambda) - \lambda\Psi_2(1-\lambda)\Big) \\
& + \hat{\Psi}(1-\lambda)^2\Big(\frac{1}{2} - \frac{1}{2\lambda} + 2\lambda\Psi_1(1-\lambda)\Big) - \hat{\Psi}(1-\lambda)^3 + \frac{3}{2\lambda}(1-\lambda)\Psi_1(1-\lambda) \\
& - \frac{1}{2}(1-\lambda)\Psi_2(1-\lambda) + 2{}_4F_3(1,1,1,1;2,2,1-\lambda;1)\Big(1 - \frac{1}{\lambda} - 2\hat{\Psi}(1-\lambda)\Big)\Bigg] \\
& + a_1\Bigg[L_\lambda^2 + L_\lambda\Big(\frac{5}{6} - \frac{1}{2\lambda} - 2\hat{\Psi}(1-\lambda) + \lambda\Psi_1(1-\lambda)\Big) + \Big(\frac{1}{2\lambda} - \frac{1}{2} + \hat{\Psi}(1-\lambda)\Big) \\
& \times\Big(-\frac{1}{3} + \hat{\Psi}(1-\lambda) - \lambda\Psi_1(1-\lambda)\Big)\Bigg]\Bigg\}.
\end{aligned} \tag{3.143}$$

The coefficients of the divergent parts are again understood in such a way, that they contain the full ϵ parts.

Poles

The calculation of the pole part is straightforward. The only difference to known poles is, that for the leading-order Green function one has to take the limit $\lambda \to n$ up to $(\lambda - n)^1$, because the function $I[1 + a\epsilon]$ has a double pole. The poles for $I[1 + a\epsilon]$ are needed up to $(\lambda - n)^0$ due to the single pole of $G(E)$. The result is:

$$\begin{aligned}
\hat{J}[0, 1+\epsilon; w(\epsilon)] = {} & \frac{C_F \alpha_s m^2 w}{16\pi\epsilon}\left[\frac{\delta^{(1)} G_C(E)}{4\pi C_F \alpha_s}\right]^{\lambda\to n} - \frac{m^2 w \beta_0}{192\pi^2\epsilon^2} G_C^{\lambda\to n}(E) \\
& + \frac{m^2}{192\pi^2\epsilon} G_C^{\lambda\to n}(E)(2a_1 w - 2\beta_0 w - \beta_0 w^{(\epsilon)}) + \frac{C_F\alpha_s m^2 w^{(\epsilon)}}{16\pi}\hat{J}[1+\epsilon, \beta_0/\epsilon + a_1(\epsilon)] \\
& + \frac{m^2}{192\pi^2} G_C^{\lambda\to n}(E)(2a_1 w^{(\epsilon)} + 2a_1^{(\epsilon)} w - 2\beta_0 w^{(\epsilon)} - \beta_0 w^{(\epsilon^2)}) \\
& + a_1 w \frac{m^4 C_F \alpha_s}{64\pi^3}\left[\frac{n}{(n-\lambda)^3} + \frac{\frac{1+n}{2} + nL_n - nS_1}{(n-\lambda)^2} + \frac{-\frac{2}{3} + \frac{1}{2n} + L_n - S_1}{(n-\lambda)}\right] \\
& + \beta_0 w \frac{m^4 C_F \alpha_s}{32\pi^3}\left[\frac{nL_n + nS_1}{(n-\lambda)^3} + \frac{-1 - \frac{n\pi^2}{3} + \frac{1+n}{2}L_n + nL_n^2 + \frac{n-3}{2}S_1 - nS_1^2 + 2nS_2}{(n-\lambda)^2}\right. \\
& + \frac{1}{2(n-\lambda)}\Big(-\frac{4}{3} - \frac{24n+7}{72}\pi^2 - \frac{2}{n} + S_1\Big(-2 - \frac{1}{n} + \frac{2n\pi^2}{3} + 5S_1 - 4nS_2\Big) \\
& \left. + S_2\Big(2n - 5\Big) + 8nS_3 - 4nS_{2,1} + L_n\Big(\frac{1}{n} - 4 - \frac{2n\pi^2}{3} - 6S_1 + 4nS_2 + L_n\Big)\Big)\right].
\end{aligned} \tag{3.144}$$

3.2.4 Coulomb and contact potential

The double insertion of the Coulomb potential with the contact term, which arises from using the equation of motion in section 2.4.2, is completely finite. Therefore, it can be easily obtained by using the result for $u = \frac{1}{2}$ from the Coulomb double insertion[1] from section 3.2.1:

$$I[\delta, 1+a\epsilon] = \int \prod_{i=1}^{5} \frac{d^{d-1}\mathbf{p}_i}{(2\pi)^{d-1}} \frac{G_C(\mathbf{p}_1, \mathbf{p}_2) G_C(\mathbf{p}_3, \mathbf{p}_4)}{[\mathbf{q}_{23}^2]^{a\epsilon+1}} G_C(\mathbf{p}_4, \mathbf{p}_5) \tag{3.145}$$

$$= \left(\frac{m}{4\pi}\right)^3 \frac{-\lambda}{m C_F \alpha_s} \sum_{j=1}^{\infty} \frac{H_\delta(j)[H^{(0)}(j) + a\epsilon H^{(1)}(j) + O(\epsilon^2)]}{j(j-\lambda)}, \tag{3.146}$$

where $\mathbf{q}_{23} = \mathbf{p}_2 - \mathbf{p}_3$, and

$$H_\delta(j) = \frac{-4\pi j\lambda}{\sqrt{-mE}(j-1-\lambda)(j-\lambda)(j+1-\lambda)}. \tag{3.147}$$

[1]Note, that H_δ is not exactly equal to H, because the Fourier transform of a delta potential is one, so $H_\delta(n) = 4\pi\cos(\pi u)\Gamma(1+2u)H(u,n)|_{u\to 1/2}$.

The remaining sum can be done only partially and a single sum is left in the result for $I[\delta, 1 + a\epsilon]$:

$$\begin{aligned} I[\delta,1+a\epsilon] &= \frac{m\lambda^2}{16\pi^2 C_F^2\alpha_s^2}\Big(1+2\lambda\Psi_1(1-\lambda)-\lambda^2\Psi_2(1-\lambda)\Big) \\ &+a\epsilon\frac{m\lambda^3}{8\pi^2 C_F^2\alpha_s^2}\Big[-\hat{\Psi}(1-\lambda)\Big(\frac{1}{\lambda}+\lambda\Psi_2(1-\lambda)\Big)-\frac{1}{3}\lambda\Psi_3(1-\lambda)+\Psi_1(1-\lambda) \\ &+\sum_{k=1}^{\infty}\frac{2(k+\lambda)\hat{\Psi}(k-\lambda)}{(\lambda-k)^3}+L_\lambda\Big(\frac{1}{\lambda}+2\Psi_1(1-\lambda)-\lambda\Psi_2(1-\lambda)\Big)\Big]. \end{aligned} \tag{3.148}$$

The order ϵ terms are kept, they multiply the β_0 dependent part of the Coulomb potential. They come only from the potential, not from the measure of the integral. This is, because parts of the Coulomb results where used here, where a subtraction is performed implicitly. The complete counter term subtracted result for the J-function is:

$$\begin{aligned} J[\delta,1+\epsilon;w] &= \frac{m\beta_0 w\lambda^3}{8\pi^2 C_F^2\alpha_s^2}\Big[-\hat{\Psi}(1-\lambda)\Big(\frac{1}{\lambda}+\lambda\Psi_2(1-\lambda)\Big)-\frac{1}{3}\lambda\Psi_3(1-\lambda) \\ &+\Psi_1(1-\lambda)+\sum_{k=1}^{\infty}\frac{2(k+\lambda)\hat{\Psi}(k-\lambda)}{(\lambda-k)^3}+L_\lambda\Big(\frac{1}{\lambda}+2\Psi_1(1-\lambda)-\lambda\Psi_2(1-\lambda)\Big)\Big] \\ &+\frac{ma_1 w\lambda^2}{16\pi^2 C_F^2\alpha_s^2}\Big(1+2\lambda\Psi_1(1-\lambda)-\lambda^2\Psi_2(1-\lambda)\Big). \end{aligned} \tag{3.149}$$

The remaining sum shows again a good convergence and will be calculated numerically with Mathematica (without a cutoff for the upper limit using Mathematica's `NSum` function).

Poles

The pole parts of this insertions are relatively easy to calculate and read:

$$\begin{aligned} \hat{J}[\delta,1+\epsilon;w] &= \frac{mw}{8\pi^2 C_F^2\alpha_s^2}\Big[a_1\Big(\frac{n^4}{(n-\lambda)^3}-\frac{3n^3}{(n-\lambda)^2}+\frac{3n^2}{n-\lambda}\Big)+\beta_0\Big(\frac{2n^4(L_n+S_1)}{(n-\lambda)^3} \\ &-\frac{n^3(3+18L_n+n\pi^2+24S_1-6nS_2)}{3(n-\lambda)^2}+\frac{n^2(3+6L_n+n\pi^2+12S_1-6nS_2)}{n-\lambda}\Big)\Big] \end{aligned} \tag{3.150}$$

The result is, as one would expect, similar to the Coulomb double insertion and contains up to second-order harmonic sums.

3.3 Triple insertions

The triple insertion part is only needed for the first-order correction to the Coulomb potential at third order. Triple insertion combinations with other potentials appear first only at fourth order.

3.3.1 Coulomb potential

The triple insertion is completely finite and is done in $d = 4$ dimensions. This calculation was done in [85] and details of the calculation were published in [35]. For completeness, some details are presented here again. The potential is generated once more by working with

$$W_i(\boldsymbol{r}_i) = \frac{1}{4\pi\Gamma(1+2u_i)\cos(\pi u_i)} \left(\boldsymbol{r}_i^2\right)^{u_i-\frac{1}{2}} , \tag{3.151}$$

and by taking the zeroth and first derivative with respect to the u_i at $u_i = 0$. The threefold insertion of the generating potential reads

$$\begin{aligned} I[1+u_1, 1+u_2, 1+u_3] &= \int \prod_{i=1}^{3} d^3\boldsymbol{r}_i \, G_C(0, \boldsymbol{r}_1; E) W_1(\boldsymbol{r}_1) G_C(\boldsymbol{r}_1, \boldsymbol{r}_2; E) \\ &\quad W_2(\boldsymbol{r}_2) G_C(\boldsymbol{r}_2, \boldsymbol{r}_3; E) W_3(\boldsymbol{r}_3) G_C(\boldsymbol{r}_3, 0; E) \qquad (3.152) \\ &= \int dr_1 dr_2 dr_3 \, \frac{r_1^{2u_1+1}}{\Gamma(1+2u_1)\cos(\pi u_1)} \frac{r_2^{2u_2+1}}{\Gamma(1+2u_2)\cos(\pi u_2)} \frac{r_3^{2u_3+1}}{\Gamma(1+2u_3)\cos(\pi u_3)} \\ &\quad \times \Big\{ G_C(0, r_1, E) G_C(r_1, r_2, E) G_C(r_2, r_3, E) G_C(0, r_3, E) \Big\} . \qquad (3.153) \end{aligned}$$

For the leading-order S-wave Coulomb Green functions, the integral representation for Green functions is used near the vertex and the sum representation for Green function between two potentials and one obtains:

$$I[1+u_1, 1+u_2, 1+u_3] = \left(\frac{m}{4\pi}\right)^4 \sum_{n=1}^{\infty} \sum_{j=1}^{\infty} \frac{H(u_1, n) K(u_2, n, j) H(u_3, j)}{n(n-\lambda) j(j-\lambda)}, \tag{3.154}$$

where the H functions here are the same as the ones presented in the Coulomb double insertion section. For the functions $K(u, n, j)$ the expansion up to the first order in u is needed (denoted with $K^{(i)}(n, j)$, where the superscript i stands for the order of the expansion and the argument u is omitted for simplicity). Then, the result is:

$$K^{(0)}(j, k) = \lambda^2 j \delta_{jk} , \tag{3.155}$$

$$K^{(1)}(j, k) = \lambda^2 \Big[I + 2j \, \delta_{nj} \left(\gamma_E + L_\lambda\right) \Big] , \tag{3.156}$$

with

$$I = \int_0^\infty ds \, 2s \ln(s) e^{-s} L_{k-1}^{(1)}(s) L_{j-1}^{(1)}(s). \tag{3.157}$$

To solve the integral I, the Laguerre polynomials are expressed through their generating functions. Then, with

$$\frac{e^{-\frac{z\,u}{1-u}}}{(1-u)^2} = \sum_{s=0}^{\infty} u^s L_s^{(1)}(z), \tag{3.158}$$

and

$$\int_0^\infty ds\, 2s\ln(s)e^{-s}\frac{e^{-\frac{s\,v}{1-v}}}{(1-v)^2}\frac{e^{-\frac{s\,w}{1-w}}}{(1-w)^2} = -\frac{2\Big[-1+\gamma_E+\ln\Big(\frac{1-vw}{(v-1)(w-1)}\Big)\Big]}{(vw-1)^2}, \tag{3.159}$$

the integral I is expressed as

$$\begin{aligned} I &= \frac{1}{(k-1)!}\frac{1}{(j-1)!}\frac{\partial^{k-1}}{\partial v^{k-1}}\frac{\partial^{j-1}}{\partial w^{j-1}}\left[-\frac{2\Big(-1+\gamma_E+\ln\Big(\frac{1-vw}{(v-1)(w-1)}\Big)\Big)}{(vw-1)^2}\right]_{v=w=0} \\ &= \begin{cases} 2+2k\Psi(k) & \text{if } k=j \\ -2\dfrac{\min(k,j)}{|j-k|} & \text{if } k\neq j \quad . \end{cases} \end{aligned} \tag{3.160}$$

Hence, the final result for $K^{(1)}(j,k)$ reads

$$K^{(1)}(j,k) = 2\lambda^2\begin{cases} 1+j[\hat{\Psi}(j)+L_\lambda] & \text{if } j=k \\ -\dfrac{\min(j,k)}{|k-j|} & \text{if } j\neq k \quad . \end{cases} \tag{3.161}$$

At this point, the threefold insertion of the perturbation potential has been expressed in terms of a double sum involving only Psi-functions. These sums converge rapidly when the energy argument is evaluated along a line parallel to the real axis as required in the calculation of the top quark pair production cross section. The final result for the J function is:

$$\begin{aligned} J^{(C)}[1,1,1;a_1+\beta_0 L_q] = \frac{m^2}{(4\pi)^4 C_F^2\alpha_s^2}\Bigg[&\beta_0^3\sum_{j=1}^\infty\sum_{k=1}^\infty\frac{H^{(1)}(j)K^{(1)}(j,k)H^{(1)}(k)}{j(j-\lambda)k(k-\lambda)} \\ &+\beta_0^2 a_1\sum_{j=1}^\infty\sum_{k=1}^\infty\frac{2H^{(0)}(j)K^{(1)}(j,k)H^{(1)}(k)+H^{(1)}(j)K^{(0)}(j,k)H^{(1)}(k)}{j(j-\lambda)k(k-\lambda)} \\ &+\beta_0 a_1^2\sum_{j=1}^\infty\sum_{k=1}^\infty\frac{2H^{(0)}(j)K^{(0)}(j,k)H^{(1)}(k)+H^{(0)}(j)K^{(1)}(j,k)H^{(0)}(k)}{j(j-\lambda)k(k-\lambda)} \\ &+a_1^3\frac{\lambda^2}{2}\Big(-\Psi_2(1-\lambda)+\frac{\lambda}{3}\Psi_3(1-\lambda)\Big)\Bigg]. \end{aligned} \tag{3.162}$$

The double sums can be in principal evaluated numerically. Here, some parts of the sum can be calculated analytically to make the calculation faster. The result for the partly analytic result is very lengthy and not given here. It can be found in the file `TTbarXSection.m`.

Poles

The pole part of the triple insertion is the most complicated one. After a long and cumbersome reduction, the result could be expressed with harmonic sums and reads:

$$\hat{J}[1,1,1;a_1+\beta_0 L_q] = \frac{m^2}{256\pi^4 C_F^2\alpha_s^2}\Bigg\{\frac{n^3}{(n-\lambda)^4}\Big[a_1+2\beta_0(L_n+S_1)\Big]^3 \tag{3.163}$$

$$
-\frac{n^2}{(n-\lambda)^3}\Bigg[2a_1^3+2a_1^2\beta_0\Big(3+6L_n+\frac{n\pi^2}{3}+8S_1-2nS_2\Big)+8a_1\beta_0^2\Big(\frac{\pi^2}{6}+3L_n
$$
$$
+\frac{n\pi^2L_n}{3}+3{L_n}^2+3S_1-\frac{S_1}{n}+\frac{n\pi^2S_1}{3}+8L_nS_1+5{S_1}^2-S_2-2nL_nS_2-2nS_1S_2
$$
$$
+nS_3-n\zeta_3\Big)+16\beta_0^3\Big(\frac{\pi^2L_n}{6}+\frac{3{L_n}^2}{2}+\frac{n\pi^2{L_n}^2}{6}+{L_n}^3+\frac{\pi^2S_1}{6}+3L_nS_1-\frac{L_nS_1}{n}
$$
$$
+\frac{n\pi^2L_nS_1}{3}+4{L_n}^2S_1+\frac{3{S_1}^2}{2}-\frac{{S_1}^2}{n}+\frac{n\pi^2{S_1}^2}{6}+5L_n{S_1}^2+2{S_1}^3-L_nS_2-n{L_n}^2S_2
$$
$$
-S_1S_2-2nL_nS_1S_2-n{S_1}^2S_2+nL_nS_3+nS_1S_3-nL_n\zeta_3-nS_1\zeta_3\Big)\Bigg]
$$
$$
+\frac{n}{(n-\lambda)^2}\Bigg[a_1^3+a_1^2\beta_0\Big(9+\frac{4\,n\,\pi^2}{3}+6\,L_n+14\,S_1-8\,n\,S_2\Big)+4a_1\beta_0^2\Big(3+\frac{\pi^2}{2}+\frac{2n\pi^2}{3}
$$
$$
+\frac{n^2\pi^4}{36}+9L_n+\frac{4n\pi^2L_n}{3}+3{L_n}^2+13S_1-\frac{3S_1}{n}+2n\pi^2S_1+14L_nS_1+11{S_1}^2-3S_2
$$
$$
-4nS_2-\frac{n^2\pi^2S_2}{3}-8nL_nS_2-12nS_1S_2+n^2{S_2}^2+9nS_3-5n^2S_4-2nS_{2,1}+4n^2S_{3,1}
$$
$$
-5n\zeta_3\Big)+8\beta_0^3\Big(\frac{\pi^2}{3}+\frac{5n\pi^4}{72}+\Big(\frac{9}{2}+\frac{2n\pi^2}{3}\Big){L_n}^2+{L_n}^3+5{S_1}^3+\Big(\frac{5n}{2}+n^2L_n\Big){S_2}^2
$$
$$
+{S_1}^2\Big(\frac{17}{2}-\frac{3}{n}+\frac{4n\pi^2}{3}+11L_n-8nS_2\Big)+\Big(2n+\frac{5n^2\pi^2}{6}+9nL_n\Big)S_3
$$
$$
-5n\Big(\frac{1}{2}+nL_n\Big)S_4+3n^2S_5+\Big(1-2nL_n\Big)S_{2,1}+\Big(2n+4n^2L_n\Big)S_{3,1}-2n^2S_{3,2}
$$
$$
-6n^2S_{4,1}+\Big(-2-2n-\frac{5n^2\pi^2}{6}\Big)\zeta_3+S_1\Big(3-\frac{2}{n}+\frac{\pi^2}{6}+\frac{2n\pi^2}{3}+\frac{n^2\pi^4}{36}
$$
$$
+\Big(13-\frac{3}{n}+2n\pi^2\Big)L_n+7{L_n}^2+\Big(-1-4n-\frac{n^2\pi^2}{3}-12nL_n\Big)S_2+n^2{S_2}^2+11nS_3
$$
$$
-5n^2S_4-2nS_{2,1}+4n^2S_{3,1}-7n\zeta_3\Big)+L_n\Big(3+\frac{\pi^2}{2}+\frac{2n\pi^2}{3}+\frac{n^2\pi^4}{36}-5n\zeta_3\Big)
$$
$$
+S_2\Big(-2+\frac{1}{n}-\frac{5n\pi^2}{6}+\Big(-3-4n-\frac{n^2\pi^2}{3}\Big)L_n-4n{L_n}^2-n^2S_3+n^2\zeta_3\Big)+6n^2\zeta_5\Big)\Bigg]
$$
$$
-\frac{1}{n-\lambda}\Bigg[2a_1^2\beta_0\Big(1+\frac{n\pi^2}{3}+2S_1-2nS_2\Big)+4a_1\beta_0^2\Big(3+n\pi^2+\frac{n^2\pi^4}{18}+\Big(2+\frac{2n\pi^2}{3}\Big)L_n
$$
$$
+4{S_1}^2+\Big(-6n-\frac{2n^2\pi^2}{3}-4nL_n\Big)S_2+2n^2{S_2}^2+S_1\Big(8+2n\pi^2+4L_n-12nS_2\Big)
$$
$$
+12nS_3-10n^2S_4-4nS_{2,1}+8n^2S_{3,1}-4n\zeta_3\Big)+8\beta_0^3\Big(1+\frac{\pi^2}{3}+\frac{n\pi^2}{3}+\frac{8n\pi^4}{45}+\frac{n^2\pi^4}{36}
$$
$$
-\frac{n^3\pi^6}{210}+\Big(1+\frac{n\pi^2}{3}\Big){L_n}^2+2{S_1}^3+\Big(4n+n^2+2n^2L_n\Big){S_2}^2+{S_1}^2\Big(7-\frac{8}{n}+\frac{5n\pi^2}{3}
$$
$$
+4L_n-10nS_2\Big)+6n^3{S_3}^2+\Big(-6n-5n^2-\frac{8n^3\pi^2}{3}-10n^2L_n\Big)S_4+24n^2S_5
$$
$$
-14n^3S_6+\frac{16S_{1,1}}{n}+\Big(-2n-\frac{2n^2\pi^2}{3}-4nL_n\Big)S_{2,1}+\Big(4n^2+\frac{4n^3\pi^2}{3}+8n^2L_n\Big)S_{3,1}
$$
$$
-14n^2S_{3,2}-34n^2S_{4,1}+28n^3S_{4,2}+40n^3S_{5,1}+8n^2S_{3,1,1}-8n^3S_{3,1,2}-8n^3S_{3,2,1}
$$

$$-24n^3S_{4,1,1}+\Big(-4n-\frac{7n^2\pi^2}{3}\Big)\zeta_3+2n^3{\zeta_3}^2+S_1\Big(5-\frac{2}{n}-\frac{2\pi^2}{3}+\frac{5n\pi^2}{3}+\frac{n^2\pi^4}{9}$$
$$+\Big(8+2n\pi^2\Big)L_n+2{L_n}^2+\Big(4-10n-\frac{4n^2\pi^2}{3}-12nL_n\Big)S_2+4n^2{S_2}^2+16nS_3$$
$$-20n^2S_4-4nS_{2,1}+16n^2S_{3,1}-8n\zeta_3\Big)+L_n\Big(3+n\pi^2+\frac{n^2\pi^4}{18}-4n\zeta_3\Big)$$
$$-2S_2\Big(1+\frac{4}{n}+n+\frac{2n\pi^2}{3}+\frac{n^2\pi^2}{6}+\Big(3n+\frac{n^2\pi^2}{3}\Big)L_n+n{L_n}^2+6n^2S_3-2n^2S_{2,1}$$
$$-2n^2\zeta_3\Big)+S_3\Big(-2+8n+\frac{11n^2\pi^2}{3}+12nL_n-4n^3\zeta_3\Big)+19n^2\zeta_5\Big)\Big]\Big\}.$$

There are up to triple nested sums in this result, and the highest order of the harmonic sums is six. Some useful relations which were used here are given in appendix C.1.

3.4 Summary of results for the S-wave Green function

In this section, the results for the Green function corrections are summarized in terms of the master functions J and I, which have been calculated in the previous sections. The Green function expanded in the strong coupling constant is given in the following notation:

$$G(E)=G_C(E)+\sum_i\left(\frac{\alpha_s}{4\pi}\right)^i\delta^{(i)}G(E)\,. \tag{3.164}$$

The leading-order Green function has been discussed in 2.4.1 and reads:

$$G_C(E)=\frac{m^2\alpha_sC_F}{4\pi}\Big(L_\lambda+\frac{1}{2}-\frac{1}{2\lambda}-\hat{\Psi}(1-\lambda)\Big)\,. \tag{3.165}$$

The first-order corrections include only the single insertion of the Coulomb potential

$$-\frac{4\pi C_F\alpha_s}{\mathbf{q}^2}(a_1+\beta_0\ln\frac{\mu^2}{\mathbf{q}^2})\,. \tag{3.166}$$

So, expressed in terms of the master functions this is

$$\delta^{(1)}G(E)=4\pi\alpha_sC_FJ^{(C)}[1;a_1+\beta_0L_q]\,. \tag{3.167}$$

In the non-relativistic power counting, at second order, one has to include the single and double insertion of the Coulomb potential (first and second line of equation (3.168)) and insertions of the $1/r^2$, delta and $\mathbf{p}^2$ potential (third and forth line in (3.168)), as well as the kinetic correction (last line in (3.168)). The last two parts have been reduced with the equation of motion (as described in section 2.4.2) and the result is:

$$\delta^{(2)}G(E)=4\pi\alpha_sC_FJ^{(C)}[1;a_2+(2a_1\beta_0+\beta_1)L_q+\beta_0^2L_q^2] \tag{3.168}$$

$$
\begin{aligned}
&+(4\pi\alpha_s C_F)^2 J^{(C)}[1,1;a_1+\beta_0 L_q] \\
&-\frac{(2\pi)^4 C_F}{m} J[\frac{1}{2}+\epsilon; b_1(\epsilon)] + \frac{(4\pi)^3 C_F}{\alpha_s m^2} J[0; v_0(\epsilon)] \\
&-\Big(\frac{16\pi^3 C_F^3 \alpha_s}{\lambda^2} J[1;1] - \frac{32\pi^4 C_F^2}{m} J[\frac{1}{2}+\epsilon; k(0)]\Big) \\
&+\Big(\frac{m C_F^4 \alpha_s^2 \pi^2}{4\lambda^4} J[\delta;1] - \frac{2\pi^2 C_F^2}{\lambda^2} G_C(E) - \frac{8\pi^3 C_F^3 \alpha_s}{\lambda^2} I[1] + (2\pi)^4 \frac{C_F^2}{2m} J[\frac{1}{2}+\epsilon; k(0)]\Big)\,.
\end{aligned}
$$

The function $k(0)$ comes from an integration after using the equation of motion and the definition is given in (2.118). At third order, corrections coming from single, double and triple insertions have to be taken into account. The corrections read:

$$
\begin{aligned}
&\delta^{(3)} G(E) = \qquad (3.169)\\
&\Big\{4\pi\alpha_s C_F J^{(C)}[1; a_3 + (2a_1\beta_1+\beta_2+3a_2\beta_0+8\pi^2 C_A^3) L_q + (\frac{5}{2}\beta_0\beta_1 + 3a_1\beta_0^2) L_q^2 + \beta_0^3 L_q^3] \\
&-\frac{4(2\pi)^4 C_F}{m}\Big(J[\frac{1}{2}+2\epsilon; \frac{1}{2\epsilon}\Big(\beta_0 b_1(\epsilon) - \frac{8}{3} C_F C_A - \frac{4}{3} C_A^2\Big) + b_2(\epsilon)] - J[\frac{1}{2}+\epsilon; \frac{\beta_0 b_1(\epsilon)}{2\epsilon}]\Big) \\
&+\frac{(4\pi)^3 C_F}{\alpha_s m^2}\Big(J[\epsilon; \frac{1}{\epsilon}\Big(\frac{7}{3} C_F - \frac{11}{6} C_A + \beta_0 v_0(\epsilon)\Big) + v_q^{(1)}(\epsilon)] \\
&+J[0; \Big(\frac{\mu^2}{m^2}\Big)^\epsilon v_m^{(1)}(\epsilon) + \Big[\Big(\frac{\mu^2}{m^2}\Big)^\epsilon - 1\Big]\frac{1}{\epsilon}\Big(\frac{C_F}{3}+\frac{C_A}{2}\Big) - \frac{1}{\epsilon}\beta_0 v_0(\epsilon)]\Big) \\
&+\frac{2(2\pi)^4 C_F^2}{m}\Big(-\frac{m C_F \alpha_s}{2\pi\lambda^2} J[1+\epsilon; \frac{1}{\epsilon}\Big(\frac{8}{3} C_A + \beta_0\Big) + v_p^{(1)}(\epsilon)] \\
&+J[\frac{1}{2}+2\epsilon; \frac{k(\epsilon)}{\epsilon}\Big(\frac{8}{3} C_A + \beta_0\Big) + v_p^{(1)}(\epsilon) k(\epsilon)] - J[\frac{1}{2}+\epsilon; \frac{k(0)}{\epsilon}\Big(\frac{8}{3} C_A + \beta_0\Big)]\Big)\Big\} \\
&+\Big\{2(4\pi\alpha_s C_F)^2 J^{(C)}[1,1; a_2 + (2a_1\beta_0+\beta_1) L_q + \beta_0^2 L_q^2] \\
&-\frac{4 C_F^2 \alpha_s (2\pi)^5}{m} J[\frac{1}{2}+\epsilon, 1+\epsilon; b_1(\epsilon)] + \frac{2(4\pi)^4 C_F^2}{m^2} J[0, 1+\epsilon; v_0(\epsilon)] \\
&+\Big(-\frac{(4\pi)^4 C_F^4 \alpha_s^2}{2\lambda^2} J[1, 1+\epsilon; 1] + \frac{256\pi^5 C_F^3 \alpha_s}{m} J[\frac{1}{2}+\epsilon, 1+\epsilon; k(0)] \\
&+\frac{32\pi^4 C_F^2}{m}(J[\frac{1}{2}+2\epsilon; k(\epsilon)(\beta_0/\epsilon + a_1(\epsilon))] - J[\frac{1}{2}+\epsilon; k(0)\beta_0/\epsilon])\Big) \\
&+2\pi C_F \alpha_s\Big(\frac{m C_F^4 \alpha_s^2 \pi^2}{\lambda^4} J[\delta, 1+\epsilon; 1] - \frac{8\pi^2 C_F^2}{\lambda^2} J[1+\epsilon; \beta_0/\epsilon + a_1(\epsilon)] \\
&-\frac{32\pi^3 C_F^3 \alpha_s}{\lambda^2} J[1, 1+\epsilon; 1] + 32\pi^4 \frac{C_F^2}{m} J[\frac{1}{2}+\epsilon, 1+\epsilon; k(0)] \\
&+8\pi^3 \frac{C_F}{\alpha_s m}(J[\frac{1}{2}+2\epsilon; k(\epsilon)(\beta_0/\epsilon + a_1(\epsilon))] - J[\frac{1}{2}+\epsilon; k(0)\beta_0/\epsilon])\Big)\Big\} \\
&+(4\pi\alpha_s C_F)^3 J^{(C)}[1,1,1; a_1+\beta_0 L_q]\,.
\end{aligned}
$$

The first (second) {}-bracket shows the single (double) insertions and the last line is the triple Coulomb insertion. Again, the $\mathbf{p}^2$ potential (first ()-bracket of the single and double insertion)

and the kinetic correction (second ()-bracket the double insertion) have been reduced with the equation of motion. Note, that there is no contribution from the kinetic correction to the single insertion part at third order. For the $1/r^2$ insertion, there appear parts of the form

$$\left[\left(\frac{\mu^2}{\mathbf{q^2}}\right)^{2\epsilon} - \left(\frac{\mu^2}{\mathbf{q^2}}\right)^{\epsilon}\right]. \tag{3.170}$$

These do not correspond to the definition of $J[1/2+a\epsilon]$, because there one always subtracts 1 from $(\mu^2/\mathbf{q^2})^{\mathbf{a}\epsilon}$ (see equation (3.5)). Therefore, the combination $(J[1/2+2\epsilon,...]-J[1/2+\epsilon,...])$ is used to recover the form of equation (3.170).

The second- and third-order results are still divergent. Only the combination with the ultrasoft corrections (at third order) and the parts coming from the external current will be finite (in the $\Gamma \to 0$ limit). The divergent part of the second-order Green function reads:

$$\delta^{(2)}G_{div} = \frac{(4\pi)^2 C_F}{6\epsilon}\left(C_F + \frac{3}{2}C_A\right) G_C(E) + \frac{2\pi\, m C_F}{\epsilon}\left(\frac{i\,\Gamma}{\alpha_s}\right). \tag{3.171}$$

The divergent third-order part of the potential insertions is:

$$\begin{aligned}
\delta^{(3)}G_{div} = \Bigg[& -\frac{1}{\epsilon^2}\left(\frac{7}{72}C_F^2 + \frac{2}{9}C_A^2 + \frac{23}{48}C_A C_F + \beta_0\left(\frac{C_A}{24}+\frac{C_F}{36}\right)\right) \\
& -\frac{1}{\epsilon}\Bigg\{\left(\frac{11}{24}-\frac{L_m}{12}\right)C_F^2 + \left(\frac{427}{324}-\frac{4\ln 2}{3}-\frac{L_m}{8}\right)C_A C_F - \left(\frac{5}{216}+\frac{2\ln 2}{3}\right)C_A^2 \\
& +\left(\frac{C_A}{24}+\frac{C_F}{54}\right)\beta_0 - \left(\frac{1}{30}-\frac{29\,n_f}{162}\right)C_F T_F + \frac{49}{216}C_A T_F n_f\Bigg\}\Bigg] 4(4\pi)^2 C_F\, G_C(E) \\
& +\left[\frac{1}{4}C_A + \frac{1}{6}C_F\right]\frac{(4\pi)^2 C_F}{\epsilon}\,\delta^{(1)}G(E) \\
& -\pi m C_F\left(\frac{i\,\Gamma}{\alpha_s}\right)\left[\frac{8C_A+15\beta_0}{9\epsilon^2} + \frac{84C_F - 388C_A + 200 n_f T_F + 66\beta_0}{27\epsilon}\right],
\end{aligned} \tag{3.172}$$

with $L_m = \ln(\mu/m)$. An additional source of divergence in the imaginary part comes from the energy dependent external current from equation (2.5). It is at second order:

$$\left(\frac{4\pi}{\alpha_s}\right)^2 \mathrm{Im}\Big(-\frac{4E}{3m}G_C(E)\Big) = -\frac{\Gamma}{\epsilon}\frac{4\pi C_F m}{3\alpha_s}, \tag{3.173}$$

and at third order:

$$\left(\frac{4\pi}{\alpha_s}\right)^3 \mathrm{Im}\Big(-\frac{E}{3m}(4c_v^{(1)}G_C(E) + d_v^{(1)} + 4\delta^{(1)}G(E))\Big) = \frac{\Gamma}{\epsilon}\frac{16\pi C_F m}{27\alpha_s}(21C_F - 5C_A + 4n_l T_F). \tag{3.174}$$

The cancelation of the divergent part with the vertex correction and the ultrasoft correction has been checked explicitly, exactly remaining with the uncanceled Γ/ϵ parts. As explained in section 2.5, these should cancel with divergences coming from the electroweak calculation.

3.5 P-wave Green function

In this section, the contribution from the P-wave parts is calculated. This corresponds to the Z-boson mediated quark pair production. The notation will be similar as for the S-wave part. For a single insertion of the potential of the form $\delta V = \frac{1}{(\mathbf{q}^2)^x}\left(\frac{\mu^2}{\mathbf{q}^2}\right)^{a\epsilon}$ the I-function is defined as:

$$I^{(P)}[x+a\epsilon] = \int \prod_i \left(\frac{d^{d-1}\mathbf{p}_i}{(2\pi)^{d-1}}\right) \tilde{G}_C(\mathbf{p}_1,\mathbf{p}_2;E) \frac{\mathbf{p}_1\mathbf{p}_4}{(\mathbf{q}^2)^x}\left(\frac{\mu^2}{\mathbf{q}^2}\right)^{a\epsilon} \tilde{G}_C(\mathbf{p}_3,\mathbf{p}_4;E)\,, \tag{3.175}$$

where $\mathbf{q} = \mathbf{p}_2 - \mathbf{p}_3$. Here, the notation $\tilde{G}_C$ is used for the full Green function including all partial waves. Then, the multiplication with $\mathbf{p_i}$ projects out the P-wave part. For the P-wave J-functions a notation similar to the S-wave calculation is used:

$$J^{(P)}[x+a\epsilon;w(\epsilon)] = \frac{1}{\epsilon} w^{(1/\epsilon)}\Big(I^{(P)}[x+a\epsilon] - I^{(P)}[x]\Big) + \Big(w + w^{(\epsilon)}\epsilon\Big) I^{(P)}[x+a\epsilon]\,. \tag{3.176}$$

The P-wave contributions starts at second order, so the double insertion is of higher order and will not be considered here.

3.5.1 Leading order

Power counting shows, that diagrams with up to three gluon exchanges for the leading-order P-wave Green function are divergent. So the Green function is divided into four parts:

$$G^{(l=1)}(E) = G^{(l=1,0ex)}(E) + G^{(l=1,1ex)}(E) + G^{(l=1,2ex)}(E) + G^{(l=1,3ex)}(E) + G^{(l=1,>3ex)}(E)\,. \tag{3.177}$$

Then, the same strategy is used as for the S-wave calculation. The first four diagrams are calculated in momentum space and the last one in coordinate space. The momentum space integrals are done with Feynman parameters and Mellin-Barnes integrals. An example of the calculation is given in the next section. The result deduced there is the same for the Green function if a is set to zero. The final results for the different parts are:

$$9G^{(l=1,0ex)}(E) = \int \frac{d^{d-1}\mathbf{p}}{(2\pi)^{d-1}} \frac{-m\mathbf{p}^2}{\mathbf{p}^2 - mE} = \frac{m\Gamma(1+\frac{1-d}{2})(-mE)^{\frac{d-1}{2}}}{2(4\pi)^{\frac{d-1}{2}}} \tag{3.178}$$

$$= \frac{m^4 C_F^3 \alpha_s^3}{64\pi\lambda^3} + O(\epsilon)\,, \tag{3.179}$$

$$9G^{(l=1,1ex)}(E) = \int \prod \frac{d^{d-1}\mathbf{p_i}}{(2\pi)^{d-1}} \frac{m^2 C_F g^2 \mathbf{p_1}\mathbf{p_2}}{(\mathbf{p}_1^2 - mE)(\mathbf{p}_1-\mathbf{p}_2)^2(\mathbf{p}_2^2-mE)} \tag{3.180}$$

$$= -\frac{m^4 C_F^3 \alpha_s^3}{16\pi\lambda^2}\left(\frac{1}{4\epsilon} + 1 + L_\lambda + O(\epsilon)\right), \tag{3.181}$$

$$9G^{(l=1,2ex)}(E) = \int \prod \frac{d^{d-1}\mathbf{p_i}}{(2\pi)^{d-1}} \frac{m^3 (C_F g^2)^2 \mathbf{p_1}\mathbf{p_3}}{(\mathbf{p}_1^2 - mE)(\mathbf{p}_1-\mathbf{p}_2)^2(\mathbf{p}_2^2-mE)(\mathbf{p}_2-\mathbf{p}_3)^2(\mathbf{p}_3^2-mE)}$$

$$= -\frac{m^4 C_F^3 \alpha_s^3}{16\pi\lambda}\left(\frac{\pi^2}{3}+1+O(\epsilon)\right), \tag{3.182}$$

$$9G^{(l=1,3ex)}(E) = \int\prod \frac{d^{d-1}\mathbf{p_i}}{(2\pi)^{d-1}} \frac{m^4(C_F g^2)^3 \mathbf{p_1}\mathbf{p_4}}{(\mathbf{p}_1^2-mE)(\mathbf{p}_1-\mathbf{p}_2)^2(\mathbf{p}_2^2-mE)(\mathbf{p}_2-\mathbf{p}_3)^2(\mathbf{p}_3^2-mE)}$$
$$\frac{1}{(\mathbf{p}_3-\mathbf{p}_4)^2(\mathbf{p}_4^2-mE)} = \frac{m^4 C_F^3\alpha_s^3}{64\pi}\left(\frac{1}{2\epsilon}+L_\lambda+c_{Real}+O(\epsilon)\right). \tag{3.183, 3.184}$$

The finite part has been done with the summation representation of the P-wave Green function:

$$G^{(l=1,>3ex)}(E) = \frac{m}{4\pi}(2\sqrt{-mE})^3\sum_{n=0}^{\infty}\frac{n!L_n^{(3)}(0)L_n^{(3)}(0)}{(n+3)!}\left(\frac{1}{(n+2-\lambda)}-\sum_{k=0}^{3}\frac{\lambda^k}{(2+n)^{k+1}}\right) \tag{3.185}$$

$$= \frac{m^4 C_F^3\alpha_s^3}{144\pi\lambda^2}\left((1-\lambda^2)\hat{\Psi}(1-\lambda)+\lambda^2\zeta_3+\frac{\pi^2\lambda}{6}\right). \tag{3.186}$$

After combining all parts, the final result reads:

$$G^{(l=1)}(E) = \frac{C_F m^3\alpha_s}{144\pi}\frac{E}{\epsilon}+\frac{C_F^3 m^4\alpha_s^3}{1152\pi\epsilon}-\frac{C_F^3 m^4\alpha_s^3}{144\pi\lambda^3}\Big(-\frac{1}{4}+\lambda+\frac{\lambda^2}{2}+\lambda L_\lambda-\frac{\lambda^3}{4}L_\lambda$$
$$-\lambda(1-\lambda^2)\hat{\Psi}(1-\lambda)-1.891\lambda^3\Big). \tag{3.187}$$

The real part from $G^{(l=1,3ex)}(E)$ has been kept, although this is not needed for the future calculation.

3.5.2 Coulomb single insertion

The leading P-wave contribution is of second order. So, for a full third-order result only the NLO P-wave corrections are needed. These correspond to a single insertion of the NLO Coulomb potential. Power counting reveals, that one has four divergent types of diagrams, as shown in figure 3.6:

$$I^{(P)}[1+a\epsilon] = I_a^{(P)}[1+a\epsilon]+2I_b^{(P)}[1+a\epsilon]+I_c^{(P)}[1+a\epsilon]+2I_d^{(P)}[1+a\epsilon]$$
$$+2I_e^{(P)}[1+a\epsilon]+2I_f^{(P)}[1+a\epsilon]+I_g^{(P)}[1+a\epsilon]. \tag{3.188}$$

The $I^{(P)}$-functions have to be calculated up to order ϵ, because one has to insert potentials of the form $\frac{1}{\epsilon}\left[\left(\frac{\mu^2}{\mathbf{q^2}}\right)^\epsilon-1\right]$, and the result is not finite. In some parts of the divergent diagrams this has been done numerically with the program `MB` [89]. The calculation of these finite parts of the P-wave Coulomb insertion will be done in coordinate space. The summation representation of the Green function for P-waves is used from equation (A.4). Some of the insertions must be subtracted from the full Green function. This is again done by taking

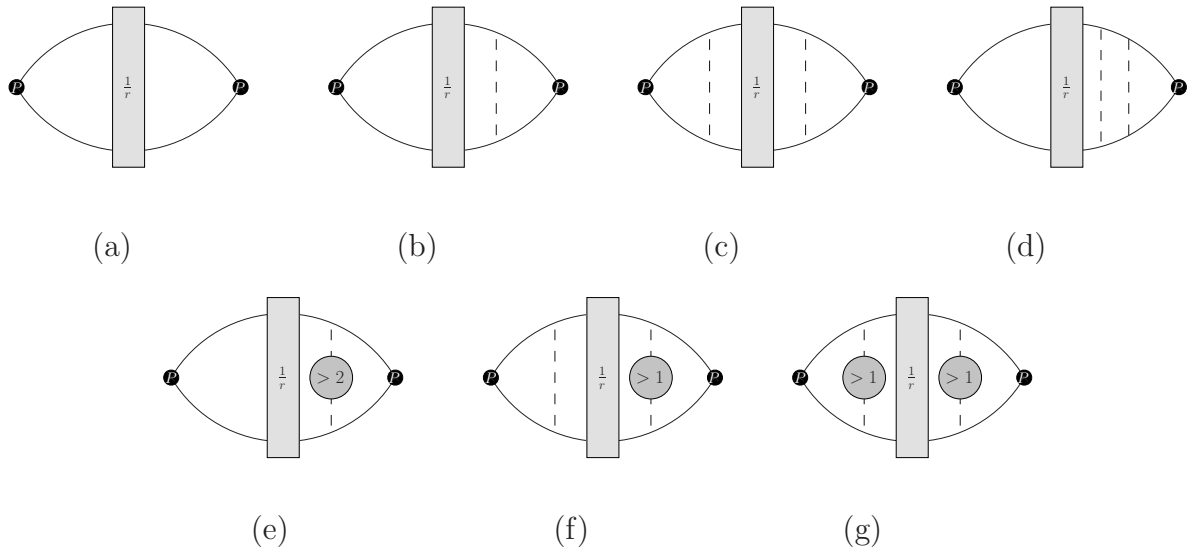

Figure 3.6: The Coulomb potential insertion for the P-waves is divided into six different parts.

the limit $\lambda \to 0$ to the appropriate order. Then, the coordinate space representation of the potentials is used. This means, that one calculates insertions of $1/r$ and of $\ln(r)/r$. As for the S-wave calculation, these insertions are generated with the potential

$$W(\boldsymbol{r}) = \frac{1}{4\pi\Gamma(1+2u_i)\cos(\pi u)} \left(\boldsymbol{r}^2\right)^{u-\frac{1}{2}} , \tag{3.189}$$

by taking the zeroth and first derivative with respect to u at $u = 0$. As will be shown in the next subsections, this leads to two types of integrals:

$$\int_0^\infty ds\, s^3 e^{-s} L_n^{(3)}(s) L_j^{(3)}(s) = (n+1)(n+2)(n+3)\delta_{nj} , \tag{3.190}$$

$$\int_0^\infty ds\, s^3 \ln(s) e^{-s} L_n^{(3)}(s) L_j^{(3)}(s) = \begin{cases} (n+1)(n+2)(n+3)\Psi(4+n) & \text{if } n = j \\ -\frac{(\min(n,j)+1)(\min(n,j)+2)(\min(n,j)+3)}{|j-n|} & \text{if } n \neq j . \end{cases} \tag{3.191}$$

The first one appears for insertions of the pure Coulomb potential and the second one for insertions of logarithmic corrections.

Part a-d

These parts are divergent and have to be done in momentum space. While the calculation is straightforward for the first parts, the last two parts are more complicated, and the result contains a numerical constant. As an example, the calculation of the third part is shown explicitly, the other parts can be done in a very similar way. The starting expression is

$$I_d^{(P)}[1+a\epsilon] = 2\int \prod_{i=1}^{3} \frac{d^{d-1}\mathbf{p}_i}{(2\pi)^{d-1}} \frac{\mathbf{p}_1^k}{\mathbf{p}_1^2 - mE} \frac{C_F^2 m^4 \alpha_s^2}{[(\mathbf{p}_1-\mathbf{p}_2)^2]^{1+a\epsilon}(\mathbf{p}_2 - mE)(\mathbf{p}_2-\mathbf{p}_3)^2} \frac{\mathbf{p}_3^k}{\mathbf{p}_3^2 - mE}$$

(3.192)

$$= \frac{2}{(4\pi)^{d-1}} \int_0^1 dxdy \frac{\Gamma(2+a\epsilon-\frac{d-1}{2})}{\Gamma(1+a\epsilon)} x^{\frac{d-1}{2}-1}(1-x)^{\frac{d-1}{2}-2-a\epsilon} y^{\frac{d-1}{2}-1}(1-y)^{\frac{d-1}{2}-2}$$
$$\times \int \frac{d^{d-1}\mathbf{p}}{(2\pi)^{d-1}} \frac{C_F^2 m^4 \alpha_s^2}{(\mathbf{p}^2-\frac{mE}{x})^{2+a\epsilon-\frac{d-1}{2}}(\mathbf{p}_2-mE)(\mathbf{p}_2^2-\frac{mE}{y})^{2-\frac{d-1}{2}}}\,, \tag{3.193}$$

where the formulas from appendix B.2 have been used to perform the $\mathbf{p}_1$ and $\mathbf{p}_3$ integral. Then, the left and right side of the denominator in the integral are written with the Mellin-Barnes representation:

$$I_d^{(P)}[1+a\epsilon] = \frac{2}{(4\pi)^{d-1}} \int_0^1 dxdy \frac{\Gamma(2+a\epsilon-\frac{d-1}{2})}{\Gamma(1+a\epsilon)} x^{\frac{d-1}{2}-1}(1-x)^{\frac{d-1}{2}-2-a\epsilon} y^{\frac{d-1}{2}-1}(1-y)^{\frac{d-1}{2}-2}$$
$$\times \frac{1}{\Gamma(2+a\epsilon-\frac{d-1}{2})\Gamma(2-\frac{d-1}{2})} \int_{-i\infty}^{i\infty} dz_1 dz_2 \Gamma(2+a\epsilon-\frac{d-1}{2}+z_2)\Gamma(\frac{d-1}{2}-2-a\epsilon)$$
$$\times \Gamma(2-\frac{d-1}{2}+z_2)\Gamma(\frac{d-1}{2}-2)\Big(\frac{-mE}{x}\Big)^{z_1}\Big(\frac{-mE}{y}\Big)^{z_2}$$
$$\times \int \frac{d^{d-1}\mathbf{p}}{(2\pi)^{d-1}} \frac{C_F^2 m^4 \alpha_s^2 \mathbf{p}^2}{(\mathbf{p}^2)^{4-d+a\epsilon+z_1+z_2}(\mathbf{p}_2-mE)}\,. \tag{3.194}$$

Now, the remaining momentum integral is performed, followed by the integration of the three Feynman parameter integrals:

$$I_d^{(P)}[1+a\epsilon] = \frac{2C_F^2 m^4 \alpha_s^2}{(4\pi)^{d-1}} \int_0^1 dxdy \frac{\Gamma(2+a\epsilon-\frac{d-1}{2})}{\Gamma(1+a\epsilon)} x^{\frac{d-1}{2}-1}(1-x)^{\frac{d-1}{2}-2-a\epsilon} y^{\frac{d-1}{2}-1}(1-y)^{\frac{d-1}{2}-2}$$
$$\times \frac{1}{\Gamma(2+a\epsilon-\frac{d-1}{2})\Gamma(2-\frac{d-1}{2})} \int_{-i\infty}^{i\infty} dz_1 dz_2 \Gamma(2+a\epsilon-\frac{d-1}{2}+z_2)\Gamma(\frac{d-1}{2}-2-a\epsilon)$$
$$\times \Gamma(2-\frac{d-1}{2}+z_2)\Gamma(\frac{d-1}{2}-2)\Big(\frac{-mE}{x}\Big)^{z_1}\Big(\frac{-mE}{y}\Big)^{z_2}$$
$$\times \int_0^1 d\xi \frac{\Gamma(5-d+a\epsilon-\frac{d-1}{2}+z_1+z_2)}{\Gamma(4-d+a\epsilon+z_1+z_2)}$$
$$\times \frac{\xi^{3-d+a\epsilon+z_1+z_2}(1-\xi)^{\frac{d-1}{2}-5+d-a\epsilon-z_1-z_2}(-mE)^{\frac{d-1}{2}-5+d-a\epsilon-z_1-z_2}}{(4\pi)^{\frac{d-1}{2}}} \tag{3.195}$$
$$= \frac{2C_F^2 m^4 \alpha_s^2 (-mE)^{\frac{d-1}{2}-5+d-a\epsilon}}{(4\pi)^{\frac{3}{2}(d-1)}} \frac{\Gamma(2+a\epsilon-\frac{d-1}{2})\Gamma(\frac{d-1}{2}-1)\Gamma(\frac{d-1}{2}-2-a\epsilon)\Gamma(\frac{d-1}{2}-2)}{\Gamma(1+a\epsilon)\Gamma(2+a\epsilon-\frac{d-1}{2})\Gamma(2-\frac{d-1}{2})\Gamma(\frac{d-1}{2})}$$
$$\times \int_{-i\infty}^{i\infty} dz_1 dz_2 \frac{\Gamma(\frac{d-1}{2}-z_1)\Gamma(\frac{d-1}{2}-1-a\epsilon)}{\Gamma(d-2-z_1-a\epsilon)} \frac{\Gamma(\frac{d-1}{2}-z_2)\Gamma(2+a\epsilon-\frac{d-1}{2}+z_2)}{\Gamma(d-2-z_2)} \tag{3.196}$$
$$\times \Gamma(5-d+a\epsilon-\frac{d-1}{2}+z_1+z_2)\Gamma(\frac{d-1}{2}-4+d-a\epsilon-z_1-z_2)\Gamma(2-\frac{d-1}{2}+z_2)\,.$$

The result is a double Mellin-Barnes integral, which can be done with the program `MB` [89]. The calculation of the other parts is quite similar, part b results in a single Mellin-Barnes integral which can be done analytically and part d is a triple integral. But, since this part

has no imaginary prefactor, only the divergent part is needed here. The number is produced again with the package `MB`. Then, the result for the P-wave J-functions can be easily obtained from the I-functions and reads (real parts are dropped):

$$J_a^{(P)}[1+\epsilon,\beta_0/\epsilon+a_1(\epsilon)] = -\frac{m^3\beta_0}{1728\pi^2}\frac{E}{\epsilon^2}+\frac{m^3 a_1}{576\pi^2}\frac{E}{\epsilon}-\frac{C_F^2m^4\alpha_s^2}{576\pi^2\lambda^2}\Big(\frac{a1^{(\epsilon)}}{4}+a_1(1+L_\lambda) +\beta_0(1+\frac{17\pi^2}{27}+2L_\lambda+L_\lambda^2)\Big)\,, \tag{3.197}$$

$$2J_b^{(P)}[1+\epsilon,\beta_0/\epsilon+a_1(\epsilon)] = -\frac{C_F^2m^4\alpha_s^2}{288\pi^2\lambda}\Big(a_1+\frac{\pi^2}{3}a_1+\beta_0(3.385752-L_\lambda-\frac{\pi^2}{3}L_\lambda)\Big)\,, \tag{3.198}$$

$$J_c^{(P)}[1+\epsilon,\beta_0/\epsilon+a_1(\epsilon)] = \frac{C_F^2m^4\alpha_s^2}{576\pi^2}\Big(\frac{L_\lambda}{128}a_1+\beta_0(-1.3888L_\lambda+L_\lambda^2)\Big)\,, \tag{3.199}$$

$$2J_d^{(P)}[1+\epsilon,\beta_0/\epsilon+a_1(\epsilon)] = \frac{C_F^2m^4\alpha_s^2}{288\pi^2}\Big(\frac{L_\lambda}{128}a_1+\beta_0(-0.3888L_\lambda+L_\lambda^2)\Big)\,. \tag{3.200}$$

The result contains the numerical values from the Mellin-Barnes integration. They are given in such a way, that the numerical accuracy is higher than the number of digits used. Since this part is a very small contribution to the complete cross section, the numerical error for the total result is negligible.

Part e

This part has no gluon exchange on the left side and more than two exchanges on the right hand side:

$$I_e^{(P)}[1+u] = \int d^3\boldsymbol{r}\, G^{(l=1,0ex)}(0,\boldsymbol{r};E)\boldsymbol{r}^2W(\boldsymbol{r})G^{(l=1,>2ex)}(\boldsymbol{r},0;E)\,. \tag{3.201}$$

One needs the zeroth and first derivative at $u=0$ to generate the correct potential. The results are:

$$I_e^{(P)}[1] = \int dr\, G^{(l=1,0ex)}(0,\boldsymbol{r};E)r^3G^{(l=1,>2ex)}(\boldsymbol{r},0;E) \tag{3.202}$$

$$= -\frac{m^3E}{36\pi}\sum_{n=0}^{\infty}\sum_{k=0}^{\infty}\frac{1}{2+n}\Big(\frac{1}{2+k-\lambda}-\frac{1}{2+k}-\frac{\lambda}{(2+k)^2}-\frac{\lambda^2}{(2+k)^3}\Big) \times\int_0^\infty ds\, s^3e^{-s}L_n^{(3)}(s)L_j^{(3)}(s) \tag{3.203}$$

$$= -\frac{m^3E}{144\pi^2}\Big(\frac{\pi^2}{6}\lambda+(1-\lambda^2)\hat{\Psi}(1-\lambda)+\lambda^2\zeta_3\Big)\,, \tag{3.204}$$

where the substitution $r\to s/(2\sqrt{-mE})$ has been made. The first derivative is:

$$\frac{\partial}{\partial u}I_e^{(P)}[1+u]|_{u=0} = 2\gamma_EI_e^{(P)}[1]+2\int dr\, G^{(l=1,0ex)}(0,\boldsymbol{r};E)r^3\ln(r)G^{(l=1,>2ex)}(\boldsymbol{r},0;E)$$
$$= \Big(2\gamma_E+\ln(-4mE)\Big)I_e^{(P)}[1]$$

$$-\frac{m^3E}{18\pi}\sum_{n=0}^{\infty}\sum_{k=0}^{\infty}\frac{1}{2+n}\Big(\frac{1}{2+k-\lambda}-\frac{1}{2+k}-\frac{\lambda}{(2+k)^2}-\frac{\lambda^2}{(2+k)^3}\Big) \tag{3.205}$$

$$\times\int_0^\infty ds\, s^3\ln(s)e^{-s}L_n^{(3)}(s)L_j^{(3)}(s) \tag{3.206}$$

$$=\ln(-4mE)I_e^{(P)}[1]-\frac{m^3E}{144\pi^2}\Bigg[\frac{\lambda^3(132-137\lambda+37\lambda^2)}{8(\lambda-2)^2(\lambda-1)}-\frac{\pi^2}{12}\lambda(10+7\lambda)-5\zeta_3\lambda^2$$

$$+\Big(\frac{3\lambda^3-11\lambda^2+2\lambda+10}{\lambda-2}\Big)\hat\Psi(1-\lambda)+2\lambda^2\sum_{k=1}^{\infty}\frac{(k^2+4k+3)\hat\Psi(k)}{(2+k)^3(2+k-\lambda)}\Bigg]. \tag{3.207}$$

The s-integrals were given for both parts in the section above, one sum has been evaluated analytically, some parts from the second sum were left. Then the result for the J-function is:

$$2J_e^{(P)}[1+\epsilon,\beta_0/\epsilon+a_1]=\frac{C_F^2m^4\alpha_s^2}{288\pi^2\lambda^2}\Bigg\{a_1\Big[\frac{\pi^2}{6}\lambda+(1-\lambda^2)\hat\Psi(1-\lambda)+\lambda^2\zeta_3\Big] \tag{3.208}$$

$$+\beta_0\Bigg[\frac{\lambda^3(132-137\lambda+37\lambda^2)}{8(\lambda-2)^2(\lambda-1)}-\frac{\pi^2}{12}\lambda(10+7\lambda)-\frac{\pi^2}{3}\lambda L_\lambda-\zeta_3\lambda^2(5+2L_\lambda)$$

$$+\Big(\frac{3\lambda^3-11\lambda^2+2\lambda+10}{\lambda-2}+2(\lambda^2-1)L_\lambda\Big)\hat\Psi(1-\lambda)+2\lambda^2\sum_{k=1}^{\infty}\frac{(k^2+4k+3)\hat\Psi(k)}{(2+k)^3(2+k-\lambda)}\Bigg]\Bigg\}.$$

Part f

This part has one gluon exchange on the left side and more than one exchange on the right hand side:

$$I_e^{(P)}[1+u]=\int d^3\boldsymbol{r}\,G^{(l=1,1ex)}(0,\boldsymbol{r};E)\boldsymbol{r}^2W(\boldsymbol{r})G^{(l=1,>1ex)}(\boldsymbol{r},0;E)\,. \tag{3.209}$$

Again, the zeroth and first derivative at $u=0$ are needed. The results are:

$$I_e^{(P)}[1]=\int dr\,G^{(l=1,1ex)}(0,\boldsymbol{r};E)r^3G^{(l=1,>1ex)}(\boldsymbol{r},0;E) \tag{3.210}$$

$$=-\frac{m^3E}{36\pi}\sum_{n=0}^{\infty}\sum_{k=0}^{\infty}\frac{\lambda}{(2+n)^2}\Big(\frac{1}{2+k-\lambda}-\frac{1}{2+k}-\frac{\lambda}{(2+k)^2}\Big)$$

$$\times\int_0^\infty ds\,s^3e^{-s}L_n^{(3)}(s)L_j^{(3)}(s) \tag{3.211}$$

$$=-\frac{m^3E}{144\pi^2}\Big(\frac{\pi^2}{6}\lambda+\lambda^2\zeta_3+(1-\lambda^2)\hat\Psi(1-\lambda)\Big), \tag{3.212}$$

where again the substitution $r\to s/(2\sqrt{-mE})$ has been made. The first derivative is:

$$\frac{\partial}{\partial u}I_e^{(P)}[1+u]|_{u=0}=2\gamma_EI_e^{(P)}[1]+2\int dr\,G^{(l=1,1ex)}(0,\boldsymbol{r};E)r^3\ln(r)G^{(l=1,>1ex)}(\boldsymbol{r},0;E)$$

$$=\Big(2\gamma_E+\ln(-4mE)\Big)I_e^{(P)}[1]-\frac{m^3E}{18\pi}\sum_{n=0}^{\infty}\sum_{k=0}^{\infty}\frac{\lambda}{(2+n)^2}\Big(\frac{1}{2+k-\lambda}-\frac{1}{2+k}$$

$$-\frac{\lambda}{(2+k)^2}\Big)\int_0^\infty ds\,s^3\ln(s)e^{-s}L_n^{(3)}(s)L_j^{(3)}(s) \tag{3.213}$$

$$
\begin{aligned}
&= \ln(-4mE) I_e^{(P)}[1] - \frac{m^3 E}{144\pi^2}\Bigg[\frac{\pi^4}{45}\lambda^2 + \frac{\pi^2}{12}(4-16\lambda-9\lambda^2) + \zeta_3\lambda(2-8\lambda) \\
&+\frac{\lambda^3(43\lambda^4-270\lambda^3+635\lambda^2-632\lambda+208)}{8(\lambda-2)^3(\lambda-1)^2} \\
&+\Big(\frac{2(\lambda^6-10\lambda^5+23\lambda^4-7\lambda^3-28\lambda^2+24\lambda-4)}{\lambda(\lambda-2)^2(\lambda-1)}\Big)\hat{\Psi}(1-\lambda) \\
&+2\lambda^3\sum_{k=1}^{\infty}\frac{(k^2+4k+2)\hat{\Psi}(k)-(k^3+6k^2+11k+6)\Psi_1(k)}{(2+k)^3(2+k-\lambda)}\Bigg]. \qquad (3.214)
\end{aligned}
$$

As for the previous part, some parts from the second sum were left in the final result. The corresponding J-function is:

$$
\begin{aligned}
2J_f^{(P)}[1+\epsilon,\beta_0/\epsilon+a_1] &= \frac{C_F^2 m^4\alpha_s^2}{288\pi^2\lambda^2}\Bigg\{a_1\Big[\frac{\pi^2}{6}\lambda+\lambda^2\zeta_3+(1-\lambda^2)\hat{\Psi}(1-\lambda)\Big] \\
&+\beta_0\Bigg[\frac{\pi^4}{45}\lambda^2+\frac{\pi^2}{12}(4-16\lambda-9\lambda^2)+\frac{\lambda^3(43\lambda^4-270\lambda^3+635\lambda^2-632\lambda+208)}{8(\lambda-2)^3(\lambda-1)^2} \\
&+\zeta_3\lambda(2-8\lambda-2\lambda L_\lambda)-\frac{\pi^2}{3}\lambda L_\lambda \qquad (3.215) \\
&+\Big(\frac{2(\lambda^6-10\lambda^5+23\lambda^4-7\lambda^3-28\lambda^2+24\lambda-4)}{\lambda(\lambda-2)^2(\lambda-1)}+2(\lambda^2-1)L_\lambda\Big)\hat{\Psi}(1-\lambda) \\
&+2\lambda^3\sum_{k=1}^{\infty}\frac{(k^2+4k+2)\hat{\Psi}(k)-(k^3+6k^2+11k+6)\Psi_1(k)}{(2+k)^3(2+k-\lambda)}\Bigg]\Bigg\}. \qquad (3.216)
\end{aligned}
$$

Part g

The last part of this insertion has two full Green functions with more than one gluon exchange on both sides:

$$
I_e^{(P)}[1+u] = \int d^3\boldsymbol{r}\, G^{(l=1,>1ex)}(0,\boldsymbol{r};E)\boldsymbol{r}^2 W(\boldsymbol{r}) G^{(l=1,>1ex)}(\boldsymbol{r},0;E)\,. \qquad (3.217)
$$

Again, the zeroth and first derivative at $u=0$ are needed. The results for this part are:

$$
\begin{aligned}
I_e^{(P)}[1] &= \int dr\, G^{(l=1,>1ex)}(0,\boldsymbol{r};E) r^3 G^{(l=1,>1ex)}(\boldsymbol{r},0;E) \qquad (3.218) \\
&= -\frac{m^3E}{36\pi}\sum_{n=0}^{\infty}\sum_{k=0}^{\infty}\Big(\frac{1}{2+n-\lambda}-\frac{1}{2+n}-\frac{\lambda}{(2+n)^2}\Big)\Big(\frac{1}{2+k-\lambda} \\
&\quad -\frac{1}{2+k}-\frac{\lambda}{(2+k)^2}\Big)\int_0^\infty ds\, s^3 e^{-s} L_n^{(3)}(s) L_j^{(3)}(s) \qquad (3.219) \\
&= -\frac{m^3E}{144\pi^2}\Big(-\frac{\pi^2}{3}\lambda-\lambda^2\zeta_3+(\lambda^2-3)\hat{\Psi}(1-\lambda)+\lambda(\lambda^2-1)\Psi_1(1-\lambda)\Big)\,. \qquad (3.220)
\end{aligned}
$$

with the same substitution as before, namely $r \to s/(2\sqrt{-mE})$. The first derivative is:

$$
\frac{\partial}{\partial u} I_e^{(P)}[1+u]|_{u=0} = 2\gamma_E I_e^{(P)}[1] + 2\int dr\, G^{(l=1,>1ex)}(0,\boldsymbol{r};E) r^3 \ln(r) G^{(l=1,>1ex)}(\boldsymbol{r},0;E)
$$

$$= \Big(2\gamma_E + \ln(-4mE)\Big) I_e^{(P)}[1] - \frac{m^3 E}{18\pi} \sum_{n=0}^{\infty} \sum_{k=0}^{\infty} \Big(\frac{1}{2+n-\lambda} - \frac{1}{2+n} - \frac{\lambda}{(2+n)^2} \Big)$$

$$\times \Big(\frac{1}{2+k-\lambda} - \frac{1}{2+k} - \frac{\lambda}{(2+k)^2} \Big) \int_0^\infty ds\, s^3 \ln(s) e^{-s} L_n^{(3)}(s) L_j^{(3)}(s) \tag{3.221}$$

$$= \ln(-4mE) I_e^{(P)}[1] - \frac{m^3 E}{144\pi^2} \Bigg[\frac{\pi^4}{45}\lambda^2 + \frac{\pi^2}{6} \frac{3\lambda^3 - 10\lambda^2 + 8\lambda + 12}{2-\lambda} + \frac{2\pi^2}{3}\lambda L_\lambda \tag{3.222}$$

$$- \frac{\lambda^3(45\lambda^4 - 358\lambda^3 + 1069\lambda^2 - 1380\lambda + 640)}{8(\lambda-2)^3(\lambda-1)^2} + \lambda(4+5\lambda)\zeta_3$$

$$+ \hat{\Psi}(1-\lambda) \Big(\frac{5\lambda^7 - 13\lambda^6 - 17\lambda^5 + 115\lambda^4 - 186\lambda^3 + 108\lambda^2 + 56\lambda - 64}{2\lambda(\lambda-2)^2(\lambda-1)}$$

$$+ \frac{\pi^2}{3}\lambda(1-\lambda^2) + \lambda(1-\lambda^2)\Psi_1(1-\lambda) \Big) + 4(1-\lambda^2)\hat{\Psi}(1-\lambda)^2$$

$$+ 2(1+\lambda-2\lambda^2)\Psi_1(1-\lambda)$$

$$- \sum_{k=1}^{\infty} \frac{2\lambda^2}{(2+k)^3(2+k-\lambda)} \Big(\lambda(\lambda-2-k)\hat{\Psi}(k) + (2+k)\lambda(1-\lambda^2)\hat{\Psi}(2+k-\lambda)$$

$$+ (k^2+4k+3)(k^2+4k+4-\lambda^2)\hat{\Psi}(3+k) - (2+k)^3(3+4k+k^2)\hat{\Psi}(3+k-\lambda)$$

$$- \lambda(2+k)(k^2+4k+3)(2+k-\lambda)\Psi_1(3+k) \Big) \Bigg]$$

As for the previous part, some parts from the second sum were left in the final result. The result for the J function reads:

$$J_g^{(P)}[1+\epsilon, \beta_0/\epsilon + a_1] = \frac{C_F^2 m^4 \alpha_s^2}{576\pi^2\lambda^2} \Bigg\{ a_1 \Big[- \frac{\pi^2}{3}\lambda - \lambda^2\zeta_3 + (\lambda^2-3)\hat{\Psi}(1-\lambda)$$

$$+ \lambda(\lambda^2-1)\Psi_1(1-\lambda) \Big] + \beta_0 \Bigg[\frac{\pi^4}{45}\lambda^2 + \frac{\pi^2}{6} \frac{3\lambda^3 - 10\lambda^2 + 8\lambda + 12}{2-\lambda} + \frac{2\pi^2}{3}\lambda L_\lambda$$

$$- \frac{\lambda^3(45\lambda^4 - 358\lambda^3 + 1069\lambda^2 - 1380\lambda + 640)}{8(\lambda-2)^3(\lambda-1)^2} + \lambda(4+5\lambda+2\lambda L_\lambda)\zeta_3$$

$$+ \hat{\Psi}(1-\lambda) \Big(\frac{5\lambda^7 - 13\lambda^6 - 17\lambda^5 + 115\lambda^4 - 186\lambda^3 + 108\lambda^2 + 56\lambda - 64}{2\lambda(\lambda-2)^2(\lambda-1)}$$

$$+ \frac{\pi^2}{3}\lambda(1-\lambda^2) + 2(3-\lambda^2)L_\lambda + \lambda(1-\lambda^2)\Psi_1(1-\lambda) \Big)$$

$$+ 4(1-\lambda^2)\hat{\Psi}(1-\lambda)^2 + 2(1+\lambda-2\lambda^2-\lambda(\lambda^2-1)L_\lambda)\Psi_1(1-\lambda)$$

$$- \sum_{k=1}^{\infty} \frac{2\lambda^2}{(2+k)^3(2+k-\lambda)} \Big(\lambda(\lambda-2-k)\hat{\Psi}(k) + (2+k)\lambda(1-\lambda^2)\hat{\Psi}(2+k-\lambda)$$

$$+ (k^2+4k+3)(k^2+4k+4-\lambda^2)\hat{\Psi}(3+k) - (2+k)^3(3+4k+k^2)\hat{\Psi}(3+k-\lambda)$$

$$- \lambda(2+k)(k^2+4k+3)(2+k-\lambda)\Psi_1(3+k) \Big) \Bigg] \Bigg\}.$$

The numerical evaluation for the remaining sums is stable for all physical values of the energy and the width. In the numerics, a cutoff is used for these sums, which is high enough to ensure that the error is much smaller than the desired precision.

Poles

The finite parts have also poles in the limit $\lambda \to n$. The poles of the total result for $J^{(P)}[1+\epsilon, \beta_0/\epsilon + a_1]$ are:

$$\hat{J}^{(P)}[1+\epsilon, \beta_0/\epsilon + a_1] = \frac{C_F^2 m^4 \alpha_s^2}{576\pi^2}\Bigg\{\frac{(n-1)}{n(\lambda-n)^2}\Big[a_1(n+1) - 2\beta_0(1+(1+n)L_n + (1+n)S_1)\Big] + \frac{1}{n^2(\lambda-n)}\Big[2a_1(n^2-1) - 2\beta_0(1-n-4n^2 - \frac{\pi^2}{3}n(n^2-1) - 2(n^2-1)L_n + 4n^2 S_1 - 2n(n^2-1)S_2)\Big]\Bigg\}. \tag{3.223}$$

This leads to corrections to energy levels and wave function which are given in the appendix 3.7. They agree with the ones found in [43].

3.6 Threshold mass

In this section, the problem of choosing an appropriate mass scheme is discussed. This is important, because in QCD, quarks cannot appear as free particles due to confinement. Therefore, they are no physical observables and their defining quantities, such as quark masses, are renormalization scheme dependent. So, it is not surprising, that for different processes, different schemes are more suitable. One can derive perturbative relations to transform the mass from scheme B to scheme A:

$$\frac{m^{(A)}}{m^{(B)}} = 1 + \sum_{n=1} k_n^{(AB)} \alpha (m^{(B)})^n.$$

The calculations in the previous sections were done in the pole mass scheme. The pole mass m^{P} is the pole of the renormalized quark propagator. This mass definition is gauge invariant in all orders of perturbation theory and has no infrared divergences [90]. But it is defined only up to an infrared ambiguity of order Λ_{QCD}, which is unprotected by the large top quark width [91]. Therefore, this definition is sensitive to infrared momenta [92], which is known as the infrared renormalon (for a review see [93]).

The threshold masses are short-distance masses and renormalon free. They are particularly useful for processes near the mass shell. Examples of threshold masses are the PS mass [94], the 1S-mass [45] and the kinetic mass scheme [95]. Here, the PS mass $m^{\mathrm{PS}}(\mu_f)$ will be used if not stated otherwise. This definition is based on the observation that the higher-order corrections to the Coulomb potential show a significant long distance sensitivity, which cancels exactly against the same sensitivity of the pole mass [94, 96]. The relation between pole mass and PS mass is:

$$m^{\mathrm{PS}}(\mu_f) = m^{\mathrm{P}} - \delta m^{\mathrm{PS}}(\mu_f)\,, \tag{3.224}$$

with

$$\delta m^{\rm PS}(\mu_f) = -\frac{1}{2} \int\limits_{|\mathbf{q}|<\mu_f} \frac{d^3\mathbf{q}}{(2\pi)^3}\, \tilde{V}_C(q)\,. \tag{3.225}$$

To convert the results obtained in the previous sections to the more useful PS mass, one must insert equation (3.224) expanded in α_s to the needed order into the PNRQCD Lagrangian. This means additional insertions proportional to $\delta m(\mu_f)$ are generated. There are no contributions from the mass shift of the potential at third order, since the mass dependent potentials appear first at second order and the mass shift generates additional two orders. But the expansion of the kinetic Lagrangian contributes at third order:

$$\psi^\dagger \left[i\partial_0 + \delta m(\mu_f) + \frac{\boldsymbol{\partial^2}}{2m}\left(1+\frac{\delta m(\mu_f)}{m}\right) + \frac{\boldsymbol{\partial}^4}{8m^3}\Big(1+O(\alpha_s v)\Big)\right]\psi\,, \tag{3.226}$$

and similar for the antiquark part. The additional insertions are the single insertion of $\frac{\boldsymbol{p^2}}{2m}\frac{\delta m(\mu_f)}{m}$ with $\delta m(\mu_f)$ expanded up to second order and the double insertion of $\frac{\boldsymbol{p^2}}{2m}\frac{\delta m(\mu_f)}{m}$ and the NLO Coulomb potential with the leading order of $\delta m(\mu_f)$ only. These parts can be reduced to known insertions with the equation of motion (given in section 2.4.2). The most complicated part is the residual mass term. Power counting shows, that the leading term of this part is of the order $\alpha_s v$ and therefore of the same order as $i\delta_0$. This means it has to be taken into account in all orders, which can be done by adding a real part to the energy, similar to the leading width term which can also be resummed in the propagator and contributes to the imaginary part of the energy. The order α_s^2 term of $\delta m(\mu_f)$ is then next-to-leading order and has to be taken into account up to triple insertions of the mass term alone and together with the potentials.

Another possibility to calculate exactly these insertions is not to start at the Lagrangian level, but to do instead the expansion for small $\delta m(\mu_f)$ directly in the cross section result. $\delta m(\mu_f)$ appears on the one hand in the mass m and in the energy. Whenever it appears in the energy, one has to keep the leading correction as an energy shift, and expand the higher orders. The reason is that the energy is $\sqrt{s}-m$ and therefore corrections to m can be large compared to the energy, even if they are small compared to the mass. These corrections start to contribute at NLO (corresponds to an expansion of the LO). The expansion of small $\delta m(\mu_f)$ if it does not appears in the energy starts with the leading order of $\delta m(\mu_f)$ which is of second order compared to the mass in the non-relativistic expansion.

Energy and mass appear in the cross section result in λ. So, the Green function has to be expanded for $\lambda \to \lambda^{\rm PS} = -\frac{m^{\rm PS} C_F \alpha_s}{\sqrt{-4m^{\rm PS}E^{\rm PS}}}$ and $E^{\rm PS} = \sqrt{s} - 2m^{\rm PS}$. For most parts of the Green function, this can be done analytically, but for Hypergeometric functions and for the sums in the Coulomb result, a numerical expansion will be used. This means, one has to take a numerical derivative of these functions. The expansion has also been done for the poles of

the Green function. The result is an additional contribution to the energy levels and wave functions.

3.7 Summary of energy levels and wave functions

Energy levels and wave function have been known since some time at NNLO [21, 97, 98]. The third-order energy level corrections have been calculated some years ago [31, 32, 35, 36] and the corrections to the wave function have been completed only recently [35, 36, 38–40] (logarithmic corrections were calculated in [99,100]($\ln^2$) and [33,34] (ln)) up to the unknown hard matching coefficients and some order ϵ parts of the potentials.

The energy levels and wave functions can be calculated from the $\lambda \to n$ poles (this corresponds to the poles $E \to E_n^{(0)}$) of the Green function. The exact structure of the Green function is known in terms of these poles, namely:

$$G(E) \overset{E\to E_n}{=} \frac{|\psi_n(0)|^2}{E_n - E} + \cdots . \tag{3.227}$$

The dots stand for the continuum contribution. If this form is expanded in the strong coupling constant, one gets the perturbative result for the poles, which must correspond exactly to the poles of the perturbative Green function. So, by comparing this expanded result with the calculated result for the poles, one can reconstruct order by order the corrections to the energy levels and wave functions:

$$\begin{aligned} G(E) &\overset{E\to E_n}{=} \frac{|\psi_n^{(0)}(0)|^2 \left(1 + \frac{\alpha_s}{4\pi} f_1 + \left(\frac{\alpha_s}{4\pi}\right)^2 f_2 + \left(\frac{\alpha_s}{4\pi}\right)^3 f_3 + \ldots\right)}{E_n^{(0)} \left(1 + \frac{\alpha_s}{4\pi} e_1 + \left(\frac{\alpha_s}{4\pi}\right)^2 e_2 + \left(\frac{\alpha_s}{4\pi}\right)^3 e_3 + \ldots\right) - E} \\ &= \frac{|\psi_n(0)|^2}{E_n^{(0)} - E}\Bigg[1 + \frac{\alpha_s}{4\pi}\left(\frac{-E_n^{(0)} e_1}{E_n^{(0)} - E} + f_1\right) + \left(\frac{\alpha_s}{4\pi}\right)^2 \left(\frac{(E_n^{(0)})^2 e_1^2}{(E_n^{(0)} - E)^2} - \frac{E_n^{(0)}(e_2 + e_1 f_1)}{E_n^{(0)} - E} + f_2\right) \\ &+ \left(\frac{\alpha_s}{4\pi}\right)^3 \left(-\frac{(E_n^{(0)})^3 e_1^3}{(E_n^{(0)} - E)^3} + \frac{(E_n^{(0)})^2 (2e_2 + e_1^2 f_1)}{(E_n^{(0)} - E)^2} - \frac{E_n^{(0)}(e_1 f_2 + e_2 f_1 + e_3)}{E_n^{(0)} - E} - f_3\right) \\ &+ O(\alpha_s^4)\Bigg], \end{aligned} \tag{3.228}$$

where the e_i and f_i are the S-wave energy level and wave function corrections at order i normalized to the leading order:

$$E_n = E_n^{(0)} \left(1 + \frac{\alpha_s}{4\pi} e_1 + \left(\frac{\alpha_s}{4\pi}\right)^2 e_2 + \left(\frac{\alpha_s}{4\pi}\right)^3 e_3 + \ldots\right) , \tag{3.229}$$

$$|\psi_n(0)|^2 = |\psi_n^{(0)}(0)|^2 \left(1 + \frac{\alpha_s}{4\pi} f_1 + \left(\frac{\alpha_s}{4\pi}\right)^2 f_2 + \left(\frac{\alpha_s}{4\pi}\right)^3 f_3 + \ldots\right) , \tag{3.230}$$

with

$$E_n^{(0)} = -\frac{m(\alpha_s C_F)^2}{4n^2}\,, \tag{3.231}$$

$$|\psi_n^{(0)}(0)|^2 = \frac{(m\alpha_s C_F)^3}{8\pi n^3}\,. \tag{3.232}$$

At third order, also the P-wave corrections have to be taken into account. They start at NNLO, so only the first-order corrections are needed for a third-order calculation. The corrections are:

$$E_n^{(P)} = E_n^{(P,0)}\left(1+\frac{\alpha_s}{4\pi}e_1^{(P)}\ldots\right), \tag{3.233}$$

$$|\psi_n^{(P)}(0)|^2 = |\psi_n^{(P,0)}(0)|^2\left(1+\frac{\alpha_s}{4\pi}f_1^{(P)}\ldots\right), \tag{3.234}$$

with

$$E_n^{(P,0)} = -\frac{m(\alpha_s C_F)^2}{4n^2}\,, \tag{3.235}$$

$$|\psi_n^{(P,0)}(0)|^2 = \frac{(m\alpha_s C_F)^5(n^2-1)}{32\pi n^5}\,. \tag{3.236}$$

Now, the distinction between Coulomb, non-Coulomb and ultrasoft corrections following the notation from [35, 38, 39][2] will be made: $e_i = e_i^C + e_i^{nC} + e_i^{us}$ and $f_i = f_i^C + f_i^{nC} + f_i^{us}$. The Non-Coulomb part appears first at second order, and the ultrasoft part at third order, so that $e_1^{nC} = e_1^{us} = e_2^{us} = 0$ and $f_1^{nC} = f_1^{us} = f_2^{us} = 0$. All results will be given for the projection to the spin triplet state.

The energy levels and wave functions will be used in the cross section calculation to resum the higher-order poles in $(E_n - E)^i$ into the exact Green function pole part. This means, the right hand side of equation (3.228) will be subtracted and the left part added back.

3.7.1 Energy levels

In this part, the results for the energy levels will be presented, separated into Coulomb, non-Coulomb and ultrasoft parts. The results for the Coulomb corrections (published in [35]) read:

$$e_1^C = 4\beta_0\, L_n + c_{E,1}^C, \tag{3.237}$$

$$e_2^C = 12\beta_0^2\, L_n^2 + L_n\Big(-8\beta_0^2 + 4\beta_1 + 6\beta_0 c_{E,1}^C\Big) + c_{E,2}^C, \tag{3.238}$$

$$\begin{aligned} e_3^C = {} & 32\beta_0^3\, L_n^3 + L_n^2\Big(-56\beta_0^3 + 28\beta_0\beta_1 + 24\beta_0^2 c_{E,1}^C\Big) + L_n\Big(16\beta_0^3 - 16\beta_0\beta_1 + 4\beta_2 \\ & -12\beta_0^2 c_{E,1}^C + 6\beta_1 c_{E,1}^C + 8\beta_0 c_{E,2}^C\Big) + c_{E,3}^C + 32\pi^2 C_A^3\Big(L_n + S_1\Big), \end{aligned} \tag{3.239}$$

[2] In [35] the non-Coulomb and ultrasoft corrections to the energy levels were combined.

where the constants $c^C_{E,i}$ are:

$$c^C_{E,1} = 2a_1 + 4S_1\beta_0, \tag{3.240}$$

$$\begin{aligned} c^C_{E,2} = {} & a_1^2 + 2a_2 + 4S_1\beta_1 + 4a_1\beta_0\Big[3S_1 - 1\Big] \\ & + \beta_0^2\Bigg[S_1\Big(12S_1 - 8 - \frac{8}{n}\Big) + 16S_2 - 8nS_3 + \frac{2\pi^2}{3} + 8n\xi(3)\Bigg], \end{aligned} \tag{3.241}$$

$$\begin{aligned} c^C_{E,3} = {} & 2a_1a_2 + 2a_3 + 2a_1^2\beta_0\Big[4S_1 - 5\Big] + 4a_2\beta_0\Big[4S_1 - 1\Big] + 4a_1\beta_1\Big[3S_1 - 1\Big] \\ & + 4S_1\beta_2 + \beta_0\beta_1\Bigg[S_1\Big(28S_1 - 16 - \frac{24}{n}\Big) + 36S_2 - 16nS_3 + \frac{7\pi^2}{3} + 16n\xi(3)\Bigg] \\ & + a_1\beta_0^2\Bigg[S_1\Big(48S_1 - 56 - \frac{32}{n}\Big) + 64S_2 - 32nS_3 + 8 + \frac{8\pi^2}{3} + 32n\xi(3)\Bigg] \\ & + \beta_0^3\Bigg[S_1\Bigg(S_1\Big(32S_1 - 56 - \frac{32}{n}\Big) + 96S_2 - 64nS_3 + 16 + \frac{16}{n} + \frac{32\pi^2}{3} + 64n\xi(3)\Bigg) \\ & + S_2\Big(8nS_2 + 16n^2S_3 - 32 - \frac{16}{n} - \frac{40n\pi^2}{3} - 16n^2\xi(3)\Big) + S_3\Big(96 + 16n + 8n^2\pi^2\Big) \\ & - 104nS_4 + 48n^2S_5 - 144S_{2,1} + 224nS_{3,1} - 32n^2S_{3,2} - 96n^2S_{4,1} - \frac{4\pi^2}{3} + \frac{2n\pi^4}{45} \\ & + \xi(3)\Big(32 - 16n - 8n^2\pi^2\Big) + 96n^2\xi(5)\Bigg]. \end{aligned} \tag{3.242}$$

The results for the non-Coulomb parts are simpler. The reason is, that they start at NNLO, so only the first-order corrections contribute to the third order. The expressions are

$$e_2^{nC}/(16\pi^2) = \frac{C_AC_F}{n} + \frac{{C_F}^2}{n}\left(\frac{2}{3} - \frac{11}{16n}\right), \tag{3.243}$$

$$\begin{aligned} e_3^{nC}/(64\pi^2) = {} & -\frac{49n_fT_FC_AC_F}{36n} + \frac{4{C_A}^2C_F}{3n}\left[\frac{197}{48} + \ln 2 + 2L_n - 2S_1\right] \\ & + \frac{C_A{C_F}^2}{n}\left[\frac{563}{108} - \frac{\ln n}{2} + \frac{8\ln 2}{3} - \frac{37S_1}{6} + \frac{\ln(C_F\alpha_s)}{2} + \frac{20L_n}{3}\right. \\ & \left. + \frac{1}{n}\Big(-\frac{97}{72} - \frac{2L_n}{3} - \frac{2S_1}{3}\Big)\right] + \frac{{C_F}^3}{3n}\left[-\frac{9}{2} + \frac{7}{2n} - \ln n - 7S_1 + \ln(C_F\alpha_s) + 8L_n\right] \\ & + \frac{{C_F}^2n_fT_F}{9n}\left[-\frac{4}{3} + \frac{5}{2n}\right] + \frac{2T_F{C_F}^2}{15n} + a_1\left[\frac{C_AC_F}{2n} + \frac{3C_F^2}{4n}\Big(1 - \frac{3}{4n}\Big)\right] \\ & + \beta_0\Bigg[C_AC_F\Big(\frac{2}{n}L_n - \frac{\pi^2}{6} + \frac{1}{2n} + S_2\Big) + {C_F}^2\Bigg(\Big(-\frac{11}{8n^2} + \frac{4}{3n}\Big)L_n \\ & - \frac{11S_1}{8n^2} + \frac{2}{3}S_2 + \frac{2}{n} + \frac{1}{24\,n^2} - \frac{\pi^2}{9}\Bigg)\Bigg]. \end{aligned} \tag{3.244}$$

Finally, the ultrasoft corrections are left for the S-wave contribution. They have been calculated some time ago [33]. There is one part of the ultrasoft corrections which corresponds to potential insertions. This part has been checked explicitly and agrees with [33]. The complete

result reads:

$$
\begin{aligned}
e_3^{us}/(64\pi^2) = {} & \frac{4{C_A}^2 C_F}{3n}\Big[-\frac{25}{12} - 2\ln 2 - \ln n - 2L_m + 3\ln(C_F\alpha_s) + S_1\Big] \\
& + \frac{{C_A}^3}{6}\Big[-\frac{5}{6} - \ln 2 - 2\ln n + 4\ln(C_F\alpha_s) - 3L_m - 2S_1\Big] \\
& + \frac{C_A {C_F}^2}{3n}\Big[-10 - 20L_m + 8S_1 - 20\ln 2 - 8\ln n + 32\ln(C_F\alpha_s) \\
& + \frac{1}{n}\Big(\frac{5}{3} + 2L_m + 2\ln 2 - 4\ln(C_F\alpha_s)\Big)\Big] \\
& + \frac{{C_F}^3}{3n}\Big[-2nL_E(n) - 8L_m - \frac{20}{3} - 8\ln 2 + 16\ln(C_F\alpha_s)\Big]. \qquad (3.245)
\end{aligned}
$$

Here, the Bethe logarithms $L[E]$ have been introduced. They are not known in an analytic form for arbitrary n. The values for the first states are:

$$
L_E(n) = (-81.5379, -37.671, -22.4818, -14.5326, -9.52642, -6.0222, \ldots)\,. \qquad (3.246)
$$

The last remaining part are the P-wave energy levels. Here, one has to calculate the first-order Coulombic corrections. The result reads:

$$
e_1^{(P)} = -2a_1 + 4\beta_0\Big(\frac{1}{1+n} + L_n + S_1\Big)\,. \qquad (3.247)
$$

This result agrees with [43], where the P-wave corrections have been first calculated.

3.7.2 Wave functions

In this section the results for the quarkonium wave function corrections will be presented. Again, the results are divided into the Coulombic part, the non-Coulomb part and the ultrasoft corrections. The results for the Coulomb corrections are:

$$
\begin{aligned}
f_1^C &= 6\beta_0\, L_n + c_{\psi,1}, && (3.248)\\
f_2^C &= 24\beta_0^2\, L_n^2 + L_n\Big(-12\beta_0^2 + 6\beta_1 + 8\beta_0 c_{\psi,1}\Big) + c_{\psi,2}, && (3.249)\\
f_3^C &= 80\beta_0^3\, L_n^3 + L_n^2\Big(-108\beta_0^3 + 54\beta_0\beta_1 + 40\beta_0^2 c_{\psi,1}\Big) + L_n\Big(24\beta_0^3 - 24\beta_0\beta_1 + 6\beta_2 && (3.250)\\
& -16\beta_0^2 c_{\psi,1} + 8\beta_1 c_{\psi,1} + 10\beta_0 c_{\psi,2}\Big) + c_{\psi,3} + 48\pi^2 {C_A}^3\Big[L_n + \frac{1}{3}\Big(S_1 + 2nS_2 - 1 - \frac{n\pi^2}{3}\Big)\Big]\,,
\end{aligned}
$$

with

$$
\begin{aligned}
c_{\psi,1} &= 3a_1 + 2\beta_0\Big[\, S_1 + 2nS_2 - 1 - \frac{n\pi^2}{3}\,\Big], && (3.251)\\
c_{\psi,2} &= 3a_1^2 + 3a_2 + 2a_1\beta_0\Big[\, 4S_1 + 8nS_2 - 7 - \frac{4n\pi^2}{3}\,\Big] + 2\beta_1\Big[\, S_1 + 2nS_2 - 1 - \frac{n\pi^2}{3}\,\Big]
\end{aligned}
$$

$$+\beta_0^2\Bigg[\,S_1\bigg(8S_1+16nS_2-20-\frac{12}{n}-\frac{8n\pi^2}{3}\bigg)+S_2\bigg(4n^2S_2+8-8n-\frac{4n^2\pi^2}{3}\bigg)$$
$$+28nS_3-20n^2S_4-24nS_{2,1}+16n^2S_{3,1}+4+\frac{(3+4n)\pi^2}{3}+\frac{n^2\pi^4}{9}+20n\xi(3)\Bigg]. \qquad (3.252)$$

$$c_{\psi,\,3}=a_1^3+6a_1a_2+3a_3+10a_1^2\beta_0\Bigg[\,S_1+2nS_2-\frac{31}{10}-\frac{n\pi^2}{3}\,\Bigg]+10a_2\beta_0\Bigg[\,S_1+2nS_2$$
$$-\frac{8}{5}-\frac{n\pi^2}{3}\,\Bigg]+8a_1\beta_1\Bigg[\,S_1+2nS_2-\frac{7}{4}-\frac{n\pi^2}{3}\,\Bigg]+2\beta_2\Bigg[\,S_1+2nS_2-1-\frac{n\pi^2}{3}\,\Bigg]$$
$$+\beta_0\beta_1\Bigg[\,S_1\bigg(22S_1+40nS_2-44-\frac{36}{n}-\frac{20n\pi^2}{3}\bigg)+S_2\bigg(8n^2S_2+14-16n-\frac{8n^2\pi^2}{3}\bigg)$$
$$+64nS_3-40n^2S_4-56nS_{2,1}+32n^2S_{3,1}+8+\frac{(21+16n)\pi^2}{6}+\frac{2n^2\pi^4}{9}+48n\xi(3)\Bigg]$$
$$+a_1\beta_0^2\Bigg[\,S_1\bigg(40S_1+80nS_2-116-\frac{60}{n}-\frac{40n\pi^2}{3}\bigg)+S_2\bigg(20n^2S_2+40-72n-\frac{20n^2\pi^2}{3}\bigg)$$
$$+140nS_3-100n^2S_4-120nS_{2,1}+80n^2S_{3,1}+48+(5+12n)\pi^2+\frac{5n^2\pi^4}{9}+100n\xi(3)\Bigg]$$
$$+\beta_0^3\Bigg[\,S_1\bigg(4S_1\Big(4S_1+16nS_2-19-\frac{6}{n}-\frac{8n\pi^2}{3}\Big)+8S_2\Big(3n^2S_2+2-14n-n^2\pi^2\Big)$$
$$+104nS_3-120n^2S_4-112nS_{2,1}+96n^2S_{3,1}+80+\frac{64}{n}+\frac{(58+56n)\pi^2}{3}+\frac{2n^2\pi^4}{3}$$
$$+120n\xi(3)\bigg)+S_2\bigg(-4n(17+2n)S_2+72n^2S_3-96n^2S_{2,1}+64n^3S_{3,1}-96+16n$$
$$-\frac{24}{n}-\frac{8(5-n)n\pi^2}{3}-8n^2\xi(3)\bigg)+S_3\bigg(-16n^3S_3+64-16n-20n^2\pi^2+32n^3\xi(3)\bigg)$$
$$+S_4\bigg(68n+40n^2+\frac{64n^3\pi^2}{3}\bigg)-312n^2S_5+144n^3S_6+S_{2,1}\bigg(48n-120+16n^2\pi^2\bigg)$$
$$-32S_{3,1}\bigg(\frac{15n}{2}+n^2+\frac{n^3\pi^2}{3}\bigg)+384n^2S_{3,2}+576n^2S_{4,1}-224n^3S_{4,2}-256n^3S_{5,1}$$
$$+256nS_{2,1,1}+64n^2S_{2,2,1}-64n^3S_{2,3,1}-448n^2S_{3,1,1}+192n^3S_{4,1,1}-8-\frac{8(2+n)\pi^2}{3}$$
$$-\frac{(83+10n)n\pi^4}{45}+\frac{4n^3\pi^6}{105}+\xi(3)\bigg(48-80n-12n^2\pi^2-16n^3\xi(3)\bigg)-40n^2\xi(5)\Bigg]. \qquad (3.253)$$

The results for the non-Coulomb part read:

$$\frac{f_2^{nC}}{16\pi^2}=C_F^2\bigg[\frac{2}{3}L_n-\frac{15}{8n^2}+\frac{4}{3n}+\frac{22}{9}-\frac{2}{3}S_1\bigg]$$
$$+C_FC_A\bigg[L_n+\frac{2}{n}+\frac{5}{4}-S_1\bigg], \qquad (3.254)$$
$$\frac{f_3^{nC}}{64\pi^2}=\bigg[\frac{7}{6}C_F^3+\frac{37}{12}C_AC_F^2+\frac{4}{3}C_A^2C_F+\beta_0\Big(\frac{4}{3}C_F^2+2C_AC_F\Big)\bigg]L_n^2$$

$$
\begin{aligned}
&+\Bigg[C_F^3\Big(-\frac{3}{2}+\frac{14}{3n}-\frac{7S_1}{3}\Big)+C_AC_F^2\Big(\frac{226}{27}+\frac{8\ln 2}{3}+\frac{37}{3n}-\frac{5}{3n^2}-\frac{37S_1}{6}\Big)\\
&\quad+C_A^2C_F\Big(\frac{145}{18}+\frac{4\ln 2}{3}+\frac{16}{3n}-\frac{8S_1}{3}\Big)+C_F^2T_F\Big(\frac{2}{15}-\frac{59}{27}n_f\Big)\\
&\quad-\frac{109}{36}C_AC_FT_F\,n_f+\beta_0\Bigg\{C_F^2\Big(\frac{16}{3}+\frac{10}{3n}-\frac{75}{16n^2}-\frac{\pi^2n}{9}-\frac{4S_1}{3}+\frac{2nS_2}{3}\Big)\\
&\quad+C_AC_F\Big(\frac{15}{8}+\frac{5}{n}-\frac{\pi^2n}{6}-2S_1+nS_2\Big)\Bigg\}\Bigg]L_n+\Big[\frac{1}{3}C_F^3+\frac{1}{2}C_AC_F^2\Big]L_mL_n\\
&+\Big[\frac{1}{12}C_F^3+\frac{1}{8}C_AC_F^2\Big]L_m^2+\Big[C_F^3\Big(\frac{1}{12}+\frac{2}{3n}-\frac{S_1}{3}\Big)+C_AC_F^2\Big(-\frac{5}{9}+\frac{1}{n}-\frac{S_1}{2}\Big)\\
&\quad+\frac{1}{15}C_F^2T_F\Big]L_m+\frac{c_{\psi,3}^{nC}}{64\pi^2}\,.
\end{aligned}
\tag{3.255}
$$

The constant term of f_3^{nC} is:

$$
\begin{aligned}
\frac{c_{\psi,3}^{nC}}{64\pi^2}&=\Big[-\frac{44}{9}-\frac{109\pi^2}{864}-\frac{25}{6n}+\frac{35}{12n^2}+S_1\Big(\frac{3}{2}-\frac{14}{3n}+\frac{7S_1}{6}\Big)-\frac{7S_2}{6}\Big]C_F^3\\
&+\Big[\frac{60479}{3888}-\frac{3247\pi^2}{5184}+\frac{1475}{108n}+\frac{\pi^2}{9n}-\frac{321}{32n^2}+\ln 2\Big(\frac{353}{54}+\frac{16}{3n}-\frac{16\ln 2}{9}\Big)\\
&\quad-S_1\Big(\frac{226}{27}+\frac{8\ln 2}{3}+\frac{37}{3n}+\frac{1}{n^2}-\frac{37S_1}{12}\Big)-S_2\Big(\frac{37}{12}+\frac{2}{3n}\Big)\Big]C_AC_F^2\\
&+\Big[\frac{3407}{432}-\frac{5\pi^2}{18}+\frac{133}{9n}+\ln 2\Big(\frac{187}{108}+\frac{8}{3n}-\frac{8\ln 2}{9}\Big)-\frac{4S_2}{3}\\
&\quad-S_1\Big(\frac{145}{18}+\frac{4\ln 2}{3}+\frac{16}{3n}-\frac{4S_1}{3}\Big)\Big]C_A^2C_F+\Big[\frac{1}{15}+\frac{4}{15n}-\frac{2S_1}{15}\Big]C_F^2T_F\\
&+\Big[-\frac{361}{108}+\frac{49\ln 2}{108}-\frac{109}{18n}+\frac{109S_1}{36}\Big]C_AC_FT_F\,n_f\\
&+\Big[-\frac{1711}{243}+\frac{7\pi^2}{648}-\frac{2\ln 2}{27}-\frac{118}{27n}+\frac{125}{24n^2}+\frac{59S_1}{27}\Big]C_F^2T_F\,n_f\\
&+\beta_0\Bigg[\Big\{\frac{1027}{648}+\frac{19}{6n}+\frac{25}{24n^2}-\frac{35\pi^2}{108}-\frac{11\pi^2n}{27}+\frac{5\pi^2}{16n}+\frac{4nS_3}{3}-\frac{2nS_{2,1}}{3}\\
&\quad-S_1\Big(\frac{10}{9}+\frac{1}{3n}+\frac{45}{16n^2}-\frac{\pi^2n}{9}+\frac{2nS_2}{3}\Big)+S_2\Big(1+\frac{22n}{9}-\frac{15}{8n}\Big)\Big\}C_F^2\\
&\quad+\Big\{\frac{7}{24}-\frac{91\pi^2}{144}-\frac{1}{4n}-\frac{5\pi^2n}{24}-S_1\Big(\frac{3}{8}+\frac{1}{2n}-\frac{\pi^2n}{6}+nS_2\Big)+S_2\Big(\frac{3}{2}+\frac{5n}{4}\Big)\\
&\quad-nS_{2,1}+2nS_3\Big\}C_AC_F\Bigg]-\frac{C_F}{6}b_2^{(\epsilon)}\,.
\end{aligned}
\tag{3.256}
$$

These results were given previously in [38], the one-loop order ϵ potential coefficient has been added in these results. The ultrasoft correction is (taken from [39]):

$$
f_3^{us}/(64\pi^2)=\Big[-2C_A^2C_F-\frac{16}{3}C_AC_F^2-\frac{8}{3}C_F^3\Big]\ln^2\alpha_s+\Big[-\frac{5}{6}C_A^2C_F-\frac{11}{6}C_AC_F^2-\frac{1}{3}C_F^3\Big]L_m^2
$$

n	1	2	3	4	5	6
δ_n^{us}	353.06	256.62	224.26	206.88	195.48	187.16

Table 3.3: Numerical result for the non-logarithmic part of the ultrasoft contribution, as defined in (3.257); n denotes the principal quantum number.

$$
\begin{aligned}
&+\left[\frac{8}{3}C_A^2C_F+\frac{20}{3}C_AC_F^2+\frac{8}{3}C_F^3\right]\ln\alpha_s L_m\\
&+\left[C_A^3+\left(\frac{52}{9}-\frac{8}{3}\ln 2-4H_n\right)C_A^2C_F+\left(6-\frac{10}{3}n^2-\frac{4}{3}\ln 2-\frac{32}{3}H_n\right)C_AC_F^2\right.\\
&\quad\left.+\left(-\frac{52}{9}-\frac{4}{3}n^2+8\ln 2-\frac{16}{3}H_n\right)C_F^3\right]\ln\alpha_s\\
&+\left[-\frac{3}{4}C_A^3+\left(-\frac{11}{3}+\frac{5}{3}\ln 2+\frac{8}{3}H_n\right)C_A^2C_F+\left(-\frac{3}{2}+\frac{5}{3}n^2+\frac{1}{3}\ln 2+\frac{20}{3}H_n\right)C_AC_F^2\right.\\
&\quad\left.+\left(5+\frac{2}{3}n^2-6\ln 2+\frac{8}{3}H_n\right)C_F^3\right]L_m+\delta_n^{us},
\end{aligned}
\tag{3.257}
$$

where $H_n=\ln\frac{C_F}{n}-\frac{1}{n}+\sum_{k=1}^{n-1}\frac{1}{k}$ and the numerical values for δ_n^{us} are given in table 3.3.

The wave function corrections from the P-waves has also been recalculated. The corrections read:

$$
f_1^{(P)}=-5a_1+2\beta_0\left(\frac{4(n^2+n-1)}{n^2-1}-\frac{\pi^2 n}{3}+5L_n-\frac{n^2+3}{n^2-1}S_1+2nS_2\right) \tag{3.258}
$$

These results agree with [43]. Their result contains still a single sum, which can be reduced to simpler harmonic sums. Note that the P-Wave contribution to the wave function is not divergent, in contrast to the full Green function. The reason is that the divergence in the Green function is proportional to the quarkonium width, and these parts have no poles in the limit $\lambda\to n$ and thus don't contribute to the wave function.

Chapter 4

The Mathematica Package

4.1 Program summary

Title of program: `TTbarXSection`

Available from: `not public`

Computer for which the program is designed and others on which it is operable: Any work-station or PC where `Mathematica` is running.

Operating system or monitor under which the program has been tested: UNIX, Windows XP, Mathematica 4.1, Mathematica 5.1

No. of bytes in program: 249 KB

Files contained: TTbarGridCalc.m, TTbarXSection.m, TTbarConstants.m, TTbarGridFile (can be created with "TTbarGridCalc.m")

Distribution format: ASCII

Typical running time: The calculation of the cross section takes about a second. The calculation of a grid file takes a couple of days, depending on the grid size.

For a quick start the user might jump directly to section 4.4.2 and use the gray shaded boxes for additional information.

4.2 Program structure

This chapter is a short user guide for the Mathematica program for the evaluation of the cross section. The calculation of the NNNLO $t\bar{t}$ production at threshold is partly analytic

and some parts contain sums (or integrals for the ultrasoft part), which have to be calculated numerically. This implicates, that the calculation of one point is too slow. Therefore the program is divided into two parts. The first one (`TTbarGridCalc`) is a precalculation of the relevant sums for a range of energies and widths. The result for those functions, which are not analytic is saved into a grid. The calculation of a typical grid takes a couple of days. This grid is used by the second part (`TTbarXSection`) to calculate the cross section as a function of different parameters. The file `TTbarConstants.m` contains a definition of further parameters, which remain usually unchanged, for example the coefficients of the potentials or the β function, but also for unknown parameters. These should be added to this file once they are calculated. For the running of the coupling the program `RunDec` [101] is used. So, for a calculation of the cross section, the following files are needed:

- `TTbarGridCalc.m` (or alternatively a precalculated gridfile)
- `TTbarXSection.m`
- `TTbarConstants.m`
- a version of `RunDec`

In the next chapter the syntax of the available commands will be explained and some relevant examples will be given in the last part.

4.3 Syntax of commands

In this section the commands included in the two main parts of the program, the calculation of the grid file and the calculation of the cross section are described. Then, the naming of the constants in the file `TTbarConstants` will be explained.

4.3.1 Part 1: The package TTbarGridCalc

The first part is the package for the calculation of the grid file. A grid file contains numbers for the needed non-analytic functions for both, the parts from potential insertions and the ultrasoft part. The structure is a two dimensional matrix. In one dimension the energy values are changed, in the second dimension the width is varied. Then, each point of this matrix is a vector where the first entry is a rescaled energy and width ($-\frac{4(E+i\Gamma)}{mC_F^2\alpha_s^2}$), and the other entries are the values for the non-analytic functions at the specific energy and width for that point. The second part of the package will use these numbers to make an interpolating function,

which can provide the values for the non-analytic functions much faster than the original function used in this part of the package.

The structure of `TTbarGridCalc` is divided into two parts, the potential insertions and the ultrasoft calculation. The potential insertions are named in the form `Ins[λ,insertion,Sum1]`. The meaning of this notation will be described in the next section and corresponds exactly to the one used in the second package file, `TTbarXSection`. The second part, the ultrasoft insertion is taken from [42]. The ultrasoft calculation is mainly based on a numerical integration. This integration is convergent for physical parameters. However, for small width, the convergence becomes worse. Therefore, in [42] an extrapolation is used to calculate the Green function for zero width. These results are implemented in this program.

The main command of this part is `TTbarGridCalc`. It creates a table with the non-analytic functions at different (rescaled) energy and width points as described above and saves the result into a file. The main input is the range in the energy and width plane as well as the difference between two neighboring points on the grid (the fineness).

`TTbarGridCalc[Energy→{StartE,EndE,StepE},Width→{StartW,EndW,StepW},"File"]`

- *Mandatory Input*:
  - `StartE`: first (lowest) energy value.
  - `EndE`: last (highest) energy value.
  - `StepE`: difference between two energy values.
  - `StartW`: first (lowest) width value.
  - `EndW`: last (highest) width value.
  - `StepW`: difference between two width values.
  - `File`: The filename for the grid file.
- *Optional Input*: -
- *Output*: No mathematica output, grid data is written in the specified file.
- *Quick Example:*

```
In[1]:=
TTbarGridCalc[Energy→{-5,1,0.1},Width→{1.1,1.9,0.1},"TTbarGrid"]
```

The first point when creating a grid is to decide which range has to be taken. This depends mainly on four values, the energy, the width, the mass and the scale. The input values for the energy and width are always for the fixed scale $\mu = 30$ GeV and the fixed mass $m = 175$ GeV. So, the input values have to be rescaled to these numbers if other values for the scale and the mass are needed. The rescaling is done in the following way. For ranges given in the form $E = [E^{(min)}, E^{(max)}]$, $\Gamma = [\Gamma^{(min)}, \Gamma^{(max)}]$, $\mu = [\mu^{(min)}, \mu^{(max)}]$ and $m = [m^{(min)}, m^{(max)}]$, the rescaled energy ranges (which have to be used as the input) are:

$$E^{(min)}_{rescaled} = E^{(min)} \frac{0.14^2}{\alpha_s(\mu^{(min)})^2} \frac{175}{m^{(max)}} \qquad E^{(max)}_{rescaled} = E^{(max)} \frac{0.14^2}{\alpha_s(\mu^{(max)})^2} \frac{175}{m^{(min)}} \tag{4.1}$$

and the width ranges have to be taken from $\Gamma^{(min)}_{rescaled}$ to $\Gamma^{(max)}_{rescaled}$:

$$\Gamma^{(min)}_{rescaled} = \Gamma^{(min)} \frac{0.14^2}{\alpha_s(\mu^{(min)})^2} \frac{175}{m^{(max)}} \qquad \Gamma^{(max)}_{rescaled} = \Gamma^{(max)} \frac{0.14^2}{\alpha_s(\mu^{(max)})^2} \frac{175}{m^{(min)}}. \tag{4.2}$$

Note also that these ranges are always for the calculation in the pole mass scheme. For calculations in other schemes a shift in the energy is performed. This shift depends on whether an exact or perturbative implementation of the threshold mass is chosen. These shifts are typically of order of a couple GeVs (and bigger in the case of an exact threshold mass implementation) and should be taken into account when choosing the energy range.

This package cannot only be used to calculate the grid file. The same definitions as used here are used in the second part. So instead of calculating the grid, it can also be taken to get the exact values for these parts without errors from the grid interpolation. An example of how to use this method is described in the last example in section 4.4.7.

4.3.2 Part 2: The package TTbarXSection

The second part is the main package to calculate the cross section and uses the grid data created with the function from the section above. This package contains on the one hand the command for the cross section calculation, but also additional commands to get the energy levels and wave functions at different orders and some useful auxiliary functions. The calculation follows the steps described in chapter 3 and the functions defined there will be used for the calculation.

Before starting the evaluation of the cross section, first the grid data has to be loaded. This can be done in two ways. The first possibility is to use a precalculated grid with the command `TTbarGridLoad`. This function interprets the grid data and uses Mathematica's `Interpolation` function to get values for all non-analytic functions in the cross sections. The second way is to load the file `TTbarGridCalc` first. This file defines the same non-analytic

functions. So the sums and integrals are evaluated directly without using the grid file. This takes significantly more time and is not recommended for regular use. It is important to load the `TTbarGridCalc` package first, before `TTbarXSection`, to ensure the correct function definition.

For both methods, these (internal) non-analytic functions are named in the same way, namely in the form `Ins[λ,insertion,Sum1]`. Such a numerical function belongs to the insertion `Ins[λ,insertion]`. These insertions correspond to the J functions described in chapter 3. The argument `insertion` stands for the type of potential which is calculated. It consist of two brackets, the first one contains the information on what type of potential it is and the second one what order in the ϵ expansion (or the exponent of logarithm) is used. The number for the type of the potential is similar to the first argument of the J functions. It is the exponent a of the insertion $1/(q^2)^a$, but here for $\epsilon = 0$. The second number stands in case of the Coulomb potential for the exponent of the logarithm in the insertion. So, the result for $\ln^a(\mu^2/q^2)/(q^2)$ is given in the function `Ins[λ,{1},{a}]`. For Non-Coulomb potentials, the function `Ins` can have one more argument for the order in the ϵ-expansion. The second one is now standing for the coefficient in front of ϵ in the exponent. For example `Ins[λ,{1/2},{a},R0]` stands for $J[1/2 + a\epsilon, 1/\epsilon]$, `Ins[λ,{1/2},{a},R1]` for $J[1/2 + a\epsilon, 1]$ and `Ins[λ,{1/2},{a},R2]` for $J[1/2+a\epsilon, \epsilon]$. The notation for the double and triple insertion is easier again, the two numbers in the first bracket stand for the two insertions with the same coding as for the single insertion and the two numbers in the second bracket for the exponent of the logarithm in exact analogy to the Coulomb single insertion.

`TTbarGridLoad["Filename"]`

- *Mandatory Input*:
  - `"Filename"`: The name (and path) of the gridfile which has to be loaded.
- *Optional Input*: -
- *Output*: -
- *Quick Example:*

```
In[1]:= TTbarGridLoad["TTbarGridFile"]
```

After loading the grid (or alternatively the file `TTbarGridCalc`), all functions of the pro-

Switcher	Potential /Coefficient
C1	Coulomb pot. ($\mathcal{V}_C^{(1)}$)
C2	Coulomb pot. ($\mathcal{V}_C^{(2)}$)
C3	Coulomb pot. ($\mathcal{V}_C^{(3)}$)
D2	Delta pot. ($\mathcal{V}_{1/m^2}^{(0)}$)
D3	Delta pot. ($\mathcal{V}_{1/m^2}^{(1)}$)
N1	$1/r^2$ pot. ($\mathcal{V}_{1/m}^{(1)}$)
N2	$1/r^2$ pot. ($\mathcal{V}_{1/m}^{(2)}$)
P2	p^2/q^2 pot. ($\mathcal{V}_p^{(0)}$)

Switcher	Potential /Coefficient
P3	p^2/q^2 pot. ($\mathcal{V}_p^{(1)}$)
K2	kinetic correction
U3	ultrasoft correction
c1	short distance coefficient $c_v^{(1)}$
c2	short distance coefficient $c_v^{(2)}$
c3	short distance coefficient $c_v^{(3)}$
d2	short distance coefficient $d_v^{(1)}$
d3	short distance coefficient $d_v^{(2)}$

Table 4.1: Coding for the switchers of potentials insertions, ultrasoft correction and short distance coefficients. The first letter denotes the correction type and the number stands for the order where the correction appears first.

gram are available. The main function is `TTbarXSection`. Its output is the value of the R-ratio defined in equation (2.1). The main inputs of this command are the energy point, several top quark properties (mass, width, scale) and the order of the calculation. With optional inputs, users can switch on or off the contributions from different potentials. The details are given on the next page and in table 4.1. It is also possible to use different mass schemes with optional inputs. There is also a command available to get energy levels and wave functions of the toponium. The syntax is similar to the cross section calculation, but instead of the energy, one has to specify the principle quantum number n.

A detailed summary of the commands and the corresponding mandatory and optional parameters is given on the following pages.

```
TTbarXSection[En,Mu,Constants→{m,w,as},Order→{ord,Potentials},
                                MassDef→MD,PoleResum→PR,Production→Prod]
```

- *Mandatory Input*:
  - `En:` The energy at which the cross section is calculated.
  - `Mu:` The renormalization scale (typical value: 30 GeV).
  - `m:` The mass of the top quark in the chosen scheme.
  - `w:` The top quark width.
  - `ord:` The order of the calculation. It has to be a number from 0 to 3, where 0 stands for LO and 3 for NNNLO.
- *Optional Input*:
  - `as:` The value of the coupling constant at the scale M_Z (mass of the Z-boson); default value: value defined in the file "TTbarConstants.m"
  - `Potentials:` Potentials is a matrix to switch on or of the different potentials, ultrasoft contribution and Wilson coefficients, the syntax is:
    `{{C1, C2, C3}, {D2, D3}, {N2, N3}, {P2, P3}, {K2}, {U3}, {c1, c2, c3}, {d2, d3}}` (see table 4.1 for the coding)
    default value: all parts switched on:
    `{{1,1,1},{1,1},{1,1},{1,1},{1},{1},{1,1,1},{1,1}}`
  - `MD:` The mass definition. Possible values are: "PS", "1S", "Pole", "PSshift" and "1Sshift".
  - `PR:` Switches the pole resummation on or off. Possible values: "On", "Off"; default value: "On".
  - `Prod:` Possibility to turn off the Z-mediated production by setting `Prod` to `"PhotonOnly"`.
- *Output*: The cross section, or more precisely the R-ratio for $t\bar{t}$ pair production.
- *Quick Example:* The cross section at energy $E = 1$ GeV, scale $\mu = 30$ GeV, for a top quark with PS mass $m = 175$ GeV, width $\Gamma = 1.5$ GeV at third order:

```
In[1]:= TTbarXSection[1,30,Constants→{175,1.5},Order→{3}]

Out[1]:= 1.18842
```

```
TTbarEnergyLevels[n,Mu,Constants→{m,as},Order→{ord,Potentials},
                                                    MassDef→MD]
```

- *Mandatory Input*:
  - `n`: The principle quantum number n.
  - `Mu`: The renormalization scale (typical value: 30 GeV).
  - `m`: The mass of the top quark in the chosen scheme.
  - `ord`: The order of the calculation. It has to be a number from 0 to 3, where 0 stands for LO and 3 for NNNLO.
- *Optional Input*:
  - `as`: The value of the coupling constant at the scale M_Z (mass of the Z-boson); default value: value defined in the file "TTbarConstants.m"
  - `Potentials`: Potentials is a matrix to switch on or of the different potentials, ultrasoft contribution and Wilson coefficients, the syntax is:
    `{{C1, C2, C3}, {D2, D3}, {N2, N3}, {P2, P3}, {K2}, {U3}, {c1, c2, c3}, {d2, d3}}` (see table 4.1 for the coding)
    default value: all parts switched on:
    `{{1,1,1},{1,1},{1,1},{1,1},{1},{1},{1,1,1},{1,1}}`
  - `MD`: The mass definition. Possible values are: "PS", "1S", "Pole", "PSshift" and "1Sshift".
- *Output*: The quarkonium S-wave energy levels for a spin triplet state.
- *Quick Example:* The ground-state energy levels at the scale $\mu = 30$ GeV for toponium with a top quark PS mass $m = 175$ GeV at third order (harmonic sums are evaluated):

```
In[1]:=
TTbarEnergyLevels[1,30,Constants→{175},Order→{3}]\\NHarmonicSum

Out[1]:= -1.61401
```

`TTbarWaveFunctions[n,Mu,Constants→{m,as},Order→{ord,Potentials},`
`MassDef→MD]`

- *Mandatory Input*:
  - `n`: The principle quantum number n.
  - `Mu`: The renormalization scale (typical value: 30 GeV).
  - `m`: The mass of the top quark in the chosen scheme.
  - `ord`: The order of the calculation. It has to be a number from 0 to 3, where 0 stands for LO and 3 for NNNLO.
- *Optional Input*:
  - `as`: The value of the coupling constant at the scale M_Z (mass of the Z-boson); default value: value defined in the file "TTbarConstants.m"
  - `Potentials`: Potentials is a matrix to switch on or of the different potentials, ultrasoft contribution and Wilson coefficients, the syntax is:
    `{{C1, C2, C3}, {D2, D3}, {N2, N3}, {P2, P3}, {K2}, {U3}, {c1, c2, c3}, {d2, d3}}` (see table 4.1 for the coding)
    default value: all parts switched on:
    `{{1,1,1},{1,1},{1,1},{1,1},{1},{1},{1,1,1},{1,1}}`
  - `MD`: The mass definition. Possible values are: "PS", "1S", "Pole", "PSshift" and "1Sshift".
- *Output*: The toponium wave function at the origin for the S-wave spin triplet state.
- *Quick Example:* The ground-state wave function at the scale $\mu = 30$ GeV for toponium with a top quark PS mass $m = 175$ GeV at third order (harmonic sums are evaluated):

```
In[1]:=
TTbarWaveFunctions[1,30,Constants→{175},Order→{3}]\\NHarmonicSum
Out[1]:= 1573.25
```

Apart from these phenomenologically related functions, the package contains several auxiliary commands. They might be used, if some other manipulations apart from those usually used for physical observables are needed. The function `Running`α`S[Mu,as]` gives the running of α_s from the value `as` at the scale of the W mass to the scale μ. The value is depending on the number of light flavours `nf`, which is predefined for the case of the top quark ($n_f = 5$) in the file `TTbarConstants`. Changing this can be done either directly in the constants file (and reloading the package) or in the Mathematica session before calling the command `Running`α`S[Mu,as]`. The recommended method is the first, to make sure that no manipulations have been made with the old value.

The next two functions are related to the energy levels and wave functions, which are defined for arbitrary quantum number n in the package. This definition contains harmonic sums, which are written as the functions `HarmSummation`. To prevent Mathematica from performing the summation automatically even if n is not fixed, the functions `HarmSummation` are left unevaluated. Instead, the function `NHarmonicSum` is introduced, which is used to give an explicit number to the harmonic sums.

`Running`α`S[Mu,as]`

- *Mandatory Input*:
  - `Mu`: The renormalization scale (typical value: 30 GeV).
- *Optional Input*:
  - `as`: The value of the coupling constant at the scale M_Z (mass of the Z-boson); default value: value defined in the file "TTbarConstants.m"
- *Output*: The strong coupling constant at the scale `Mu`.
- *Quick Example:* The strong coupling constant at 30 GeV and the standard value of `as` (here `as`=0.1176):

```
In[1]:= Running$\alpha$S[30]

Out[1]:= 0.14139265407766518629
```

`NHarmonicSum[expression]`

- *Mandatory Input*:
  - `expression:` An expression containing harmonic sums with numerical argument. If the argument of the harmonic sum is not numeric the function tries to evaluate the sum, which can lead to errors.
- *Optional Input*: -
- *Output*: Expression where all harmonic sums and nested harmonic sums are replaced by their numerical value.
- *Quick Example:*

`HarmSummation[n,index]`

- *Mandatory Input*:
  - `n:` argument of the harmonic sum.
  - `index:` index of the harmonic sum in the form `{a,b,c,...}` where a, b and c are the indices.
- *Optional Input*: -
- *Output*: No direct output, only when the function `NHarmonicSum` is used.
- *Quick Example:*

4.3.3 The definition file TTbarConstants.m

The file `TTbarConstants.m` contains the definitions for several constants, which can be changed in this file. The first sort of constants are the ones which define the general properties of the quarkonium and QCD. These are the charge of the up-type quark `eU`, the axial vector coupling of the top quark and electron are `at` and `ae`, the corresponding vector couplings are `vt` and `ve` and the third component of the weak isospin are `T3t` and `T3e` for top quark and electron respectively. θ`w` is the weak mixing angle and `nl` the number of light flavours (should

be set to 5 for the top and 4 for the bottom quark). The group theory factors of $SU(3)$ are denoted by `cF`, `cA` and `T`.

The constants from the second part are related to the running of the coupling. First, the default value of the coupling (α`SmZ`) at the scale of the Z boson mass (`mZ`) is defined. Note that this is just a standard value and can be changed by several commands (implemented as an optional argument). Then the β-functions are defined up to the three-loop coefficient. The coefficients are taken from [71, 102–106].

After this, the potential coefficients are introduced. The notation is similar to the one used in chapter 2. For example the coefficient a_1 is denoted as `a1` or the coefficient $v_q^{(\epsilon)}$ as `vq`ϵ.

The next part defines the hard Wilson coefficients c_i and d_1. The partly unknown constant part of c_3 is defined as `c3constant` and should be added to this file once it is calculated.

Finally, the last part contains the definitions of the threshold masses. Predefined masses include the PS mass and the 1S mass. The factorization scale, which is needed for the PS mass is defined as μ`f`. The threshold masses are then given in the form of corrections to $\delta m^{\mathrm{TM}}(\mu_f)$, defined in equation (3.224), where TM stands for the corresponding threshold mass. These corrections are named δ`mTM[order,"TM"]`, where `order` stands for the order of the perturbative correction and `TM` stands for the name of the threshold mass (for example "PS" or "1S"). It is easy to implement a new threshold mass permanently in this file. An example how to do this is given in section 4.4.5. The command `TTbarXSection` knows then automatically about the new mass definition.

4.4 Examples

In this section, some useful examples for the use of the packages are presented. The number of the Mathematica input and output is given is such a form, that the user can see where a restart of the kernel has been done. If consecutive numbering is used, some previous inputs might be necessary to use the command.

4.4.1 Grid calculation

Before starting the calculation of a new grid, the first part of the package must be loaded.

```
In[1]:=  <<TTbarGridCalc.m;
```

Then the upper and lower value of the rescaled energy and width have to be calculated. This is explained in detail in section 4.3.1. In this example, the cross section for energies in the

pole scheme from -5 to 1 GeV are needed, the width should change from 1.4 to 1.5 GeV, the scale from 20 to 60 GeV and the mass will be in the range from 170 to 180 GeV. Then, the rescaled energy range is according to equation (4.1):

$$E^{(min)}_{rescaled} = -5\frac{0.14^2}{0.15275^2}\frac{175}{180}GeV = -4.1GeV \qquad E^{(max)}_{rescaled} = 1\frac{0.14^2}{0.12553^2}\frac{175}{170}GeV = 1.3GeV \tag{4.3}$$

The value for the strong coupling constant at a specific scale can be calculated with the function `Running`α`S` (included in `TTbarXSection`). Similarly, with equation (4.2) the rescaled width is:

$$\Gamma^{(min)}_{rescaled} = \Gamma^{(min)}\frac{0.14^2}{0.15275^2}\frac{175}{180} = 1.14GeV \qquad \Gamma^{(max)}_{rescaled} = \Gamma^{(max)}\frac{0.14^2}{0.12553^2}\frac{175}{170} = 1.92GeV. \tag{4.4}$$

Then, the command for this grid file with an energy and width step of 0.1 GeV is:

```
In[2]:= TTbarGridCalc[Energy→{-4.1,1.3,0.1},Width→{1.1,1.9,0.1},"TTbarGrid"]
```

The grid data is then written in the file `TTbarGrid`. A few seconds after the command `TTbarGridCalc` is started, an estimated finishing time is given. This is a rough estimate taking into account the processor speed.

4.4.2 Preparation for cross section calculation

First, the program
tt TTbarXSection must be loaded. Please include the path, if the location is not included in Mathematica's `$Path` variable.

```
In[1]:=  <<TTbarXSection.m;
```

The next step is to specify and load the grid file with the precalculated grid data. This is necessary for the first four examples. In the last one, a possibility is shown, how the non-analytic parts can be calculated directly without using the precalculation. This will a take a few minutes per point, so usually it is very useful to use the grid data. The grid data can be loaded with:

```
In[2]:= TTbarGridLoad["TTbarXSectionGridFile"]
```

Here `"TTbarXSectionGridFile"` is the name of the grid file. After this, all functions are available and some typical examples are explained in the following subsections.

4.4.3 Complete cross section at different orders

The first example is the cross section for different orders. Here, one is interested in the full cross section including all parts and in the standard mass scheme, which is the PS scheme. Then, the following commands give the cross sections at LO, NLO, NNLO and NNNLO at the energy value of -1, the scale of $\mu = 30$ GeV, a top mass of 175 GeV and the width of 1.5 GeV:

```
In[3]:= TTbarXSection[-1,30,Constants→{175,1.5},Order→{0}]
Out[3]:= 0.52805
In[4]:= TTbarXSection[-1,30,Constants→{175,1.5},Order→{1}]
Out[4]:= 0.303885
In[5]:= TTbarXSection[-1,30,Constants→{175,1.5},Order→{2}]
Out[5]:= 0.559662
In[6]:= TTbarXSection[-1,30,Constants→{175,1.5},Order→{3}]
Out[6]:= 0.547919
```

The calculation of each point takes of the order of a second, and might therefore be too slow for making a plot directly. So, it is useful to perform a precalculation when a plot of the cross section is needed. For example an interpolation can be used as follows for the third-order plot of the energy range from -1 to 3:

```
In[7]:= TTbarInt=Interpolation[Table[{En,
       TTbarXSection[En,30,Constants→{175,1.5},Order→{3}]},{En,-1,3,0.1}]]
Out[7]:=InterpolatingFunction[{{-1,3}},<>]
In[8]:= Timing[TTbarInt[-1]]
Out[8]:= {0.Second, 0.547919}
```

Then, the function `TTbarInt` can be plotted very fast as a function of the energy. Similar functions should then be used for every order.

4.4.4 Contributions from different potentials

In the second example it is shown how to switch on and off different contributions. For a physical analysis this is not needed, but it might be useful if some parts have to be checked separately. First, only the Coulomb potential insertions are calculated, then only the ultrasoft part and finally for example only the third-order double insertion.

To calculate only the part coming from Coulomb potentials, all other parts have to be

switched off. This will be done by using the optional argument of `Order` in `TTbarXSection`. In this option, the first three numbers define the Coulomb potential and have to be switched on (which means that this value is 1). The other numbers stand for the Non-Coulomb parts, the ultrasoft correction and the short distance coefficients and are switched off (or more precisely put to 0) in this example. So, the command for the Coulomb only cross section at third order for the same parameters as in the previous example is:

```
In[9]:= TTbarXSection[1,30,Constants→{175,1.5},
            Order→{3 {{1,1,1},{0,0},{0,0},{0,0},{0},{0},{0,0,0},{0,0}}}]
Out[9]:= 1.06823
```

Similarly for the ultrasoft part only the corresponding parameters are set to one, all others to zero. But this time the leading-order Green function (which is always included, even if all parts are set to zero) will be subtracted to get the pure ultrasoft correction:

```
In[10]:= TTbarXSection[1,30,Constants→{175,1.5},
            Order→{3, {{0,0,0},{0,0},{0,0},{0,0},{0},{1},{0,0,0},{0,0}}}]-
             TTbarXSection[1,30,Constants→{175,1.5},
            Order→{3, {{0,0,0},{0,0},{0,0},{0,0},{0},{0},{0,0,0},{0,0}}}]
Out[10]:= 0.182092
```

A more complicated example is the double insertion. This cannot be switched on directly, so one has to take all parts which contribute to the double insertion at third order first. This includes automatically some contributions from the single insertion (at second order). These have to be subtracted. So, all potentials up to second order are switched on and the single insertions is subtracted in the following way:

```
In[11]:= TTbarXSection[1,30,Constants→{175,1.5},
            Order→{3 {{1,1,0},{1,0},{1,0},{1,0},{1},{0},{1,1,0},{1,0}}}]-
            TTbarXSection[1,30,Constants→{175,1.5},
            Order→{2 {{1,1,0},{1,0},{1,0},{1,0},{1},{0},{1,1,0},{1,0}}}]
Out[11]:= -0.234938
```

In the same way one can also get only single insertions or only triple insertions.

4.4.5 Cross section in different mass schemes

The next example is the use of different mass schemes. It is also shown how to implement a different scheme from those provided in the package.

There are two ways of using a mass scheme different from those given in the file `TTbarConstants`. The first is a permanent implementation, which is useful if the mass scheme will be used frequently. Then, the definitions have to be added at the end of the file `TTbarConstants`. As an example the following lines have been added to the file (this has to be done before loading the package):

```
δmTM[0,"MyDef"] = 10 αS/π;
δmTM[1,"MyDef"] = 100 (αS/π)^2;
δmTM[2,"MyDef"] = 1000 (αS/π)^3;
δmTM[3,"MyDef"] = 10000 (αS/π)^4;
```

Then the command for this definition would be:

```
In[12]:= TTbarXSection[-1,30,Constants→{175,1.5},
            Order→{3},MassDef->"MyDef"]
Out[12]:= 1.20033
```

The other possibility is to define the mass scheme before calling the cross section calculation, so for example:

```
In[13]:= δmTM[0,"MyDef"] = 10 αS/π; δmTM[1,"MyDef"] = 100 (αS/π)^2;
            δmTM[2,"MyDef"] = 1000 (αS/π)^3; δmTM[3,"MyDef"] = 10000 (αS/π)^4;
In[14]:= TTbarXSection[-1,30,Constants→{175,1.5},
            Order→{3},MassDef->"MyDef"]
Out[14]:= 1.20033
```

However, the first method is recommended, so the definitions are permanent and can be used again in a later session without defining the mass scheme again.

4.4.6 Photon mediated cross section

For comparison with other calculations it might be useful to consider only the photon mediated cross section and suppressing the Z exchange. This can be done by adding the command

`Production->"PhotonOnly"`. The complete R-ratio is defined in (2.1) by

$$R = \frac{\sigma(e^+e^- \to t\bar{t} + X)}{\sigma(e^+e^- \to \mu^+\mu^-)} = 12\pi \mathrm{Im}\Big[e_t^2 \Pi^{(v)}(q^2) - \frac{2q^2}{q^2 - M_Z^2} v_e v_t e_t \Pi^{(v)}(q^2) + \Big(\frac{q^2}{q^2 - M_Z^2}\Big)^2 (v_e^2 + a_e^2)(v_t^2 \Pi^{(v)}(q^2) + a_t^2 \Pi^{(a)}(q^2))\Big], \tag{4.5}$$

and the optional command `Production->"PhotonOnly"` gives only the contribution coming from the first term (proportional to e_t^2). Another possibility to exclude some of the contributions is to set the relevant prefactors to zero. So, instead of using

```
In[15]:= TTbarXSection[-1,30,Constants→{175,1.5},
            Order→{3},Production->"PhotonOnly"]
Out[15]:= 0.534374
```

one could also first set v_e and a_e to zero and calculate then the full cross section. The coefficients v_e and a_e are defined as `ve` and `ae` (see section 4.3.3), so the command would be:

```
In[16]:= ve=0; ae=0; TTbarXSection[-1,30,Constants→{175,1.5},Order→{3}]
Out[16]:= 0.534374
```

This might be useful for example if one is interested in the P-wave contribution only. This could be calculated by setting `vt` and `et` to zero.

4.4.7 Cross section at zero width for positive energies

Finally it is shown how the program can be used to calculate the cross section at zero width for positive energies. This region in parameter space is usually not covered by a grid file. There is a possibility to use exact results for the non-analytic functions instead of using the grid. This can be done by loading the package `TTbarGridCalc` instead of the grid file. The definitions of the sums are the same as in the program `TTbarXSection`, so the result will be the exact cross section without the error from the grid interpolation. So, first a new kernel is started and the `TTbarGridCalc` package is loaded (due to Mathematicas handling of definitions, this has to be done before loading the `TTbarXSection` file):

```
In[1]:= <<TTbarGridCalc.m;
```

This contains the same definitions for the non-analytic functions and so they are calculated exactly instead of using the grid data. Now, as usual, the `TTbarXSection` file is loaded:

```
In[2]:= <<TTbarXSection.m;
```

With this method, the calculation will take a few minutes per point, so it is recommended to use a grid file for typical values for the input parameters. At zero width however, the calculation is faster than for higher values, because the ultrasoft part, which is the most time consuming, is already precalculated (see section 4.3.1). After loading both packages, one can now use the usual command for the cross section:

```
In[3]:= TTbarXSection[1,30,Constants→{175,0.00001},
            Order→{3},MassDef→"Pole"]
Out[3]:= 1.102
```

Note that a small positive width has been used instead of taking exactly zero to ensure that the integral is taken along the correct contour. Another important point is that this calculation can only be done for positive energy values (in the pole scheme), because the hypergeometric functions from the Coulomb insertion result are ill defined for negative energies and zero width.

4.4.8 Toponium energy levels and wave functions

With the package it is also possible to get numerical values for the wave function and energy levels. Analytical expressions can be obtained by clearing the numerical values for the parameters (like `cF` or `cA`) from the memory. In this example, only the numerical evaluation is shown. First the package has to be loaded again.

```
In[1]:= <<TTbarXSection.m;
```

For energy levels and wave functions no grid data is necessary, so the commands are directly available. Then, the third-order ground-state ($n = 1$) energy level of the S-wave state at the scale $\mu = 30$ GeV and a mass of $m = 175$ GeV is:

```
In[2]:= TTbarEnergyLevels[1,30,Constants→{175},Order→{3}]
Out[2]:= -1.61401
```

The wave function at third order for the same state is:

```
In[3]:= TTbarWaveFunctions[1,30,Constants→{175},Order→{3}]
Out[3]:= 1573,25
```

So, the third-order correction only (normalized to the leading order) for the energy level and wave function is:

```
In[4]:=(TTbarEnergyLevels[1,30,Constants→{175},Order→{3}]
            -TTbarEnergyLevels[1,30,Constants→{175},Order→{2}])
            /TTbarEnergyLevels[1,30,Constants→{175},Order→{0}]
Out[4]:= -0.0135455

In[5]:=(TTbarWaveFunctions[1,30,Constants→{175},Order→{3}]
            -TTbarWaveFunctions[1,30,Constants→{175},Order→{2}])
            /TTbarWaveFunctions[1,30,Constants→{175},Order→{0}]
Out[5]:= -0.0335683
```

The commands for different values of the mass, the width or the scale can be obtained similarly to the cross section case.

Chapter 5

Phenomenology

In this chapter, the phenomenological applications of the results are discussed. First, the corrections to the energy levels and wave functions of heavy quarkonium systems are analyzed. These corrections are needed for the cross section, in order to resum poles, which become large at threshold, into the denominator. They can also be used to examine top quark properties, like the mass corrections (from energy levels) or the decay constant (from the wave function). In the second part, the third order effects on the top-antitop pair production threshold in electron-positron annihilation are shown and a detailed analysis of the new results is given. For all results obtained here, unknown coefficients are set to zero (for the three-loop Coulomb coefficient the Padé estimates are used) and only QCD corrections are taken into account. Electroweak corrections are missing and might have a significant impact on the results, but a full calculation is currently not available for this process.

5.1 Quarkonium energy levels and wave functions

In this first part, the size of the corrections of the energy levels and wave functions is discussed for both, the bottomonium and the toponium. Near the threshold, where $E \to E_n^{(0)}$, the two point function can be written in terms of the bound state poles and the residue Z_n:

$$\Pi(q^2) = \frac{N_c}{2m^2} \frac{Z_n}{E_n - (E + i\,\epsilon)} + \text{non-pole.} \tag{5.1}$$

The residue is given by

$$Z_n = c_v \Big[c_v - \frac{E_n}{m} \Big(1 + \frac{d_v}{3} \Big) + \cdots \Big] \times |\psi_n(0)|^2. \tag{5.2}$$

So, written in an expanded form, defining $Z_n = |\psi_n^{(0)}(0)|^2 \, (1 + \sum_k (\alpha_s/4\pi)^k z_k)$, the coefficients z_i read:

$$z_1 = 2c_v^{(1)} + f_1, \tag{5.3}$$

$$z_2 = 2c_v^{(2)} + {c_v^{(1)}}^2 + 2c_v^{(1)} f_1 + f_2 - \frac{4}{3}\frac{16\pi^2 E_n^{(0)}}{m\alpha_s^2}, \tag{5.4}$$

$$z_3 = 2c_v^{(3)} + 2c_v^{(1)}\left(c_v^{(2)} + f_2\right) + \left(2c_v^{(2)} + {c_v^{(1)}}^2\right) f_1 + f_3 - \frac{16\pi^2 E_n^{(0)}}{m\alpha_s^2}\left[\frac{d_v^{(1)}}{3} + \frac{4}{3}\left(c_v^{(1)} + e_1 + f_1\right)\right]. \tag{5.5}$$

Note that in contrast to the wave function, the residue is finite, because it is a physical quantity. It has been checked explicitly that the divergences coming from the wave function and the short-distance coefficients cancel. The residue Z_n is related to the leptonic decay width $\Gamma([q\bar{q}]_n \to l^+l^-)$ of the nth S-wave quarkonium state by

$$\Gamma([q\bar{q}]_n \to l^+l^-) = \frac{4\pi N_c e_q^2 \alpha^2 Z_n}{3m^2}. \tag{5.6}$$

The similar relation holds also for the P-wave residue, which is related to the decay of the P-wave state. Summarized, the wave function describes the decay of the quarkonium and the energy levels can be observed as corrections to the quarkonium masses. In the next subsections, the corrections to the masses will be discussed first, followed by an examination of the quarkonium residues.

5.1.1 Quarkonium masses

First, a numerical version of the general result for the S-state energy levels for the spin-triplet case with $n_f = 4$ (bottomonium) and $n_f = 5$ (toponium) will be given. For the first three states $n = 1, 2, 3$, the result for $n_f = 4$ is:

$$M_{\Upsilon(1S)} = 2m_b - \frac{4}{9}m_b\alpha_s^2\Big[1 + \Big(3.590 + 2.653\,L_1\Big)\alpha_s + \Big(19.52 + 12.07\,L_1 + 5.277\,{L_1}^2\Big)\alpha_s^2 + \Big(111.1 + 15.30\,\ln\alpha_s + 93.67\,L_1 + 27.59\,{L_1}^2 + 9.332\,{L_1}^3\Big)\alpha_s^3\Big], \tag{5.7}$$

$$M_{\Upsilon(2S)} = 2m_b - \frac{1}{9}m_b\alpha_s^2\Big[1 + \Big(4.916 + 2.653\,L_2\Big)\alpha_s + \Big(27.67 + 17.34\,L_2 + 5.277\,{L_2}^2\Big){\alpha_s}^2 + \Big(158.2 + 8.647\,\ln\alpha_s + 132.4\,L_2 + 41.59\,{L_2}^2 + 9.332\,{L_2}^3\Big)\alpha_s^3\Big], \tag{5.8}$$

$$M_{\Upsilon(3S)} = 2m_b - \frac{4}{81}m_b\alpha_s^2\Big[1 + \Big(5.800 + 2.653\,L_3\Big)\alpha_s + \Big(34.49 + 20.86\,L_3 + 5.277\,{L_3}^2\Big)\alpha_s^2 + \Big(206.8 + 6.305\,\ln\alpha_s + 165.7\,L_3 + 50.92\,{L_3}^2 + 9.332\,{L_3}^3\Big)\alpha_s^3\Big]. \tag{5.9}$$

Here, m_b is the bottom quark pole mass, and as before $L_n = \ln(n\mu/(m_b C_F \alpha_s(\mu)))$. The third-order result for $n = 1$ has already been obtained in [107], the other results are new and were published in [35]. It is already obvious, that the series will not converge, due to

the huge series coefficients. The reason is, as already explained in section 3.6, that the pole mass suffers from a renormalon effect [92,108] which is not present in the physical observable itself [94,96]. Therefore it is more useful to use a threshold mass definition. The results will be given also in the potential-subtracted (PS) scheme [94] in the following.

The bottomonium results will now be examined at the "natural" renormalization scale μ, where the logarithms vanish, so $L_n = \ln(n\mu/(M_b C_F \alpha_s(\mu))) = 0$. M_b is the bottom quark mass in the chosen scheme (denoted by m_b in the pole scheme and $m_{b,\mathrm{PS}}$ in the PS scheme). For $\Lambda_{\mathrm{QCD}}^{(n_f=4)} = 290.4\,\mathrm{MeV}$, and with the four-loop running of α_s, the "natural" scale is realized at $\mu = (2.02,\ 1.30,\ 1.03)$ GeV (for $n = 1,2,3$) with $m_b = 5\,\mathrm{GeV}$, and $\mu = (1.91, 1.23, 0.98)$ GeV with $m_{b,\mathrm{PS}}(2\,\mathrm{GeV}) = 4.6\,\mathrm{GeV}$. Using the relation between the pole and PS mass, $M_{\Upsilon(nS)}$ is reexpressed in terms of $m_{b,\mathrm{PS}}$ taking into account that μ_f/m_b counts as one power of α_s. With $m_b = 5\,\mathrm{GeV}$, $m_{b,\mathrm{PS}} \equiv m_{b,\mathrm{PS}}(2\,\mathrm{GeV}) = 4.6\,\mathrm{GeV}$ the result (separated in Coulomb and Non-Coulomb plus ultrasoft part) reads:

$$\begin{aligned}
M_{\Upsilon(1S)} &= 2m_b + E_1^{(0)}\Big[1 + 1.09_{\mathrm{NLO}} + \Big(1.42 + 0.36_{nC}\Big)_{\mathrm{N^2LO}} + \Big(2.29 + 0.28_{nC+us}\Big)_{\mathrm{N^3LO}}\Big] \\
&= 2m_{b,\mathrm{PS}} + E_{1,\mathrm{PS}}^{(0)}\Big[1 + 0.19_{\mathrm{NLO}} + \Big(0.07 - 0.23_{nC}\Big)_{\mathrm{N^2LO}} + \Big(0.09 - 0.19_{nC+us}\Big)_{\mathrm{N^3LO}}\Big], \quad (5.10) \\
M_{\Upsilon(2S)} &= 2m_b + E_2^{(0)}\Big[1 + 1.91_{\mathrm{NLO}} + \Big(3.84 + 0.35_{nC}\Big)_{\mathrm{N^2LO}} + \Big(8.64 + 0.18_{nC+us}\Big)_{\mathrm{N^3LO}}\Big] \\
&= 2m_{b,\mathrm{PS}} + E_{2,\mathrm{PS}}^{(0)}\Big[1 + 0.26_{\mathrm{NLO}} + \Big(0.26 - 0.05_{nC}\Big)_{\mathrm{N^2LO}} + \Big(0.37 - 0.03_{nC+us}\Big)_{\mathrm{N^3LO}}\Big], \quad (5.11) \\
M_{\Upsilon(3S)} &= 2m_b + E_3^{(0)}\Big[1 + 2.69_{\mathrm{NLO}} + \Big(7.06 + 0.34_{nC}\Big)_{\mathrm{N^2LO}} + \Big(20.10 - 0.03_{nC+us}\Big)_{\mathrm{N^3LO}}\Big] \\
&= 2m_{b,\mathrm{PS}} + E_{3,\mathrm{PS}}^{(0)}\Big[1 + 0.25_{\mathrm{NLO}} + \Big(0.41 - 0.03_{nC}\Big)_{\mathrm{N^2LO}} + \Big(0.69 + 0.00_{nC+us}\Big)_{\mathrm{N^3LO}}\Big], \quad (5.12)
\end{aligned}$$

with

$$E_{n,\mathrm{PS}}^{(0)} = -\frac{(\alpha_s C_F)^2 m_{b,\mathrm{PS}}}{4n^2} + \frac{2\mu_f C_F \alpha_s}{\pi}. \quad (5.13)$$

While the series did not converge in the pole scheme, even with vanishing logarithms, the situation is different in the PS scheme. For the latter, the coefficients are slowly decreasing for the ground state, but for higher excited states a convergence can not be seen. The reason is, that for $n > 1$, the scale is near or below 1 GeV and a perturbative treatment is no longer justified. Another observation is, that the Coulomb correction increases with n, while the Non-Coulomb corrections become smaller. The reason for this is that the characteristic distance scale (the "Bohr radius") increases $\langle r_n \rangle \sim n$, hence the relative effect of the short-range Non-Coulomb interactions decreases for the excited states.

Now, the experimental Υ(1S) mass $M_{\Upsilon(1S)} = 9.460\,\mathrm{GeV}$ can be used to extract the bottom PS mass at NNNLO, as was done in [109] at NNLO. In figure 5.1 the extracted PS mass is shown as a function of the renormalization scale μ at LO (black long dashes), NLO

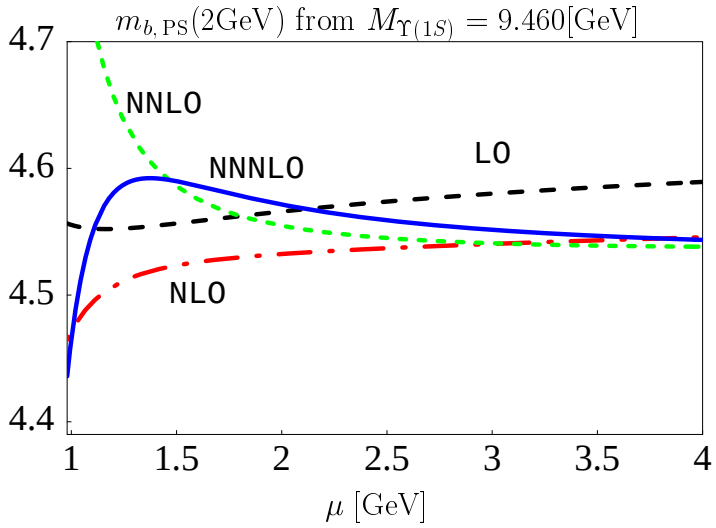

Figure 5.1: The bottom PS mass, $m_{b,\mathrm{PS}}(2\,\mathrm{GeV})$, extracted from the experimental value $M_{\Upsilon(1S)} = 9.460\,\mathrm{GeV}$ as a function of renormalization scale μ at LO (long dashes, black), NLO (long-short dashes, red), NNLO (short dashes, green) and NNNLO (solid, blue).

(red long-short dashed), NNLO (green short dashed) and NNNLO (blue solid). Varying μ from 1.25 GeV to 4 GeV, the NNNLO correction is never larger than about 30 MeV, and the error from the scale dependence is of similar size. Therefore, a ± 30 MeV error will be assigned to $m_{b,\mathrm{PS}}$ from the truncation of the perturbative expansion. The uncertainty in $\alpha_s(M_Z) = 0.118 \pm 0.003$ results in a ± 10 MeV error on $m_{b,\mathrm{PS}}$. The largest uncertainty in the determination of the bottom quark mass from the Υ(1S) mass is then from non-perturbative effects. The perturbative approximation is justified when the ultrasoft scale $m_b(C_F\alpha_s)^2 \gg \Lambda_{\mathrm{QCD}}$, in which case the leading non-perturbative contributions is expressed in terms of the gluon condensate [110, 111]

$$\delta M^{\mathrm{np}}_{\Upsilon(1S)} = \frac{624\pi m_b}{425} \frac{\langle \alpha_s GG \rangle}{(m_b C_F \alpha_s)^4}. \tag{5.14}$$

The numerical estimate is strongly dependent on the choice of scale in α_s in the denominator. Referring to [109] for a more detailed discussion of the non-perturbative correction, the final result of this analysis is

$$m_{b,\mathrm{PS}}(2\,\mathrm{GeV}) = (4.57 \pm 0.03_{\mathrm{pert.}} \pm 0.01_{\alpha_s} \pm 0.07_{\mathrm{non-pert.}})\,\mathrm{GeV}\,. \tag{5.15}$$

Because of the small third-order correction, the bottom quark mass remains practically unchanged compared to the second-order analysis of [109], and so does the $\overline{\mathrm{MS}}$ mass determined from (5.15). Further improvement of the mass determination by this method requires a quantitative understanding of non-perturbative effects.

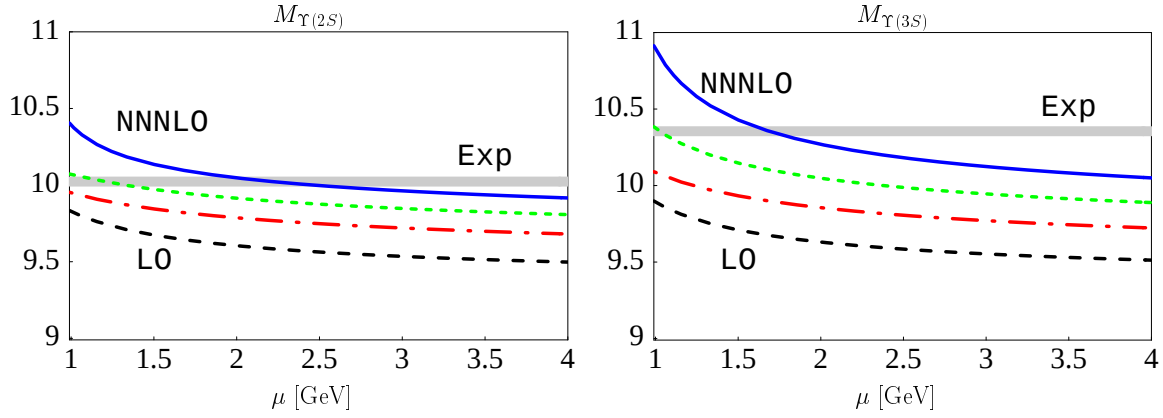

Figure 5.2: Predicted masses of the Υ(2S) and Υ(3S) as a function of the renormalization scale μ. The lines refer to LO (long dashes, black), NLO (long-short dashes, red), NNLO (short dashes, green) and NNNLO (solid, blue). The widths of the bands for the experimental mass values are exaggerated.

With the result of $m_{b,\mathrm{PS}}$, a prediction of the masses of the excited S-level states can be performed. Here, the spin-triplet states Υ(2S) and Υ(3S) are considered. The successive approximations up to the third order are shown in figure 5.2 for $m_{b,\mathrm{PS}} = 4.57\,\mathrm{GeV}$ as a function of the renormalization scale. For μ between 2 GeV and 4 GeV, it appears that the large third-order correction brings the theoretical result closer to the observed masses. However, at the natural scales 1.23 GeV ($n = 2$) and 0.98 GeV ($n = 3$) the NNLO result agrees well with the data, and the NNNLO correction renders the prediction too large. As is apparent from the figure, the conclusion is that the perturbative computation of bottomonium masses is applicable only to the ground state, $n = 1$, while the excited states, involving larger distances, appear to be in the non-perturbative regime. It can be seen from (5.11) and (5.12) that the NNNLO term for $n > 1$ is dominated by the Coulomb correction.

A similar analysis can now be done for the top quark case. For the spin-triplet toponium, $n_f = 5$, the series for the three lowest states reads:

$$M_{t\bar{t}(1S)} = 2m_t - \frac{4}{9}m_t\alpha_s^2\Big[1 + \Big(3.201 + 2.440\,L_1\Big)\alpha_s + \Big(16.43 + 9.718\,L_1 + 4.467\,{L_1}^2\Big)\alpha_s^2 + \Big(87.26 + 15.30\ln\alpha_s + 72.22\,L_1 + 20.06\,{L_1}^2 + 7.267\,{L_1}^3\Big)\alpha_s^3\Big]\,, \tag{5.16}$$

$$M_{t\bar{t}(2S)} = 2m_t - \frac{1}{9}m_t\alpha_s^2\Big[1 + \Big(4.421 + 2.440\,L_2\Big)\alpha_s + \Big(23.41 + 14.18\,L_2 + 4.467\,{L_2}^2\Big)\alpha_s^2 + \Big(118.42 + 8.647\,\ln\alpha_s + 99.75\,L_2 + 30.96\,{L_2}^2 + 7.267\,{L_2}^3\Big)\alpha_s^3\Big]\,, \tag{5.17}$$

$$M_{t\bar{t}(3S)} = 2m_t - \frac{4}{81} m_t \alpha_s^2 \Bigg[1 + \Big(5.234 + 2.440\, L_3 \Big) \alpha_s + \Big(28.33 + 17.16\, L_3 + 4.467\, {L_3}^2 \Big) \alpha_s^2 + \Big(153.2 + 6.305\, \ln \alpha_s + 124.2\, L_3 + 38.23\, {L_3}^2 + 7.267\, {L_3}^3 \Big) \alpha_s^3 \Bigg] , \tag{5.18}$$

where m_t is top quark pole mass.

At this point it is important to mention that toponium bound states do not exist in nature due to the large decay width $\Gamma_t \sim 1.5\,\text{GeV}$ of the top quark. However, the remnant of the 1S toponium state should be visible as an enhancement in the cross section $e^- e^+ \to t\bar{t}X$ near threshold. The convergence of the series expansion for the toponium 1S mass is therefore a good measure for the accuracy to which the top quark mass might be determined from this cross section [14].

The method suggested in [21, 112] relies on determining $m_{t,\text{PS}} \equiv m_{t,\text{PS}}(20\,\text{GeV})$ from the cross section measurement and obtaining the top quark $\overline{\text{MS}}$ mass from $m_{t,\text{PS}}$, since both relations are expected to be expressible in terms of well-behaved perturbative expansions. Adopting $m_{t,\text{PS}} = 175\,\text{GeV}$, $n_f = 5$, $\Lambda_{\text{QCD}}^{(n_f=5)} = 208\,\text{MeV}$ and the natural scale $\mu = 32.6\,\text{GeV}$, where $L_n = 0$, the result is:

$$M_{t\bar{t}(1S)} = (350 + 0.85 + 0.05 - 0.13 + 0.01)\,\text{GeV} = 350.78\,\text{GeV}. \tag{5.19}$$

The sum of the series varies only by about 60 MeV when the scale is taken between 15 and 60 GeV, although the convergence is no longer satisfactory at the lower scale as will be discussed in the cross section analysis. The small uncertainty implies that $m_{t,\text{PS}}$ can be determined with little theoretical error from the cross section. Then, the largest uncertainty in the determination of the top quark $\overline{\text{MS}}$ mass results from the unknown four-loop coefficient in the relation between the $\overline{\text{MS}}$ mass and the pole mass, which is needed to convert $m_{t,\text{PS}}$ to the $\overline{\text{MS}}$ mass, as already observed in [21]. This uncertainty is estimated to be around 100 MeV (see table 2 of [14]).

5.1.2 Quarkonium residue

The quarkonium residue can be obtained from the wave function and the short-distance coefficients, as explained in the beginning of this section. For the ground state of top and bottom quarkonia, the following results are obtained:

$$Z_{1S(t\bar{t})} = \Big\{ 1 + \Big[3.66\, L_1 - 2.13 \Big] \alpha_s(\mu) + \Big[8.93\, L_1^2 - 6.14\, L_1 + 10.46 - 7.26\, L_m \Big] \alpha_s^2(\mu) + \Big[18.17\, L_1^3 - 20.26\, L_1^2 + (110.82 - 11.57\, L_m)\, L_1 - 22.27\, L_{US} - 16.35\, L_m^2 - 22.65\, L_m + (22.60 + 0.0015\, a_3 + 0.32\, \delta_\epsilon + 0.0645\, \delta c_3) \Big] \alpha_s^3(\mu) \Big\} \times |\psi_{1S(t\bar{t})}^{(0)}(0)|^2 , \tag{5.20}$$

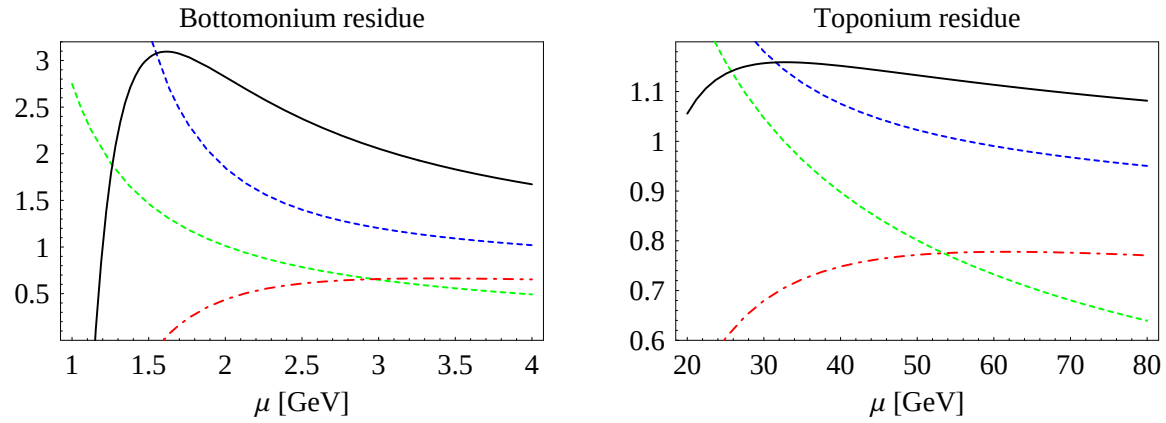

Figure 5.3: The scale dependence of the residue of the two-point function for the bottomonium (left) and toponium (right), normalized by its zeroth order value at $\mu = mC_F\alpha_s(\mu)$. The dashed green line is LO, the dash-dotted red line NLO, the dashed blue line is NNLO and the solid line is the NNNLO result.

$$
\begin{aligned}
Z_{1S(b\bar{b})} = \Big\{ & 1 + \Big[3.98\, L_1 - 2.00\Big]\alpha_s(\mu) + \Big[10.55\, L_1^2 - 6.51\, L_1 + 11.19 - 7.44\, L_m\Big]\,\alpha_s^2(\mu) \\
& + \Big[23.33\, L_1^3 - 23.12\, L_1^2 + (125.14 - 14.59\, L_m)\; L - 22.27\, L_{US} - 17.36\, L_m^2 - 26.61\, L_m \\
& + (17.44 + 0.0015\, a_3 + 0.32\, \delta_\epsilon + 0.0645\, \delta c_3)\Big]\,\alpha_s^3(\mu)\Big\} \times |\psi_{1S(b\bar{b})}(0)|^2\,,
\end{aligned}
\tag{5.21}
$$

where $|\psi^{(0)}_{1S(Q\bar{Q})}(0)|^2 = (mC_F\alpha_s(\mu))^3/(8\pi)$ is the LO Coulomb wave function, and the logarithms are defined as usual: $L_1 = \ln\left(\mu/(mC_F\alpha_s(\mu))\right)$, $L_{US} = \ln\left(e^{5/6}\mu/(2m\alpha_s^2(\mu))\right)$ and $L_m = \ln(\mu/m)$. The numerical size of the corrections will be examined for the following values: for the top quark, $m_t = 175$ GeV, $\mu = m_t\, C_F\, \alpha_s(\mu) = 32.62$ GeV; for the bottom quark, $m_b = 5$ GeV, $\mu = m_b\, C_F\, \alpha_s(\mu) = 2.02$ GeV. Then, the following numbers for the toponium and bottomonium ground state at $\mu = mC_F\alpha_s(\mu)$ are obtained:

$$
Z_{1S(t\bar{t})} = \frac{(C_F\, m_t\, \alpha_s)^3}{8\pi}\Big[1 - 2.13\, \alpha_s + 22.7\, \alpha_s^2 + 4.6\, \alpha_s^3\Big]\,, \tag{5.22}
$$

$$
Z_{1S(b\bar{b})} = \frac{(C_F\, m_b\, \alpha_s)^3}{8\pi}\Big[1 - 2.00\, \alpha_s + 17.9\, \alpha_s^2 + 30.9\, \alpha_s^3\Big]\,, \tag{5.23}
$$

where the coupling constant is $\alpha_s = 0.14,\, 0.304$ for the top and bottom quarkonia, respectively. At third order, a good convergence is observed. While first and second order results are quite large, at third order the corrections are relatively small. They are at the order of 1.3% for the toponium and around 9% for the bottomonium. As expected, the perturbative expansion is not so good for the bottom case, due to the large coupling constant at the characteristic scale of the bottomonium. However, these results have to be interpreted with great care, due to the neglected missing parts. As will be discussed later in more detail for

the cross section, especially the non-n_f terms of the short-distance coefficient can have a big impact on the result.

As an indication of the theoretical uncertainty coming from perturbation theory, the scale dependence of the result will now be examined. Figure 5.3 shows the scale dependence of the ground-state pole residue for bottomonium (left) and toponium (right) at different orders in perturbation theory. It is observed, that the scale dependence is reduced at third order for the top quark case resulting in a relatively flat curve. This indicates that the normalization of the cross section peak might be under control now. The situation is different for the bottomonium. Due to the breakdown of perturbation theory at the bottom scale, the result shows a strong scale dependence of the order of 50%.

5.2 Top quark cross section

In this chapter, several issues related to the third-order correction to the toponium production cross section at the linear collider are examined. First, the behavior of the perturbative series is investigated, followed by a study of the scale dependence. Then, the sensitivity to several input parameters is tested. The result is still incomplete due to the missing c_3 and b_2^ϵ coefficient, so a complete analysis is not possible. The relevance of these unknown parts is inspected in the subsequent subsection. Then, the effects of different mass definitions and of the pole resummation are discussed. After this, a comparison with the resummed (partly known) NNLL result is done. Finally, the continuation to the continuum and the inclusion of further effects is outlined.

If not stated otherwise, the following parameters will be used: the top quark mass (in the PS scheme, if not stated otherwise) is set to $m_t = 175$ GeV, the top width to $\Gamma = 1.5$ GeV, the strong coupling at the scale $M_Z = 91.1876$ GeV is set to $\alpha_s(M_Z) = 0.1176$. The missing part of the short-distance coefficient and the $O(\epsilon)$ part of b_2 are neglected. The typical scale of the plots is $\mu = 30$ GeV.

5.2.1 Perturbative behavior and scale dependence

In this section, the results for the third-order corrections are presented and a comparison with the lower orders is done, followed by an analysis of the scale dependence.

Figure 5.4 shows the results up to the third order. The first observation is, that the LO, NNLO and NNNLO curves are quite similar, but the NLO result differs significantly. For all orders, the peak position is relatively stable, while the normalization of the peak is much lower for the first-order corrections. The new result is, that the third order stabilizes the

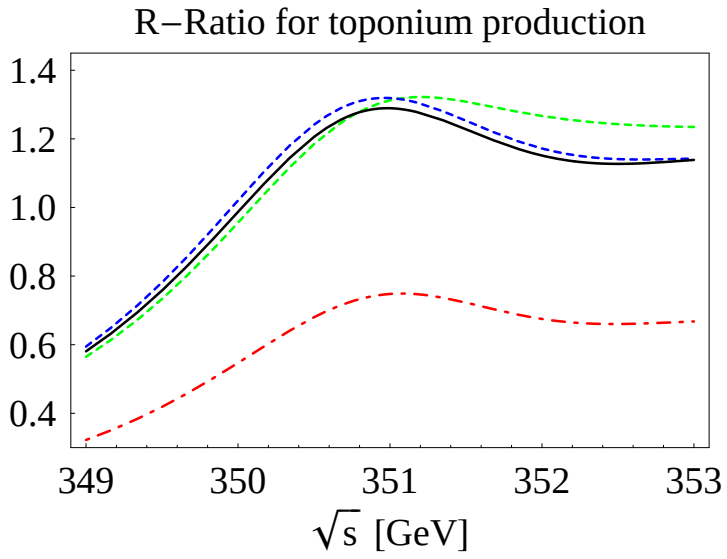

Figure 5.4: The cross section for $t\bar{t}$-production in the PS Scheme for LO (green dashed line), NLO (red dash-dotted), NNLO (blue dashed) and NNNLO (black solid).

perturbative series. To understand this behavior, an analysis of the different parts of the cross section will be done in section 5.2.6.

A first important check of the result is the scale dependence. This scale uncertainty is unphysical and a relic of perturbation theory. Thus it must vanish in an exact result. The variation of the cross section due to scale variations can therefore be used as an estimate of the theoretical error of the result coming from perturbation theory.

The typical scale of the problem is the energy at the Bohr radius $\mu_B \sim 30$ GeV. This corresponds to the scale where $\mu = C_F m \alpha_s(\mu)$, so the logarithms of the form $\ln(\mu/(C_F m \alpha_s))$ are suppressed. Naively, the variation of the scale would be performed from $\mu_B/2$ to $2\mu_B$. But from the analysis of the Coulomb potential it is known, that too low scales lead to a breakdown of perturbation theory [35, 85]. This has been deduced from a comparison of the Coulombic perturbative result with the numerical solution of the Schrödinger equation. In the latter, the insertions of the Coulomb potential (up to third order) have been taken into account for all iterations, while for the perturbative result only the iterations up to third order have been used. So, for example the triple insertion of the second-order potential or the double insertion of the first- with the third-order potential is included in the solution of the Schrödinger equation, while it is of higher order in the perturbative approach. So, the difference of the two results comes exactly from the higher iterations of the potentials (up to third order). This difference is shown in figure 5.5. In the left diagram it can be seen that for $\mu = 30$ GeV the numerical and perturbative solution coincide at third order. But from

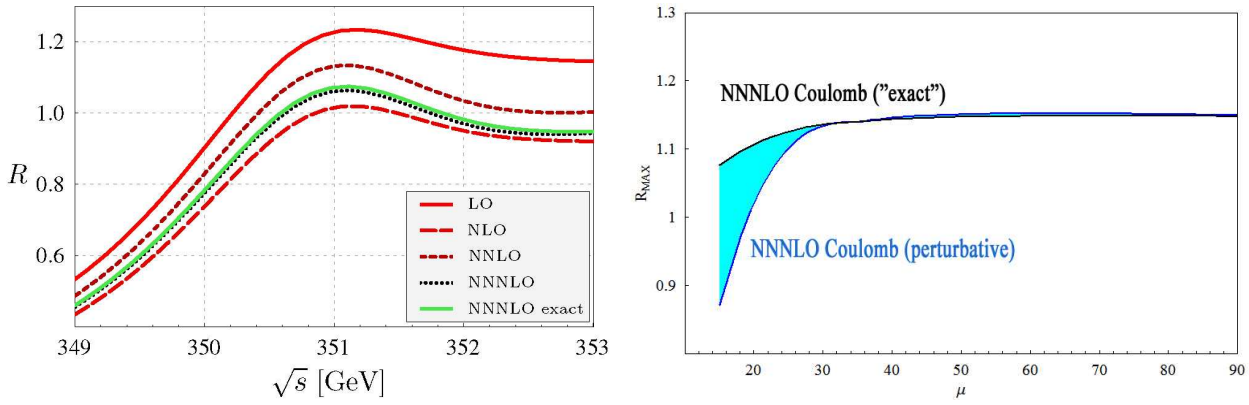

Figure 5.5: The left figure shows the Coulomb cross section coming only from the Coulomb potential insertion for the perturbative and numerical ("exact") solution for $\mu = 30$ GeV (taken from [35]). The right figure shows the scale dependence of the height of the peak for both results.

the right diagram, where the scale dependence of the peak height is shown, it is obvious that this is not true for smaller scales. The turquoise area is the difference of the perturbative and numerical result. It turns out that dropping the higher iterations is leading to a big falloff of the peak height for the perturbative result at scales smaller than about 25 GeV. The falloff is not so pronounced for the numerical solution and can thus be explained as an artifact of perturbation theory. This analysis has been done only for the Coulomb potential. The reason is that this part is finite, and thus can be treated quantum mechanically. The other potential insertions are divergent and a finite result is only obtained by adding the contribution from the short-distance coefficient. Nevertheless, the analysis for the Coulomb potential shows, that the scale has to be chosen above 25 GeV to get a stable result. So, the scale variation in this section is chosen from 25-60 GeV.

Figure 5.6 shows a comparison of the scale variation of the second- (red band) and third-order (black band) result. There is a significant reduction of the scale uncertainty at third order. The variation leads to an error estimate of about 3% for the normalization of the peak. The error of the peak position is too small too be observed from this figure. Figure 5.7 shows explicitly the effect of the scale for the peak position and the height of the peak. The reduced scale dependence of the third-order peak position is more obvious from these diagrams. The error from perturbative effects is around 30 MeV, which is of the same order as the target precision which can be reached by the experiment.

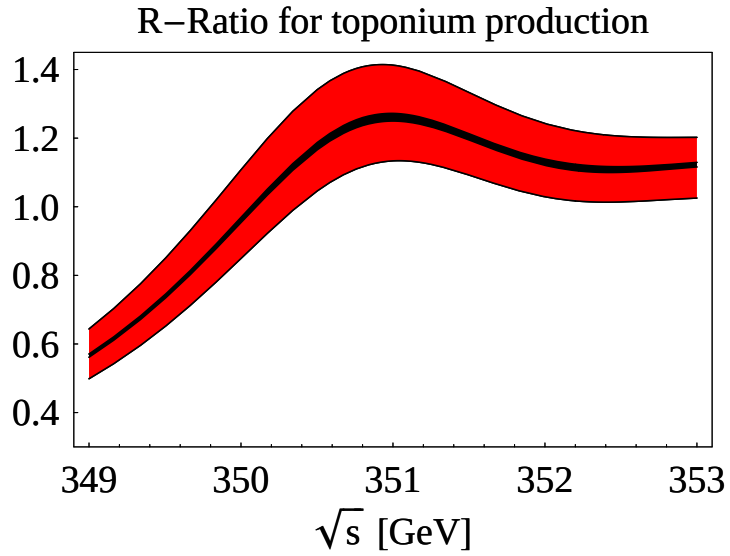

Figure 5.6: Scale dependence of the NNLO (red band) and NNNLO (black band) result for scales varied from $\mu = 25$ GeV (upper bound) and $\mu = 60$ GeV (lower bound).

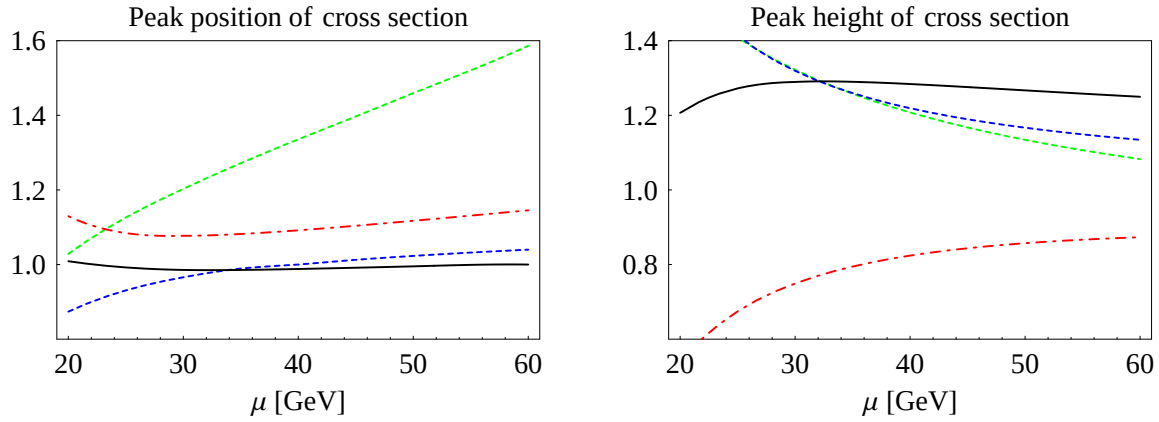

Figure 5.7: Scale dependence of the peak position (left figure) and peak height (right figure) for LO (green dashed line), NLO (red dash-dotted), NNLO (blue dashed) and NNNLO (black solid).

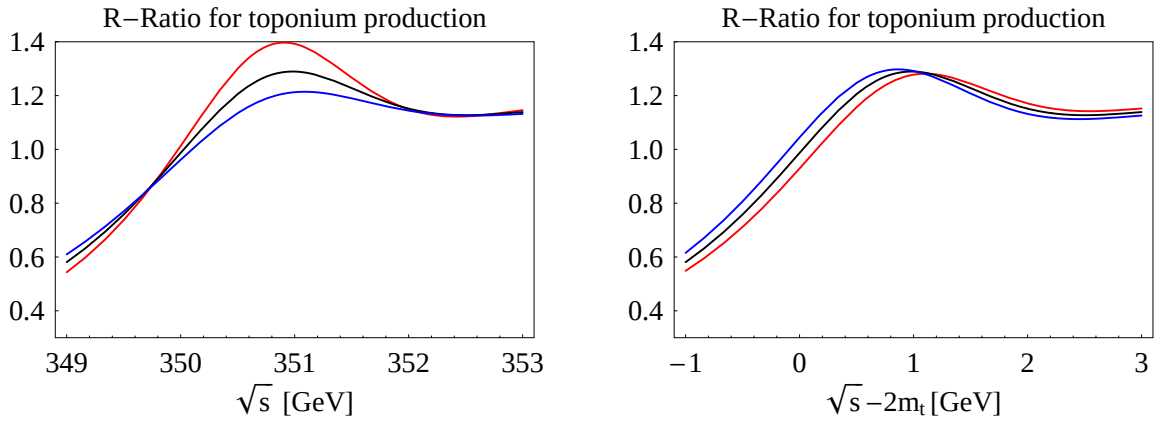

Figure 5.8: Left diagram: Variation of the top quark width Γ_t. The upper line (red) corresponds to $\Gamma_t = 1.3$ GeV, the middle line to $\Gamma_t = 1.5$ GeV and the lower line (blue) to $\Gamma_t = 1.7$ GeV. Right diagram: Variation of the top quark mass from $m_t = 165$ GeV (red line) to $m_t = 175$ GeV (black line) and $m_t = 185$ GeV (blue line).

5.2.2 Parameter analysis

The final aim of a cross section measurement will be not only the extraction of the top quark mass, but a combined fit of different parameters. Such an analysis has been done for example in [13]. In this section the effect of the mass, the width and the strong coupling constant are examined.

Figure 5.8 shows the variation of the top quark mass and width, and figure 5.9 shows the variation of the strong coupling constant. The result is, that the width variation results in a variation of about 20% for the height of the cross section peak. The effect of the mass variation seems to be small, but note that on the x-axis $2m_t$ has been subtracted to show only the quarkonium effect. So, the full mass variation is shifting the cross section horizontally by a large amount and is the dominant effect. The effect of a variation of the strong coupling constant from $\alpha_s(M_Z) = 0.115 - 0.12$ is relatively small and can be estimated to around 15% for the height of the peak and about 100 MeV for the peak position. The current value for $\alpha_s(M_Z) = 0.118$ [10] is the middle curve.

The result of these numbers is, as was already observed by [13] for the second-order calculation, that the mass measurement from this process will be very good (due to the high sensitivity of the cross section on the mass), but the result for the width and the coupling will have much bigger (relative) errors.

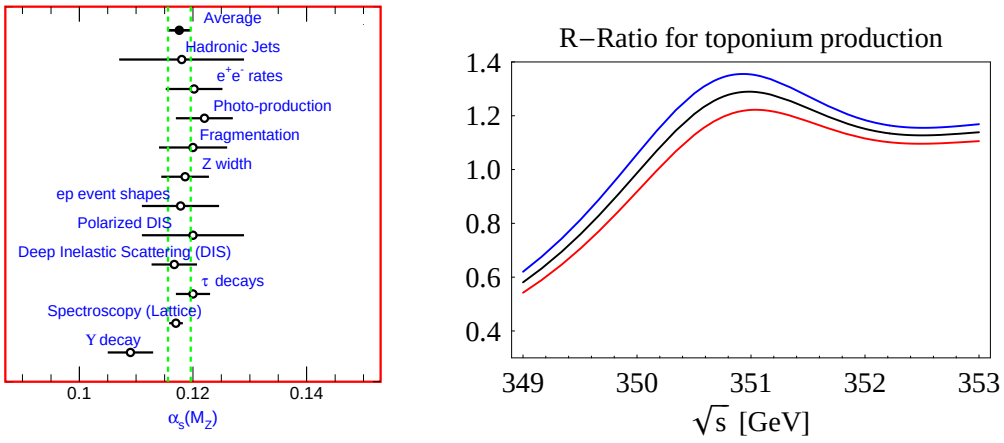

Figure 5.9: Left diagram: Uncertainty for the strong coupling constant (taken from [10]). Right diagram: Variation of the strong coupling from $\alpha_s(M_Z) = 0.115$ (red line) to $\alpha_s(M_Z) = 0.118$ (black line) and $\alpha_s(M_Z) = 0.12$ GeV (blue line).

5.2.3 Size of unknown contributions

For the results of the previous sections, the unknown parameters have been neglected (or Padé estimates have been used for a_3). However, some of them might have a significant impact on the cross section. The unknown parameters are on the one hand from the potential matching (the three-loop coefficient of the Coulomb potential a_3 and the order ϵ part of the two-loop coefficient of the $1/r^2$ potential $b_2^{(\epsilon)}$) and on the other hand the non-n_f (and non-logarithmic) parts of the three-loop short-distance coefficient.

The left part of figure 5.10 shows the sensitivity of the cross section on variations of a_3 and $b_2^{(\epsilon)}$. For the Coulomb three-loop coefficient, Padé estimates are known. The variation is done in a range from $a_3 = 0.25\, a_3^{Pade}$ to $a_3 = 4\, a_3^{Pade}$. The difference in the cross section is very small, given that Padé estimates are usually reliable and don't vary in such a big range.

In the right part of figure 5.10, the parameter $b_2^{(\epsilon)}$ is changed. The black line corresponds to $b_2^{(\epsilon)} = 0$ which is the value used in every other plot. To get a rough idea of the size of this coefficient, the ration of $b_i^{(\epsilon)}/b_i$ is assumed to stay approximately the same for different i (where i is the loop order). Then, one gets:

$$b_2^{(\epsilon),est} \approx \frac{b_1^{(\epsilon)}}{b_1} b_2 = -11.4573\,. \tag{5.24}$$

To be conservative the range is taken from $+4b_2^{(\epsilon),est}$ to $-4b_2^{(\epsilon),est}$. The variation of the cross section for this range is extremely small, and therefore it is reasonable to ignore the effect of $b_2^{(\epsilon)}$ in the following.

The situation is different for the unknown parts of c_3. Figure 5.11 shows the result for this variation. The difference is not negligible and an important effect. The black line

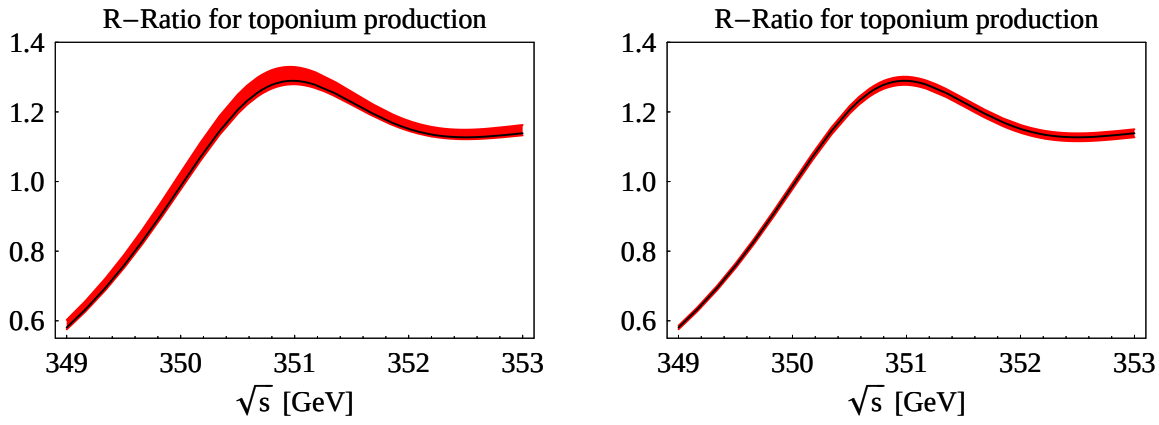

Figure 5.10: Left diagram: Variation of the three-loop Coulomb potential coefficient from $a_3 = 0.25\, a_3^{Pade}$ (lower line) to $a_3 = 4\, a_3^{Pade}$ (upper line). Right diagram: Variation of the order ϵ part of the Non-Abelian two-loop potential coefficient from $b_2^{(\epsilon)} = -45.8291$ (lower line) to $b_2^{(\epsilon)} = +45.8291$ (upper line).

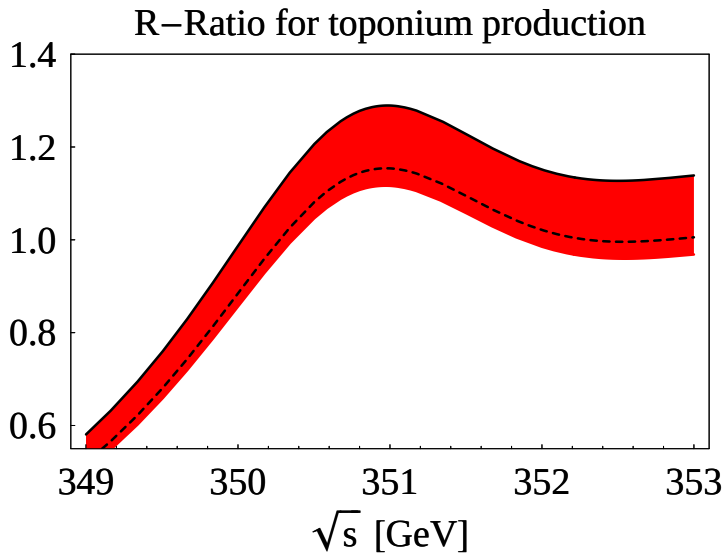

Figure 5.11: Variation of the non-n_f part of the three-loop short-distance coefficient from $c_{v,\not n_f}^{(3)} = 0$ (upper line) to $c_{v,\not n_f}^{(3)} = -47635$ (lower line). The dashed line corresponds to $c_v^{(3,constant)} = 0$ or $c_{v,\not n_f}^{(3)} = -c_{v,n_f}^{(3)}$.

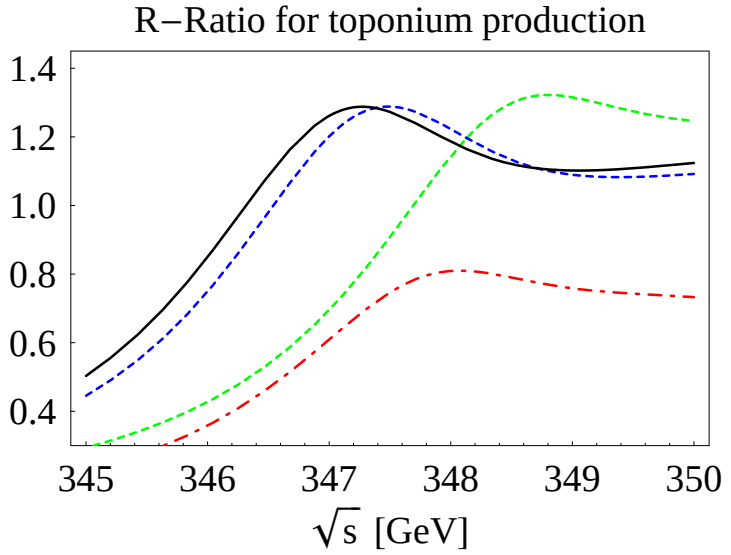

Figure 5.12: The cross section for $t\bar{t}$-production in the Pole Scheme for LO (green dashed line), NLO (red dashed), NNLO (blue dashed) and NNNLO (black solid).

corresponds again to the result where the unknown part is ignored. The dotted curve is for the situation where the complete constant part of c_3 (including the known n_f terms) is ignored and the lower bound of the range is an estimate of the unknown part by the similar method used for $b_2^{(\epsilon)}$. Here the assumption is that the ratio of non-n_f parts of different orders stays approximately the same:

$$c_{v,\not{n}_f}^{(3)} = \frac{c_{v,\not{n}_f}^{(2)}}{c_{v,\not{n}_f}^{(1)}} c_{v,\not{n}_f}^{(2)} = -47635\,. \tag{5.25}$$

The total effect from such a variation is about 20%, and therefore one has to include this coefficient for a meaningful result.

5.2.4 Mass definitions

In this section, the effect of different mass definitions is discussed. As explained in section 3.6, it is crucial to use a threshold mass definition. For completeness, in figure 5.12 the result in the pole mass scheme is given. Here, there is no clear sign of convergence in the perturbative behavior. The reason is the renormalon effect which has been described in 3.6. This result will not be considered further in the following.

The convergence is improved by using threshold mass definitions. There are two ways to implement these. The first is a perturbative expansion of the mass terms in the Lagrangian. The second method is a simple mass shift. This corresponds to taking the perturbations

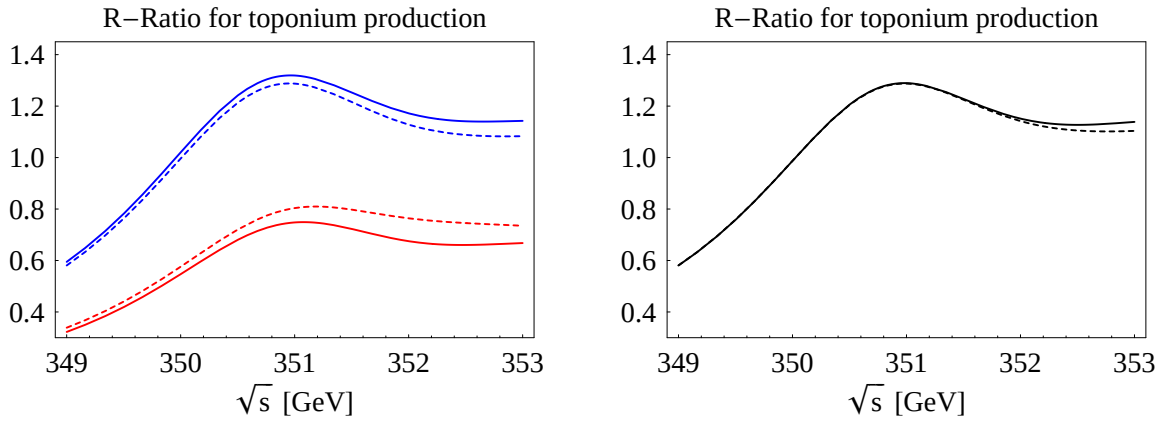

Figure 5.13: Comparison of different implementations of the PS scheme. The dotted lines show the result for the shifted and the solid line for the perturbative implementation. The left diagram shows the NLO (red) and NNLO (blue) result, the right diagram the NNNLO cross section.

into account at all orders. The difference of both methods is shown in figure 5.13. The left diagram shows the first- and second-order corrections and the right diagram the third order. For the shifted result solid lines are used, and the perturbative implementation is given with dotted lines. The observation is, that for the second and third order the two methods lead to a significant difference in the cross section normalization, while at third order both methods lead nearly to the same result. This is what was expected, because the difference between both methods are the higher iterations of the corrections due to the threshold mass terms, and at third order more of these corrections are included in the perturbative result.

The next question is, how important the choice of the threshold mass scheme is. To examine this, exemplary the difference between the PS scheme and the 1S scheme will be discussed. Figure 5.14 shows the result for the different orders in the 1S scheme. If compared with the same figure in the PS scheme (figure 5.4), the first observation is that the peak position is at a different energy value. The reason is that the input for the calculation is different. While in the PS scheme, the PS mass is set to 175 GeV, for the 1S figure the 1S mass is at 175 GeV. So, in fact an energy shift of $m_t^{PS} - m_t^{1S}$ has to be made to get the same peak position for both schemes. However, the shape of the corrections is very similar for the PS and 1S scheme. This can also be seen from figure 5.15, where the scale dependence of the peak position and height of the peak are compared at second and third order. Again the shift of the peak position due to the different mass input can be seen, but the scale dependence itself is very similar for the two schemes. For the peak height, shown on the left side of figure 5.15, the results for the two schemes are very similar. In fact, the effect of the mass scheme

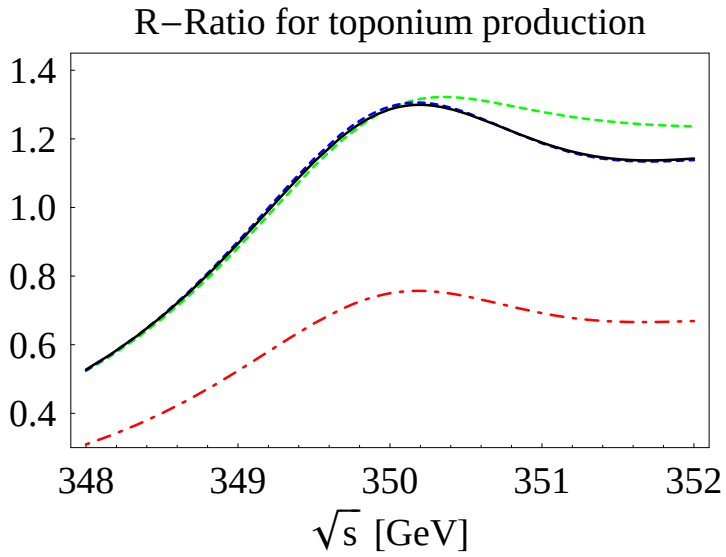

Figure 5.14: The cross section for $t\bar{t}$-production in the 1S Scheme for LO (green dashed line), NLO (red dashed), NNLO (blue dashed) and NNNLO (black solid).

is much smaller than the scale dependence itself.

5.2.5 Resummation effects

In this section, the effect of the pole resummation is analyzed. The resummation of the threshold poles is explained in section 3.7. The right diagram of figure 5.16 shows the third-order result including the resummation (solid lines) and without resummation (dashed lines) for two different implementations of the threshold mass scheme. In the pole scheme the effect of the pole resummation is very big. The shifted implementation is a simple energy shift, so the big pole scheme effects translate also into big effects of the shifted PS scheme. This is not only observed at third order, but also in lower orders, as can be seen from the left diagram in figure 5.16.

Interestingly, it seems, that a perturbative PS scheme implementation cures this problem. There, the effect of the pole resummation is much smaller. However, after the resummation both implementation lead to the same result. The reason that the pole resummation in the perturbative implementation is so small is because of additional mass terms which are added. These have also a pole structure, which is similar to the expanded results. So the two effects cancel.

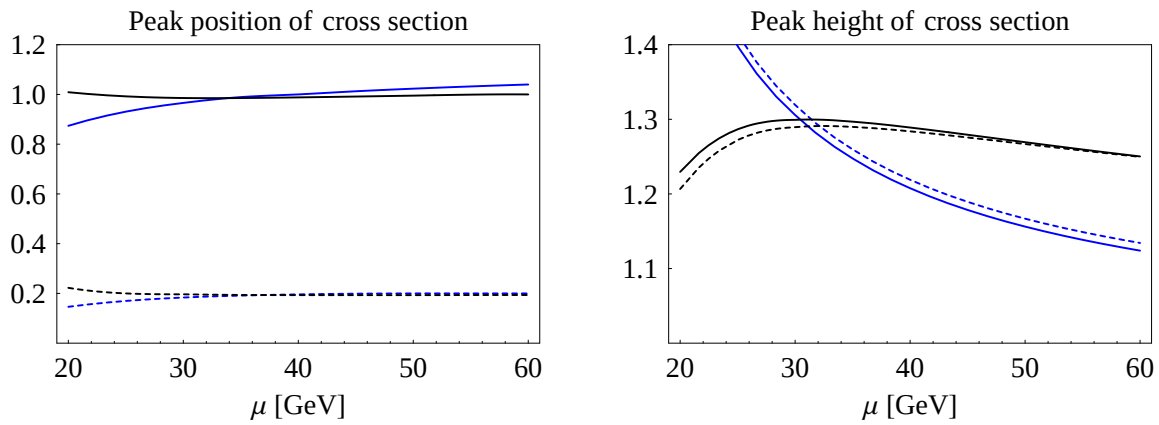

Figure 5.15: Scale dependence of the peak position (left) and peak height (right) of the NNLO (blue) and NNNLO (black) cross section for the 1S (dotted lines) and PS (ssolid lines) scheme.

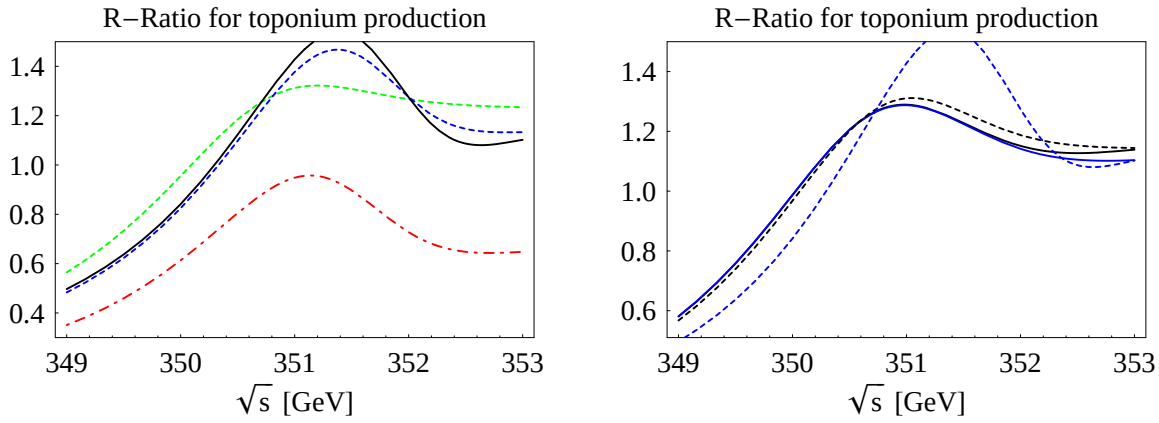

Figure 5.16: Left diagram: The cross section in the PS Scheme (shift implementation) without resummation for LO (green dashed line), NLO (red dash-dotted), NNLO (blue dashed) and NNNLO (black solid). Right diagram: The third order cross section with (solid lines) and without (dashed lines) resummation for the PS shifted (blue) and perturbative (black) implementation.

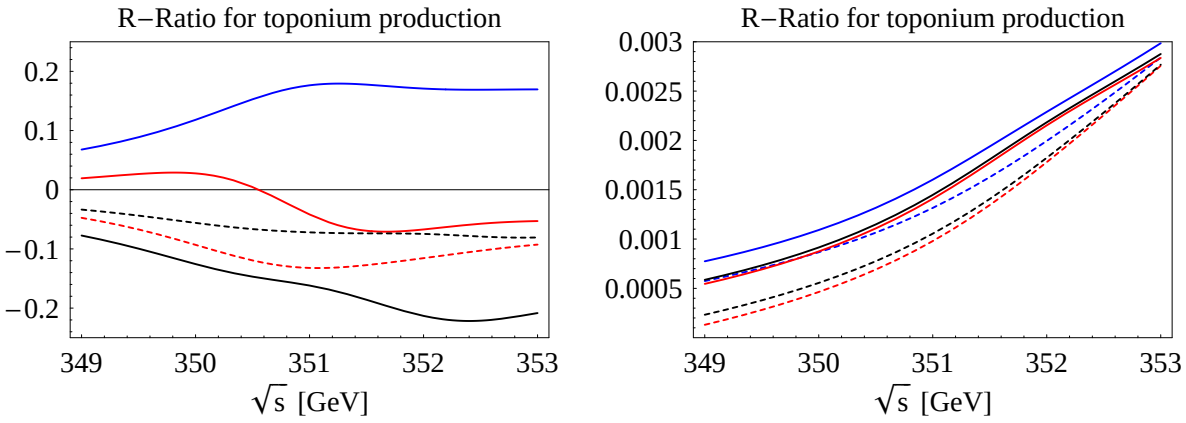

Figure 5.17: Left diagram: Size of different contributions for the S-wave cross section. The dotted lines are the third-order correction only and the solid lines the complete (first plus second- plus third-order) corrections for Coulomb potential (black), non-Coulomb potentials (red) and ultrasoft part (blue). Right diagram: P-Wave contribution to the cross section.

5.2.6 Analysis of insertions

In this section, different parts of the cross section are discussed. Three different types can be distinguished, the Coulomb potential insertions, the non-Coulomb insertions and the ultrasoft corrections. The P-wave contributions are discussed separately. There is an ambiguity in defining the non-Coulomb potentials and the ultrasoft correction, because the counter term potential which is subtracted from the potentials and added back to the ultrasoft corrections can be defined differently[1]. Only the combined result is finite and meaningful. However, in this section the two are separated to show the size of the individual parts. The left diagram of figure 5.17 shows the three contributions. The solid lines are the subsequently added contributions up to third order, and the dotted lines are the third order contributions only. The ultrasoft correction appears only at third order, so here both curves are the same. It can be seen, that the third-order Coulomb corrections are small (about 5%), while at third order, ultrasoft and non-Coulomb parts are quite big (around $10-20\%$), but with opposite sign. So, the total contribution is small. The P-wave contributions to the total cross section are tiny, as was already observed in previous papers. The result agrees well with the results using other regularization schemes [24, 43–45]. Note that usually a different normalization is chosen for the plots there. The scale dependence which is already very small for the leading order P-wave part is reduced further for the NLO result and the effect on the complete result can be neglected.

[1] At third order, also the Coulomb potential has such a term. But the effect of this term is quite small, so that the ambiguity in choosing the separation is negligible for this analysis.

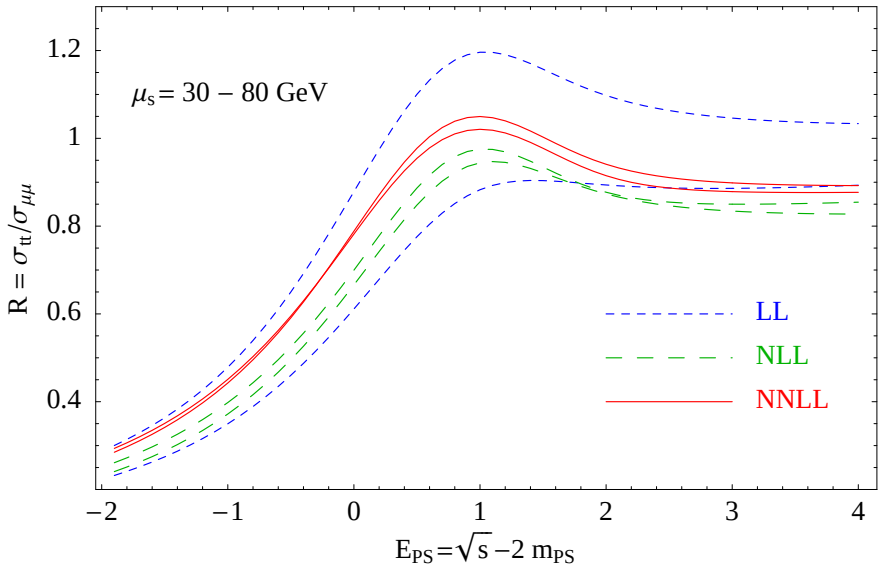

Figure 5.18: Cross section in the RG improvement version for LL, NLL and NNLL for an input of $m_t^{PS} = 175$ GeV for different scales (taken from [30])

5.2.7 Comparison with NNLL results

The presented results will now be compared to the second-order resummed results (NNLL). These are only partially known [28–30], but the unknown terms are expected to be considerably small. The main difference between the NNNLO and the NNLL result is, that the fixed-order approach includes the constant (non-logarithmic) term at third order, while the NNLL result contains higher powers of the logarithms coming from second order. However, it has been shown, that the main difference of the NNLL and NNLO result comes from the third-order logarithms, which are also included in the NNNLO result. This can be seen in figure 5.19. The notation "NNNLO" means the complete second order plus the third-order logarithms and the curve for "NNLL" includes also higher logarithms. The results from [30], shown in figures 5.18 and 5.19, can be compared with those discussed in the previous sections. The observation is, that the difference in the peak position is about 50 MeV, thus of the order of the target precision and the normalization is changed by about 5%. This leads to the conclusion that the third-order constant effects cannot be ignored to achieve the aimed accuracy. For a serious comparison, the missing constants have to be taken into account, which in the case of the short-distance coefficient can have a significant effect.

5.2.8 Outlook

In this section, a brief outlook of the remaining work will be given. For the QCD corrections some missing parts have to be calculated and the effect of these parts were discussed in

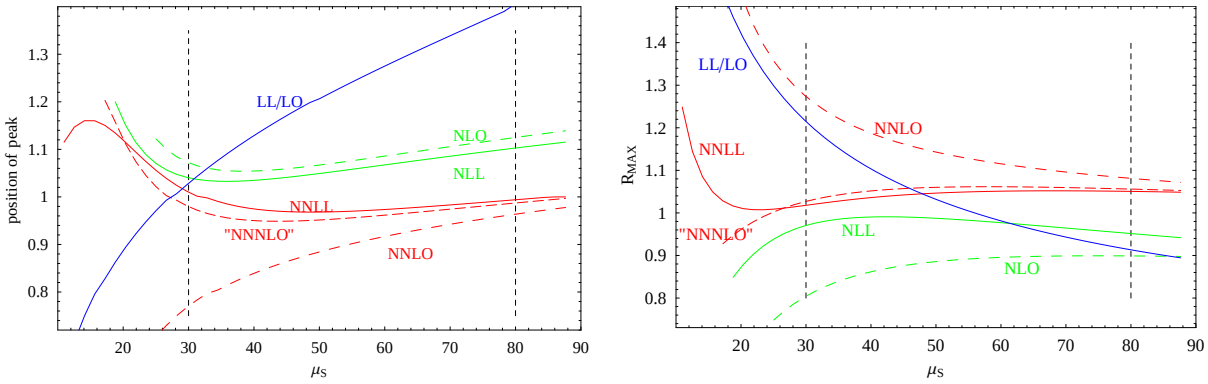

Figure 5.19: Left diagram: Scale dependent variation of the peak height in the RG improved result for different orders. Right diagram: Scale dependent variation of the peak position in the RG improved result for different orders (both taken from [30])

section 5.2.3. On top of the QCD corrections, a combined QCD and electroweak result not only desirable, but necessary due to uncanceled Γ/ϵ divergencies. First steps towards the electroweak result have been done [25–27]. However, there is still a lot of ongoing work at the moment on this topic.

Another point to mention is, that this result is only valid at threshold, due to the non-relativistic approach. So, a continuation to the continuum limit has to be performed in the end. For energies well above threshold, the usual perturbation theory can be applied. Results up to two loops ($O(\alpha_s)$) and some three-loop results for the QCD corrections are available [113–115]. Figure 5.20 shows the continuation done for the second-order results [45]. The observation is, that the perturbative corrections as well as the scale dependence are lower for the non-relativistic result in the possible overlap region around $355 - 360$ GeV (for a top mass of $m_t = 175$ GeV).

Finally an important task is to consider initial-state radiation and beam effects. They can play an important role for the precision of the mass measurement [116–118]. The observed cross section is the theoretical result (calculated in this work) folded with luminosity spectrum $\mathcal{L}(x)$:

$$R^{exp}(\sqrt{s}) = \int_0^1 dx \mathcal{L}(x) R(x^2\sqrt{s}). \tag{5.26}$$

Figure 5.21 shows, the influence of these effects on the cross section. The upper curve is the theoretical prediction (here at NNLO). After adding the biggest effect, namely the initial-state radiation, the curve is shifted down by about 30%. Further addition of beamstrahlung and single-beam energy spread lower the curve even more. In the end no distinct peak will be visible. This will effect significantly the mass measurement. Although for the mass, the peak position is the important quantity, which is very stable as seen in the previous sections, due

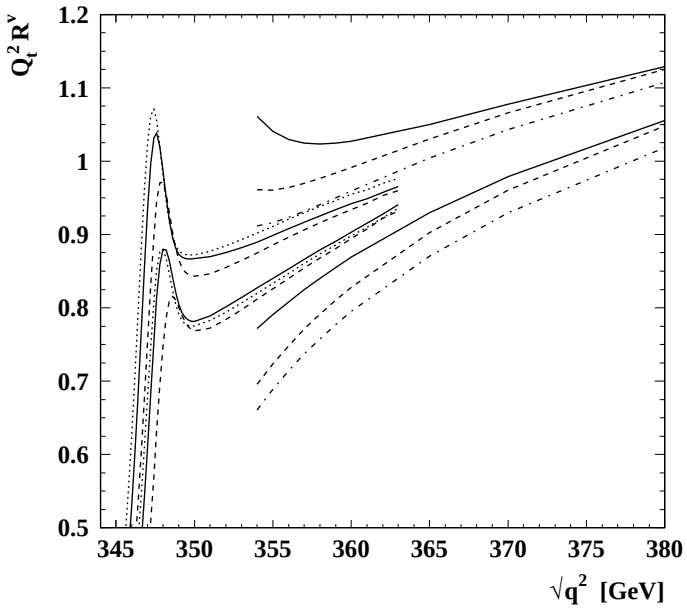

Figure 5.20: Continuation from threshold to continuum region, taken from [45]. The lower curves are NLO for the threshold region and $O(\alpha_s)$ for the continuum, the upper curves are NNLO and $O(\alpha_s^2)$. The parameters are $\alpha_s(M_Z) = 0.118$, $\Gamma_t = 1.43$ GeV, $m_t = 175$ GeV, The solid, dotted and dash-dotted lines are for different scales. The result for the $O(\alpha_s^2)$ correction has been taken from [114].

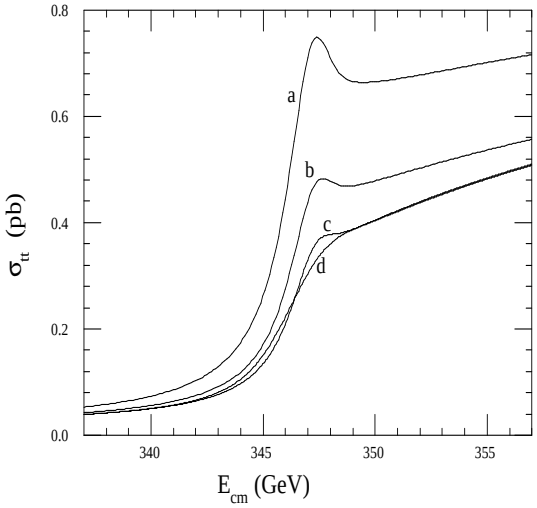

Figure 5.21: Influence of initial state radiation and beam effects on the cross section (taken from [116]). The theoretical cross section is given by curve (a). The following energy redistribution effects have been applied to the theory for the remaining curves: (b) initial-state radiation (ISR); (c): ISR and beamstrahlung; (d): ISR, beamstrahlung, and single-beam energy spread.

to these experimental effects, the uncertainty in the height of the peak will play an important role. The reason is, that the exact position cannot be determined so precisely, so a complete fit to the shape of the cross section is needed.

A further application of the results obtained would be the determination of the bottom quark mass with sum rules (see for example [119]). To be able to perform this, an option has been implemented in the Mathematica package to get the result for the cross section of bottomonium production for positive energies[2].

[2]This can be obtained by setting $n_f = 4$, $m = m_b$ and $\Gamma = 0$.

Chapter 6

Conclusion

The precise knowledge of the top quark mass is important to check the Standard Model predictions. Quantum corrections make it possible to observe effects beyond the Standard Model, from energy regions, which are not directly available at colliders in the near future. The best measurement of the top quark mass can be obtained at the ILC from the top quark pair production. The QCD corrections to this process have been examined in this work. The results are very promising and lead to the conclusion, that the aimed accuracy of less than 50 MeV seams to be feasible.

This work presents the third-order QCD corrections from potential insertions. The matching to one-loop order has been performed and the insertions of the resulting potentials have been calculated. Together with the recently calculated ultrasoft corrections, the QCD cross section at third order is now almost completed. The results have been implemented in a Mathematica package, which makes them easily accessible for further use. For a complete QCD correction, there are still some unknown matching coefficients. It was shown, that at least one of these missing parts has a significant effect on the cross section. There is currently ongoing effort on the calculation of these coefficients, so a full QCD calculation might be completed soon.

It has been shown, that the uncertainty of the cross section normalization which was observed at second order could be significantly reduced. The error from perturbation theory has been estimated to about 5%. This is near the range of the aimed uncertainty of about 3% and an inclusion of missing effects might improve this, because uncanceled divergences indicate, that adding the corresponding counterpart will also lead to a cancelation of scale dependent logarithms and thus to a reduction of the uncertainty. So, the remaining task is to include electroweak effects as well as finally initial-state radiation and beamstrahlung to get a realistic shape of the cross section.

In the future, one might go even further, and use the results from this work to get a renor-

malization group improved calculation at NNNLL. However, this seems to be hardly feasible with current techniques. Other applications of the results obtained, are the determination of the third-order corrections to the bottom quark mass with sum rules.

Appendix A

Representations for the Coulomb Green function

In the calculation, two different representation for the Coulomb resummed Green function are used. The first one is the integral representation [120] for the S-wave Green function:

$$G_C(0,r,E) = \frac{m\sqrt{-mE}}{2\pi} e^{-r\sqrt{-mE}} \int_0^\infty dt e^{-2rt\sqrt{-mE}} \left(\frac{1+t}{t}\right)^\lambda, \tag{A.1}$$

with $\lambda = -\frac{mC_F\alpha_S}{2\sqrt{-mE}}$. The second one is a representation using Laguerre polynomials $L_n^{2l+1}(x)$, derived in [111, 121]. The S-wave part reads:

$$G^{l=0}(r_1,r_2,E) = \frac{m\sqrt{-mE}}{2\pi} \sum_{n=0}^\infty \frac{L_n^{(1)}(2r_1\sqrt{-mE})L_n^{(1)}(2r_2\sqrt{-mE})}{(n+1)(n+1-\lambda)} e^{-\sqrt{-mE}(r_1+r_2)}. \tag{A.2}$$

Then:

$$G^{l=0}(0,r,E) = \frac{m\sqrt{-mE}}{2\pi} e^{-\sqrt{-mE}r} \sum_{n=0}^\infty \frac{L_n^{(1)}(2r\sqrt{-mE})}{(n+1-\lambda)}. \tag{A.3}$$

A similar representation for P-waves is:

$$G^{(l=1)}(r_1,r_2,E) = \frac{m}{4\pi}(2\sqrt{-mE})^3 e^{-\sqrt{-mE}(r_1+r_2)} \sum_{n=0}^\infty \frac{n! L_n^{(3)}(2r_1\sqrt{-mE})L_n^{(3)}(2r_2\sqrt{-mE})}{(n+3)!(n+2-\lambda)}, \tag{A.4}$$

and

$$G^{(l=1)}(0,r,E) = \frac{m}{3\pi}(2\sqrt{-mE})^3 e^{-\sqrt{-mE}r} \sum_{n=0}^\infty \frac{L_n^{(3)}(2r\sqrt{-mE})}{(n+2-\lambda)}. \tag{A.5}$$

The integral representation is mainly used for Green functions near the vertex, and the Laguerre represention for Green functions between potentials (for double and triple potential insertions). For P-waves the sum representation has been used in every part of the coordinate space calculation.

In some parts of the calculations, where divergences occur, the full Green function is splittet into several parts using the notation:

$$G(E) = G^{(0ex)}(E) + G^{(1ex)}(E) + ... + G^{(n\,ex)}(E) + G^{(>n\,ex)}(E). \tag{A.6}$$

Then, the Green function without gluon exchange is given by:

$$G^{(0ex)}(\mathbf{p}_1, \mathbf{p_2}, E) = \frac{m(2\pi)^{d-1}\delta^{d-1}(\mathbf{p}_1 - \mathbf{p}_2)}{\mathbf{p}_1^2 - mE}. \tag{A.7}$$

The next part has one gluon exchange and reads:

$$G^{(1ex)}(\mathbf{p}_1, \mathbf{p_2}, E) = \frac{m^2 C_F g_s^2}{(\mathbf{p}_1^2 - mE)(\mathbf{p}_1 - \mathbf{p}_2)^2(\mathbf{p}_2 - mE)}, \tag{A.8}$$

and so one for more gluon exchanges. The parts with infinite number of exchanges are needed in the coordinate space representation. This can be calculated from the formulas above by subtracting the relevant number of exchanges. This subtraction can be done by taking the limit $\lambda \to 0$. This corresponds to a suppression of the strong coupling constant and thus a suppression of gluon exchanges. The zeroth order of the limit $\lambda \to 0$ corresponds to the Green function without exchanges, the first order to the Green function with one exchange and so on.

Appendix B

Master Integrals

In this chapter, the results for integrals which are used in the calculation are given. They are divided into three parts. The first section contains integrals which were used for the calculation of the one-loop correction to the potentials, the second sort of integrals are momentum integrals which were used to calculate the divergent parts of potential insertions, and finally the result for integrals which appear when using the integral representation of the Green function to calculate the finite parts of potential insertions are presented.

B.1 Integrals for potential matching

The integrals in this section are all calculated using Feynman parameters. The calculation is straightforward, so here only the results are presented here. The reader interested in more details is referred to the next section, where the integrals are also solved with Feynman parameters and all details are given. For the calculation of the hard region two diagrams are encountered, the box diagram and a crossed box diagram (denoted by $h1$ and $h2$ respectively). The master integrals needed for these diagrams are:

$$I^{1}_{h1}[a] := \int \frac{d^d\mathbf{k}}{(2\pi)^{d-1}} \frac{1}{(k^2)^a(k^2+2mk_0)(k^2-2mk_0)} \tag{B.1}$$

$$= \frac{i(-m^2)^{-a}}{(4\pi)^2} e^{\gamma_E \epsilon} \left(\frac{\mu^2}{m^2}\right)^{\epsilon} \frac{\Gamma(a+\epsilon)\Gamma(1-2\epsilon-2a)}{\Gamma(2-2\epsilon-a)}, \tag{B.2}$$

$$I^{k0}_{h1}[a] := \int \frac{d^d\mathbf{k}}{(2\pi)^{d-1}} \frac{k_0}{(k^2)^a(k^2+2mk_0)(k^2-2mk_0)} \tag{B.3}$$

$$= \frac{im(-m^2)^{-a}}{(4\pi)^2} e^{\gamma_E \epsilon} \left(\frac{\mu^2}{m^2}\right)^{\epsilon} \frac{\Gamma(a+\epsilon)\Gamma(2-2\epsilon-2a)}{\Gamma(3-2\epsilon-a)}, \tag{B.4}$$

$$I^{jl}_{h1}[a] := \int \frac{d^d\mathbf{k}}{(2\pi)^{d-1}} \frac{k_j k_l}{(k^2)^a(k^2+2mk_0)(k^2-2mk_0)} \tag{B.5}$$

$$= \frac{i(-m^2)^{-a}}{(4\pi)^2}\frac{m^2\delta_{ij}}{2}e^{\gamma_E\epsilon}\left(\frac{\mu^2}{m^2}\right)^{\epsilon}\frac{\Gamma(a+\epsilon-1)\Gamma(3-2\epsilon-2a)}{\Gamma(4-2\epsilon-a)}, \tag{B.6}$$

and

$$I^1_{h2}[a] := \int \frac{d^d\mathbf{k}}{(2\pi)^{d-1}}\frac{1}{(k^2)^a(k^2-2mk_0)^2} \tag{B.7}$$

$$= \frac{i(-m^2)^{-a}}{(4\pi)^2}e^{\gamma_E\epsilon}\left(\frac{\mu^2}{m^2}\right)^{\epsilon}\frac{\Gamma(a+\epsilon)\Gamma(2-2\epsilon-2a)}{\Gamma(2-2\epsilon-a)}, \tag{B.8}$$

$$I^{k0}_{h2}[a] := \int \frac{d^d\mathbf{k}}{(2\pi)^{d-1}}\frac{k_0}{(k^2)^a(k^2-2mk_0)^2} \tag{B.9}$$

$$= \frac{im(-m^2)^{-a}}{(4\pi)^2}e^{\gamma_E\epsilon}\left(\frac{\mu^2}{m^2}\right)^{\epsilon}\frac{\Gamma(a+\epsilon)\Gamma(3-2\epsilon-2a)}{\Gamma(3-2\epsilon-a)}, \tag{B.10}$$

$$I^{jl}_{h2}[a] := \int \frac{d^d\mathbf{k}}{(2\pi)^{d-1}}\frac{k_jk_l}{(k^2)^a(k^2-2mk_0)^2} \tag{B.11}$$

$$= \frac{i(-m^2)^{-a}}{(4\pi)^2}\frac{m^2\delta_{ij}}{2}e^{\gamma_E\epsilon}\left(\frac{\mu^2}{m^2}\right)^{\epsilon}\frac{\Gamma(a+\epsilon-1)\Gamma(4-2\epsilon-2a)}{\Gamma(4-2\epsilon-a)}. \tag{B.12}$$

In the soft region there is only one type of denominator. The relevant master integrals are:

$$I^1_s[a] := \int \frac{d^d\mathbf{k}}{(2\pi)^{d-1}}\frac{1}{(k^2)^a(k-q)^2k_0^a} = \frac{i}{16\pi^{3/2}}\frac{(-1)^ae^{\gamma_E\epsilon}q^{-a}\Gamma(1-\epsilon-\frac{a}{2})^2\Gamma(\frac{a}{2}+\epsilon)}{\Gamma(\frac{1+a}{2})\Gamma(2-a-2\epsilon)}\left(\frac{\mu^2}{q^2}\right)^{\epsilon}, \tag{B.13}$$

$$I^j_s[a] := \int \frac{d^d\mathbf{k}}{(2\pi)^{d-1}}\frac{k_j}{k^2(k-q)^2k_0^a} \tag{B.14}$$

$$= \frac{iq_j}{16\pi^{3/2}}\frac{(-1)^ae^{\gamma_E\epsilon}q^{-a}\Gamma(1-\epsilon-\frac{a}{2})\Gamma(2-\epsilon-\frac{a}{2})\Gamma(\frac{a}{2}+\epsilon)}{\Gamma(\frac{1+a}{2})\Gamma(3-a-2\epsilon)}\left(\frac{\mu^2}{q^2}\right)^{\epsilon}, \tag{B.15}$$

$$I^{jl}_s[a] := \int \frac{d^d\mathbf{k}}{(2\pi)^{d-1}}\frac{k_jk_l}{k^2(k-q)^2k_0^a} \tag{B.16}$$

$$= \frac{i(q^2\delta_{ij}+q_jq_l(a-4+2\epsilon))}{32\pi^{3/2}}\frac{(-1)^ae^{\gamma_E\epsilon}q^{-a}\Gamma(2-\epsilon-\frac{a}{2})^2\Gamma(\frac{a}{2}+\epsilon-1)}{\Gamma(\frac{1+a}{2})\Gamma(4-a-2\epsilon)}\left(\frac{\mu^2}{q^2}\right)^{\epsilon}. \tag{B.17}$$

Note that the $\overline{MS}$ factor is included in the integration measure and is given explicitly after the integration.

B.2 Momentum Integrals for insertions

The following integrals are needed for the potential insertions, when formally divergent diagrams are calculated. These have do be done in momentum space. There are four types of integrals, which have been used extensively during the calculation:

$$I^1_1[a] := \int \frac{d^{d-1}\mathbf{p}}{(2\pi)^{d-1}}\frac{1}{(\mathbf{p}^2-mE)^a} = \frac{\Gamma(a-\frac{d-1}{2})}{(4\pi)^{\frac{d-1}{2}}(-mE)^{a-\frac{d-1}{2}}\Gamma(a)}, \tag{B.18}$$

$$I^2_{112}[a,b,c] := \int \frac{d^{d-1}\mathbf{k}}{(2\pi)^{d-1}}\frac{d^{d-1}\mathbf{l}}{(2\pi)^{d-1}}\frac{1}{(\mathbf{k}^2-mE)^a(\mathbf{l}^2-mE)^b[(\mathbf{l}-\mathbf{k})^2]^c}$$

$$= \int \frac{d^{d-1}\mathbf{k}}{(2\pi)^{d-1}}\frac{d^{d-1}\mathbf{l}}{(2\pi)^{d-1}}\frac{2^{d-1-2c}}{[(\mathbf{l}-\mathbf{k})^2-mE]^a[(\mathbf{l}+\mathbf{k})^2-mE]^b[\mathbf{k}^2]^c} \tag{B.19}$$

$$= \int \frac{d^{d-1}\mathbf{k}}{(2\pi)^{d-1}}\frac{2^{d-1-2c}}{[\mathbf{k}^2]^c}\int \frac{d^{d-1}\mathbf{l}}{(2\pi)^{d-1}}\int_0^1 dx\frac{\Gamma(a+b)}{\Gamma(a)\Gamma(b)}\frac{x^{a-1}\bar{x}^{b-1}}{[\mathbf{l}^2+2\mathbf{lk}(1-2x)+\mathbf{k}^2-mE]^{a+b}} \tag{B.20}$$

$$= \int \frac{d^{d-1}\mathbf{k}}{(2\pi)^{d-1}}\frac{2^{d-1-2c}}{[\mathbf{k}^2]^c}\int_0^1 dx\frac{\Gamma(a+b-\frac{d-1}{2})}{(4\pi)^{\frac{d-1}{2}}\Gamma(a)\Gamma(b)}\frac{x^{a-1}\bar{x}^{b-1}}{[\mathbf{k}^2(4x\bar{x})-mE]^{a+b-\frac{d-1}{2}}} \tag{B.21}$$

$$= \frac{2^{d-1-2c}\Gamma(a+b+c-\frac{d-1}{2})}{(4\pi)^{\frac{d-1}{2}}\Gamma(a)\Gamma(b)\Gamma(c)}\int_0^1 dx\frac{x^{a-1}\bar{x}^{b-1}}{(4x\bar{x})^{a+b-\frac{d-1}{2}}}\int \frac{d^{d-1}\mathbf{k}}{(2\pi)^{d-1}}\int_0^1 dy\frac{y^{a+b-\frac{d-1}{2}-1}\bar{y}^{c-1}}{[\mathbf{k}^2-\frac{y}{4x\bar{x}}mE]^{a+b+c-\frac{d-1}{2}}} \tag{B.22}$$

$$= \frac{2^{d-1-2c}\Gamma(a+b+c-d+1)}{(4\pi)^{d-1}\Gamma(a)\Gamma(b)\Gamma(c)}\int_0^1 dx\frac{x^{a-1}\bar{x}^{b-1}}{(4x\bar{x})^{a+b-\frac{d-1}{2}}}\int_0^1 dy\frac{y^{a+b-\frac{d-1}{2}-1}\bar{y}^{c-1}}{(-\frac{y}{4x\bar{x}}mE)^{a+b+c-d+1}} \tag{B.23}$$

$$= \frac{(-mE)^{d-a-b-c-1}\Gamma(a+b+c-d+1)}{(4\pi)^{d-1}\Gamma(a)\Gamma(b)\Gamma(c)}\int_0^1 dx x^{a+c-\frac{d+1}{2}}\bar{x}^{b+c-\frac{d+1}{2}}\int_0^1 dy y^{\frac{d-3}{2}-c}\bar{y}^{c-1} \tag{B.24}$$

$$= \frac{\Gamma(a+b+c-d+1)\Gamma(a+c-\frac{d-1}{2})\Gamma(b+c-\frac{d-1}{2})\Gamma(\frac{d-1}{2}-c)}{(4\pi)^{d-1}(-mE)^{1-d+a+b+c}\Gamma(a)\Gamma(b)\Gamma(a+b+2c-d+1)\Gamma(\frac{d-1}{2})}, \tag{B.25}$$

$$I^1_{22}[a,b] := \int \frac{d^{d-1}\mathbf{k}}{(2\pi)^{d-1}}\frac{1}{[(\mathbf{p}-\mathbf{k})^2]^a[(\mathbf{l}-\mathbf{k})^2]^b} \tag{B.26}$$

$$= \int \frac{d^{d-1}\mathbf{k}}{(2\pi)^{d-1}}\frac{\Gamma(a+b)}{\Gamma(a)\Gamma(b)}\int_0^1 dx\frac{x^{a-1}\bar{x}^{b-1}}{[x(\mathbf{p}-\mathbf{k})^2+\bar{x}(\mathbf{l}-\mathbf{k})^2]^{a+b}} \tag{B.27}$$

$$= \int_0^1 dx x^{a-1}\bar{x}^{b-1}\frac{\Gamma(a+b)}{\Gamma(a)\Gamma(b)}\int \frac{d^{d-1}\mathbf{k}}{(2\pi)^{d-1}}\frac{1}{[\mathbf{k}^2-2\mathbf{k}(x\mathbf{l}-\bar{x}\mathbf{p})+x\mathbf{l}^2+\bar{x}\mathbf{p}^2]^{a+b}} \tag{B.28}$$

$$= \int_0^1 dx\frac{x^{a-1}\bar{x}^{b-1}}{(4\pi)^{\frac{d-1}{2}}}\frac{\Gamma(a+b-\frac{d-1}{2})}{\Gamma(a)\Gamma(b)}\frac{(x\bar{x})^{\frac{d-1}{2}-a-b}}{[(\mathbf{l}-\mathbf{p})^2]^{a+b-\frac{d-1}{2}}} \tag{B.29}$$

$$= \frac{1}{(4\pi)^{\frac{d-1}{2}}}\frac{\Gamma(a+b-\frac{d-1}{2})}{\Gamma(a)\Gamma(b)}\frac{\Gamma(\frac{d-1}{2}-a)\Gamma(\frac{d-1}{2}-b)}{\Gamma(d-1-a-b)}\frac{1}{[(\mathbf{l}-\mathbf{p})^2]^{a+b-\frac{d-1}{2}}} \tag{B.30}$$

$$I^1_{12}[a,b] := \int \frac{d^{d-1}\mathbf{k}}{(2\pi)^{d-1}}\frac{1}{[\mathbf{k}^2-mE]^a[(\mathbf{p}-\mathbf{k})^2]^b} \tag{B.31}$$

$$= \int \frac{d^{d-1}\mathbf{k}}{(2\pi)^{d-1}}\int_0^1 dx\frac{\Gamma(a+b)}{\Gamma(a)\Gamma(b)}\frac{\bar{x}^{a-1}x^{b-1}}{[\mathbf{k}^2-2x\mathbf{kp}+x\mathbf{p}^2-\bar{x}mE]^{a+b-\frac{d-1}{2}}} \tag{B.32}$$

$$= \int_0^1 dx\frac{1}{(4\pi)^{\frac{d-1}{2}}}\frac{\Gamma(a+b-\frac{d-1}{2})}{\Gamma(a)\Gamma(b)}\frac{x^{b-1}\bar{x}^{\frac{d-1}{2}-b-1}}{[x\mathbf{p}^2-mE]^{a+b-\frac{d-1}{2}}}. \tag{B.33}$$

In these results, a, b and c can stand for any number (integer or non-integer).

B.3 Mellin-Barnes Method and Integrals

In some parts of the calculation of momentum space integrals, the Mellin-Barnes representation is used to simplify the numerator. This method is based on the identy:

$$\frac{1}{(X+Y)^{\lambda}} = \frac{1}{\Gamma(\lambda)}\frac{1}{2\pi i}\int_{-i\infty}^{+i\infty} dz\Gamma(\lambda+z)\Gamma(-z)\frac{Y^z}{X^{\lambda+z}}. \tag{B.34}$$

Here, the integration has to be performed in such a way that all poles from Γ function with positive z are to the left of the contour and all poles from Γ function with negative z argument are to the right. A detailed summary of this method with some examples is given in [88]. In the appendix of [88], one can also find a table of master integrals which where used in this calculation. A modification from the Mellin-Barnes integral $D.53$ from [88] using the conventions listed there is:

$$\frac{1}{2\pi i}\int_{-i\infty}^{i\infty} dz\frac{\Gamma(\lambda_1+z)\Gamma(\lambda_2+z)\Gamma^*(\lambda_3+z)\Gamma(-\lambda_3-z)\Gamma(-z)}{\Gamma(\lambda_4+z)} \tag{B.35}$$

$$= \frac{\Gamma(\lambda_1-\lambda_3)\Gamma(\lambda_3)\Gamma(\lambda_2-\lambda_3)}{\Gamma(1+\lambda_1+\lambda_2-\lambda_3)}\Big(-\frac{\lambda_3}{\lambda_1\lambda_2}-\Psi(\lambda_1)-\Psi(\lambda_2)+\Psi(\lambda_3)+\Psi(1+\lambda_1+\lambda_2-\lambda_3)\Big)$$

$$\frac{1}{2\pi i}\int_{-i\infty}^{i\infty} dz\frac{\Gamma(\lambda_1+z)\Gamma(\lambda_2+z)\Gamma(\lambda_3+z)\Gamma^*(-\lambda_3-z)\Gamma(-z)}{\Gamma(\lambda_4+z)} \tag{B.36}$$

$$= \frac{\Gamma(\lambda_1+\lambda_3)\Gamma(-\lambda_3)\Gamma(\lambda_2+\lambda_3)}{\Gamma(1+\lambda_1+\lambda_2+\lambda_3)}\Big(\frac{\lambda_3}{\lambda_1\lambda_2}-\Psi(\lambda_1)-\Psi(\lambda_2)+\Psi(\lambda_1+\lambda_3)+\Psi(\lambda_2+\lambda_3)\Big),$$

where $\lambda_4 = \lambda_1+\lambda_2+1$.

B.4 Coordinate Space Integrals for insertions

The integrals from this section are needed for the finite part of the potential insertion, when using the integral representation of the Green function. They can be done with Mathematica (using some obvious substitutions in some parts):

$$\int_0^{\infty}\left(\Big(\frac{1+t}{t}\Big)^{\lambda}-1-\lambda\ln\frac{1+t}{t}\right) = G^{(\bar{1})}(0,0,E), \tag{B.37}$$

$$\int_0^{\infty}\left(\Big(\frac{1+t}{t}\Big)^{\lambda}-1-\lambda\ln\frac{1+t}{t}\right)\ln(1+t) \tag{B.38}$$

$$= \lambda-\lambda\frac{\pi^2}{6}+\frac{1}{2}\lambda(1+\lambda){}_4F_3(1,1,1,2+\lambda;2,2,3;1) \tag{B.39}$$

$$= (\lambda-1)\Big(\gamma_E+\Psi(1-\lambda)\Big)-\frac{\lambda}{2}\Big(\gamma_E+\Psi(1-\lambda)\Big)^2-\frac{\lambda}{2}\Big(\frac{\pi^2}{2}-\Psi_1(1-\lambda)\Big), \tag{B.40}$$

$$\int_0^{\infty}\left(\Big(\frac{1+t}{t}\Big)^{\lambda}-1-\lambda\ln\frac{1+t}{t}\right)\ln^2(1+t) = \lambda\frac{\pi^2}{3}-2\lambda-2\lambda\zeta_3 \tag{B.41}$$

$$+\lambda(1+\lambda){}_5F_4(1,1,1,1,2+\lambda;2,2,2,3;1)$$

$$= \frac{\pi^2}{6}(3\lambda - 1) + (\lambda - 1)\Big(\gamma_E + \Psi(1-\lambda)\Big)^2 - \frac{\lambda}{3}\Big(\gamma_E + \Psi(1-\lambda)\Big)^3 - (\lambda - 1)\Psi_1(1-\lambda) \quad \text{(B.42)}$$

$$+\Big(\gamma_E + \Psi(1-\lambda)\Big)\Big(2 - 2\lambda - \frac{\pi^2\lambda}{6} + \lambda\Psi_1(1-\lambda)\Big) - \frac{1}{3}\lambda\Psi_2(1-\lambda) - \frac{8}{3}\lambda\zeta_3\,. \quad \text{(B.43)}$$

The Hypergeometric functions in the final result are all finite for physical values of λ. However, if using unphysical values, especially small width with negative energy, the Hypergeometric functions are not well defined.

Appendix C

The $\lambda \to n$ limit

To get the total cross section a resummation of energy levels and wave functions is performed into the full Green function described in section 5.1. To get these functions, the limit $\lambda \to n$ of the Green function has to be taken, and the results can be read off from the poles in this limit. For the calculation of this limit, three different methods depending on the structure of the Green function are used. The first structure is the one containing only completely analytic formulas, the second one is the part with single sums, and the third one is for the parts d and e from the delta potential single insertion.

Analytic Results The $\lambda \to n$ poles of the analytic parts come from the poles of the $\Psi_i(1-\lambda)$ functions. So, the expansion of the Ψ-functions for negative integer arguments is needed, which is given by

$$\Psi_i(-m+\epsilon) = \frac{i!}{(-\epsilon)^{i+1}} + \sum_{j=i}^{\infty} \frac{(-1)^k \epsilon^{k-i}}{(k-i)!} \Big(\Psi_k(n+1) + ((-1)^k - 1)\Psi_k(1) \Big). \tag{C.1}$$

With this result, all analytic parts can be expanded in this limit[1].

Summation parts The parts with summations over the variable k have additional poles from the functions $\Psi(k-\lambda)$ in the sum over k. To extract these, one can separate three cases:

$$a)\ k = n, \qquad b)\ k < n, \qquad c)\ k > n.$$

The third case is similar to the analytic parts and gets contributions only from $\Psi_i(1-\lambda)$ functions. The first and second part get additional singularities from $\Psi(k-\lambda)$. Then, one can use equation (C.1) to substitute the Ψ functions which contribute to the poles. The

[1]The Hypergeometric function from the Coulomb insertions are treated differently. For details of that calculation see [85].

remaining sums can be written in such a way, that the final result consist only of harmonic sums and nested harmonic sums.

Delta potential single insertion parts d and e The sums for parts d and e for the single insertion of the delta potential are more complicated and have also Γ functions with nontrivial $\lambda \to n$ pole structure. Here, it is more difficult to write the poles in terms of harmonic sums. However, one can easily get the poles for any specific quantum number n. By assuming then a specific form of the expression for arbitrary n, one can get the coefficients in front of the assumed functions and check the result for any specific number n. So, here a kind of smart guessing or sometimes called 'experimental mathematics' has been performed.

C.1 Harmonic sums and Zeta functions

In the pole result of the basic functions sums are encountered, which could be written as (multiple) nested harmonic sums

$$S_a(n) = \sum_{k=1}^{n} 1/k^a, \qquad S_{a,b}(n) \equiv \sum_{k=1}^{n} \frac{1}{k^a} S_b(k), \qquad S_{a,b,c}(n) \equiv \sum_{k=1}^{n} \frac{1}{k^a} S_{b,c}(k), \tag{C.2}$$

and zeta functions

$$\zeta(a) = \sum_{k=1}^{\infty} 1/k^a, \qquad \zeta(a,b) \equiv \sum_{k=1}^{\infty} \frac{1}{k^a} S_b(k-1), \qquad \zeta(a,b,c) \equiv \sum_{k=1}^{\infty} \frac{1}{k^a} S_{b,c}(k-1). \tag{C.3}$$

Several reduction formula have been used to get a short final result. Relations for harmonic sums can usually be derived more easily as for zeta functions, since the latter are infinite harmonic sums. A very useful reduction formula for double nested zeta functions is the one that relates the sum of two zeta functions with inverse order of arguments to the unnested zeta function (see for example [122]):

$$\zeta(r,s) + \zeta(s,r) = \zeta(r)\zeta(2) - \zeta(r+s). \tag{C.4}$$

There is another useful identity discovered by Euler if one of the arguments is even and one odd:

$$\zeta(r,s) = -\frac{1}{2}\zeta(r+s) + \sum_{j=1, j\in odd}^{r+s} \left[\binom{j-1}{s-1} + \binom{j-1}{r-1} \right] \zeta(j)\zeta(r+s-j), \tag{C.5}$$

for r even and s odd. More formulas for double zeta functions can be found in [122]. The more complicated case of the triple zeta function has also been covered in the literature. The

following formulas were used and are taken from [123]:

$$\zeta(2,1,1) = \zeta(4), \tag{C.6}$$
$$\zeta(2,1,2) = \frac{9}{2}\zeta(5) - 2\zeta(3)\zeta(2), \tag{C.7}$$
$$\zeta(2,2,1) = -\frac{11}{2}\zeta(5) + 3\zeta(3)\zeta(2), \tag{C.8}$$
$$\zeta(3,1,1) = 2\zeta(5) - \zeta(3)\zeta(2), \tag{C.9}$$
$$\zeta(4,1,1) = \frac{23}{16}\zeta(6) - \zeta(3)^2, \tag{C.10}$$
$$\zeta(2,1,3) = -\frac{13}{16}\zeta(6) + \zeta(3)^2, \tag{C.11}$$
$$\zeta(3,2,1) = -\frac{203}{48}\zeta(6) + 3\zeta(3)^2, \tag{C.12}$$
$$\zeta(2,2,2) = \frac{3}{16}\zeta(6), \tag{C.13}$$
$$\zeta(3,1,2) = \frac{53}{24}\zeta(6) - \frac{3}{2}\zeta(3)^2, \tag{C.14}$$
$$\zeta(2,3,1) = \frac{53}{24}\zeta(6) - \frac{3}{2}\zeta(3)^2. \tag{C.15}$$

Higher order nested sums are also available in the literature but not needed for the calculation performed in this work.

Bibliography

[1] T. E. W. Group, f. t. CDF and D. Collaborations, *A Combination of CDF and D0 Results on the Mass of the Top Quark*, arXiv:0803.1683 [hep-ex].

[2] S. Heinemeyer, W. Hollik, D. Stockinger, A. M. Weber and G. Weiglein, *Precise prediction for M(W) in the MSSM*, *JHEP* **08** (2006) 052 [hep-ph/0604147].

[3] S. Heinemeyer, W. Hollik and G. Weiglein, *Electroweak precision observables in the minimal supersymmetric standard model*, *Phys. Rept.* **425** (2006) 265–368 [hep-ph/0412214].

[4] A. Djouadi *et. al.*, *Supersymmetric contributions to electroweak precision observables: QCD corrections*, *Phys. Rev. Lett.* **78** (1997) 3626–3629 [hep-ph/9612363].

[5] A. Djouadi *et. al.*, *Leading QCD corrections to scalar quark contributions to electroweak precision observables*, *Phys. Rev.* **D57** (1998) 4179–4196 [hep-ph/9710438].

[6] S. Heinemeyer and G. Weiglein, *Leading electroweak two loop corrections to precision observables in the MSSM*, *JHEP* **10** (2002) 072 [hep-ph/0209305].

[7] J. Haestier, S. Heinemeyer, D. Stockinger and G. Weiglein, *Electroweak precision observables: Two-loop Yukawa corrections of supersymmetric particles*, *JHEP* **12** (2005) 027 [hep-ph/0508139].

[8] **CDF** Collaboration, F. Abe *et. al.*, *Observation of top quark production in $\bar{p}p$ collisions*, *Phys. Rev. Lett.* **74** (1995) 2626–2631 [hep-ex/9503002].

[9] **D0** Collaboration, S. Abachi *et. al.*, *Observation of the top quark*, *Phys. Rev. Lett.* **74** (1995) 2632–2637 [hep-ex/9503003].

[10] **Particle Data Group** Collaboration, W. M. Yao *et. al.*, *Review of particle physics*, *J. Phys.* **G33** (2006) 1–1232.

[11] I. Borjanovic *et. al.*, *Investigation of top mass measurements with the ATLAS detector at LHC*, *Eur. Phys. J.* **C39S2** (2005) 63–90 [hep-ex/0403021].

[12] M. Duda, *Top mass measurement at CMS*, *Acta Phys. Polon.* **B38** (2007) 417–426.

[13] M. Martinez and R. Miquel, *Multi-parameter fits to the t anti-t threshold observables at a future e+ e- linear collider*, *Eur. Phys. J.* **C27** (2003) 49–55 [hep-ph/0207315].

[14] A. H. Hoang *et. al.*, *Top-antitop pair production close to threshold: Synopsis of recent NNLO results*, *Eur. Phys. J. direct* **C2** (2000) 1 [hep-ph/0001286].

[15] T. Appelquist and H. D. Politzer, *Orthocharmonium and e+ e- annihilation*, *Phys. Rev. Lett.* **34** (1975) 43.

[16] V. S. Fadin and V. A. Khoze, *Threshold behavior of heavy top production in e+ e- collisions*, *JETP Lett.* **46** (1987) 525–529.

[17] M. J. Strassler and M. E. Peskin, *The heavy top quark threshold: QCD and the Higgs*, *Phys. Rev.* **D43** (1991) 1500–1514.

[18] G. T. Bodwin, E. Braaten and G. P. Lepage, *Rigorous QCD analysis of inclusive annihilation and production of heavy quarkonium*, *Phys. Rev.* **D51** (1995) 1125–1171 [hep-ph/9407339].

[19] A. H. Hoang and T. Teubner, *Top quark pair production at threshold: Complete next-to- next-to-leading order relativistic corrections*, *Phys. Rev.* **D58** (1998) 114023 [hep-ph/9801397].

[20] K. Melnikov and A. Yelkhovsky, *Top quark production at threshold with $O(\alpha_s^2)$ accuracy*, *Nucl. Phys.* **B528** (1998) 59–72 [hep-ph/9802379].

[21] M. Beneke, A. Signer and V. A. Smirnov, *Top quark production near threshold and the top quark mass*, *Phys. Lett.* **B454** (1999) 137–146 [hep-ph/9903260].

[22] O. I. Yakovlev, *Top quark production near threshold: NNLO QCD correction*, *Phys. Lett.* **B457** (1999) 170–176 [hep-ph/9808463].

[23] T. Nagano, A. Ota and Y. Sumino, *$O(\alpha_s^2)$ corrections to $e^+e^- \to t\bar{t}$ total and differential cross sections near threshold*, *Phys. Rev.* **D60** (1999) 114014 [hep-ph/9903498].

[24] A. A. Penin and A. A. Pivovarov, *Analytical results for $e^+e^- \to t\bar{t}$ and $\gamma\gamma \to t\bar{t}$ observables near the threshold up to the next- to-next-to-leading order of NRQCD*, *Phys. Atom. Nucl.* **64** (2001) 275–293 [hep-ph/9904278].

[25] A. H. Hoang and C. J. Reisser, *Electroweak absorptive parts in NRQCD matching conditions*, *Phys. Rev.* **D71** (2005) 074022 [hep-ph/0412258].

[26] A. H. Hoang and C. J. Reisser, *On electroweak matching conditions for top pair production at threshold*, *Phys. Rev.* **D74** (2006) 034002 [hep-ph/0604104].

[27] D. Eiras and M. Steinhauser, *Complete Higgs mass dependence of top quark pair threshold production to order alpha alpha(s)*, *Nucl. Phys.* **B757** (2006) 197–210 [hep-ph/0605227].

[28] A. H. Hoang, A. V. Manohar, I. W. Stewart and T. Teubner, *A renormalization group improved calculation of top quark production near threshold*, *Phys. Rev. Lett.* **86** (2001) 1951–1954 [hep-ph/0011254].

[29] A. H. Hoang, A. V. Manohar, I. W. Stewart and T. Teubner, *The threshold t anti-t cross section at NNLL order*, *Phys. Rev.* **D65** (2002) 014014 [hep-ph/0107144].

[30] A. Pineda and A. Signer, *Heavy quark pair production near threshold with potential non-relativistic QCD*, *Nucl. Phys.* **B762** (2007) 67–94 [hep-ph/0607239].

[31] B. A. Kniehl and A. A. Penin, *Ultrasoft effects in heavy quarkonium physics*, *Nucl. Phys.* **B563** (1999) 200–210 [hep-ph/9907489].

[32] Y. Kiyo and Y. Sumino, *$O(\alpha_s^5 m)$ quarkonium 1S spectrum in large β_0 approximation and renormalon cancellation*, *Phys. Lett.* **B496** (2000) 83–88 [hep-ph/0007251].

[33] B. A. Kniehl, A. A. Penin, M. Steinhauser and V. A. Smirnov, *Heavy-quarkonium creation and annihilation with $O(\alpha_s^3 \ln \alpha_s)$ accuracy.*, *Phys. Rev. Lett.* **90** (2003) 212001 [hep-ph/0210161].

[34] A. H. Hoang, *Three-loop anomalous dimension of the heavy quark pair production current in non-relativistic QCD*, *Phys. Rev.* **D69** (2004) 034009 [hep-ph/0307376].

[35] M. Beneke, Y. Kiyo and K. Schuller, *Third-order Coulomb corrections to the S-wave Green function, energy levels and wave functions at the origin*, *Nucl. Phys.* **B714** (2005) 67–90 [hep-ph/0501289].

[36] A. A. Penin, V. A. Smirnov and M. Steinhauser, *Heavy quarkonium spectrum and production / annihilation rates to order $\beta_0^3\alpha_s^3$*, *Nucl. Phys.* **B716** (2005) 303–318 [hep-ph/0501042].

[37] P. Marquard, J. H. Piclum, D. Seidel and M. Steinhauser, *Fermionic corrections to the three-loop matching coefficient of the vector current*, *Nucl. Phys.* **B758** (2006) 144–160 [hep-ph/0607168].

[38] M. Beneke, Y. Kiyo and K. Schuller, *Third-order non-Coulomb correction to the S-wave quarkonium wave functions at the origin*, *Phys. Lett.* **B658** (2008) 222–229 [arXiv:0705.4518 [hep-ph]].

[39] M. Beneke, Y. Kiyo and A. A. Penin, *Ultrasoft contribution to quarkonium production and annihilation*, *Phys. Lett.* **B653** (2007) 53–59 [arXiv:0706.2733 [hep-ph]].

[40] M. Beneke, Y. Kiyo, A. Penin and K. Schuller, *NNNLO correction to the toponium and bottomonium wave- functions at the origin*, arXiv:0710.4236 [hep-ph].

[41] M. Beneke, Y. Kiyo and K. Schuller, *NNNLO results on top-quark pair production near threshold*, arXiv:0801.3464 [hep-ph].

[42] M. Beneke and Y. Kiyo, *Ultrasoft contribution to heavy-quark pair production near threshold*, 0804.4004.

[43] A. A. Penin and A. A. Pivovarov, *Top quark threshold production in gamma gamma collision in the next-to-leading order*, *Nucl. Phys.* **B550** (1999) 375–396 [hep-ph/9810496].

[44] J. H. Kuhn and T. Teubner, *Axial contributions at the top threshold*, *Eur. Phys. J.* **C9** (1999) 221–228 [hep-ph/9903322].

[45] A. H. Hoang and T. Teubner, *Top quark pair production close to threshold: Top mass, width and momentum distribution*, *Phys. Rev.* **D60** (1999) 114027 [hep-ph/9904468].

[46] M. Beneke and V. A. Smirnov, *Asymptotic expansion of Feynman integrals near threshold*, *Nucl. Phys.* **B522** (1998) 321–344 [hep-ph/9711391].

[47] A. H. Hoang, M. Jezabek, J. H. Kuhn and T. Teubner, *Radiation of heavy quarks*, *Phys. Lett.* **B338** (1994) 330–335 [hep-ph/9407338].

[48] W. E. Caswell and G. P. Lepage, *Effective Lagrangians for bound state problems in QED, QCD, and other field theories*, *Phys. Lett.* **B167** (1986) 437.

[49] B. A. Thacker and G. P. Lepage, *Heavy quark bound states in lattice QCD*, *Phys. Rev.* **D43** (1991) 196–208.

[50] G. P. Lepage, L. Magnea, C. Nakhleh, U. Magnea and K. Hornbostel, *Improved nonrelativistic QCD for heavy quark physics*, *Phys. Rev.* **D46** (1992) 4052–4067 [hep-lat/9205007].

[51] A. V. Manohar, *The HQET/NRQCD lagrangian to order alpha/m^3*, *Phys. Rev.* **D56** (1997) 230–237 [hep-ph/9701294].

[52] A. Pineda and J. Soto, *Matching at one loop for the four-quark operators in NRQCD*, *Phys. Rev.* **D58** (1998) 114011 [hep-ph/9802365].

[53] M. E. Luke and M. J. Savage, *Power counting in dimensionally regularized NRQCD*, *Phys. Rev.* **D57** (1998) 413–423 [hep-ph/9707313].

[54] M. Beneke, A. Signer and V. A. Smirnov, *Two-loop correction to the leptonic decay of quarkonium*, *Phys. Rev. lett.* **80** (1998) 2535–2538 [hep-ph/9712302].

[55] A. Czarnecki and K. Melnikov, *Two-loop QCD corrections to the heavy quark pair production cross section in e^+e^- annihilation near the threshold*, *Phys. Rev. lett.* **80** (1998) 2531–2534 [hep-ph/9712222].

[56] B. A. Kniehl, A. Onishchenko, J. H. Piclum and M. Steinhauser, *Two-loop matching coefficients for heavy quark currents*, *Phys. Lett.* **B638** (2006) 209–213 [hep-ph/0604072].

[57] A. Pineda and J. Soto, *Effective field theory for ultrasoft momenta in NRQCD and NRQED*, *Nucl. Phys. Proc. Suppl.* **64** (1998) 428–432 [hep-ph/9707481].

[58] M. Beneke, *Perturbative heavy quark-antiquark systems*, hep-ph/9911490.

[59] N. Brambilla, A. Pineda, J. Soto and A. Vairo, *Potential NRQCD: An effective theory for heavy quarkonium*, *Nucl. Phys.* **B566** (2000) 275 [hep-ph/9907240].

[60] M. E. Luke, A. V. Manohar and I. Z. Rothstein, *Renormalization group scaling in nonrelativistic QCD*, *Phys. Rev.* **D61** (2000) 074025 [hep-ph/9910209].

[61] P. Labelle, *Effective field theories for QED bound states: Extending nonrelativistic QED to study retardation effects*, *Phys. Rev.* **D58** (1998) 093013 [hep-ph/9608491].

[62] B. A. Kniehl, A. A. Penin, V. A. Smirnov and M. Steinhauser, *Potential NRQCD and heavy-quarkonium spectrum at next-to- next-to-next-to-leading order*, *Nucl. Phys.* **B635** (2002) 357–383 [hep-ph/0203166].

[63] N. Brambilla, A. Pineda, J. Soto and A. Vairo, *The heavy quarkonium spectrum at order m alpha(s)**5 ln(alpha(s))*, *Phys. Lett.* **B470** (1999) 215 [hep-ph/9910238].

[64] W. Fischler, *Quark - anti-Quark Potential in QCD*, *Nucl. Phys.* **B129** (1977) 157–174.

[65] A. Billoire, *How Heavy Must Be Quarks in Order to Build Coulombic q anti-q Bound States*, *Phys. Lett.* **B92** (1980) 343.

[66] Y. Schroder, *The static potential in QCD*, *Ph.D. Thesis* (1999). DESY-THESIS-1999-021.

[67] M. Peter, *The static quark-antiquark potential in QCD to three loops*, *Phys. Rev. Lett.* **78** (1997) 602–605 [hep-ph/9610209].

[68] M. Peter, *The static potential in QCD: A full two-loop calculation*, *Nucl. Phys.* **B501** (1997) 471–494 [hep-ph/9702245].

[69] Y. Schroder, *The static potential in QCD to two loops*, *Phys. Lett.* **B447** (1999) 321–326 [hep-ph/9812205].

[70] F. A. Chishtie and V. Elias, *RG/Pade estimate of the three-loop contribution to the QCD static potential function*, *Phys. Lett.* **B521** (2001) 434–440 [hep-ph/0107052].

[71] O. V. Tarasov, A. A. Vladimirov and A. Y. Zharkov, *The gell-mann-low function of QCD in the three loop approximation*, *Phys. Lett.* **B93** (1980) 429–432.

[72] N. Brambilla, X. Garcia i Tormo, J. Soto and A. Vairo, *The logarithmic contribution to the QCD static energy at NNNNLO*, *Phys. Lett.* **B647** (2007) 185 [hep-ph/0610143].

[73] N. Brambilla, A. Pineda, J. Soto and A. Vairo, *The infrared behaviour of the static potential in perturbative QCD*, *Phys. Rev.* **D60** (1999) 091502 [hep-ph/9903355].

[74] B. A. Kniehl, A. A. Penin, M. Steinhauser and V. A. Smirnov, *Nonabelian $\alpha_s^3/(m_q r^2)$ heavy-quark-antiquark potential*, *Phys. Rev.* **D65** (2002) 091503 [hep-ph/0106135].

[75] S. Wuester, *Heavy quark potential at order α_s^2/m^2 [in German]*, *Diploma Thesis* (2003).

[76] M. Jezabek and J. H. Kuhn, *QCD Corrections to Semileptonic Decays of Heavy Quarks*, *Nucl. Phys.* **B314** (1989) 1.

[77] A. Czarnecki and K. Melnikov, *Two-loop QCD corrections to top quark width*, *Nucl. Phys.* **B544** (1999) 520–531 [hep-ph/9806244].

[78] K. G. Chetyrkin, R. Harlander, T. Seidensticker and M. Steinhauser, *Second order QCD corrections to Gamma(t –> W b)*, *Phys. Rev.* **D60** (1999) 114015 [hep-ph/9906273].

[79] J. H. Kuhn, *Weak interactions of quarkonia*, *Acta Phys. Polon.* **B12** (1981) 347.

[80] I. I. Y. Bigi, Y. L. Dokshitzer, V. A. Khoze, J. H. Kuhn and P. M. Zerwas, *Production and Decay Properties of Ultraheavy Quarks*, *Phys. Lett.* **B181** (1986) 157.

[81] C. Collaboration, *First direct limit on the top quark lifetime*, CDF note 8104.

[82] M. Beneke, N. Kauer, A. Signer and G. Zanderighi, *Towards pair production near threshold with unstable particle effective theory*, *Nucl. Phys. Proc. Suppl.* **152** (2006) 162–167 [hep-ph/0411008].

[83] M. Beneke, A. P. Chapovsky, A. Signer and G. Zanderighi, *Effective theory approach to unstable particle production*, *Phys. Rev. Lett.* **93** (2004) 011602 [hep-ph/0312331].

[84] M. Beneke, P. Falgari, C. Schwinn, A. Signer and G. Zanderighi, *Four-fermion production near the W pair production threshold*, *Nucl. Phys.* **B792** (2008) 89–135 [0707.0773].

[85] K. Schuller, *Analytical and numerical analyis of the higher order coulomb green function [in German]*, *Diploma Thesis* (2004).

[86] T. Huber and D. Maitre, *HypExp, a Mathematica package for expanding hypergeometric functions around integer-valued parameters*, *Comput. Phys. Commun.* **175** (2006) 122–144 [hep-ph/0507094].

[87] T. Huber and D. Maitre, *HypExp 2, Expanding Hypergeometric Functions about Half-Integer Parameters*, arXiv:0708.2443 [hep-ph].

[88] V. A. Smirnov, *Evaluating Feynman Integrals*. Springer Tracts in Modern Physics (Volume 211). Springer Verlag, 2004.

[89] M. Czakon, *Automatized analytic continuation of Mellin-Barnes integrals*, *Comput. Phys. Commun.* **175** (2006) 559–571 [hep-ph/0511200].

[90] A. S. Kronfeld, *The perturbative pole mass in QCD*, *Phys. Rev.* **D58** (1998) 051501 [hep-ph/9805215].

[91] M. C. Smith and S. S. Willenbrock, *Top-quark pole mass*, *Phys. Rev. Lett.* **79** (1997) 3825–3828 [hep-ph/9612329].

[92] M. Beneke and V. M. Braun, *Heavy quark effective theory beyond perturbation theory: Renormalons, the pole mass and the residual mass term*, *Nucl. Phys.* **B426** (1994) 301–343 [hep-ph/9402364].

[93] M. Beneke, *Renormalons*, *Phys. Rept.* **317** (1999) 1–142 [hep-ph/9807443].

[94] M. Beneke, *A quark mass definition adequate for threshold problems*, *Phys. Lett.* **B434** (1998) 115–125 [hep-ph/9804241].

[95] I. I. Y. Bigi, M. A. Shifman, N. Uraltsev and A. I. Vainshtein, *High power n of m_b in beauty widths and $n = 5 \to \infty$ limit*, *Phys. Rev.* **D56** (1997) 4017–4030 [hep-ph/9704245].

[96] A. H. Hoang, M. C. Smith, T. Stelzer and S. Willenbrock, *Quarkonia and the pole mass*, *Phys. Rev.* **D59** (1999) 114014 [hep-ph/9804227].

[97] A. A. Penin and A. A. Pivovarov, *Bottom quark pole mass and $|V_{cb}|$ matrix element from $R(e^+e^- \to b\bar{b})$ and $\Gamma_{sl}(b \to cl\nu_l)$ in the next-to-next-to-leading order*, *Nucl. Phys.* **B549** (1999) 217–241 [hep-ph/9807421].

[98] K. Melnikov and A. Yelkhovsky, *The b quark low-scale running mass from Υ sum rules*, *Phys. Rev.* **D59** (1999) 114009 [hep-ph/9805270].

[99] B. A. Kniehl and A. A. Penin, *Order $\alpha_s^3 \ln^2(1/\alpha_s)$ corrections to heavy- quarkonium creation and annihilation*, *Nucl. Phys.* **B577** (2000) 197–208 [hep-ph/9911414].

[100] A. V. Manohar and I. W. Stewart, *Running of the heavy quark production current and $1/v$ potential in QCD*, *Phys. Rev.* **D63** (2001) 054004 [hep-ph/0003107].

[101] K. G. Chetyrkin, J. H. Kuhn and M. Steinhauser, *RunDec: A Mathematica package for running and decoupling of the strong coupling and quark masses*, *Comput. Phys. Commun.* **133** (2000) 43–65 [hep-ph/0004189].

[102] D. J. Gross and F. Wilczek, *Ultraviolet behavior of Non-Abelian gauge theories*, *Phys. Rev. Lett.* **30** (1973) 1343–1346.

[103] H. D. Politzer, *Reliable perturbative results for strong interactions?*, *Phys. Rev. Lett.* **30** (1973) 1346–1349.

[104] D. R. T. Jones, *Two Loop Diagrams in Yang-Mills Theory*, *Nucl. Phys.* **B75** (1974) 531.

[105] W. E. Caswell, *Asymptotic Behavior of Nonabelian Gauge Theories to Two Loop Order*, *Phys. Rev. Lett.* **33** (1974) 244.

[106] T. van Ritbergen, J. A. M. Vermaseren and S. A. Larin, *The four-loop beta function in quantum chromodynamics*, *Phys. Lett.* **B400** (1997) 379–384 [hep-ph/9701390].

[107] A. A. Penin and M. Steinhauser, *Heavy quarkonium spectrum at O(alpha(s)**5 m(q)) and bottom / top quark mass determination*, *Phys. Lett.* **B538** (2002) 335–345 [hep-ph/0204290].

[108] I. I. Y. Bigi, M. A. Shifman, N. G. Uraltsev and A. I. Vainshtein, *The Pole mass of the heavy quark. Perturbation theory and beyond*, *Phys. Rev.* **D50** (1994) 2234–2246 [hep-ph/9402360].

[109] M. Beneke and A. Signer, *The bottom MS-bar quark mass from sum rules at next-to-next-to-leading order*, *Phys. Lett.* **B471** (1999) 233–243 [hep-ph/9906475].

[110] H. Leutwyler, *How to Use Heavy Quarks to Probe the QCD Vacuum*, *Phys. Lett.* **B98** (1981) 447.

[111] M. B. Voloshin, *Precoulombic asymptotics for energy levels of heavy quarkonium*, *Sov. J. Nucl. Phys.* **36** (1982) 143.

[112] M. Beneke, *New results on heavy quarks near threshold*, hep-ph/9806429.

[113] K. G. Chetyrkin, J. H. Kuhn and A. Kwiatkowski, *QCD corrections to the e+ e- cross-section and the Z boson decay rate: Concepts and results*, *Phys. Rept.* **277** (1996) 189–281.

[114] K. G. Chetyrkin, A. H. Hoang, J. H. Kuhn, M. Steinhauser and T. Teubner, *Massive quark production in electron positron annihilation to order alpha(s)**2*, *Eur. Phys. J.* **C2** (1998) 137–150 [hep-ph/9711327].

[115] R. V. Harlander and M. Steinhauser, *rhad: A program for the evaluation of the hadronic R-ratio in the perturbative regime of QCD*, *Comput. Phys. Commun.* **153** (2003) 244–274 [hep-ph/0212294].

[116] R. Frey *et. al.*, *Top quark physics: Future measurements*, `hep-ph/9704243`.

[117] S. T. Boogert and D. J. Miller, *Questions about the measurement of the e+ e- luminosity spectrum*, `hep-ex/0211021`.

[118] D. Cinabro, *The t anti-t threshold and machine parameters at the NLC*, `hep-ex/0005015`.

[119] J. H. Kuhn and M. Steinhauser, *Determination of alpha(s) and heavy quark masses from recent measurements of R(s)*, *Nucl. Phys.* **B619** (2001) 588–602 [`hep-ph/0109084`].

[120] E. H. Wichmann and C. H. Woo, *Integral representation for the non-relativistic Coulomb Green's function*, *J. Math. Phys.* **2** (1961) 178–180.

[121] M. B. Voloshin, *Nonperturbative effects in hadronic annihilation of heavy quarkonium*, *Sov. J. Nucl. Phys.* **40** (1984) 662–667.

[122] R. E. Crandall and J. P. Buhler, *On the evaluation of Euler Sums*, *Exp.Math.* **3** (1994) No.4.

[123] J. M. Borwein and R. Girgesohn, *Evaluation of triple Euler Sums*, *El.Journ.Comb.* **3** (1996) R23.

Danksagung - Acknowledgement

An dieser Stelle möchte ich mich bei allen bedanken, die zum Gelingen dieser Arbeit beigetragen haben.

Zuerst danke ich Professor Dr. Martin Beneke für die Bereitstellung dieses interessanten Themas, für die außerordentlich gute und kompetente Betreuung und die Überprüfung vieler Ergebnisse. Ich danke außerdem Professor Dr. Werner Bernreuther, der sich als Koreferent zur Verfügung gestellt hat. I am very grateful for the help from Dr. Yuichiro Kiyo, for the fruitful collaboration, countless discussions and many checks of the results.

Ich möchte mich auch bei meinen langjährigen Bürokollegen Silja Brensing, Marc Hitschfeld und Leonard Meyer für viele fachliche Diskussionen und die stets angenehme gemeinsame Zeit bedanken. Außerdem danke ich allen Kollegen des dritten und vierten Flures für die gute Atmosphäre.

Für die finanzielle Förderung bedanke ich mich beim DFG-Graduiertenkolleg "Elementarteilchenphysik an der TeV-Skala".

Sehr dankbar bin ich meinen Eltern Karl und Sofia Schuller, nicht nur für die finanzielle und materielle Unterstützung, sondern auch für den uneingeschränkte Rückhalt, den ich jederzeit hatte. Nicht zuletzt danke ich Isabell Wolf für die moralische Unterstützung während der gesamten Zeit.

Curriculum Vitae

Kurt Schuller

geboren	am 14.08.1978 in Mediasch (Rumänien)
Staatsangehörigkeit	deutsch
Familienstand	ledig

Schulbildung

1984-1989	Grundschule (Şeica Micâ/Rumänien)
1989-1998	Städtisches Gymnasium an der Bayreuther Straße (Wuppertal)
1998	Abitur

Wehrdienst

1998-1999	Lehr- und Unterstützungszentrum für Operative Information (Mayen)

Universitätsausbildung

1999-2004	Physikstudium an der Rheinisch-Westfälischen Technischen Hochschule (Aachen)
2002-2008	Wirtschaftswissenschaftliches Zusatzstudium an der Rheinisch-Westfälischen Technischen Hochschule (Aachen)
2004	Diplom-Physiker (Betreuer: Prof. M. Beneke)
2008	Master of Business Administration (Betreuer: Prof. W. Breuer)
2004-2008	Doktorarbeit in Physik an der Rheinisch-Westfälischen Technischen Hochschule (Aachen)